



**Characterisation of microglia's  
inflammatory response and investigation  
of the effect of mesenchymal stem cells-  
conditioned media**

Samantha White

A thesis presented in the fulfilment of the requirement for the  
degree of doctor of philosophy

STRATHCLYDE INSTITUTE OF PHARMACY AND BIOMEDICAL  
SCIENCES

UNIVERSITY OF STRATHCLYDE

2017

## **Declaration**

*This thesis is the result of the author's original research. It has been composed by the author and has not been previously submitted for examination which has led to the award of a degree.*

*The copyright of this thesis belongs to the author under the terms of the United Kingdom Copyright Acts as qualified by University of Strathclyde Regulation 3.50. Due acknowledgement must always be made of the use of any material contained in, or derived from, this thesis.*

Signed:

Date:

## Acknowledgments

First and foremost, I would like to offer my sincere gratitude to my supervisor's Dr Hilary Carswell, Dr Michele Zagnoni and Prof Robin Plevin for all their contributions, guidance and support. I would especially like to thank Hilary for her constant encouragement and patience throughout the last 4 years, and for her reassurance during my tough times. A big thank you to Michele, who became an unexpectedly massive part of my project, and an additional supervisor, thank you for all your patience when trying to explain 'engineering' to me! Thank you to Robin for his constant support and advice throughout my time at Strathclyde, as an undergraduate student and during my PhD.

I would like to thank our collaborators, Dr Eliza Zanier, Dr Francesca Pischiutta, Prof Parolini Ornella and Dr Antonietta Silini, thank you for allowing me to part of such an exciting project, and for all your input to my PhD, it was a pleasure to work with you all.

I am grateful for the generous financial support from the BBSRC DTP which was essential for conducting this work.

It would not have been possible for me to complete my PhD without the help of so many people. Thanks to the very knowledgeable Dr Rothwell Tate for his expertise in PCR, your teaching and patience is sincerely appreciated! A massive thanks to Dr Craig McKittrick for all his guidance and patience teaching me the stroke models. A big thanks to Dr Kathleen Grabert, a fantastic scientist who gave me so much support when I was pulling my hair out trying to successfully isolate microglial cells. It was a pleasure spending our Colorado experience together, I still laugh when I think about our constant dehydration, you on that luggage holder and of course it was my pleasure introducing you to 'The Kardashians'. I would like to thank Theresa Christ for all her help and support in engineering, especially with all the gradient and microscope work!

My thanks and appreciation is extended to all the staff in the biological procedures unit, I could not have completed my *in vivo* work without you all! I would like to personally thank Carol and Lee, both of whom went out their way to help me. All our chats and your help managed to keep me sane when I was in the unit all day, every

day and was stressed to my max! Thank you to all my SIPBS colleagues for their constant help and advice.

Throughout my PhD I have made many friends who I will no doubt be friends with for life. Dr Josie Fullerton, thank you for all your pep talks, for all the hilarious desk chat and of course letting me work for you as your very own PA! Haha! I started my PhD journey with Claire McCluskey (AKA big Dave, Half pint, Edna, Pat) now one of my best friends. We cried in the toilets during the really hard times and we cried with laughter during the good times. We have had so many laughing fits which made my PhD experience so enjoyable and fun! I would say that I will miss you but I still get to see you every day at work so all is good in life!

I would not be at this stage in my life if it wasn't for the love and support of my family, friends and my partner Jye. I need to give a big shout out to my longest friend Mo, ever since we were house mates in St Andrews and you taught me first year Maths, you have always been there for me, cheering me on and supporting me!

Thank you to Sandra and Iain especially in the past few months for the cooking, cleaning and even doing our washing so I could keep writing! A massive thank you to my Mum, the strongest woman I know. She has always supported me, and made sure that I always had everything I needed and more. She is my best friend and my inspiration and I wouldn't be where I am now if it wasn't for her. Thank you to my Granny and Grampie for all their support, guidance and encouragement. Granny, your hard work and determination after your stroke truly inspired me to keep going when times are tough. You have always called me your 'clever Granddaughter' - it has been so encouraging to know how proud you all are of me.

Last but not least, I need to say an enormous thanks to my partner in crime, and best friend, Jye. Your persistent motivation and never-ending support throughout not only my PhD but also the past 9 years has been amazing. You have always believed in me, supported me and motivated me to do anything that I want to. Thank you for putting up with all my stressing, crying and moaning during my PhD! I couldn't have done it without you, whether it was you cleaning the house, giving me a lift in at crazy o'clock or letting us get our big fluffy baby Rex, you always know how to cheer me up and make me smile.

## Poster communications

Glasgow Neuroscience Day Meeting, Caledonian University, UK (16<sup>th</sup> January 2015)  
The effect of ischaemia on the DUSP-4 knockout mouse.

Scottish Cardiovascular Forum, Queens Medical Research Institute, UK (7<sup>th</sup> February 2015)  
The effect of ischaemia on the DUSP-4 knockout mouse.

BNA 2015 Festival of Neuroscience, EICC, UK (12<sup>th</sup>-15<sup>th</sup> April 2015)  
The effect of ischaemia on the DUSP-4 knockout mouse.

Scottish Neuroscience Meeting, St Andrews, UK (28<sup>th</sup> August 2015)  
Establishing microglial cultures in microfluidic devices for future investigations into stem cell-microglial cell interactions.

Microglia in the brain conference, Colorado, USA (12<sup>th</sup>-16<sup>th</sup> June 2016)  
An *in vitro* model of microglia migration after stroke.

Brain, Berlin, Germany (1<sup>st</sup>-4<sup>th</sup> April 2017)  
An *in vitro* model of microglia migration after stroke. *JOURNAL OF CEREBRAL BLOOD FLOW AND METABOLISM* (Vol. 37, pp. 406-407).

## **Oral communications**

SIPBS Cell biology, neuroscience and cardiovascular research day, SIPBS, UK (August 2014) The immunomodulation of neural stem cells in the ischaemic brain.

2<sup>nd</sup> Pre-clinical stroke symposia, University of Strathclyde, UK (18<sup>th</sup> June 2015)  
Establishing microglial cultures in microfluidic devices for future investigations into stem cell-microglial cell interactions.

SIPBS Annual Symposium, University of Strathclyde, UK (20<sup>th</sup> August 2015)  
Establishing microglial cultures in microfluidic devices for future investigations into stem cell-microglial cell interactions.

Glasgow Neuroscience Meeting, University of Strathclyde, UK (15<sup>th</sup> January 2016)  
An *in vitro* model of microglia migration: relevant to stroke.

3<sup>rd</sup> Pre-clinical stroke symposia, University of Nottingham, UK (26<sup>th</sup>-27<sup>th</sup> June 2017)  
The effect of hAMSC-CM on microglia's inflammatory response after stroke.

## **Awards and Prizes**

**AWERB 3Rs Grant-** Establishing primary microglial cultures from adult mice using microfluidics technology to reduce numbers of animals used for future investigations into microglial-stem cell interactions after stroke. *Dr Hilary Carswell, Dr Michele Zagnoni and Ms Samantha White.*

**Best oral presentation-** Glasgow Neuroscience Meeting 2016

**Best oral presentation-** 3<sup>rd</sup> Pre-clinical stroke symposia 2017

## **Manuscripts in preparation**

White, S., Zagnoni, M and Carswell, H. V. O. (2017) Responses of A Microglial Cell Line Derived from Spontaneously Immortalized Murine Microglia, SIM-A9, to pro- and anti-inflammatory stimuli: signalling, migration and molecular profiles. *J Neuroinflammation*

White, S., Plevin, R., Zagnoni, M., Zanier, E., Pischiotta, F., Parolini, O., Silini, A and Carswell, H. V. O. (2017) Modulation of microglia inflammatory and migratory responses by human amniotic mesenchymal stem cell conditioned media. *Stroke*.

## Abstract

Stroke is the second single most common cause of death and the largest cause of disability worldwide, highlighting the urgent need for new treatments. Mesenchymal stem cell transplantation aids regeneration and repair in animal models of ischaemia, possibly, at least in part, via interaction with microglia, modulating their inflammatory response into an anti-inflammatory phenotype favouring regeneration. Evidence shows that the beneficial effects of cell therapy are due to the release of soluble factors, raising the possibility of cell-free therapeutic strategy. Our collaborators on the current project, Pischuitta *et al.*, (2016) recently provided evidence of the comparable effects of human amniotic stem cells (hAMSC) and hAMSC-conditioned media. They found that both hAMSC and hAMSC-CM treatments induced up-regulation of the microglia marker, CD11b. In order to investigate the potential for hAMSC-CM to modulate microglia, several *in vitro* and *in vivo* approaches were utilised.

The aims of this thesis were to characterise the signalling and polarisation of SIM-A9 cells; establish a consistent protocol for the isolation of highly pure microglia from the mouse brain; establish and optimise an *in vitro* microglia migration model; and to examine the effects of hAMSC-CM on SIM-A9 cells microglial cells on signalling, polarisation and migration *in vitro* and on polarisation *in vivo*.

The results revealed the ability of SIM-A9 microglial cells to be polarised in to a pro-inflammatory phenotype (induced with LPS), with the expression of pro-inflammatory genes *Il1 $\beta$*  and *Nos2* significantly increasing; as well as an anti-inflammatory phenotype (induced with IL-4), which led to the expression of the anti-inflammatory gene, *Arg1* to significantly increase. Protocols used to extract primary microglia from the neonatal and adult mouse did not produce purity, reproducibility or good survival in culture.

We showed that the addition of hAMSC-CM significantly reduced mRNA expression of *Il1 $\beta$* , *Tnfa* and *Ccl2* in LPS-induced microglia. Using a multi-disciplinary approach, an *in vitro* microglia migration model that is a better representation of the stroke environment was established, optimised and characterised. This work showed that LPS significantly inhibited glutamate-induced migration of microglial cells, while IL-4 treatment enhanced migration. Interestingly, addition of hAMSC-CM reversed the



inhibitory effect of LPS on glutamate-induced migration. Translating our *in vitro* findings *in vivo*, we then investigated the effect of hAMSC-CM after stroke, using the mouse stroke model. It was concluded that hAMSC-CM, injected 3 hours after stroke, had no effect on inflammatory markers after 24 hours of recovery.

In conclusion, we have shown that hAMSC-CM can modulate microglial cells from a pro-inflammatory phenotype into an anti-inflammatory phenotype. Therefore, hAMSC-CM has an anti-inflammatory effect that may be beneficial after stroke.

## Table of contents

<b>Declaration</b> .....	<b>I</b>
<b>Acknowledgments</b> .....	<b>II</b>
<b>Poster communications</b> .....	<b>IV</b>
<b>Oral communications</b> .....	<b>V</b>
<b>Awards and Prizes</b> .....	<b>V</b>
<b>Manuscripts in preparation</b> .....	<b>VI</b>
<b>Abstract</b> .....	<b>VII</b>
<b>Table of contents</b> .....	<b>IX</b>
<b>List of figures</b> .....	<b>XIV</b>
<b>List of tables</b> .....	<b>XVII</b>
<b>List of abbreviations</b> .....	<b>XVIII</b>
<b>Chapter 1: General Introduction</b> .....	<b>1</b>
1.1 Introduction to Stroke .....	2
1.2 Mechanisms of tissue damage in ischaemic stroke .....	2
1.3 Inflammatory mechanisms in ischaemic stroke .....	5
1.4 Microglia .....	7
1.4.1 Introduction to microglia .....	7
1.4.2 Microglia in the healthy brain .....	8
1.4.3 Activation of microglia .....	10
1.4.4 Microglia migration .....	14
1.4.5 Modelling microglia <i>in vitro</i> .....	15
1.4.6 Microglia response after ischaemic damage .....	17

1.5 Modulation of the immune system for treatment of stroke.....	20
1.6 Introduction to stem cell therapy for stroke .....	22
1.6.1 Immunomodulatory effects of MSCs .....	23
1.6.2 Do we need stem cells or can we use their juices? The effect of hAMSC-CM.....	29
1.7 Aims and thesis overview .....	33

**Chapter 2: Signalling and polarisation of microglial cell line SIM-A9 in response to LPS, IL-4 and hAMSC-CM..... 34**

2.1 Introduction and aims .....	35
2.2 Materials and Methods .....	38
2.2.1 Cell culture.....	38
2.2.2 Immunoblotting of cell lysates .....	39
2.2.3 RNA analysis .....	42
2.2.4 Quantitative real-time polymerase chain reaction (qRT-PCR) .....	44
2.2.5 Mouse cytokine proteome profiler .....	47
2.2.6 Nitric oxide assay.....	48
2.2.7 Isolation of microglia from the mouse brain .....	48
2.2.8 Statistical analysis.....	53
2.3 Results .....	54
2.3.1 LPS activated the NF- $\kappa$ B signalling pathway in a time and concentration dependent manner in SIM-A9 microglia cells.....	54
2.3.2 The effect of hAMSC-CM on specific transcription factors expression in microglia .....	59
2.3.3 Validation and characterisation of the polarisation of SIM-A9 microglia..	62
2.3.4 hAMSC-CM promotes anti-inflammatory properties in microglia while dampening the pro-inflammatory properties.....	67

2.3.5 Establishment of primary microglia cell isolation and culture.....	75
2.4 Discussion.....	81
2.4.1 Characterisation of the signalling of SIM-A9 microglia cell line.....	81
2.4.2 The effects of hAMSC-CM on signalling pathways in SIM-A9 microglia cells .....	82
2.4.3 The effect of LPS and IL-4 on inflammatory mediators in SIM-A9 cells ..	83
2.4.4 The effect of hAMSC-CM on inflammatory mediators in SIM-A9 cells ....	85
2.4.5 Establishment of primary microglia cell isolation and culture.....	87
2.4.6 Methodological limitations .....	90

<b>Chapter 3: Establishment and characterisation of an <i>in vitro</i> model of microglia migration that is relevant to stroke and investigation of the effects of hAMSC-CM.....</b>	<b>91</b>
3.1 Introduction and aims .....	92
3.2 Materials and Methods .....	98
3.2.1 BV-2 cells .....	98
3.2.2 Microfluidic device preparation.....	98
3.2.3 Insertion of cells into the microfluidic devices.....	100
3.2.4 Gradient characterisation.....	100
3.2.5 Set up of migration experiments.....	101
3.2.6 Real-time imaging.....	101
3.2.7 Analysis of cell migration.....	103
3.3 Results .....	105
3.3.1 Microglia cells survive and proliferate within microfluidic devices .....	107
3.3.2 Optimisation of coatings of microfluidic devices .....	109
3.3.3 Results from readily available devices .....	110
3.3.4 New generation of devices.....	116

3.3.5 The effect of LPS and IL-4 treatment on glutamate-induced migration in SIM-A9 microglia cells .....	119
3.3.6 The effect of hAMSC-CM treatment on glutamate-induced migration in SIM-A9 microglia cells .....	124
3.4 Discussion.....	127
3.4.1 The use of microfluidic technology to study microglia migration .....	127
3.4.2 A glutamate gradient induces migration of SIM-A9 microglial cells.....	129
3.4.3 The effect of LPS and IL-4 treatment on glutamate-induced migration in SIM-A9 microglia cells .....	130
3.4.4 The effect of hAMSC-CM treatment on glutamate-induced migration in SIM-A9 microglia cells .....	131
3.4.5 Methodological limitations .....	133

**Chapter 4: Establishment of the middle cerebral artery occlusion model in mice and investigation of the effect of hAMSC-CM on the acute inflammatory response post-MCAO .....** **134**

4.1 Introduction and aims .....	135
4.2 Materials and methods .....	138
4.2.1 Surgical Techniques .....	138
4.2.2 Experimental protocol .....	141
4.2.3 Intravenous injection of hAMSC-CM .....	144
4.2.4 Bederson scoring .....	144
4.2.5 Termination of Experiment and Processing Tissue .....	145
4.2.6 Measurement of ischaemic damage and oedema .....	148
4.2.7 Collection of plasma from blood samples.....	149
4.2.8 RNA extraction from regional brain homogenates using RNeasy Plus Universal Mini kit .....	149
4.3. Results .....	151

4.3.1 Result from study 1: Reproducibility of the ILT model in mice .....	151
4.3.2 Results from study 2: hAMSC-CM study .....	152
4.4 Discussion.....	160
4.4.1 Reproducibility of the ILT model in mice.....	160
4.4.2 The effect of hAMSC-CM on inflammatory marker expression after a 45 min MCAO in mice.....	161
4.4.3 Methodological limitations .....	167
<b>Chapter 5: General Discussion.....</b>	<b>168</b>
5.1 Summary of aims and results .....	169
5.1.1 Summary of main findings.....	169
5.2 Future directions .....	170
5.3 Further implications .....	172
5.3.1 What are the mechanisms involved in hAMSC-CM modulation of microglia? .....	172
5.3.2 Clinical relevance.....	173
<b>Chapter 6: Refences .....</b>	<b>175</b>

## List of figures

### Chapter 1

- Figure 1.1. Overview of pathophysiology mechanisms in the ischaemic brain. .... 3
- Figure 1.2. Schematic representation of microglia functional states in the healthy murine brain..... 9
- Figure 1.3. Schematic diagram showing various morphological and functional states of microglia. .... 18
- Figure 1.4. A summary of mechanisms of MSC therapy-related neuroprotection... 28
- Figure 1.5. Categories of molecules secreted by placenta-derived stem cells..... 32

### Chapter 2

- Figure 2.1. Schematic diagram of microglia isolation using Percoll gradient and CD11b magnetic microbeads..... 52
- Figure 2.2. Time dependent LPS-induced I $\kappa$ B $\alpha$  degradation in SIM-A9 microglia cells. .... 55
- Figure 2.3. Time dependent LPS-induced P65 phosphorylation in SIM-A9 microglia cells. .... 56
- Figure 2.4. Concentration dependent LPS-induced I $\kappa$ B $\alpha$  degradation in SIM-A9 microglia cells. .... 57
- Figure 2.5. Concentration dependent LPS-induced P65 phosphorylation in SIM-A9 microglia cells. .... 58
- Figure 2.7. The effect of LPS and IL-4 activation of SIM-A9 microglia cells on *I11 $\beta$* , *Nos2* and *Arg1* expression..... 63
- Figure 2.8. The effect of LPS and IL-4 activation of SIM-A9 microglia cells on iNOS expression. .... 64
- Figure 2.9. The effect of LPS and IL-4 activation of SIM-A9 microglia cells on Arginase 1 expression. .... 65

Figure 2.10. The effect of LPS and IL-4 activation of SIM-A9 microglia cells on nitrite production.....	66
Figure 2.11. The effect of hAMSC-CM on <i>Il1<math>\beta</math></i> , <i>Tnfa</i> , <i>Nos2</i> , <i>Ccl2</i> and <i>Arg1</i> expression in SIM-A9 microglia cells.....	68
Figure 2.12. The effect of hAMSC-CM and LPS on the morphology of SIM-A9 microglia cells. ....	70
Figure 2.13. The effect of hAMSC-CM on nitrite production in SIM-A9 microglia cells. ....	71
Figure 2.14. The effect of hAMSC-CM on pro- and anti-inflammatory mediators in SIM-A9 cell lysates. ....	73
Figure 2.15. Quantification of Proteome Profiler Mouse Cytokine Array.....	74
Figure 2.16. Flow cytometry analysis of extracted microglia from a neonatal mouse brain using the shaking method (Protocol 1).....	75
Figure 2.17. Flow cytometry analysis and images of extracted microglia from an adult mouse brain using a Percoll gradient and CD11b magnetic beads (Protocol 2). ....	78
Figure 2.18. Images of extracted microglia from a neonatal mouse at day 3 in culture.....	79
Figure 2.19. Flow cytometry analysis of extracted microglia from a neonatal mouse brain using the tissue dissociation kit and CD11b+ magnetic beads (Protocol 4)...	80
<b>Chapter 3</b>	
Figure 3.1. Schema of a physiologically relevant <i>in vitro</i> model for migration studies .....	94
Figure 3.2. Static gradient generator.....	96
Figure 3.3. Example of microfluidic devices. ....	99
Figure 3.4. Example of an experimental set-up using an on-stage incubator. ....	102
Figure 3.5. Snapshot images demonstrating manual cell tracking of BV-2 microglia cells within microfluidic devices.....	103
Figure 3.6. Schematic illustrating the definitions in the 2D cell trajectory plots. ....	104



Fig 3.7. DAPI and Propodium iodide stained BV-2 microglia cells 6 days after insertion into microfluidic devices.....	108
Figure 3.8. The effect of PDL and fibronectin coating on BV-2 microglia cell motility. ....	109
Figure 3.9. BV-2 microglia cells within device 2. ....	110
Figure 3.10. Images of BV-2 cells in device 3, illustrating uneven cell distribution 24 hours after seeding. ....	112
Figure 3.11. A gradient can successfully be established within microchannels in device 4. ....	113
Figure 3.12. The effect of a glutamate and ADP gradient on BV-2 microglia cells. ....	115
Figure 3.13. Characterisation of the gradient development. ....	118
Figure 3.14. LPS inhibited glutamate-induced SIM-A9 microglia cell migration in microfluidic devices.....	121
Figure 3.15. IL-4 enhanced glutamate-induced SIM-A9 microglia cell migration in microfluidic devices.....	122
Figure 3.16. Modulation of glutamate-induced migration by LPS and IL-4. ....	123
Figure 3.17. hAMSC-CM reverses the inhibitory effect of LPS on glutamate-induced SIM-A9 microglia cell migration in microfluidic devices. ....	125
Figure 3.18. hAMSC-CM reversed the inhibitory effect of LPS on glutamate-induced microglia migration.....	126
<b>Figure 4</b>	
Figure 4.2. A schematic representation of the intraluminal filament middle cerebral artery occlusion surgery.....	140
Figure 4.1. Experimental and treatment protocol for study 2. ....	142
Figure 4.3. The eight distinct anatomical landmarks collected for quantification of lesion and oedema volume. ....	147
Figure 4.4. (A) Infarct volume and (B) Oedema percentage in animals 72 hours post MCAO.....	152
Figure 4.5. Flow-chart showing total experimental animals used in study 2. ....	153

Figure 4.6. The effect of hAMSC-CM on ipsilateral striatal pro-inflammatory gene expression 24 hours after MCAO..... 157

Figure 4.7. The effect of hAMSC-CM on ipsilateral striatal anti-inflammatory gene expression 24 hours after MCAO..... 159

## **Chapter 5**

Figure 5.1. Five chamber microfluidic device. .... 171

## **List of tables**

### **Chapter 2**

Table 2.1. Details of primary and secondary antibodies used for each protein of interest..... 41

Table 2.2. Sequence of oligonucleotides of housekeeping genes and genes of interest. Primers used in qRT-PCR with annealing temperature of 60°C..... 45

Table 2.3. Thermal profile of standardised qRT-PCR..... 46

Table 2.4. Experimental protocols used for microglia isolations and the rationale, and result from each protocol. .... 76

### **Chapter 3**

Table 3.1. A summary of the five microfluidic devices used in this chapter. .... **Error! Bookmark not defined.**

### **Chapter 4**

Table 4.1. Details of the experimental methods for study 2 as advised by the ARRIVE guidelines. .... 143

Table 4.2. Bederson neurological examination grading system ..... 145

Table 4.5. Sequence of oligonucleotides of housekeeping genes and genes of interest. Primers used in qRT-PCR with an annealing temperature of 60°C..... 150

Table 4.6. Results of the Bederson neurological scoring examine in experimental animals 24 hours post MCAO in study 2. .... 154

Table 4.7. Key features of the published and unpublished work carried out on the effects of hAMSC or hAMSC-CM after TBI, MCAo or OGD. .... 162

## List of abbreviations

ADP	Adenosine diphosphate
AMPA	$\alpha$ -amino-3-hydroxy-5-methyl-4-isoxazolepropionic acid
ANOVA	analysis of variance
Arg	arginase
ATP	Adenosine triphosphate
BBB	blood brain barrier
BMMSCs	bone marrow mesenchymal stem cells
Ca <sup>2+</sup>	calcium
CCA	common carotid artery
CCL2	chemokine ligand 2
cDNA	complementary DNA
CM	conditioned media
CNS	central nervous system
DAMPS	damage-associated molecular patterns
DAPI	4',6-Diamidino-2-Phenylindole, Dihydrochloride
DMEM	Dulbecco's modified eagle medium
DNA	deoxyribonucleic acid
ECA	external carotid artery
ECL	electrochemiluminescence

EDTA	ethylenediaminetetraacetic acid
FACS	fluorescence-activated cell sorting
FCS	fetal bovine serum
FDA	food and drug administration
GAPDH	glyceraldehyde 3-phosphate dehydrogenase
GM-CSF	granulocyte macrophage colony-stimulating factor
H&E	haematoxylin and eosin
HAPI	highly aggressively proliferating immortalised microglia cell line
HCL	hydrochloric acid
HSP	heat shock protein
hUCB	human umbilical cord blood
i.p	intraperitoneal
IC	intracerebral
ICA	internal carotid artery
IFN	interferon
IGF-1	insulin growth factor-1
IL	interleukin
IL-R	interleukin receptor
ILT	intraluminal thread
iNOS	inducible Nitric Oxide Synthase
IP3	inositol triphosphate

iPSCs	induced pluripotent stem cells
IV	intravenous
K <sup>+</sup>	potassium ions
LHS	left-hand side
LPS	lipopolysaccharide
MAPK	mitogen-activated protein kinases
MCA	middle cerebral artery
MCA <sub>o</sub>	middle cerebral artery occlusion
M-CSF	macrophage colony-stimulating factor
MiR	micro-RNA
Mrc1	mannose receptor C-type-1
mRNA	messenger RNA
MSCs	mesenchymal stem cells
MyD88	myeloid differentiation primary response 88
Na <sup>+</sup>	sodium ions
NF-κB	nuclear factor kappa-light-chain-enhancer of activated B cells
NMDA	N-methyl-D-aspartic acid receptor
nNOS	neuronal Nitric Oxide Synthase
NO	nitric oxide
NPCs	neuronal progenitor cells
NSC	neuronal stem cells

O <sub>2</sub>	oxygen
occA	occipital artery
OGD	oxygen-glucose deprivation
PBS	phosphate-buffered saline
PCR	polymerase chain reaction
PDL	Poly-D-lysine
PDMS	polydimethylsiloxane
p-ERK	phosphorylated-extracellular signal-regulated kinase
PI	propidium iodide
p-IkBa	phosphorylated- IkBa
p-JNK	phosphorylated-c-Jun N-terminal kinases
PLC	phospholipase C
PLL	Poly-L-lysine
PM	primary microglia
pMSCs	placental mesenchymal stem cells
PRR	pattern recognition receptor
PTA	ptergopalatine
qRT-PCR	quantitative real time-PCT
RHS	right-hand side
RNA	ribonucleic acid
ROS	reactive oxygen species

RT	reverse transcriptase
SEM	standard error of the mean
SIM-A9	spontaneously immortalised microglia cell line
SOC3	suppressor of cytokine signalling 3
STA	superior thyroid artery
TBS	tris-buffered saline
TBST	tris-buffered saline-tween
TGF- $\beta$	transforming growth factor $\beta$
Th	T helper cell
TLR	toll like receptor
TNF	tumour necrosis factor
tPA	tissue plasminogen activator
Treg	T regulatory cells
UCB-SC	umbilical cord blood-stem cells
UDP	uridine diphosphate
UV	ultraviolet

# **Chapter 1: General Introduction**



## 1.1 Introduction to Stroke

Globally, in 2013 there were 6.5 million stroke deaths, making stroke the 2<sup>nd</sup> leading cause of death behind ischaemic heart disease. In 2014, on average, every 4 minutes someone died of a stroke (Benjamin *et al.*, 2017). Every 2 seconds, someone in the world will have a stroke, with the burden of stroke (due to illness, disability and early death) set to double worldwide within the next 15 years (Feigin *et al.*, 2014). Most conventional risk factors for stroke include age, smoking, diabetes, hypertension and obesity.

There are three main pathological types of stroke, ischaemic, haemorrhagic and subarachnoid haemorrhagic with ischaemic being most prevalent contributing to 87% of all strokes (Sierra *et al.*, 2011). The most common mechanism of haemorrhagic stroke is hypertensive small vessel disease that subsequently ruptures. Ischaemic stroke is a consequence of thrombosis or following embolic occlusion of a cerebral blood vessel arising from the heart or atherosclerotic plaques. Potential causes of emboli from the heart include atrial fibrillation, cardiac valve disease and patent foramen ovale and these conditions are associated with an increased risk of ischaemic stroke (Warlow *et al.*, 2003).

Recombinant tissue plasminogen activator (tPA) administration can restore blood flow by clot lysis and cause reperfusion (Moskowitz *et al.*, 2010) and is the only current FDA-approved treatment available for ischaemic stroke. tPA must be given within 3-4.5 hours of symptom onset, which leads to only 3-8% of eligible patients receiving treatment (Peña *et al.*, 2017). Without more effective treatments, rehabilitation or preventative treatment the cost of stroke can only increase.

## 1.2 Mechanisms of tissue damage in ischaemic stroke

There are many pathophysiological processes involved that lead to cell death (**figure 1.1**), all of which are time dependent, occurring over minutes, hours or days. Within the ischaemic core, where blood flow is most severely restricted, necrotic cell death occurs within minutes. Around the ischaemic core lies the penumbra area, this area may remain viable for several hours after an ischaemic event due to the collateral arteries that supply the penumbral zone (Fisher, 2004). Hence the degree of ischaemia and timing of reperfusion can determine the outcome for the individual cells (Doyle *et al.*, 2008).

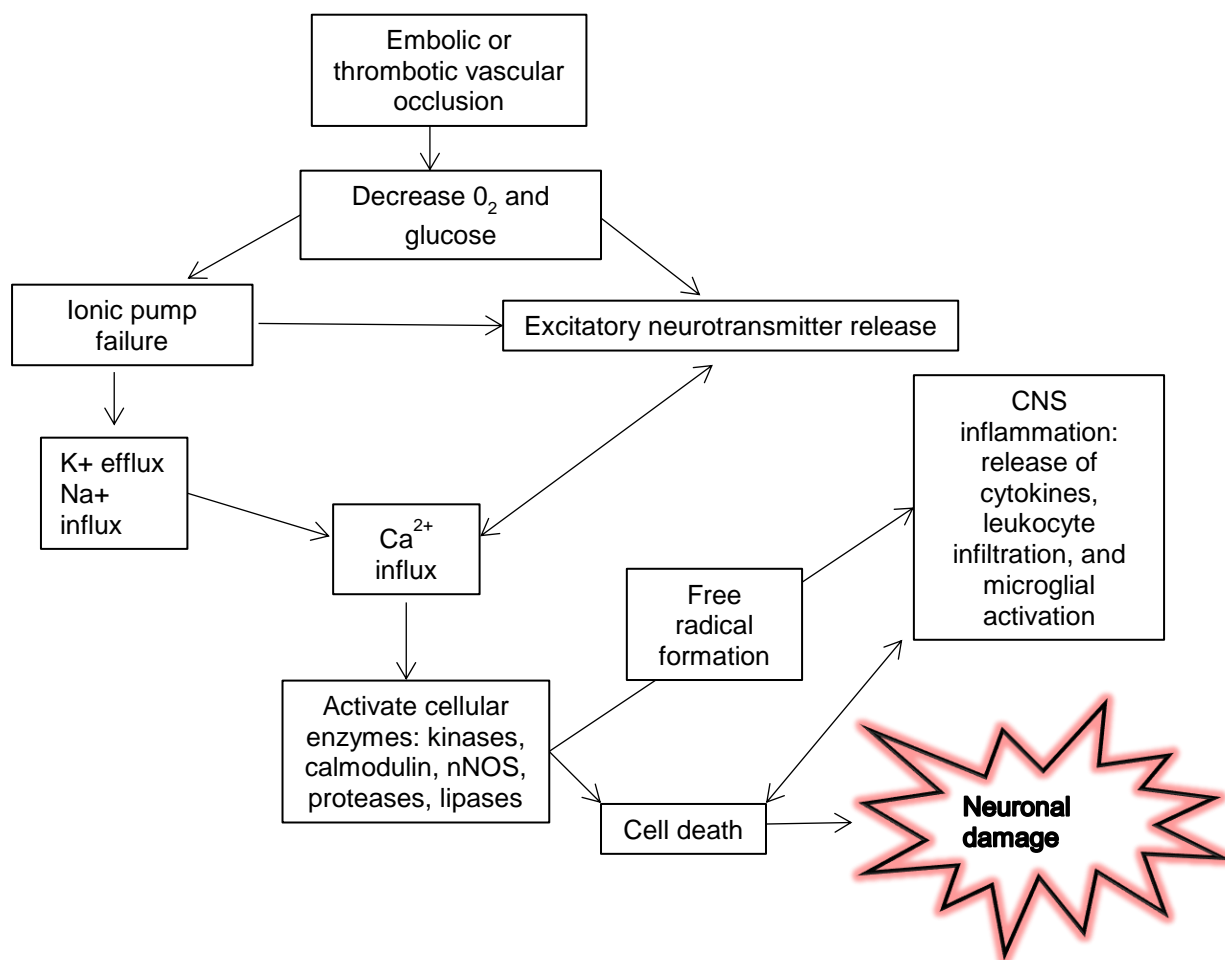


**Figure 1.1. Overview of pathophysiology mechanisms in the ischaemic brain.**

An embolic or thrombotic vascular occlusion leads to a limited supply of oxygen and glucose in the ischaemic core. The restricted supply of energy leads to ionic pump failure which causes depolarisation of neurons and subsequently excitatory neurotransmitter release. Activation of the glutamate receptors causes an increase in intracellular  $\text{Ca}^{2+}$ ,  $\text{Na}^+$  while  $\text{K}^+$  is released into the extracellular space. The universal intracellular messenger  $\text{Ca}^{2+}$  over-activates numerous enzymes systems such as kinases, calmodulin, nNOS, proteases and lipases. Free radicals are generated which damage membranes, mitochondria and DNA and induce the formation of inflammatory mediators which lead to microglia activation and leukocyte infiltration. These processes and products ultimately lead to cell death and neuronal damage. Schema adapted from Dirnagl *et al.*, (1999).

Focal impairment of cerebral blood flow restricts the delivery of substances, particularly oxygen and glucose (Dirnagl *et al.*, 1999). Despite the brain accounting for less than 2% of the body's total mass, at rest the brain uses up 20% of the oxygen needed by the body (Raichle, 2001). This is essential to generate sufficient adenosine tri-phosphate (ATP) to maintain and restore ionic gradients. After ischaemia, mitochondrial inhibition of ATP synthesis leads to ATP being consumed within 2 minutes, causing neuronal plasma membrane depolarisation. This ultimately leads to neuronal plasma membrane depolarisation release of  $K^+$  and entry of  $Na^+$  into cells (Doyle *et al.*, 2008). Hence, ischaemic insults induce changes in the balance of ion gradients across membranes, which are caused by reduced energy production. Failure to maintain ion gradients results in depolarisation of cell membranes. Membrane depolarisation leads to glutamate release, an excitatory neurotransmitter, and subsequent activation of the AMPA and NMDA receptors. Glutamate and its receptors are implicated in the pathology of stroke in two main ways; excessive accumulation of glutamate in the extracellular space during ischaemia and the subsequent activation of glutamate receptors in postsynaptic cells (Nishizawa, 2001). In addition to direct neurotoxicity of glutamate on neurons, glutamate activation also leads to further increase of intracellular  $Ca^{2+}$ ,  $Na^+$  and  $Cl^-$  levels, leading to cytotoxic oedema and further toxic events (Dirnagl *et al.*, 1999). Therefore, during ischaemia  $Ca^{2+}$  levels are increased in cells, also increased by activation of voltage-dependent  $Ca^{2+}$  channels. An increase in the universal second messenger,  $Ca^{2+}$  triggers a series of events that influence the development of tissue damage. One such event is nitric oxide (NO) synthesized by the  $Ca^{2+}$ -dependent enzyme, neuronal nitric-oxide synthase (NOS) that reacts with a superoxide anion to form the highly reactive species, peroxynitrite, promoting tissue damage.

Ischaemic neurons depolarise and cells in the core region can never repolarise, however, cells in the penumbra can repolarise at the cost of consuming more energy. These same cells can depolarise again in response to glutamate or  $K^+$ , this repetitive depolarisation is called 'peri-infarct' depolarisations and can contribute to infarct size (Dirnagl *et al.*, 1999). These high levels of  $Ca^{2+}$ ,  $Na^+$  and ADP cause the mitochondria to produce high levels of reactive oxygen species. Neurons contain low levels of antioxidants so are particularly vulnerable (Doyle *et al.*, 2008). The  $Ca^{2+}$ -related activation of intracellular second messenger systems, the increase of free radicals as well as hypoxia itself, triggers activation of the inflammatory response.

### 1.3 Inflammatory mechanisms in ischaemic stroke

Minutes to hours after onset of cerebral ischemia a cascade of inflammatory events is initiated. The brain responds to ischaemic injury with an acute and sustained inflammatory process, consisting of the rapid activation of microglia, inflammatory mediator production, and infiltration of various inflammatory cells leading to ischaemic brain injury (Jin *et al.*, 2010).

Dying and dead cells release 'danger signals' that activate the immune system. Some of these signals, like the nucleotides ATP and UDP are released by cells under stress when the cell membrane is still intact and set the stage for the subsequent inflammatory responses (Ladecola and Anrather, 2012). When cells start to die, a different signalling landscape emerges; endogenous molecules, called damage-associated molecular patterns (DAMPs) such as high-mobility group box 1 (HMGB1), hyaluronan, or heat shock proteins (HSP) are released from dying cells. Many DAMPs, are sensed by toll-like receptors (TLRs); sensors of the innate immune system that are widely expressed on microglia, and perivascular macrophages. Downstream of DAMP-receptor signalling, inflammatory mediators such as cytokines, chemokines and NO are released, contributing to cell death and subsequently leading to dysfunction of the blood brain barrier (BBB) (Macrez *et al.*, 2011).

As previously mentioned reactive oxygen species are produced in the ischaemic brain, this triggers the activation of complement, platelets and endothelial cells. Minutes after ischaemia, the adhesion molecule P-selectin is expressed on endothelial cells and pro-inflammatory signals are generated. The expression of adhesion molecules on endothelial cells, leukocytes and microglia lead to subsequent infiltration of damaged tissue by neutrophils, macrophages and T cells (Badoer 2010). Acutely (4 to 24 hours) after ischaemic injury circulating inflammatory cells begin to adhere to and migrate along the damaged endothelium lining the cerebral vasculature and start to infiltrate into the brain parenchyma owing to the breakdown of the BBB (Tobin *et al.*, 2014). The initial cell type to infiltrate the CNS from the periphery is the neutrophil, leukocytes that are an important cell type belonging to the innate immune system which transmigrate approximately 4-6 hours after ischaemic onset in the rodent stroke model (Wang *et al.*, 2007; Lakhan *et al.*, 2009).

The mechanisms in which neutrophils exerts its pathogenesis in stroke is excessive production of ROS, release of proinflammatory cytokines and chemokines, release of

elastase and MMPs and by enhancing the expression of leukocyte  $\beta$ 2-integrins and adhesion molecules (Jin *et al.*, 2010). Different populations of lymphocytes can exert beneficial or detrimental functions after stroke. Ordinarily lymphocytes are excluded from the CNS but appear within 24 hours in the post-ischaemic brain (Doyle *et al.*, 2008). Infiltrating T cells are the main source of IFN- $\gamma$ , which mediates delayed neurotoxic effects in the ischaemic brain tissue (Chamorro *et al.*, 2012). In a mouse model of stroke, activated  $\gamma\delta$ T cells infiltrated the brain and in turn produced proinflammatory cytokines, IFN- $\gamma$  and IL-17 within hours of ischemia onset (Shichita *et al.*, 2009). The roles of specific lymphocyte populations during stroke are complex and are still extensively researched (Fu *et al.*, 2015).

Mast cells are resident in the brain, located on or near the cerebrovasculature particularly within the dura, on the brain side of the BBB, with a high percentage of mast cells in contact with astrocyte end-feet (Khalil *et al.*, 2007). It has been reported that mast cell degranulation plays a pivotal role in the inflammatory response. Mast cells contain and release an array of mediators such as histamine, proteases and TNF- $\alpha$ , which can potentially decrease the integrity of the BBB leading to vasogenic oedema, through the degradation of ECM and tight junction proteins, such as MMP-9 (McKittrick *et al.*, 2015).

Astrocytes have a typically protective role in ischaemia, by the production of anti-inflammatory cytokines, growth factors and by forming a glial scar; which acts to protect the brain from further ischaemic damage by creating a barrier around the damaged tissue (Kahle and Bix, 2013).

Macrophages also play a role by producing pro-inflammatory cytokines that contribute to the endothelial expression of adhesion molecules and to blood brain barrier (BBB) damage that leads to infiltration of leukocytes (Iadecola and Anrather, 2011). After macrophage and neutrophil infiltration, lymphocytes begin to infiltrate the brain as well. In addition to above, dendritic cells are also implicated in ischaemic injury (Jin *et al.*, 2010). Circulating dendritic cells may be recruited into the infarcted brain and thereby trigger cerebral immune reactions in the brain. It has been shown that dendritic cells are present in the ischaemic brain in a rat model of stroke with a correlation between dendritic cell numbers and brain lesion area (Kostulas, 2002).

It should be noted that systemic inflammation following stroke has a substantial influence on the post-ischaemic inflammatory reaction (McColl *et al.*, 2009). Infection

is a major complication of acute stroke and causes increased mortality and morbidity. It has been elucidated that splenic marginal zone B cells play an important role in the infection observed post stroke. McCulloch *et al.*, (2017) reported that stroke caused a marked loss of splenic marginal zone B cells, this was linked to a suppression of circulating IgM, which was accompanied by spontaneous bacterial lung infection.

Microglia are the tissue-resident macrophage in the CNS, a key cellular element and they are recognised to serve as the brain and spinal cords' innate immune system. Microglial cells are active within minutes of onset of ischaemia peaking at 72 hours, and although immediate activation of microglia after insult results in an increase in infarct damage, in the long term microglia activation appears to be neuroprotective (Badoer, 2010).

## **1.4 Microglia**

### **1.4.1 Introduction to microglia**

Franz Nissl and F. Robertson first described microglia cells in 1880 and showed that microglia are related to macrophages. Later in 1913, they were renamed a "third element", Santiago Ramón Cajal pointed out that these cells were different from neurons and astrocytes. The third element was later identified as oligodendrocytes and microglia. Poi Rio Hortega was the first to call the cells microglia, around 1920. He went on to characterise microglia response to brain lesions in 1927 and after years of research became the 'father of microglia'. The field has since then expanded enormously and now microglia are thought to represent an important nexus between neurological and immunological activity in the CNS (Nayak *et al.*, 2014). Georg Kreutzberg coined the term "microglial sensor of pathology" which captures the essences of microglia cell function.

In the adult mouse brain, microglia constitute 5-12% of all glia cells. Distribution of microglia is different in different regions of the brain. A cardinal paper by Grabert *et al.*, (2016) demonstrated that microglia have distinct region-dependent transcriptome identities. In the young adult brain, differences in bioenergetic and immunoregulatory pathways are the major source of heterogeneity and suggested that cerebellar and hippocampal microglia exist in a more immune-vigilant state. It was also concluded that microglia age in a regionally variable manner with aged microglia displaying partial loss of the core young microglia identity distinct from a macrophage-like signature (Grabert *et al.*, 2016).

The precise origin of microglia during brain development has been a matter of controversy for decades. It took approximately two decades to confirm the yolk sac origin of microglia by genetic fate-mapping experiments (Prinz and Priller, 2014). Seminal work performed by Ginhoux *et al.*, (2010) showed that microglia are the progeny of primitive macrophage from the yolk sac that invade the developing CNS. It can now be concluded that microglia originate from primitive myeloid progenitors arising from the yolk sac before embryonic day 8 (Ginhoux *et al.* 2010). In addition, it should also be noted that microglia are a genetically distinct cell type in the mononuclear phagocyte system (Ginhoux *et al.*, 2010).

#### **1.4.2 Microglia in the healthy brain**

Resident microglia cells in the healthy adult brain persists during adulthood via constant self-renewal without turnover from circulating blood progenitors (Ginhoux *et al.*, 2010) (**figure 1.2**). Microglia survey the brain to detect infection or cell damage or cell death. Fundamental functions in the healthy brain includes affecting neuronal activity, synaptic connectivity and programmed cell death (Madry and Attwell, 2015). *In vivo* it has been shown that microglia processes do not just randomly screen the extracellular space but contact neuronal somata and synapses in an activity-dependent fashion (Tremblay *et al.*, 2010).

Microglia also play an important role in synaptic pruning (eliminating excessive synapses) in the developing brain, which is critical for the proper maturation of synaptic circuits (Paolicelli *et al.*, 2011). Many newly discovered functions depend on the enormous process motility of non-activated, ramified microglia and their surveillance of the brain parenchyma (Madry and Attwell, 2015).

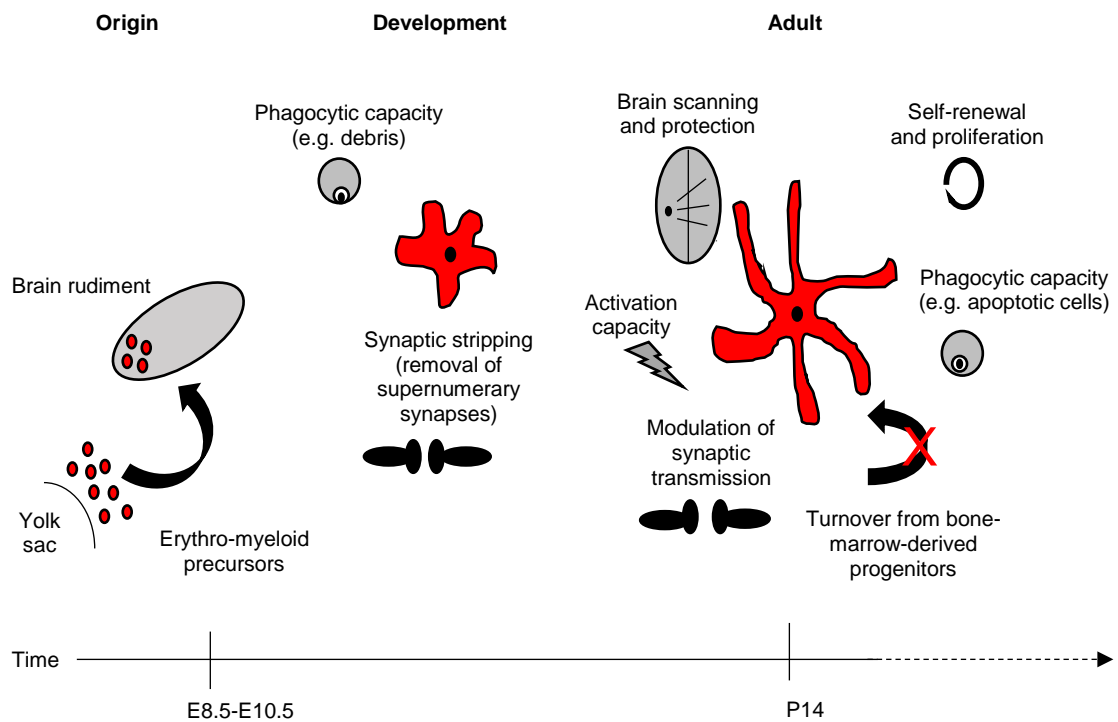


**Figure 1.2. Schematic representation of microglia functional states in the healthy murine brain.** Microglia arise from erythro-myeloid precursors in the embryonic yolk sac and populate the brain rudiment during early development. Microglia cell population is maintained by self-renewal, without the contribution of bone marrow-derived progenitors. In the adult healthy brain, microglia continuously survey the brain and readily react to any potential threat to CNS homeostasis. Phagocytic microglia can detect and quickly remove damaged or dying neurons, preventing further damage to neighbouring cells. During developmental stages, microglia phagocytic capacity is particularly important to prune supernumerary synapses. Microglia has also been suggested to modulate neuronal activity by influencing synapse transmission (synaptic stripping). Under specific conditions, microglia are able to remove dysfunctional synapses by physically interacting with functional neurons. Schematic adapted from (Sousa *et al.*, 2017).



Microglia are highly dynamic and undergo extreme remodelling processes throughout their lifespan (Nimmerjahn *et al.*, 2005). This behaviour requires tightly controlled regulation of the movement of cell processes, cell motility, cell morphology, phagocytosis, immune functions, and the secretion of molecular mediators. These functions are tightly and precisely controlled by several signalling pathways (EIAli and Rivest, 2016).

In the healthy brain, microglia express numerous inhibitory proteins and interact with neurons to form a 'brake' on inflammation maintaining cells in a quiescent state (Patel *et al.*, 2013). The endogenous mechanism in the form of neuronal-glia interactions may prevent excessive microglia activation in the CNS. Following ischaemic stroke, these interactions may be disrupted due to neuronal death and structural tissue damage. Examples of various inhibitory proteins include: CD200/CD200R1, CD200 glycoprotein is expressed on neurons, while CD200R1 is expressed on the surface of all myeloid origin cells. Similarly, CX3CL1 (fractalkine), a cell surface bound chemokine constitutively expressed by neurons, suppresses microglia activation through its microglia receptor, CX3CR1. CX3CL1 can be either secreted or membrane bound, when it is membrane bound, neuronal CX3CL1 binds to microglia CX3CR1 and maintains microglia in a quiescent state. Cleaved CX3CL1 acts as a chemokine to induce microglia chemotaxis. Signal-regulatory protein alpha (SIRP $\alpha$ ) is expressed on myeloid cells including microglia, binds integrin associated protein CD47 on neurons keeping microglia silenced and thereby suppressing phagocytosis (Patel *et al.*, 2013).

### **1.4.3 Activation of microglia**

In the presence of a threat, microglia rapidly become activated. Activated microglia are associated with fewer and shorter processes, becoming amoeboid with a large soma. This is compared with 'resting' microglia which are typically associated with a ramified morphology, having many long processes. Microglia are extremely plastic cells and undergo a variety of structural changes based on their location and systems needed. This level of plasticity is required to fulfil the vast variety of functions that microglia perform. The morphological and functional spectrum of microglia is highly regulated *in vivo* resulting in various intermediate states in activation. Schwartz *et al.*, (2006) suggested microglia 'comprise of a family of cells with diverse phenotypes' to

explain observations on their seemingly contradictory 'beneficial' or 'destructive' properties under various experiment conditions.

Microglia phenotypes are mirrored on the macrophage M1/M2 phenotype where the classically activated cells (M1) is induced by IFN- $\gamma$ , PAMPS, (such as lipopolysaccharides (LPS)) or cytokines, resulting in a pro-inflammatory phenotype. The opposing phenotype, the alternatively activated (M2), activated by IL-4 and generally thought to dampen down the immune response (Chhor *et al.*, 2013). Direct transfer of the idea of immune polarization to microglial cells was frequently performed by researchers world-wide without further testing its applicability (Mittelbronn, 2014). In CNS pathologies, microglia cells are nonclonal and show a high degree of plasticity as well as intermixture with peripheral blood borne macrophages (Mittelbronn, 2014).

Prof Richard Ransohoff, highly recognised in the current field for his contributions, recently published an article where he discussed the problems with the current paradox of categorisation of microglia (Ransohoff, 2016). His working hypothesis is that cortical microglia respond most directly to loss of signalling from injured neurons. It has been widely proposed that microglia activation states can be identified using two pro- and anti-inflammatory markers, iNOS and Arg1, respectively. This assumes that the full expression profile of reactive microglia can be characterised by examining one or a few gene products which is not the case (Ransohoff, 2016). The challenge with the current paradox is between *in vitro* and *in vivo*, *in vitro* conditions mimic the original tissue on a basic level, but often excludes complex interactions between cells and their signalling molecules. The activation signatures defined *in vitro* are highly influenced by factors that are often overlooked but that are important *in vivo*. Whole genome studies do not support the long established concept of the macrophage/microglia polarisation with microglia *in vivo* showing no clear bias towards either phenotype (Chiu *et al.*, 2013). Recent evidence shows various overlapping and novel phenotypes that the current M1/M2 dogma cannot account for (Martinez and Gordon, 2014; Prinz and Priller, 2014). For some time now, concepts such as 'resting' and 'activated' microglia have also been questions. They are considered simplistic and do not reflect microglia movement dynamism nor their functional plasticity (Ransohoff and Perry, 2009).

The role of M1 and M2 stimuli needs to be considered in their dynamic complexity, beyond the current bipolar dogma. It must however be recognised that this is an emerging concept, with the majority of publications remaining to use this paradox, making it difficult to move on from the M1/M2 concept. Throughout the present work, we will refer to the activation of microglia as having either pro- or anti-inflammatory traits based on the expression levels of various typical markers.

#### **1.4.3.1 Triggers- Signalling pathways**

The first line of defence is the activation of the innate immune system. Pattern recognition receptors (PRRs) recognise PAMPS and DAMPS. There are three major receptor families, TLR, nucleotide-binding oligomerization domain (NOD)-like receptors (NLRs) and the retinoic acid-inducible gene-1 (RIG-1)-like receptors (RLRs). Activation of these receptors induces specific signalling pathways that are involved in modulating microglia functions. TLR activation stimulates the recruitment of specific intracellular adaptor proteins, namely the myeloid differentiation primary response gene-88 (Myd88) that leads to induction of the nuclear factor kappa-light-chain-enhancer of activated B cells (NF- $\kappa$ B) signalling pathway (EiAli and Rivest, 2016). TLR4 is the prominent LPS receptor that can lead to activation of LPS-responsive cells and subsequently causes upregulation of pro-inflammatory genes via NF- $\kappa$ B. Interestingly, the most prominent TLRs on microglia are TLR4 and TLR2, both of which are upregulated after ischemia (Patel *et al.*, 2013).

The NF- $\kappa$ B transcription factor family is a pleiotropic regulator of many cellular signalling pathways, playing an important role specifically in inflammation, cell cycle and cell survival. In mammals, there are five different members of the NF- $\kappa$ B family, p65 (RelA), RelB, c-Rel, p50/p105 (NF- $\kappa$ B1) and p52/p100 (NF- $\kappa$ B2) (Schmitz and Baeuerle, 1991). NF- $\kappa$ B is activated by a wide variety of agents including viruses, bacterial toxins such as LPS, oxidative stress such as free radicals, and inflammatory stimuli such as cytokines. Agents such as IL-4, IL-13 and IL-10 interferons and corticosteroids are known to block the specific signalling transductions and suppress NF- $\kappa$ B activation (Shih *et al.*, 2015). It has been shown that microglia responses to injury triggered by endogenous ligands for TLR and TLR signalling are mediated through the NF- $\kappa$ B pathway (Akira and Takeda, 2004).

Activation of NF- $\kappa$ B involves two steps: release of inhibitory I $\kappa$ B subunit; and nuclear translocation of the activated factor. In unstimulated cells, I $\kappa$ B $\alpha$  or I $\kappa$ B $\beta$  selectively

bind to the p50/p65 heterodimer and masks their nuclear localisation signal (NLS), preventing their nuclear translocation (Baeuerle and Henkel, 1994). Upon activation, the IKK complex phosphorylates I $\kappa$ B $\alpha$ , priming it for subsequent ubiquitylation and proteasome-mediated degradation. Dissociation of the I $\kappa$ B $\alpha$  induces NF- $\kappa$ B heterodimers to become located to the nucleus and bind to specific gene promoters to modulate the expression of pro- and anti-inflammatory proteins (Napetschnig and Wu, 2013).

NF- $\kappa$ B is activated via two distinct kinase-pathways, the classical/canonical and alternative/non-canonical NF- $\kappa$ B pathway, with the canonical pathway being the most extensively studied. The canonical pathway is mediated through activation of a variety of cell surface receptors, including IL-1 receptor, TLRs and TNF receptors, in response to proinflammatory mediators like IL-1, LPS and TNF. The inactive NF- $\kappa$ B resides in the cytoplasm and associates or links with the natural biological inhibitor I $\kappa$ B. The NF- $\kappa$ B function and nuclear translocation ability are sequestered in the cytoplasm and nuclear compartments, respectively. The I $\kappa$ B family members include, I $\kappa$ B $\alpha$ , I $\kappa$ B $\beta$ , p105/I $\kappa$ B $\gamma$ , p100 (precursor of p52) and I $\kappa$ B $\epsilon$  (Whiteside *et al.*, 1997). Each of these prevents NF- $\kappa$ B from binding to DNA by masking its DNA binding domain. Treatment of cells with various stimuli (e.g. LPS) activates I $\kappa$ B for ubiquitin-dependent degradation through the 26s proteasome complex, resulting in the release and nuclear translocation of NF- $\kappa$ B (Thanos and Maniatis, 1995). The non-canonical NF- $\kappa$ B pathway can be triggered by the activation of members of the TNF-receptor superfamily. The canonical pathway activation is rapid and independent of protein synthesis, compared to the non-canonical pathway where activation requires NF- $\kappa$ B inducing kinase (NIK) synthesis and accumulation (Sun, 2011).

#### **1.4.3.2 Consequences of microglia activation**

Activated microglia clear any toxic cell debris such as damaged cells or infected microorganisms by phagocytosis (Pocock and Kettenmann, 2007). In the absence of neuronal control signals, anti-inflammatory cytokines and other restricting mechanisms, microglia become overactivated and continue to release pro-inflammatory cytokines as well as producing a range of neurotoxic factors including TNF- $\alpha$  and NO.

Microglia express a wide range of cytokine receptors that play a crucial role in modulating microglia cell function. Among these cytokines, TNF- $\alpha$ , TGF- $\beta$  and

interleukin signalling pathways play major roles. IL-1 $\beta$  signalling pathways potentiate microglia proinflammatory responses, this cytokine is essentially produced in the early stages of the innate immune response engagement, in response to TLR/Myd88/NF- $\kappa$ B activation (Herx *et al.*, 2000).

Chemokines are small chemotactic cytokines that possess the ability to induce chemotaxis in nearby responsive cells. All chemokines mediate their effects following their release as soluble molecules that generate a chemotactic gradient for cell mobilization and migration except CX3CL that mediates its effect either as a soluble molecule or a membrane-anchored molecule. Following TLR activation, CCL2 is produced by microglia, thus acting in an autocrine and paracrine manner. In parallel, the CCL2/CCR2 signalling pathways play a central role in regulating peripheral leukocyte recruitment and infiltration into the brain during inflammatory reactions (EIAli and Rivest, 2016).

#### **1.4.4 Microglia migration**

Microglia motility can be classified into functionally and mechanistically distinct modes: 1) Baseline surveillance with apparently random non-directed process movement and 2) Microglia chemotaxis, an 'alert mode' in response to cell or tissue damage with highly targeted movement of microglia processes towards the injury site. Both depend on cytoskeletal changes arising from highly motile bundles of actin filaments (Madry and Attwell, 2015).

*In vivo*, 'inactive' microglia cells respond to chemoattractant agents by sending out their processes, however, in comparison, the less ramified and partly activated microglia in culture instead migrate by translocating their cell bodies (Honda *et al.*, 2001; Ohsawa *et al.*, 2012; Orr *et al.*, 2009). ATP/ADP-induced chemotaxis, is dependent on G<sub>i</sub>-coupled P2Y receptors. Expression of P2Y<sub>12</sub> receptor protein on the surface of ramified microglia *in vivo* is particularly enriched at the tips of the leading processes during chemotaxis (Dissing-Olesen *et al.*, 2014). ATP/ADP-induced P2Y<sub>12</sub> receptor activation leads to phospholipase C (PLC) and Ca<sup>2+</sup>-dependent phosphorylation of the serine/threonine kinase Akt, as well as PI3K-mediated Akt phosphorylation (Irina *et al.*, 2008).

The most studied substances that are released from the injured cells that are responsible for the increase in motility and chemotaxis of microglia to the site of injury include fractalkine, chemokine ligand 21 (CCL21) and ATP. CX3CL1 and CCL21 are

chemokines, released from nerve terminals, that diffuse to engage receptors on microglia increasing their motility and inducing chemotaxis (Liu *et al.*, 2009). ATP, released from injured cells, also increases the motility and chemotaxis of the processes of nearby microglia to the injured site by acting on microglial P2Y<sub>12</sub> purinergic receptors (Honda *et al.*, 2001; Haynes *et al.*, 2006). The most ubiquitous transmitter in the brain is glutamate which exists at very high concentrations in neurons and glial cells. Despite this, glutamate-induced microglia migration is less studied and characterised than other chemoattractant agents. Microglia possess glutamate receptors, in particular group III metabotropic receptors (mGlu4,6,8) and group II metabotropic receptors (mGlu2,3,) (Biber *et al.*, 2007). Evidence suggests that glutamate can mediate rapid chemotactic response from microglia cells (Liu *et al.*, 2009; Domercq *et al.*, 2013). Therefore, it is likely that glutamate acting on microglia could affect the motility and direction of migration of the cells, for instance towards regions of high extracellular glutamate released due to high levels of synaptic transmission or the direct release of glutamate from neurons following ischemia or excitotoxic insults. Using *in vitro* microfluidic technology to help replicate the *in vivo* environment we investigate this possibility in the present work.

#### **1.4.5 Modelling microglia *in vitro***

The development of *in vitro* microglia cultures was undoubtedly an innovative tool that contributed to a greater understanding and characterisation of microglial cells, which were not possible to be studied *in vivo*. Presently, there are many models of microglia and microglia-like cell lines used to examine neuroinflammation. These include primary microglia cultures, which are either retrovirus transformed or non-retrovirus transformed. Primary and immortalised microglia cells share similarities but are also separated by crucial differences that must be considered when choosing an appropriate model for the research aims (Stansley *et al.*, 2012).

Primary microglia are very popular due to the similarities in phenotype to *in vivo* cells. These cells can be derived from the adult or most commonly the neonatal mouse or rat. Protocols for isolating microglia from both neonatal and adult were developed in the 1990s. The most widely used method for isolation of glia cells was mechanical shake off. Introduction of magnetic cell sorting using CD11b microbeads improved not only the yield of microglia cells but also ensured separation of microglia from astrocytes (Sousa *et al.*, 2017). Advantages of using microglia directly from an animal

are the functional characteristics that these cells possess, such as secretory products and cell surface markers, which closely resemble endogenous microglia (Stansley *et al.*, 2012). However, there are some drawbacks to using primary microglia; extensive preparations are needed for each experiment, making it more time consuming; the financial and ethical cost of using animals; and a low cell number is generated which could limit experiments. It should also be noted that primary microglia cells may not be completely homogenous for microglia as astrocytes or oligodendrocytes may also remain in the culture (Stansley *et al.*, 2012).

By genetically immortalising the primary microglia, you can obtain cells that have faster proliferation rates and a more homogenous population. Despite their universal usage, immortalised cell lines are prone to an increased inflammatory state and are sensitive to genetic drift and morphological changes (Sousa *et al.*, 2017). In 1985, the first immortalised cell line emerged by infecting the cells with two retroviral oncogenes, *raf* and *myc*. Two commonly used cell lines are the BV-2 and N9 cells that are derived from mouse and rat respectively. The validity of BV-2 cells as a sufficient substitute for primary microglia has been debated. A study conducted by Horvath *et al.*, (2008) compared several parameters in rat primary to the BV-2 cell line. The study revealed that BV-2 cells have similar functions as primary microglia but not to the same extent, with BV-2 cells exerting a less pronounced response than primary cells when responding to LPS (Henn *et al.*, 2009; Horvath *et al.*, 2008). It was concluded that data obtained from BV-2 cells may not be creditable if it is not reproduced in primary microglia (Horvath *et al.*, 2008), while others report that BV-2 cells appear to be a valid substitute for primary microglia in many experimental settings (Henn *et al.*, 2009). The N9 microglia cell line has also been shown to upregulate proinflammatory genes in response to LPS, similarly to BV-2 cells, including *Nos2*, *Cos2*, *Tnf* and *Il1 $\beta$* . There are a few microglial cell lines that are highly proliferative microglia which are not genetically modified. The highly aggressively proliferating immortalised (HAPI) cell line, and colony stimulating factor-1 dependent EOC cells are examples of spontaneously immortalised microglial cell lines. These cells are easily cultured however, they require colony-stimulating factor-1 (CSF-1) in order to be maintained, which may alter their phenotype. The recently available simultaneously immortalised microglia (SIM)-A9 cell line are not dependent on a specific growth factor to maintain immortalisation. SIM-A9 cells have been shown to retain typical microglia characteristics after cloning responding to primary

inflammatory stimuli in a similar manner as primary microglia (Nagamoto-Combs *et al.*, 2014).

#### **1.4.6 Microglia response after ischaemic damage**

After ischaemic brain injury, microglia rapidly migrate towards the lesion site and exacerbate tissue injury by producing inflammatory cytokines. On the other hand, microglia also contribute to tissue repair and remodelling by clearing up debris and producing anti-inflammatory cytokines (Ma *et al.*, 2016) (**figure 1.3**). Evidence suggest that microglia can be beneficial and are key in recovery and repair after ischaemic brain damage by secreting anti-inflammatory cytokines such as IL-10 and TGF- $\beta$ , which act to quell inflammation (Neumann *et al.*, 2006; Denes *et al.*, 2007; Thored *et al.*, 2009; Madinier *et al.*, 2009).

The balance of these effects may depend on the location of microglia, the degree of ischemia, and the timing after injury. In the ischaemic core, where blood flow is reduced to zero, cell death is nearly universal by 24 hours (Morrison and Filosa, 2013). Immediately after 60 minutes of focal ischemia without reperfusion, microglia/macrophages in the striatum (ischaemic core) significantly increased the number of their processes. 24 hours later, the microglia/macrophages in the ischaemic core showed a reduction in the number of processes, had significantly shorter processes and increased CD11b expression indicating activation and the formation of amoeboid morphology (Morrison and Filosa, 2013). While in the penumbral area, microglia were observed to be highly ramified (resting) (Perego *et al.*, 2011).

During ischemia of the brain, there is a dramatic increase in the duration of the contact time with neuronal synapses (approximately 1 hour compared to 5 minutes in the healthy brain) and this is associated with an increased loss of synapses (Wake *et al.*, 2009), suggesting that the enhanced contact time with neurons is detrimental and accounts for the increased neuronal loss that occurs with occlusion of the middle cerebral artery (MCA) (Wake *et al.*, 2009). There is some consensus in the literature suggesting that immediate activation of microglia after an ischaemic insult results in neuronal toxicity and increased infarct damage. In the longer term, activation of microglia appears to be neuroprotective by promoting clearance of dead cells and secretion of neutrophils to promote survival of neurons (Wake *et al.*, 2009).



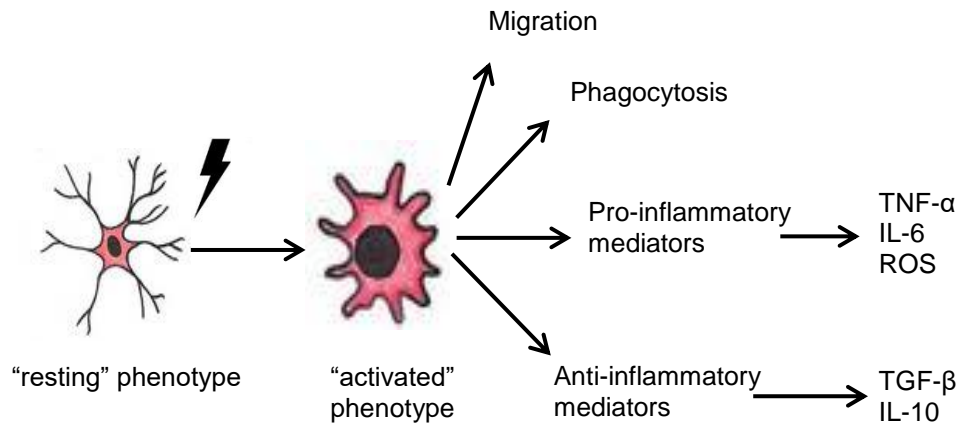


**Figure 1.3. Schematic diagram showing various morphological and functional states of microglia.** A key initial event in the ischaemic pathway is the rapid activation of resident immune cells, mainly microglia. Microglia display prominent changes in morphology which is associated with various functional states. After ischaemic insult, chemoattractant factors such as ADP and glutamate are released from dying neurons in the core, in response to these microglia can migrate to the sites of ischaemic tissue injury to increase phagocytotic uptake of cellular debris. Depending on their activation state, microglia may promote a pro-inflammatory environment which can be detrimental, or they can promote an anti-inflammatory environment which can lead to regeneration and repair.

It has been suggested that post ischaemic proliferation of resident microglia is neuroprotective by modulating the micromilieu. Selective ablation of proliferating resident microglia by expression of thymidine kinase (TK) protein under the control of the CD11b promoter after transient middle cerebral artery occlusion (MCAO) was associated with an increase in the size of ischaemic lesion, and an increase in the number of apoptotic cells, predominately neurons (Lalancette-Hébert *et al.*, 2007).

Monocyte chemoattractant protein-1 (CCL2) is a chemokine that plays a major role in driving inflammatory monocyte invasion into sites of post ischaemic inflammation. Mice deficient in CCR2, the receptor for CCL2, showed reduced infarct sizes and significantly reduced oedema formation in the affected ischaemic hemisphere compared with normal mice (Napoli and Neumann, 2009).

Microglia cytokine production can be observed as early as 1 hour after stroke. Microglia have been reported to be the primary source of IL-1 $\beta$  in a biphasic time course which peaks at 1 hour and 24 hours (Schielke *et al.*, 1998). Microglia have also been reported to be the main source of IL-6, TGF- $\beta$ , and IL-10 after ischemia (Ceulemans *et al.*, 2010). Within 4 hours after stroke, TNF- $\alpha$  production can be seen within and surrounding the infarct. Microglia/macrophages production of TNF- $\alpha$  can be measured 6, 12 and 24 hours after ischaemic stroke (Gregersen *et al.*, 2000). The role of TNF- $\alpha$  production in ischaemic stroke remains controversial, with some studies reporting that TNF- $\alpha$  antagonism results in improved outcomes (McCoy and Tansey, 2008) while other studies concluded that TNF- $\alpha$  is important in hippocampal and striatal neurogenesis (McCoy and Tansey, 2008).

Local accumulation of NO is also involved in the inflammatory cascade after stroke (Patel *et al.*, 2013). Equipped with inducible nitric oxide synthase (iNOS), proinflammatory microglia are partially responsible for the changes in expression level of NO after injury. The role of NO in ischemia is inconsistent in literature, and evidence for both protective and deleterious roles have been reported (Lalancette-Hébert *et al.*, 2007; Patel *et al.*, 2013). Protective effects of endothelial NO (eNOS), includes inducing vasodilation and improving reperfusion.

A study which suggested the protective role of microglia after stroke was carried out by Neumann and colleagues. Using 3D reconstruction images, they proposed that immediately after oxygen-glucose deprivation (OGD), microglia are activated by injured neurons and engage in close cell-cell contact with the first neuronal layer (capping). It was purposed that this 'capping' could ensue the early recognition and fast phagocytic removal of dying/dead neurons, providing protection for the neurons by minimising the exposure time and dose of these cells to cytotoxic cell contents/debris released from dead/dying neurons (Neumann *et al.*, 2006).

#### **1.4.6.1 Mediators of microglia activation after ischemia**

Galectin-3 serves as an important survival factor in microglia survival, proliferation and migration. Absence of galectin-3 lead to areas of increased infarction and enhanced neuronal apoptosis after MCAO (Taylor and Sansing, 2013). This indicates that galectin-3 may play an important role in reducing cell death and infarction after cerebral ischemia. Secreted protein acidic rich in cysteine (SPARC) is a matricellular

protein that regulates growth factors and the assembly of the extracellular matrix. A role for SPARC in microglia toxicity has been suggested leading to poor outcome after ischemia (Taylor and Sansing, 2013).

High motility group protein B1 (HMGB1) may act as a cytokine to activate microglia after ischemia (Kim *et al.*, 2006). HMGB1 induces activation via the receptor for advanced glycation end products (RAGE) receptor on both microglia and blood-derived macrophages after ischemia. Chemokine receptor CX3CR1, as discussed in **section 1.4.2** is expressed at high levels on murine microglia under homeostatic conditions. CX3CL1 expression is upregulated within 48 hours after MCAO and downregulated by 7 days. Reports suggest that it may play a role in microglia/macrophage cell recruitment into the infarcted region (Tarozzo *et al.*, 2002). In contrast, mice genetically deficient for either CX3CR1 or CX3CL1 have reduced infarct volumes after MCAO (Fumagalli *et al.*, 2013; Dénes *et al.*, 2008).

Microglia cells have metabotropic and ionotropic receptors that link to intracellular calcium signalling (Noda *et al.*, 2000). Increasing concentrations of extracellular glutamate activates these metabotropic glutamate receptors on microglia leading to a pro-inflammatory phenotype (Chapman *et al.*, 2000). Glutamate receptors both ionotropic and metabotropic, upon activation allow influx of Ca<sup>2+</sup> into the cell. Ca<sup>2+</sup> signalling and levels of Ca<sup>2+</sup> have a great impact on microglia response and function resulting in the release of NO and cytokines (Murugan *et al.*, 2013).

### **1.5 Modulation of the immune system for treatment of stroke**

Considering the detrimental consequences of the immune response after stroke, as well as the beneficial contribution, modulating the immune system could be an appealing strategy. Modulation of the immune system is not a new concept; with many immunotherapies currently being explored. Blockade of the IL-1 receptor with the antagonist IL-1ra has also been attempted for treatment of ischaemic stroke. A randomised phase IIa trial that included 34 patients with acute stroke showed that recombinant human IL-1Ra was safe and seemed to provide some benefits, particularly to patients with cortical infarcts (Emsley *et al.*, 2005). Scores on the NIH stroke scale reduced by a median of 4 points for at least three months and by just one point among patients receiving a placebo. Interestingly markers of biological activity including neutrophil and total white cell counts, C reactive protein and IL-6 concentration were lower in IL-1Ra treated patients (Emsley *et al.*, 2005). A recent

study has shown that administration of IL-1Ra improves stroke outcome in both young and aged/co-morbid rats. It was shown to be neuroprotective by increasing stem cell proliferation, and enhancing neuroblast migration and the number of newly born neurons after cerebral ischemia (Pradillo *et al.*, 2017).

The observation of upregulation of E-selectin expression on the endothelium systemically within a few hours of focal cerebral ischemia prompted investigation of E-selectin as a possible therapy. Evidence suggest that transnasal E-selectin tolerization attenuates cerebral ischaemic damage in experimental stroke and studies are currently underway to prepare for clinical trials of E-selectin for secondary prevention of stroke (Fu *et al.*, 2015).

An example of another immunotherapy for ischaemic stroke is fingolimod, an agonist of four sphingosine-1-phosphate (S1P) receptors (S1P1, S1P3, S1P4 and S1P5). In stroke, fingolimod reduces the number of circulating lymphocytes by preventing their egress from lymph nodes thus preventing early infiltration of lymphocytes to the brain and local activation of microglia. Fingolimod has shown potential in the clinic with short term neurological improvements and no safety concerns. Collectively, the fast action of fingolimod on multiple lymphocyte subsets, which ceased promptly after the dose, might be instructive in future selection of immunomodulatory drugs in stroke trials.

Many other drugs such as the antibody Natalizumab which blocks  $\alpha_4$ -integrin and the broad-spectrum tetracycline antibiotic minocycline have also been investigated for treatment of ischaemic stroke (Fu *et al.*, 2015).

Considering the success of various immunomodulatory therapies in pre-clinical models of stroke, in this thesis, we explore the potential of stem cell conditioned media to modulate microglial cells.

## 1.6 Introduction to stem cell therapy for stroke

Stem cells are undifferentiated biological cells that can differentiate into specialised cells and can divide through mitosis to produce more stem cells (Terskikh *et al.*, 2006). A cardinal feature of stem cells is their ability to self-renew, where cells divide to give rise to at least one daughter cell that maintains the multipotent character of its parent cell (Anderson, 2001).

During injury, due to stem cells' capacity to asymmetrically divide, one daughter cell will leave the niche to differentiate while one daughter cell will remain in the niche as a stem cell, keeping a healthy balance between stem cell population and differentiated cells. Despite this, neural stem cells have a limited capacity to regenerate and the small population of endogenous stem cells seem unable to fully restore function after damage. This has led to the potential of transplantation cell replacement therapy after cerebral damage such as ischemia.

Stem cells, with their ability to act simultaneously on multiple targets, driving the damaged microenvironment from a toxic to a more protective/regenerative activation state, are a promising strategy (Gennai *et al.*, 2015; Eckert *et al.*, 2013; Zhang *et al.*, 2013). Adult stem cells are multipotent cells found in developed organisms, which replace cells that have died or lost function with diseases such as in stroke. Human cells that have been used in these experimental studies fall into three categories, neural stem/progenitors cells (NSC/NPCs) cultured from fetal tissue, immortalised neural cell lines and hematopoietic/endothelial progenitor or stromal cells isolated from bone marrow, placenta, umbilical cord, peripheral blood or adipose tissue and induced pluripotent stem cells (iPS) (Bhasin *et al.*, 2013).

Over the past years there has been progress in which NSCs are transplanted into experimentally lesioned animals to assay their capacity to repair. It was initially thought that the seminal property of NSCs were their multipotency and their ability to repair was down to replacement of lost neurons and glia. It has now been shown that as well as cell replacement they are also capable of increasing plasticity in the host brain (Price and Williams, 2001).

A variety of stem cells including embryonic, bone marrow, neuronal and induced pluripotent stem cells (iPSCs) have been shown to improve stroke outcome (Daadi *et al.*, 2008, Schwarting *et al.*, 2008, Hicks *et al.*, 2009, Kawai *et al.*, 2010). Different stem cells and their derivatives of rodent and human origin can survive, differentiate

into neurons and restore function after transplantation in the stroke-damaged brain (Ding *et al.*, 2013). It was shown that the conditionally immortalised neural stem cell line, MHP36 promoted neuronal differentiation, synaptic plasticity and axonal projections after a focal MCA occlusion in mice (Patkar *et al.*, 2012). Human fetal neural progenitor cells, injected in the cortical peri-infarct tissue 24 hours after permanent MCAO promoted cell proliferation in the subventricular zone and increased angiogenesis in the peri-infarct regions (Locatelli *et al.*, 2009). Conditioned immortalised NSCs have been shown to decrease motor impairments in a rat stroke model, possibly by promoting angiogenesis and improving cerebral blood flow (Ding *et al.*, 2013).

A major disadvantage is that a comprehensive understanding of stem cells mechanism of action is lacking, but one concept that is now emerging is that tissue replacement is likely to constitute only a minor contribution to the therapeutic effect. Multiple mechanisms of action of stem cells include the secretion of tropic factors, increase synaptic plasticity, cellular replacement and immunomodulation (Kalladka and Muir, 2014).

It is evident from preclinical studies that mesenchymal stromal cells (MSCs) secrete a plethora of growth factors which are associated with direct anti-apoptotic effects and modulation of inflammatory responses within the ischaemic tissue resulting in reduced neural damage (Caplan, 1991). With these mechanisms in mind, MSCs may be a good choice for stroke therapy because they secrete a variety of bioactive substances, including trophic factors, and extracellular vesicles, which may be associated with enhanced neurogenesis, angiogenesis and synaptogenesis. Interestingly, MSCs are thought to play important roles in attenuating inflammation (Acosta *et al.*, 2015; Kim *et al.*, 2009).

### **1.6.1 Immunomodulatory effects of MSCs**

Human mesenchymal stromal cells (hMSC) injected into the hippocampus of adult mice one day after transient global ischaemia were shown to have major inflammatory modulatory effects. Microarray assays indicated that ischaemia up-regulated 586 mouse genes, of which hMSC down regulated more than 10%, most related to inflammatory and immune responses (Ohtaki *et al.*, 2008). Bone marrow-derived stromal cells (BMSCs) injected through the tail vein down-regulated and attenuated inflammatory damage, restored brain tissue and improved functional outcomes by

modulating IL-17/IL-23 axis which is known to have a role in the development of infarction (Ma *et al.*, 2013).

In an *in vitro* oxygen-glucose deprivation (OGD) model using M17 neuronal cells, MSCs facilitated neuron recovery and attenuated inflammation after OGD injury (Huang *et al.*, 2014). Pro-inflammatory cytokine, IL-6 secretion from MSCs increased 25% after exposure to OGD stressed M17 neuroblastoma cells, this was blocked using an antibody for IL-6 and this in turn diminished the rescuing effects of MSCs. The role of IL-6 as an anti-inflammatory cytokine is mediated through its inhibitory effects on TNF- $\alpha$  and IL-1. A cytokine analysis on conditioned media from OGD-stressed and MSC-rescued cultures showed that one day post rescue there was a significant decrease in TNF- $\alpha$  levels in MSC-rescued cultures when compared with OGD-stressed only cultures (Huang *et al.*, 2014).

BMSC transplantation led to a significant increase in T regulatory (Treg) cells while  $\gamma\delta$ T cells were reduced in the ischaemic hemisphere (Wang *et al.*, 2014). This suggests that BMSCs have the ability to modulate T cell sub-populations as well as cytokine profile, however, the mechanisms underlying regulation of Tregs by BMSC remain unclear. Burr *et al.*, (2013) discuss the interaction between BMSC and Tregs further, they report it has been shown that cell contact, soluble mediators (prostaglandin E2, IL-10 and TGF- $\beta$ ) and indirect induction via manipulation of other antigen-presenting cells all appear to have vital roles.

As demonstrated, MSCs are attractive cells due to their capacity for proliferation, multilineage differentiation and immunomodulatory properties. These cells were first identified and isolated from bone marrow (BMMSCs) and have since emerged as promising therapeutic strategy. The process of isolating MSCs from bone marrow is complex and painful. However, in comparison, all placental tissues/fluids are easily available after birth, without invasive procedures, and their use is free from any ethical issues (Lu *et al.*, 2002). As such, stem cells derived from waste fetal placental tissues are a more preferred source (Ding *et al.*, 2015). Kranz *et al.*, (2010) showed that placental cells can produce immunosuppressive effects. Placental MSCs (pMSC) displayed suppression of allogenic T-cell proliferation that was mediated by the tryptophan-degrading enzyme indoleamine 2, 3-dioxygenase (IDO).

The first preclinical use of placenta-derived MSCs for stroke took place in 2001 (Chen *et al.*, 2001). It was reported that IV-infused human umbilical cord blood-stem cells

(UCB-SC) improved functional recovery in rats after MCAO (Chen *et al.*, 2001). Amniotic stem cells have since been shown to migrate to the site of ischaemic injury and improve functional recovery after MCAO (Weise *et al.*, 2014; Li *et al.*, 2012). In order to establish if transplanted cells are required to enter the brain to be effective, the mechanisms of UCB-SC cell-induced recovery have been investigated. Despite studies reporting the migration of transplanted cells into the injury area, evidence suggest that there is no need for cells to enter the brain to be effective. Cells administered systemically have been shown to induce functional recovery after MCAO through the secretion of trophic factors (Borlongan *et al.*, 2004).

This immunomodulatory capability of UCB-SC has been reported to be a potential mechanism for mediating restoration after stroke. Human UCB-SC could reduce ischemia-induced infiltration of granulocytes, monocytes and activation of astrocytes and microglia in adults and pups. A reduction in pro-inflammatory cytokines and NF- $\kappa$ B activity after stroke was observed upon treatment with UCB-SC (Vendrame *et al.*, 2006; Newcomb *et al.*, 2006).

Along similar lines, treatment with human umbilical cord blood (HUCB) cells 48 hours after middle cerebral artery occlusion (MCAO) altered the migration and lectin-binding profile of infiltrating immune cells, these cells represented a pro-inflammatory phenotype. This study showed that HUCB cells block the migration of pro-inflammatory cells to the injured site. The authors demonstrated that lectin binding to immune cell surfaces increased 66% in vehicle-treated animals from 51 hours to 72 hours, but the numbers of lectin-binding cells in peri-infarct regions where immune cells traffic to the striatum reduced in HUCB treated animals. The injection of the HUCB cells was administered at 48 hours post-MCAO, importantly, CD11b-positive, isolectin-binding microglia displaying amoeboid shape were first observed within the infarct at 48 hours post-MCAO. This paper suggests the importance of timing of treatments aimed at targeting the immune cell response in order to achieve efficacy (Leonardo *et al.*, 2010).

Human umbilical cord MSCs have been shown to be neuroprotective in mice after MCAO by modulating the peripheral immune system. Cheng *et al.*, (2015) demonstrated that the neurological deficit was ameliorated and brain oedema, infarct volume was significantly decreased from 72 hours to 1 week post-MCAO with hUC-MSC treatment via tail vein injection within 30 minutes after stroke. hUC-MSCs



attenuated the levels of inflammatory factors such as IL-1, TNF- $\alpha$ , IL-23, and IL-17 in peripheral blood serum and the ischaemic hemisphere after stroke. hUC-MSCs significantly decreased the level of Th17 cells at 24 hours and increased the level of Tregs at 72 hours post-MCAO in peripheral immune system, the level of TGF- $\beta$  in blood serum was enhanced by hUC-MSCs (Cheng *et al.*, 2015).

Several clinical studies have taken place using placenta stem cells for acute brain injury. A pilot study to assess the safety of human umbilical cell tissue-MSC delivered by a catheter to treat stroke of the MCA territory was conducted (Jiang *et al.*, 2013). Four males with stroke were treated with 20 million hUCT-MSC between 11 and 50 days after the stroke onset. After transplant there was no sign of immune response (fever or rash), demonstrating the feasibility of intra-arterial delivery of hUCT-MSC (Jiang *et al.*, 2013). It should be noted that the trial was not powered to assess hUCT-MSC efficacy and no conclusions could be drawn about the therapy potential. Presently, there are eight on-going phase I or II clinical trials using placenta-derived stem cells for acute brain injuries, seven targeting ischaemic stroke and one cerebral haemorrhage (Zanier *et al.*, in press, *Cell transplantation*).

There is a plethora of evidence demonstrating the ability of umbilical cord derived MSCs in stroke, improving behavioural recovery (Boltze *et al.*, 2005) along with angiogenic and neurogenic effects (Borlongan *et al.*, 2004). hUCT-MSC also improved functional recovery in rats after MCAO, possibly by reducing peripheral and cerebral pro-inflammatory cytokines observed for both hUCB-MSC (Kim *et al.*, 2012) and hUCT-MSC (Zhu *et al.*, 2014). As discussed, ischemia triggers inflammation which subsequently causes microglia activation. A plethora of studies have reported a direct effect of MSCs on microglia, as such it has now emerged that MSC therapy may improve outcomes of brain injury by modulating microglia activation (**figure 1.4**).

It has been demonstrated that BM-MSCs possess the ability to inhibit microglia activation, maintaining the resting phenotype through inhibition of the expression and release of inflammatory molecules and stress-associated proteins (Zhou *et al.*, 2009; Giunti *et al.*, 2012; Yan *et al.*, 2013; Liu *et al.*, 2014). BM-MSCs induced a microglia phenotype defined as *Arg1*-high, *CD86*-high, *CD206*-high, *Il10*-high, *Ccl2*-high and *Tnfa*-low cells (Hegyí *et al.*, 2014). Studies have concluded that BM-MSCs are capable of inhibiting microglia proliferation upon LPS stimulation while modulating the levels of NO, IL-6 and TNF- $\alpha$  (Jose *et al.*, 2014; Ooi *et al.*, 2010; Rahmat *et al.*, 2013).

Evidence shows that the ability of MSCs to suppress activation of microglia causes a delay of neuronal death (Ohmi *et al.*, 2003). BM-MSC treatment reduces the expression of inflammatory cytokines in LPS-activated microglia and subsequently reduces aquaporin-4 expression and apoptosis of astrocytes after cerebral injury (Tang *et al.*, 2014). Both neurological deficit and brain oedema and infarct volume were significantly decreased post ischaemic stroke with BM-MSC treatment via tail vein injection (Tang *et al.*, 2014).

The current evidence for the potential of placenta-derived cell therapy for stroke is promising. Studies indicate that placenta-derived stem cells improve functional recovery after MCAO, most likely by promoting angiogenesis, neurogenesis and through potent immunomodulatory effects that all contribute to the resolution of the inflammatory response after stroke, facilitating post ischaemic recovery.

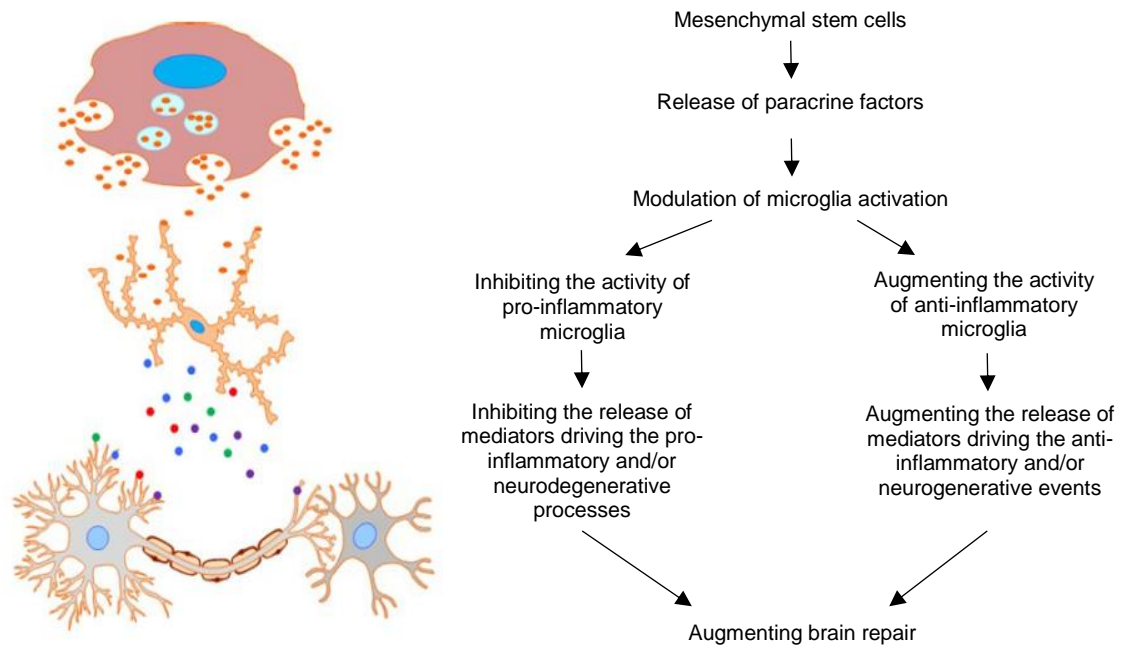


**Figure 1.4. A summary of mechanisms of MSC therapy-related neuroprotection.**

MSCs have been shown to modulate microglia's inflammatory response post stroke. Microglia are activated rapidly in response to central nervous system injury and produce proinflammatory cytokines, growth factors, reactive oxygen species, nitric oxide and glutamate. Pro-inflammatory microglia are associated with tissue destruction, whereas anti-inflammatory microglia facilitate repair and regeneration. MSC therapy has been shown to modulate microglia by inhibiting the pro-inflammatory activity while increasing the anti-inflammatory mechanism, thus improving the outcome after ischaemic damage. Adapted from (Hsuan *et al.*, 2016).

Of all the placental derived cells, amniotic cells are the least explored. The human umbilical cord starts developing on the 5<sup>th</sup> week of gestation and continues to grow until 50 cm in length. Stem cells can be derived from various parts of the umbilical cord, including amniotic membrane, Wharton's jelly, cord lining and the perivascular region (Ding *et al.*, 2015). Collaborators in the current project have provided evidence of the protective effects of human amniotic membrane derived MSCs (hAMSCs) in a mouse model of traumatic brain injury. ICV (intracerebroventricular) and IV (intravenous) transplanted hAMSC induced functional improvement of sensorimotor deficits. Functional improvement was associated with histological protective modifications, like neuronal and vessel rescue in the peri-confusional cortex and the stimulation of endogenous neurogenesis (Pischiutta *et al.*, 2016).

### **1.6.2 Do we need stem cells or can we use their juices? The effect of hAMSC-CM**

Evidence showing that the beneficial effects of cell therapy are due to the release of soluble factors raises the possibility of a cell-free therapeutic strategy. A cell-free therapy would overcome important issues related to intrinsic cells heterogeneity and safety concerns. *In vitro* (Pischiutta *et al.*, 2016) and *in vivo* (Fraga *et al.*, 2013; Teixeira *et al.*, 2015) evidence shows that the conditioned media from placenta-derived cell cultures can induce effects similar to their cell counterparts. The hAMSC-CM composition is influenced by different factors, besides the organ of origin, and the donors genetic background, several variables such as the cell density, cell passage, culture medium, days of collection or presence of preconditioned stimuli may affect the release of soluble molecules. Pischiutta *et al.*, (2016) recently provided evidence of comparable effects of hAMSC and hAMSC-CM treatments. They found that both hAMSC and hAMSC-CM treatments induced up-regulation of CD11b compared to when exposed to OGD, and Ym1 signalling was upregulated by both hAMSC and hAMSC-CM.

Many cell-released soluble factors have been proposed as mediators of the protection and different classes of molecules have been investigated (**figure 1.5**). More than 90 cytokines belonging to the families of interleukins, tumour necrosis factors, interferons, colony-stimulating factors, growth factors and chemokines are amongst the secretion products of umbilical MSCs. These proteins may have a potential role

for stroke recovery in view of their anti-inflammatory and immunomodulatory effects, angiogenesis, wound healing and neurogenesis (Deng-Bryant *et al.*, 2015).

Nucleic acids are another class of molecules that have recently aroused great interest. Micro-RNA (miRNA) are small noncoding sequences of RNA that can regulate the gene expression on target cells. In the brain, miRNA-21 mediates neuronal and microglia survival after ischaemic injury, reducing the levels of the apoptosis-inducing factor Fas ligand (FasL), miRNA-181 regulates the expression levels of the anti-inflammatory cytokine, IL-10 in astrocytes and reduces the neuronal apoptosis induced by microglia activated after an ischaemic insult, suppressing TNF- $\alpha$  expression (Hutchison *et al.*, 2013). miRNA-126 has been shown to play an important role in hUCB-MSC induced protection. These beneficial effects were attenuated in mice treated with hUCB-MSC where miRNA-126 expression was inhibited (Zhang *et al.*, 2012).

Metabolites are small molecules (MW < 2000 Da) that include endogenous compounds (peptides, lipids, amino acids, nucleic acids, CHO, organic acids, vitamins). Using an *in vitro* model of OGD with cortical organotypic brain slices, Pischitta *et al.*, (2016) demonstrated that the conditioned media (CM) from hAMSC was protective and they identified a CM sub fraction containing small metabolites (MW < 700 Da) with marked protective properties. Further analyses of the CM active sub fraction by profiling six metabolic classes identified a pool of selectively enriched metabolites. These included molecules such as lysine, taurine, alpha-aminoadipic acid and spermidine, all for which neuroprotective effects have been reported (Menzie *et al.*, 2013; Kondoh *et al.*, 2010). The secretome of placenta-derived stem cells holds great promise for the treatment of stroke. The exact mechanisms of action are still not clear and numerous factors, rather than any single one, probably contribute synergistically to the neuroprotective effects.

Recent studies have suggested that hAMSC-CM may exert its effects through modulation of microglia. Pischitta *et al.*, (2016) reported that hAMSC and hAMSC-CM treatment after OGD induced an upregulation of the leukocyte marker CD11b compared to OGD alone. This indicates that hAMSC and hAMSC-CM may have a direct effect on microglia. The only study (as far as we are aware) that investigates the effect of MSC-CM on microglial cells directly, concluded that MSC-CM treatment is capable of modulating microglia's pro-inflammatory phenotype (Ooi *et al.*, 2014).

The authors reported that MSC-CM significantly reduced the mRNA and protein expression levels of pro-inflammatory cytokines (IL-6 and TNF) in microglia activated by LPS. In addition, MSC-CM significantly reduced the protein expression of NF- $\kappa$ B, JNK, and c-Jun, while increasing the expression levels of anti-inflammatory cytokine IL-10 and MKP-1 in activated BV-2 cells (Ooi *et al.*, 2015). As discussed, microglia play an important role in tissue repair and re-organisation. These beneficial effects must be considered when developing therapeutic approaches based on interrupting post-ischaemic inflammation. By modulating the immune response, MSC-CM may be capable to harness the advantageous effects for example, the repair mechanisms while dampening down the deleterious response that leads to damage. The question remains, is hAMSC-CM capable of modulating microglia and if so, is it this modulation of microglia that is responsible for the beneficial effects of hAMSC-CM observed so far?

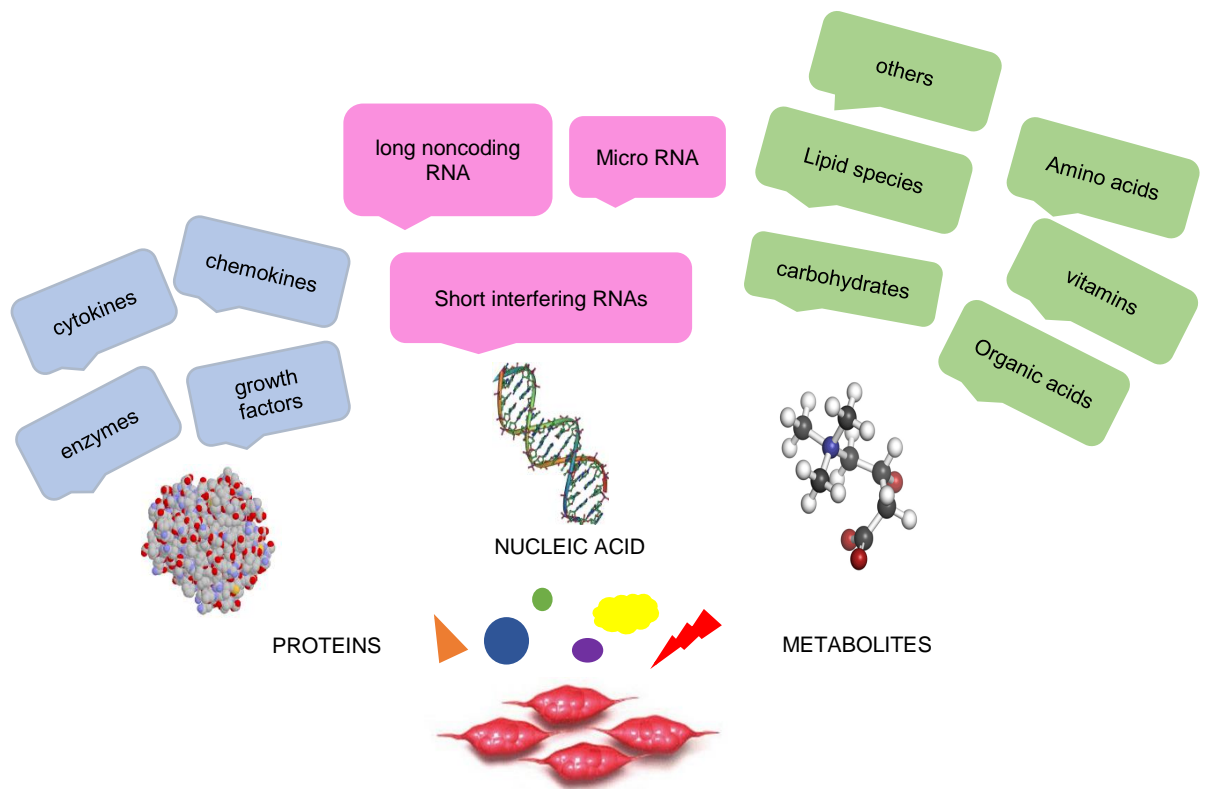


**Figure 1.5. Categories of molecules secreted by placenta-derived stem cells.**

## 1.7 Aims and thesis overview

The aim of this thesis is to investigate the potential for hAMSC-CM to modulate microglia's inflammatory response *in vitro* and *in vivo* after ischaemic stroke. In chapter 2, the first goal was to characterise the novel microglia SIM-A9 cell line, using opposing stimuli, LPS and IL-4 to elicit different phenotypes and responses. To assess the activation and phenotype of microglia, several techniques were utilised including immunoblotting to analyse signalling, PCR for gene expression, the Griess assay for nitrite production and cytokine array analysis. Following on from this, we describe several techniques that were used to try and isolate primary microglia cells. As discussed above, hAMSC-CM has been shown to improve recovery after stroke and TBI, however, the precise interaction of hAMSC-CM and microglia directly remains unknown. The aim of the project is therefore to establish whether hAMSC-CM is capable of modulating microglia's inflammatory response *in vitro* and *in vivo*.

In chapter 3, a multidisciplinary approach was taken to establish a more relevant model of microglia migration. The aim of these experiments was to establish, optimise and characterise an *in vitro* model of microglia migration that is a better representation of the stroke environment. The effect of hAMSC-CM on microglia migration was also examined.

Translating our *in vitro* findings *in vivo*, chapter 4 investigated the effects of hAMSC-CM *in vivo* using the mouse stroke model. hAMSC-CM was injected into stroke mice and inflammatory markers were measured using PCR 24 hours post stroke.



**Chapter 2: Signalling and polarisation of  
microglial cell line SIM-A9 in response to  
LPS, IL-4 and hAMSC-CM**

## 2.1 Introduction and aims

It is now acknowledged that inflammation plays a major pathophysiology role in ischaemic stroke (Iadecola and Anrather, 2011). Almost immediately after the onset of brain ischemia, microglia are activated and mediators are produced (Zhao *et al.*, 2007). Microglia undergo dramatic morphologic alterations upon activation, changing from the resting ramified phenotype into activated amoeboid, releasing a variety of soluble factors, such as cytokines and chemokines, which are pro-inflammatory and which play a critical role in the inflammatory response associated with post-ischemia (Hu *et al.*, 2014).

Microglia activates the innate immune response through their pattern recognition receptors (PRRs) which induce a pro-inflammatory response via down-stream nuclear factor- kappa B (NF- $\kappa$ B) and mitogen-activated protein kinase (MAPK) signalling (Svensson *et al.*, 2011). In the present study, the spontaneously immortalised microglia cell line (SIM-A9) established by Nagamoto-Combs *et al.*, (2014), was used for reasons described in **section 3.4**. Due to the novelty of SIM-A9 cells, there is limited published work with the microglia cell line. Current published work on SIM-A9 cells covers various functions, but regarding inflammation and signalling, very little has been carried out. It was demonstrated that cofilin, the actin-binding factor, is involved in SIM-A9 cell activation, working through NF- $\kappa$ B and JAK/STAT pathways. The study shows the involvement of cofilin by the use of siRNA knockdown paradigms (Alhadidi and Shah, 2017). Farrell and colleagues induced chronic inflammation in SIM-A9 cells through application of 2.5 ng/ml LPS for 10 days, showing the production and release of several cytokines and chemokines (Farrell *et al.*, 2016). Additionally, a recent study using SIM-A9 cells investigated the effect of the anti-depressant fluoxetine on IL-6 production highlighting the role of the *TNFAIP3* gene in fluoxetine's effects (Hung *et al.*, 2017).

It has been shown that SIM-A9 cells, were responsive to exogenous inflammatory stimulation with lipopolysaccharide (LPS) triggering NF- $\kappa$ B signalling cascades which resulted in TNF- $\alpha$  secretion (Nagamoto-Combs *et al.*, 2014). However, Nagamoto-Combs *et al.*, (2014) investigated a single time point after LPS stimulation (5 minutes) of phospho-I $\kappa$ B (p-I $\kappa$ B) at a single dose of LPS (25 ng/mL) and failed to show a significant activation of the NF- $\kappa$ B pathway. Previous studies have failed to fully characterise activation of signalling pathways, in terms of agonist concentration and

a time course of activation, thus ensuring optimal conditions for investigating the signalling pathway. Given the potential role of NF- $\kappa$ B signalling in controlling inflammatory responses of microglia, we further characterise the NF- $\kappa$ B pathway in these cells and investigate the consequence of activation. Specifically, the present study characterised the time and concentration dependent effects of LPS-induced I $\kappa$ B $\alpha$  degradation and P65 phosphorylation in SIM-A9 microglia cells.

Furthermore, LPS increased levels of iNOS, while IL-4 stimulation increased arginase 1 levels, demonstrating that SIM-A9 cells can switch their profiles to pro- or anti-inflammatory phenotype respectively (Nagamoto-Combs *et al.*, 2014). However, Nagamoto-Combs *et al.*, (2014) only examined the effect of 24-hour stimulation of LPS (2.5 ng/mL) on TNF $\alpha$ , nitrite production, iNOS and COX-2 whereas effect of IL-4 on Arg1 only was investigated. Given the balance of responses to pro- and anti-inflammatory stimuli are pivotal to the damaging or reparative effects of microglia, the present study examined the effects of both LPS and IL-4 on SIM-A9 microglia cells at two time points (4 hours and 24 hours) on *Il1 $\beta$* , *Nos2*, *Arg1*, *Nos2* and nitrite production.

While microglia can be destructive in repair and recovery, their presence is needed to alleviate injury (Taylor and Sansing, 2013), the balance of these processes opens up possibilities of modulation microglia to harness their beneficial properties while dampening down their damaging effects. As discussed in **section 1.6.2**, studies have highlighted a possible effect of stem cell conditioned media on microglia that harness their beneficial properties. Ooi *et al.*, 2014 demonstrated that MSC-conditioned media significantly reduced mRNA and protein expression levels of pro-inflammatory cytokines (*Il6* and *Tnfa*) in microglia activated by LPS. In addition to these findings, the same study revealed that MSC-CM significantly reduced the protein expression of NF- $\kappa$ B, JNK and c-Jun in BV-2 microglia cells (Ooi *et al.*, 2014).

The experiments presented in the current chapter were aimed to elucidate the effects of the human amniotic mesenchymal stromal cells secretome (hereby referred to as hAMSC-CM (or CM in figures)) in modulating microglia activation by analysing microglia pro- and anti-inflammatory factors and signalling pathways.

As detailed in the introduction, the use of microglia cell lines such as the BV-2, HAPI, N9 and SIM-A9 in replacement for primary microglia are often criticised in neuroinflammation research. BV-2 and HAPI cell cultures were shown to only partially

model primary microglia (Horvath *et al.*, 2008). On the other hand, studies have concluded that BV-2 cells appear to be a valid substitute for primary microglia in many experimental settings (Henn *et al.*, 2009). Likewise SIM-A9, since they are spontaneously immortalised microglia cells may be suitable for initial studies and optimisation of experiment parameters, however, it should always be carefully considered and acknowledged that responses in cell lines may be less pronounced than in primary cultures (Henn *et al.*, 2009). In mindfulness of the differences and relevance of cell lines compared to primary cells as detailed in chapter 1, we attempted to isolate primary microglia cells suitable for examining the effects of hAMSC-CM.

The aims of the work described in this chapter were to:

1. Characterise the signalling and activation of SIM-A9 cells;
2. Examine the effects of hAMSC-CM in LPS-activated microglia;
3. Establish and validate an optimal protocol to enable efficient and consistent isolation of highly pure microglia from the mouse brain.

## **2.2 Materials and Methods**

### **2.2.1 Cell culture**

#### **2.2.1.1 SIM-A9 cells**

SIM-A9 cells from the mouse C57BL/6 from the laboratory of Kumi Nagamoto-Combs (Nagamoto-Combs *et al.*, 2014), University of North Dakota were purchased from Kerfast, Boston, USA. These cells were harvested from the cerebral cortex of C57BL/6 mice and spontaneously immortalised (SIM) so they could aggressively proliferate to confluency (Nagamoto-Combs *et al.*, 2014). To minimise bias and ensure purity of the cell line, clonal cells were cultured separately in several wells, allowed to expand in DMEM/F12 medium containing serum, and clone A9 were arbitrarily selected (Nagamoto-Combs *et al.*, 2014). In the present work, in culture, SIM-A9 cells were grown in DMEM/F12 containing 5% heat-inactivated donor horse serum, 10% heat-inactivated-fetal bovine serum, 1.5 µg/ml penicillin/ streptomycin/ neomycin. Cells were either sub cultured, plated or inserted into microfluidic devices before reaching 90% confluency by harvesting with cold PBS containing 1mM EDTA, 1mM EGTA and 1mg/ml glucose.

#### **2.2.1.2 hAMSC- Conditioned media**

1ml Eppendorf tubes containing either control media or hAMSC-CM were received frozen from our collaborators Prof Ornella Parolini at Università Cattolica del Sacro Cuore, Milano. The media was transferred immediately into -80°C where it was stored. The control medium was Neurobasal medium with added B27 supplement, P/S (1% final) [penicillin (100U/ml), streptomycin (100ug/ml)] + L-Glutamine 1% (2mM final). The control, non-conditioned media was made in the Ornella lab by plating the Neurobasal complete medium for 5 days at 37 °C (5% CO<sub>2</sub>). After 5 days the media was collected, centrifuged at 300 x g for 10 minutes and then filtered using a 0.8 µM filter. The media was then frozen at -80 °C until use. A 50% mix of hAMSC-CM: Control media was used for all hAMSC-CM experiments. LPS (*E.Coli*, serotype 026:B6, L2762, Sigma, UK) was added together with control media or hAMSC-CM to the microglia cultures except for the protein expression studies of signalling pathways (NF-κB, p65, ERK and JNK), where SIM-A9 microglia were treated with LPS in the last 30 minutes of the 24 hour incubation with control media or hAMSC-CM.

## **2.2.2 Immunoblotting of cell lysates**

### **2.2.2.1 Preparation of samples for SDS-page and immunoblot**

Cells were grown in 12-well plates, once reaching 70% confluency cells were then rendered quiescent for 24 hours and stimulated with 1 µg/ml of LPS or 20 ng/ml of recombinant mouse IL-4 (BD Biosciences, UK) for the desired time. For hAMSC-CM experiments the hAMSC-CM and control media was applied to the cells 24 hours before addition of LPS (1 µg/ml). The plates were then placed on ice to stop the stimulation. Cells were immediately washed with ice-cold PBS before adding 150 µl of pre-heated Laemmli sodium dodecyl sulphate (SDS) sample buffer (63 mM Tris HCl (pH 6.8), 2 mM Na<sub>4</sub>P<sub>2</sub>O<sub>7</sub>, 5 mM EDTA, 10% glycerol (v/v), 2% SDS (w/v) and 0.007% (w/v) bromophenol blue to which, 50 mM dithiothreitol (DTT) was added immediately before use). Cells were scraped from wells and lysates drawn repeatedly through a 16-gauge needle attached to a 1 ml syringe to shear chromosomal DNA. Samples were transferred to a 1.5 ml microfuge tube, the lid pierced and boiled for 5 minutes at 95°C to denature proteins and stored at -20°C until required for SDS-polyacrylamide gel electrophoresis.

### **2.2.2.2 SDS-polyacrylamide Gel Electrophoresis**

Gel kit apparatus was assembled before adding distilled water to check the glass plates were flush and not leaking. Resolving gel was prepared using required amount of acrylamide: [N, N'-methylenebis-acrylamide (37:5:1), 0.375 M Tris (pH 8.8), 0.1% (w/v) SDS and 0.05% (w/v) ammonium persulphate]. Polymerisation of the resolving gel was initiated by the addition of 0.05% (v/v) N, N, N', N'-tetramethylethylenediamine (TEMED). The gel solution was poured into the assembled glass plates (Bio-Rad) until 2-3 inches from the top. A thin layer of 0.1% SDS solution was added to the gel, to prevent drying and to disperse bubbles. Once the gel was set, the 0.1% SDS was discarded, the stacking gel solution [5% (w/v) acrylamide, 125 mM Tris-HCl (pH 6.8), 0.1% (w/v) SDS, 0.05% (w/v) ammonium persulphate, 0.1% (v/v) TEMED] was then made and added directly on top of the resolving gel, the appropriate Teflon welled combs were then slotted into the glass plates. Once the gel was set the comb was removed, the wells were washed with sterile distilled water. Gels were placed in the specified western blot tank and this was filled with running buffer [24.8 mM Tris, 191.8 mM glycine, 0.1% SDS], 10-20 µl of sample were loaded in the appropriate wells, run concurrently with a pre-stained SDS protein marker of known molecular weights at

120V for approximately 105 minutes. The resolved proteins on the gel were then transferred to nitrocellulose membranes. The gel was placed on top of the nitrocellulose membrane and sandwiched between two Whatmann 3MM papers and two fibrous blotting pads (Bio-Rad). The cassette(s) were then placed in a Biorad mini trans-blot electrophoresis tank along with an ice pack. The tank was then filled with transfer buffer [25 mM Tris, 192 mM glycine, 20% (v/v) methanol] and was left to run for 1 hour 45 minutes at a constant current of 300 mA. Membranes were blocked at 1 hour at room temperature in 5% (w/v) non-fat dry milk diluted in Tris buffered saline solution containing Tween 20 (TBST) (20 mM Tris-base, 137 mM NaCl and 0.1% (v/v) Tween 20, pH 7.6). Then membranes were incubated overnight in primary antibody (**Table 2.1**) prepared in 3% BSA in TBST buffer. The following day the membranes were washed for 5 x 5 minutes in TBST buffer then incubated for 2 hours at room temperature with either horseradish peroxidase conjugated anti-mouse or anti-rabbit IgG prepared in 3% BSA in TBST. Finally, blots were washed for 5 x 5 minutes with TBST buffer and immunoreactive protein bands were detected by incubation with enhanced chemiluminescence (ECL) (Amersham International Plc) for 3 minutes. The membranes were blotted on a paper towel, mounted onto an exposure to Kodak X-OMAT LS film for the appropriate time under darkroom conditions and developed by KODAK M35-M X-OMAT processor. After development, signals of the scanned autoradiographs were quantified by densitometry using a GS-800 densitometer and Quantity One Image software (version 4.5.2, BioRad). All blots were stripped (see below) and re-probed for GAPDH. All proteins investigated were normalised to GAPDH and calculated as a fold change compared to the control sample.

Primary antibody	Company	Dilution/ Incubation	Secondary antibody	Company	Dilution/ Incubation
I $\kappa$ B- $\alpha$	Cell Signalling Technology	1/1,500 (4°C)	Anti-Rabbit IgG-HRP antibody	Jackson Immuno-Research (USA)	1/7,500 (RT)
p-P65	Cell Signalling Technology	1/1,500 (4°C)	Anti-Rabbit IgG-HRP antibody	Jackson Immuno-Research (USA)	1/7,500 (RT)
p-ERK	Santa Cruz Biotechnology	1/3,000 (4°C)	Anti-Rabbit IgG-HRP antibody	Jackson Immuno-Research (USA)	1/7,500 (RT)
p-SAPK/JNK (T183/Y185)	Cell Signalling Technology	1/5,000 (4°C)	Anti-Rabbit IgG-HRP antibody	Jackson Immuno-Research (USA)	1/7,500 (RT)
Arginase 1	BD Transduction Laboratories	1/4,000 (4°C)	Anti-Mouse IgG-HRP antibody	Jackson Immuno-Research (USA)	1/7,500 (RT)
iNOS	Millipore	1/6,000 (4°C)	Anti-Rabbit IgG-HRP antibody	Jackson Immuno-Research (USA)	1/7,500 (RT)
GAPDH	Abcam	1/80,000 (4°C)	Anti-Mouse IgG-HRP antibody	Jackson Immuno-Research (USA)	1/7,500 (RT)

**Table 2.1. Details of primary and secondary antibodies used for each protein of interest**



### **2.2.2.3 Reprobing of Nitrocellulose Membrane**

Antibodies were stripped from the nitrocellulose membrane by incubating for 1 hour in 15 ml stripping buffer (100 mM  $\beta$ -mercaptoethanol, 2% sodium dodecyl sulphate, 62.5 mM Tris-HCl, pH 6.7) at 70 °C on a shaker (Stuart Science Equipment). After the incubation period, the stripping buffer was discarded and membrane rinsed in TBST buffer for 3 x 5 minutes washes to remove residual stripping buffer. Finally, immunological detection of protein was carried out as described above, starting from day 2.

## **2.2.3 RNA analysis**

### **2.2.3.1 RNA extraction**

SIM-A9 cells were seeded in 6-well plates, rendered quiescent for 24 hours, and then stimulated with 1  $\mu$ g/ml of LPS or 20 ng/ml of recombinant mouse IL-4 (BD Biosciences, UK) for 4 or 24 hours. Total RNA was isolated from SIM-A9 cells using the ISOLATE II RNA Mini Kit (Bioline, UK), following the manufacturer's instructions. Microglia cells were harvested as follows: Cell-culture medium was aspirated from the wells using a P1000 and stored for NO assays and cytokine array experiments. Cells were washed once with PBS and then lysed with 350  $\mu$ l buffer RLY supplemented with  $\beta$ -mercaptoethanol ( $\beta$ -ME). To reduce viscosity and to clear the lysate, the sample was loaded into a ISOLATE II filter in a collection tube (2 ml) and centrifuged for 1 minute at 11,000 x g. The filter was then discarded and 350  $\mu$ l of 70% ethanol was added to the homogenised lysate and was mixed using a pipette 5 times. The lysate was loaded onto an ISOLATE II RNA Mini Column (blue) and centrifuged for 30 seconds at 11,000 x g. In order to dry the membrane, 350  $\mu$ l Membrane Desalting Buffer (MEM) was added to each sample and centrifuged at 11,000 x g for 1 minute. For each preparation, 10  $\mu$ l of reconstituted DNase I was added to 90  $\mu$ l Reaction Buffer (RDN). The tube was gently flicked to mix before 95  $\mu$ l of the DNase I reaction mixture was directly applied onto the centre of the silica membrane and incubated at room temperature for 15 minutes. The membrane was washed with 200  $\mu$ l wash buffer RW1 for 30 seconds at 11,000 x g, followed by 600  $\mu$ l wash buffer RW2 for the same centrifuge conditions. A final wash with 250  $\mu$ l wash buffer RW2 for 2 minutes 11,000 x g was carried out to dry the membrane completely. The RNA was eluted with 60  $\mu$ l RNase-free water at 11,000 x g for 1

minute. All samples were analysed for yield and quality using NanoDrop (described below) and were stored at -80°C.

### **2.2.3.2 RNA quality assessment**

NanoDrop (ND-2000C, Thermo Scientific) (220-750 nm) spectrophotometer was used to measure total RNA concentration. The nanodrop allows measurement of RNA concentration by the absorbance of light at  $\lambda = 260$  nm (A260). The software displays the sample absorption curves as well as the calculated RNA concentration and ratios. The purity of RNA was defined using the A260/A280 ratio, which should range around 1.8, and A260/A230 ranging from 2.0- 2.2. All extracted RNA samples had acceptable purity and yield ratios.

### **2.2.3.3 cDNA synthesis**

For the analysis of relative gene expression, mRNA requires conversion to complementary DNA (cDNA), a process called reverse transcription (RT). Depending on the amount of RNA and the required amount of cDNA a total reaction volume of 20  $\mu$ l was used. Total RNA was reverse transcribed to cDNA using Tetro cDNA Synthesis Kit (Bioline, UK). RNA concentrations were normalised between samples to 2  $\mu$ g using RNase-free water to make a final volume of 12  $\mu$ l. A reverse transcriptase 'RT +' master mix was then prepared: 1  $\mu$ l of oligo-dT (500 ng/ $\mu$ l) as the first-strand synthesis primer, 1  $\mu$ l of 10 mM dNTP mixture, 5  $\mu$ l of 5x RT Buffer, 1  $\mu$ l RNase Inhibitor and 1  $\mu$ l of Tetro Reverse Transcriptase (200 g/ $\mu$ l). To check for the presence of persisting contaminating genomic DNA, an additional master mix 'RT-master mix' containing all of the cDNA synthesis components and total RNA with the exception of replacing 1  $\mu$ l of Tetro Reverse Transcriptase (200 g/ $\mu$ l) with 1  $\mu$ l of RNase-free water. 8  $\mu$ l of the relevant master mix was transferred into each tube along with the RNA/water mix. The reactions were incubated for 1 hour at 45 °C, the reaction was then terminated by incubating at 85 °C for 5 minutes before being chilled on ice. The samples were diluted 1:5 using 1x RT buffer and stored at -20 °C.

#### 2.2.4 Quantitative real-time polymerase chain reaction (qRT-PCR)

To ensure high-quality, reproducible, and biologically relevant results, the qRT-PCR assays were performed using the practices laid out in the Minimum Information for Publication of Quantitative Real-Time PCR Experiments (MIQE) guidelines when possible (Bustin *et al.*, 2009).

qRT-PCR was utilised to quantitatively assess the amplification of fluorescent probe labelled target cDNA originally generated from RNA. SYBR Green, which intercalates into amplified DNA strands, was chosen as fluorescent DNA binding dye. Primers were designed using the publicly available Primer Blast of NCBI (<https://www.ncbi.nlm.nih.gov/tools/primer-blast/>), which combines the primer designing tool Primer3 and BLAST to screen generated primers across a user-specified database and assess primer-specificity (Ye *et al.*, 2012). Both sense and anti-sense (**Table 2.2**) were produced by Integrated DNA Technologies (IDT) (USA). The PCR master mix consisted of 10 µl ready-to-use SYBR™ Green (ThermoFisher Scientific, UK), 0.8 µl 10 µM sense primer, 0.8 µl 10 µM anti-sense primer, 1 µl of cDNA and 8 µl RNase free water to make a total reaction volume of 20 µl. qRT-PCR was carried out using the StepOne Plus real-time PCR system (Applied Biosystems, UK) and the thermal profile is detailed in **Table 2.3**.

Gene name	Forward primer	Reverse primer
<i>Sdha</i>	TATGGTGCAGAAGCTCGGAAGGAG	CCCAAACGGCTTCTTCTGCTGTC
<i>Qars</i>	TGGTTATGCCAAGGCCAACAATG	TGTATAACCCAGCCAGGTCACCATG
<i>Casc3</i>	TTGCAGCCACGGGAACTTCG	TCTGCCGCTGGGATGAGTAACG
<i>B2m</i>	CACTGACCGCCTGTATGCTATCC	TTCAATGTGAGGCGGGTGAAC
<i>Nos2</i>	CACACTGGCCTCCCTCTGAAAAG	AAGGACTCTGAGGCTGTGTGGTGG
<i>Il1<math>\beta</math></i>	TCCTGAACTCAACTGTGAAATGCCAC	GACAGCCCAGGTCAAAGGTTTGG
<i>Chil3</i>	GCCAGCAGAAGCTCTCCAGAAGC	CACATCAGCTGGTAGGAAGATCCCAG
<i>Arg1</i>	CAAATTGTGAAGAACCCACGGTCTG	GCTTCCAAGTCCAGACTGTGGTC
<i>Tnfa</i>	CCCACGTCGTAGCAAACCA	AGAACCTGGGAGTAGACAAGGT
<i>Ccl2</i>	AGCTGTAGTTTTTGTCAACCAAGC	GACCTTAGGGCAGATGCAGT

**Table 2.2. Sequence of oligonucleotides of housekeeping genes and genes of interest. Primers used in qRT-PCR with annealing temperature of 60°C.**

Step	Temperature	Duration	Number of cycles
UDG activation	50°C	2 minutes	1
Dual-Lock™ DNA polymerase	95°C	2 minutes	1
Denature	95°C	15 seconds	40
Anneal/extend	60°C	1 minute	

**Table 2.3. Thermal profile of standardised qRT-PCR.**

#### **2.2.4.1 Quantification method**

The gene expression of each gene was quantified using the cycle of threshold (Ct), which is the point at which the fluorescence of SYBR Green rises above the fluorescence background. The StepOne software automatically set the baseline signal and threshold of signal fluorescence. The relative expression of a target gene is calculated using the  $\Delta\Delta\text{Ct}$  method proposed by Livak & Schmittgen (2001). This method compares Ct values between the target gene and the endogenous reference gene to examine the changes in gene expression between control and treated samples.

At first the  $\Delta\text{Ct}$  was determined by subtracting the Ct of the reference gene from the Ct of the target gene:

$$\Delta\text{Ct} = \text{Ct (Target)} - \text{Ct (Reference)}$$

The  $\Delta\Delta\text{Ct}$  results from the subtraction of the  $\Delta\text{Ct}$  of the control sample (e.g. untreated) from the  $\Delta\text{Ct}$  of the samples of interest (e.g. treated):

$$\Delta\Delta\text{Ct} = (\Delta\text{Ct treated}) - (\Delta\text{Ct untreated})$$

The relative expression in the treated sample is then equal to  $2^{-\Delta\Delta\text{Ct}}$ .

#### **2.2.4.2 Selecting the reference gene**

The reference gene is used to normalise differences in the cDNA concentration added in each PCR reaction. Thus, the mRNA expression of this gene must remain stable between samples and treatments. Genes selected from the literature surveying appropriate mouse reference gene were Glutaminyl tRNA synthetase (*QARS*), Beta-2 microglobulin (*B2M*), Cancer Susceptibility 3 (*CASC3*) and Succinate dehydrogenase complex, subunit A, flavoprotein variant (*SDHA*). The PCR results for each sample was passed through RefFinder (<http://150.216.56.64/referencegene.php?type=reference#>) and the most stable gene was used for each treatment. *B2M* was found to be the most stable for LPS treatment, and *SDHA* for IL-4.

#### **2.2.5 Mouse cytokine proteome profiler**

Determination of the relative levels of selected mouse cytokines and chemokines was measured in cell lysate samples using a commercially available proteome profiler kit, Mouse cytokine array panel A- ARY006 (R&D Systems, Abingdon, UK). The protocol was carried out following the manufacturer's guidelines as follows. The array membrane was blocked for one hour on a rocking platform using blocking buffer provided and then aspirated. Samples (700 µg protein/ml), containing detection antibody cocktail (1:250) were applied to the membrane and incubated overnight at 4°C on a rocking platform. The membrane was then washed 3 x 10 minutes in 20 ml wash buffer provided and then incubated with streptavidin-HRP conjugate at room temperature for 30 minutes. Again, the membrane washed 3 x 10 minutes in 20 ml buffer and then blotted dry and placed on a plastic sheet protector. Next, the membrane was overlaid with 1 ml chemical reagent mix provided in a dark room. The membrane was removed from the plastic sheet provider and wrapped in cling film and any air bubbles smoothed out. Finally, the membrane was placed in an autoradiography cassette and exposed to x-ray film for multiple periods between 1-10 minutes.

### **2.2.6 Nitric oxide assay**

Cell supernatants were thawed and centrifuged for 3 minutes at 11,000 x g to remove any cell debris. Nitrite was detected in the supernatant by using the Griess assay. Nitrite is detected and analysed by formation of a red pink colour upon treatment of a  $\text{NO}_2^-$ -containing sample with the Griess assay. For this, 50  $\mu\text{l}$  of culture supernatant from each sample was transferred to a 96-well plate in triplicate and added with the same volume of Griess reagent (1% sulfanilamide/0.1% N-1-naphthylethylenediamine dihydrochloride/2.5% phosphoric acid; all from Sigma-Aldrich, USA). Absorbance was read at 530 nm (POLARstar Omega Plate Reader, BMG LABTECH, Germany) after 10 minute incubation. Nitrite concentration was calculated with reference to a standard curve of freshly prepared sodium nitrite (0 to 100  $\mu\text{M}$ ).

### **2.2.7 Isolation of microglia from the mouse brain**

#### **2.2.7.1 Protocol 1. The shaking method**

##### **Isolation and culture of murine microglia cells via enzymatic digestion**

The base of a 75  $\text{cm}^2$  culture flask was coated overnight with 5 ml Poly-D-lysine (10  $\mu\text{g}/\text{ml}$ ), the next day excess poly-D-lysine was removed and the flask washed once with PBS. The following procedures were carried out in a sterile cell culture hood. Five neonatal C57BL/6J mice (1-3 days old) were culled by decapitation, the heads were placed straight into a beaker with 70% alcohol for 15-30 seconds. The decapitated heads were removed and all excess bloody and alcohol was removed using a sterile gauze. The skin over the skull was cleared using straight forceps to peel away the skin and fully expose the skull. The brain was gently lifted away from the skull base and placed onto a small culture dish containing a small volume of DEPC treated 1x Hank's balanced salt solution (HBSS, without calcium and magnesium, ThermoFisher, UK). The meningeal lining was gently removed and the brain cleaned and placed into a new culture dish with 2 ml of trypsin/ EDTA (0.05%/ 0.02%). Using a pair of corneal scissors, the brain was minced into a fine slurry before being transferred into a 15 ml centrifuge tube using a 5 ml serological pipette. The same volume of trypsin/ EDTA (0.05%/ 0.02%) was added and the tube was placed into the incubator at 37  $^\circ\text{C}$ / 5%  $\text{CO}_2$  for 10 minutes to allow for enzymatic disaggregation. After the allocated time, DMEM with 10% FCS was added to the suspension (1:1 ratio) to

neutralise the trypsin. The single cell suspension was gently agitated by moving the solution up and down 20 times using a 3.5 ml plastic transfer pipette. The suspension was allowed to stand for 1 minute at room temperature to allow any larger pieces to precipitate. This supernatant was then passed through a 70  $\mu$ M nylon cell strainer into another 100 ml beaker. The process of agitation using a 3.5 ml plastic transfer pipette with more DMEM with 10% FCS and straining was repeated twice. All the filtrated fluid was then gently transferred into a 50 ml centrifuge tube using a serological pipette. This was then centrifuged in a cooled (4 °C) centrifuge at 190 x g for 8 minutes. The supernatant was discarded and the cell pellet resuspended in 15 ml DMEM containing 15% FCS. The resuspended cells were added to the poly-D-lysine coated flask and incubated at 37 °C in a humidified 5% CO<sub>2</sub> atmosphere. After 3 days, the DMEM was replaced with a fresh DMEM, 10% FCS. After this, the medium was changed every alternate day using a 1:1 mix of fresh DMEM, 10% FCS and the supernatant of the medium of the flask in order to remove any dead cells while retaining existing growth factors previously released by the cells. The cells were used for purification once they reached 80-90% confluency (10-14 days).

#### **Purification of microglia cells from the mixed glia cell culture**

The medium was replaced with DMEM, 15% FCS 24 hours prior to purification. The microglia cells can be detached from the flask using a heated orbital shaker, the flask was placed on the shaker at 240 rpm for 1.5- 2 hours (37 °C). The suspension was transferred into a 50 ml centrifuge tube and centrifuged at 190 x g for 8 minutes. The supernatant was discarded and the cell pellet resuspended in fresh DMEM, 15% FCS, the cells were then seeded onto a 24-well tissue culture plate (pre-coated with poly-D-lysine). The cells were plated  $7.5 \times 10^4$  cells/well, and incubated at 37 °C in a humidified 5% CO<sub>2</sub> atmosphere. The medium was replaced every 2 days with fresh DMEM, 10% FCS. The cell purity was assessed via flow cytometry using the CD11b monoclonal antibody, as discussed in **section 2.2.7.5**.



### 2.2.7.2 Protocol 2. Percoll gradient and CD11b Magnetic beads

#### Generation of myelin-free mixed brain cell suspension by density gradient

C57Bl/6J mice were transcardially perfused (see **section 4.2.5**) with ice-cold saline to minimise contamination of red blood cells. The brain was removed, transferred into ice-cold DEPC treated 1x Hank's balanced salt solution (HBSS, without calcium and magnesium, ThermoFisher, UK) and finely minced to allow a fast cooling of the tissue. The minced brains were centrifuged for 5 minutes at 400 x g at room temperature (RT). Following the aspiration of the supernatant, the pellet was resuspended in 10 ml of enzyme cocktail. The enzyme cocktail consisted of the following components and stock concentrations: 50 U/ml collagenase D (Gibco, UK, 50 $\mu$ L), 100  $\mu$ g/ml N $\alpha$ -Tosyl-L-lysine chloromethyl ketone hydrochloride (Sigma, UK, 10 $\mu$ L), 5 U/ml DNase I (Roche, Switzerland, 50 $\mu$ L) and 8.5 U/ml dispase (Gibco, UK, 250 $\mu$ L) in 9.64 ml HBSS. The minced brain regions were incubated with the enzyme cocktail for 1h at 37°C under gentle rotation using the MACSmix™ tube rotator (Miltenyi Biotec, UK). The minced and digested brain tissue was transferred to a 15 ml Dounce homogeniser and homogenised on ice with 20 passes using the large clearance pestle. The homogenised cell suspension was transferred to a new tube containing an equal volume of 10% foetal bovine serum (FBS, GE Healthcare, Sweden) in HBSS to stop the enzymatic reaction. Following centrifugation for 5 minutes at 4°C and 400 x g (no brake), the supernatant was aspirated and the pellet resuspended in 16 ml of 35% Percoll made from isotonic Percoll (1 volume of 10 x HBSS, 9 volumes of Percoll; GE Healthcare, Sweden). For the density gradient, samples were split equally into 2 x 8 ml and carefully overlaid with 5 ml HBSS before resting on ice for 5 minutes. Samples were centrifuged for 45 minutes at 800 x g (no brake) at 4°C. Following the Percoll spin, different layers were observed (**Figure 2.1**). Mixed cells formed a pellet below the 35% Percoll, in between the Percoll and HBSS was the myelin layer. The supernatant including the myelin layer was carefully removed. 1 ml of HBSS was added to the cell pellet and samples were re-combined in a new myelin free tube. To dilute and remove the excess of Percoll, samples were topped up to 5ml using HBSS, centrifuged for 5 minutes at 4°C and 300 x g and the supernatant was removed.

### **Immunomagnetic bead separation**

The washed cell pellet from the Percoll gradient was resuspended in 90  $\mu$ L MACS buffer (1x PBS, pH 7.2, 0.5% Bovine Serum Albumin (BSA), 2mM ethylenediaminetetraacetic acid (EDTA)) and transferred into a new tube. MACS buffer was prepared using the manufacturer's guidelines (Miltenyi Biotec, UK). Following the addition of 10  $\mu$ l CD11b microbeads (Miltenyi Biotec, UK) the cell-bead-mix was incubated for 15 minutes at 4°C under gentle rotation. Microglia which are CD11b<sup>+</sup>, will bind to anti-CD11b labelled microbeads. Meanwhile pre-cooled LS columns (Miltenyi Biotec, UK) were placed in a magnetic field of the MACS separator and washed with 3 ml of MACS buffer. The bead-cell-suspension was washed with 500  $\mu$ l of MACS buffer and applied onto the LS column (**Figure 2.1**). The empty tube was rinsed with additional 500  $\mu$ L of MACS buffer which was then also applied onto the column before washing the column with 9 ml of MACS buffer. Microglia bound to microbeads remain within the column due to the magnetic field whereas unbound cells flow through and form the non-selected part of the sample. After the complete flow through of MACS buffer LS columns were removed from the magnetic field and placed into a 15 ml tube. After the addition of 5 ml MACS buffer into the column, bead bound microglial cells were flushed out by firmly pushing a plunger into the column. Finally, cells were pelleted for 5 minutes at 300 x g at 4°C and were plated at onto a poly-L-lysine coated 12-well plate. The cell purity was assessed via flow cytometry using the CD11b monoclonal antibody (**section 2.2.7.5**).

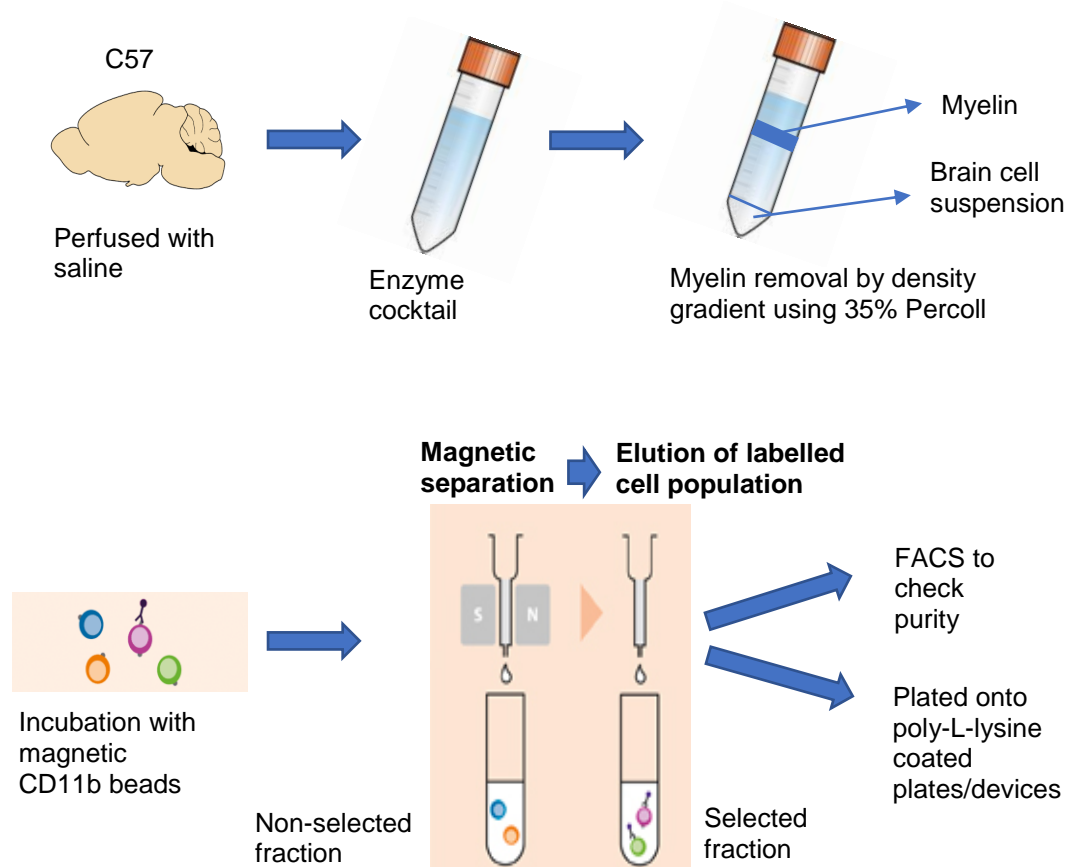


**Figure 2.1. Schematic diagram of microglia isolation using Percoll gradient and CD11b magnetic microbeads.** Myelin removal by density gradient using 35% Percoll. Mixed brain cell suspension separated from myelin. Magnetic bead separation for microglia isolation using CD11b labelled magnetic beads.

### 2.2.7.3 Protocol 3: Shaking dissociation and CD11b magnetic microbeads

This protocol is a combination of protocol 1 and protocol 2 and based on the method described by Marek *et al.*, (2008). The first half of the protocol was as described in Protocol 1: Isolation and culture of murine microglia cells via enzymatic digestion. Once a mixed glia cell culture was established using neonatal mice, purification was proceeded as Protocol 2: Immunomagnetic bead separation. The cell purity was assessed via flow cytometry using the CD11b monoclonal antibody (**section 2.2.7.5**).

#### **2.2.7.4 Protocol 4: Neural Tissue Dissociation kit, GentleMACS™ and CD11b magnetic microbeads**

Neonatal mice were harvested as described in protocol 1. Brains were dissociated using a GentleMACS™ Dissociator (Miltenyi Biotec, UK) and Neural Tissue Dissociation Kit P (Miltenyi, Biotec, UK) following manufactures instructions. Once a mixed cell suspension was achieved, purification was carried using CD11b magnetic microbeads as described in protocol 2.

#### **2.2.7.5 Microglia purity check using Flow cytometry**

Each sample was resuspended in FACS buffer (0.1% BSA in 1x PBS) and incubated for 20 minutes with 1 µg/ml anti-CD16/CD32 (Biolegend, UK) to block non-specific binding to Fc receptors. CD11b-PE (Miltenyi Biotec, UK) was incubated for 20 minutes in the dark at 4 °C. The excess of unbound antibodies was removed by washing and then centrifuged for 5 minutes at 400 x g and samples were resuspended in 2 ml FACS buffer. This was repeated one more time before cells were resuspended in 0.5 ml FACS buffer and analysed using a BD FACSCanto system and BD FACSDiva software (both BD Biosciences).

#### **2.2.8 Statistical analysis**

Statistical analysis was performed using the graph and statistics software of GraphPad Prism (GraphPad Software Inc., USA). All data is shown as mean ± SEM unless otherwise stated. Further details of which statistical tests were used are given in each individual figure legend.

## 2.3 Results

### 2.3.1 LPS activated the NF- $\kappa$ B signalling pathway in a time and concentration dependent manner in SIM-A9 microglia cells

Microglia are equipped with a set of PRRs on their cell surface for the detection of PAMPs or DAMPs, leading to induction of a pro-inflammatory response via downstream NF- $\kappa$ B and MAPK signalling. In order to characterise the signalling and activation of SIM-A9 cells, components of the NF- $\kappa$ B pathway were examined. A representative time course for the degradation of I $\kappa$ B- $\alpha$  and therefore corresponding activation of NF- $\kappa$ B signalling in the presence of LPS is shown in **figure 2.2**. Relative protein expression was calculated by using the total loading volume as a normalisation method. Fold change was calculated as a change compared to the control (dotted line). A significant degradation of I $\kappa$ B- $\alpha$  compared to the control (dotted line) (2-fold change) was observed at 30 and 45 minutes (**figure 2.2**). To validate that this result was due to increased NF- $\kappa$ B signalling, the subsequent phosphorylation of P65 (p-P65) was measured (**figure 2.3**), where there is a significant upregulation of p-P65 after 30 minutes of LPS stimulation (2-fold change), remaining significantly upregulated after 90 minutes, compared to control.

To ensure the optimal concentration of LPS was used, a concentration study was carried out. 10 ng/ml failed to cause significant degradation of I $\kappa$ B- $\alpha$ , whereas, 100 ng/ml significantly activated degradation of I $\kappa$ B- $\alpha$  after 30 and 60 minutes compared to control. A concentration of 1  $\mu$ g/ml LPS produced significant degradation after 15, 30 and 60 minutes (**figure 2.4**). These results corroborate nicely with the phosphorylation of P65, where a concentration of 1  $\mu$ g/ml LPS induced a significant upregulation of p-P65 at 15, 30 and 60 minutes versus control (**figure 2.5**).

The findings from these experiments suggest that LPS successfully induced NF- $\kappa$ B signalling in SIM-A9 microglia cells which was maximum at 30 minutes with 1  $\mu$ g/ml LPS.

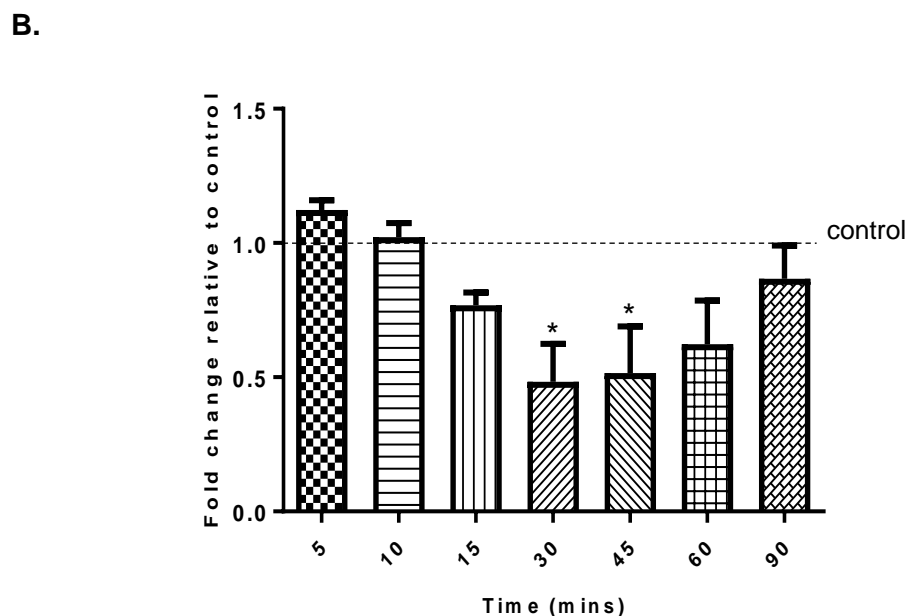
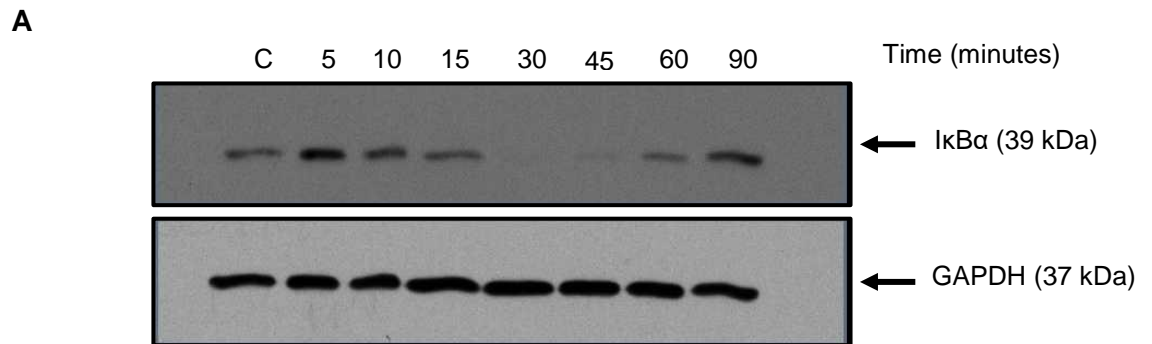


**Figure 2.2. Time dependent LPS-induced IkBα degradation in SIM-A9 microglia cells.** SIM-A9 cells were exposed to LPS (1  $\mu\text{g/ml}$ ) for the indicated periods. IkBα degradation was assessed by immunoblotting and data was normalised against the internal loading control, GAPDH. A representative of one of four immunoblots is shown **(A)**. Densitometric analysis of immunoblots were performed **(B)**, data shown as mean  $\pm$  SEM and are representative of four independent experiments. Data are expressed as fold change in expression vs. control treatment (dashed line). \* $P \leq 0.05$ , versus control. One-way ANOVA, Dunnett's post-test.

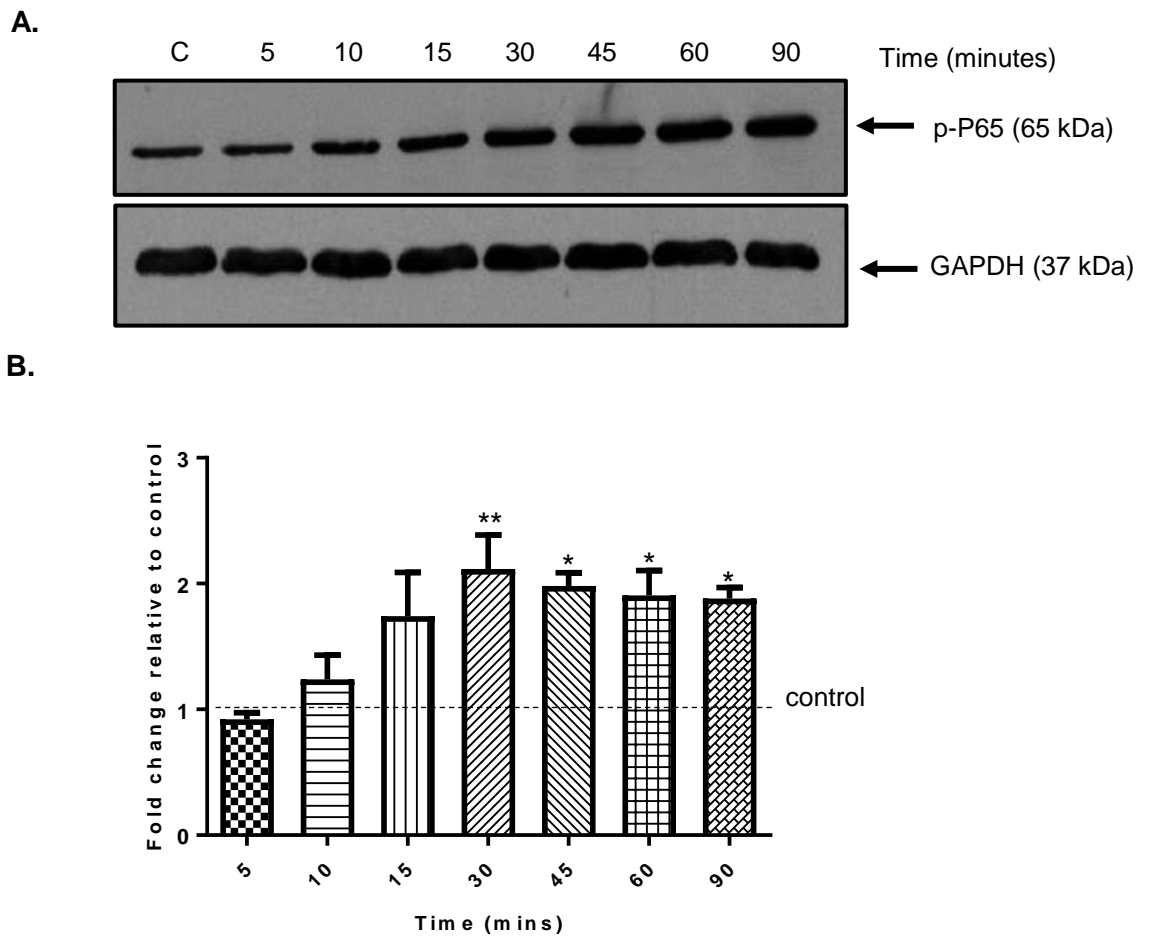


**Figure 2.3. Time dependent LPS-induced P65 phosphorylation in SIM-A9 microglia cells.** SIM-A9 cells were exposed to LPS (1  $\mu\text{g/ml}$ ) for the indicated periods. P65 phosphorylation was assessed by immunoblotting and data was normalised against the internal loading control, GAPDH. A representative of one of three immunoblots is shown **(A)**. Densitometric analysis of immunoblots were performed **(B)**, data shown as mean  $\pm$  SEM and are representative of three independent experiments. Data are expressed as fold change in expression vs. control treatment (dashed line). \* $P \leq 0.05$ , versus control. One-way ANOVA, Dunnett's post-test.

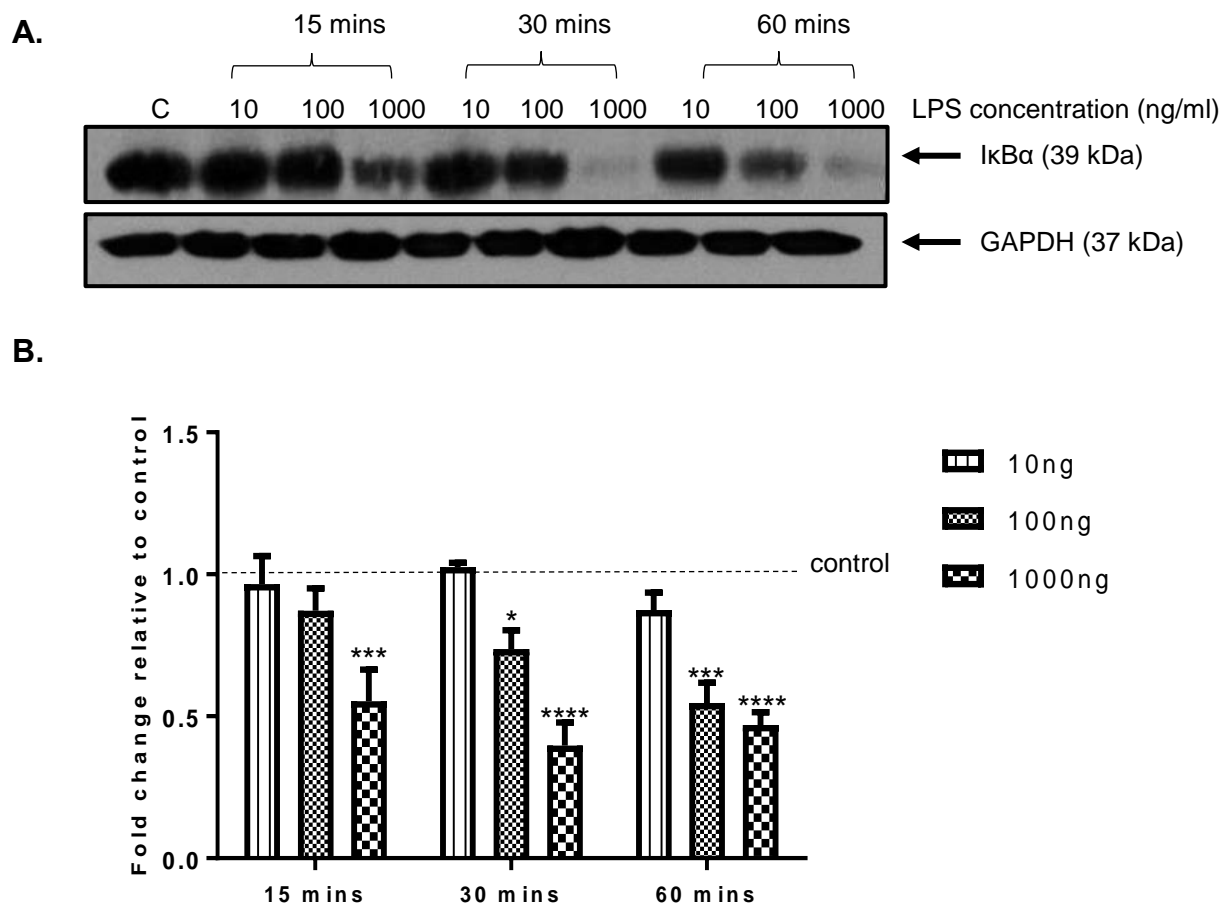


**Figure 2.4. Concentration dependent LPS-induced IkB $\alpha$  degradation in SIM-A9 microglia cells.** SIM-A9 cells were exposed to varying concentrations of LPS (10 ng, 100 ng and 1000 ng/ml) for the indicated periods. IkB $\alpha$  degradation was assessed by immunoblotting and data was normalised against the internal loading control, GAPDH. A representative of one of three immunoblots is shown **(A)**. Densitometric analysis of immunoblots were performed **(B)**, data shown as mean  $\pm$  SEM and are representative of three independent experiments. Data are expressed as fold change in expression vs. control treatment (dashed line). \* $P \leq 0.05$ , \*\* $P \leq 0.01$  \*\*\* $P \leq 0.001$ , \*\*\*\* $P \leq 0.0001$  versus control, Two-way ANOVA, Dunnett's post-test.



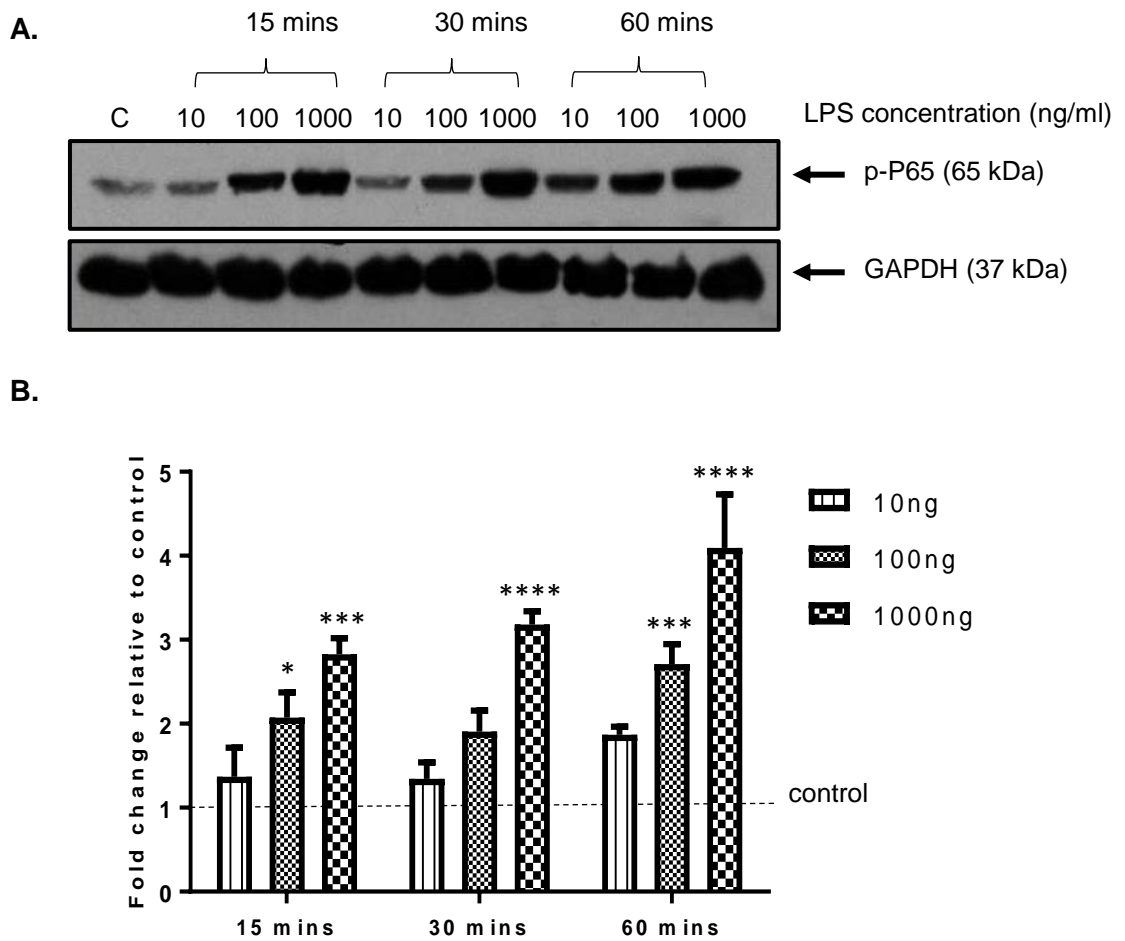
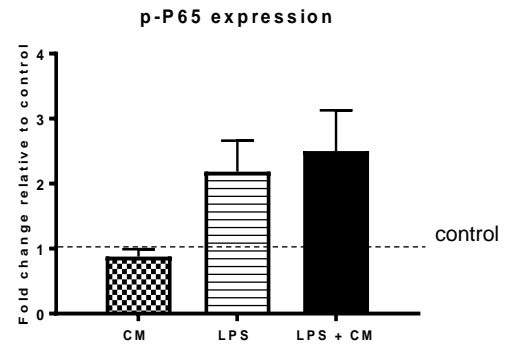
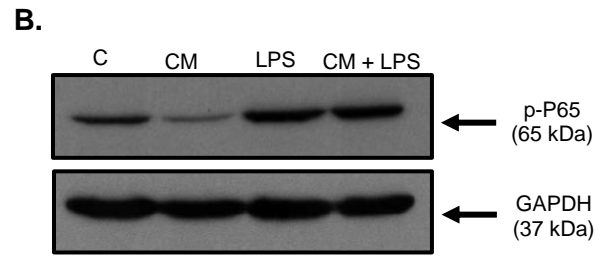
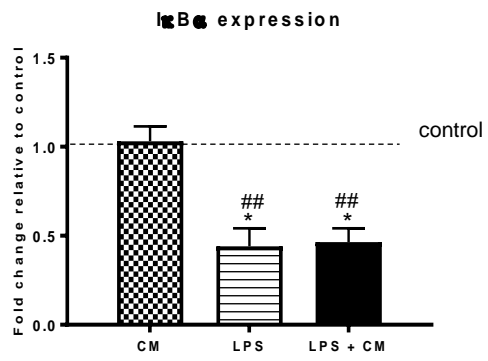
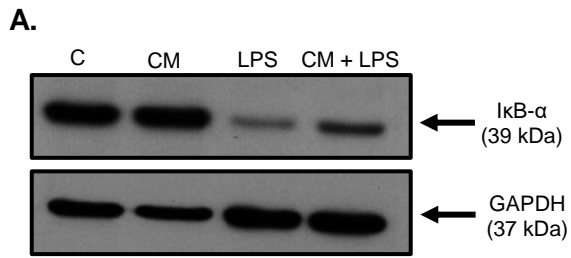


**Figure 2.5. Concentration dependent LPS-induced P65 phosphorylation in SIM-A9 microglia cells.** SIM-A9 cells were exposed to varying concentrations of LPS (10 ng, 100 ng and 1000 ng/ml) for the indicated periods. P65 phosphorylation was assessed by immunoblotting and data was normalised against the internal loading control, GAPDH. A representative of one of three immunoblots is shown **(A)**. Densitometric analysis of immunoblots were performed **(B)**, data shown as mean  $\pm$  SEM and are representative of three independent experiments. Data are expressed as fold change in expression vs. control treatment (dashed line). \* $P \leq 0.05$ , \*\* $P \leq 0.01$  \*\*\* $P \leq 0.001$ , \*\*\*\* $P \leq 0.0001$ , versus control. Two-way ANOVA, Dunnett's post-test.

### **2.3.2 The effect of hAMSC-CM on specific transcription factors expression in microglia**

The potential involvement of hAMSC-CM in modulation of microglia signalling was explored by performing immunoblotting to measure components of the NF- $\kappa$ B and MAPK pathway, as these are commonly found to be associated with inflammation.

An LPS concentration of 1  $\mu$ g/ml and a stimulation time of 30 minutes was chosen for this study; due to the previous study showing that these were the optimal conditions to induce maximal activation of the NF- $\kappa$ B pathway. SIM-A9 microglia were induced with LPS in the last 30 minutes of the 24 hour incubation with hAMSC-CM, giving us four groups in total (control media (control); hAMSC-CM (CM); LPS + control media (LPS); LPS + hAMSC-CM (LPS + CM)). There was a significant degradation of I $\kappa$ B- $\alpha$  in the LPS and LPS + CM treated groups compared to the control and to the CM only group. A one-way ANOVA was carried out between all groups for each signalling component (I $\kappa$ B- $\alpha$ , p-P65, p-ERK and P-JNK) and each test found that there were no significant differences between CM and CM + LPS or between LPS and LPS + CM (**figure 2.6**). Together these results demonstrate that hAMSC-CM had no effect on the NF- $\kappa$ B or MAPK pathway after 30 minutes LPS stimulation.



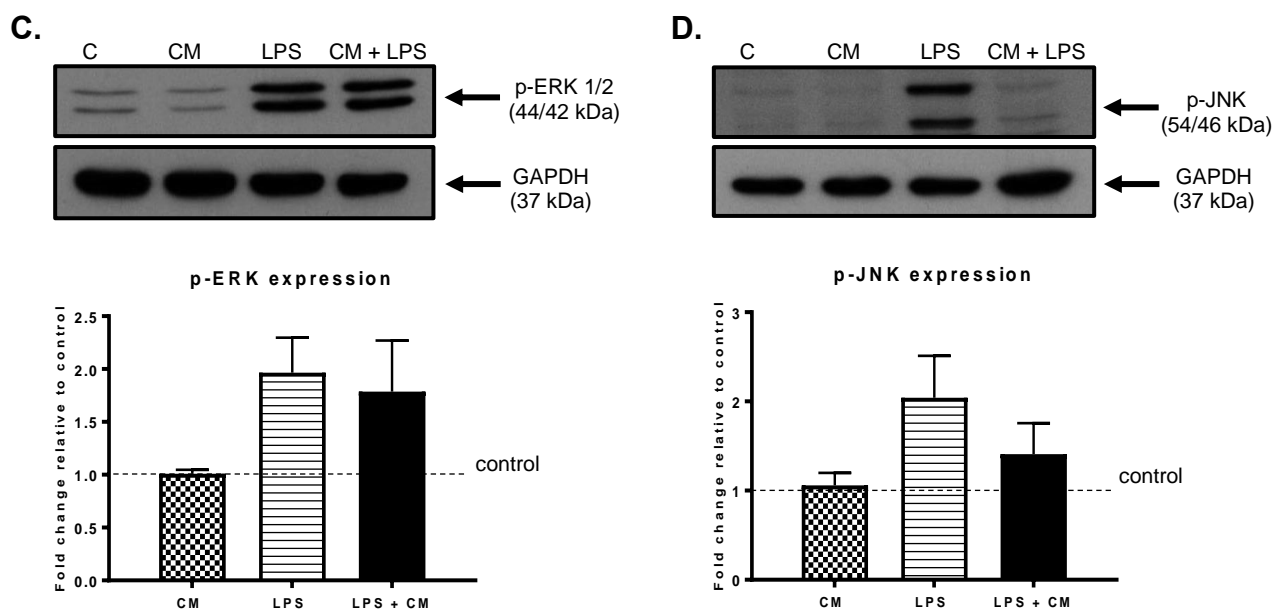


**Figure 2.6. hAMSC-CM had no effect on the NF $\kappa$ B or MAPK pathway in SIM-A9 microglia after 30 minutes of LPS stimulation.** SIM-A9 cells were exposed to either control media (control), hAMSC-CM alone (CM), LPS (1  $\mu$ g/ml) (LPS in control media), or LPS (1  $\mu$ g/ml) + hAMSC-CM (LPS + CM). Control media and hAMSC-CM were applied 24 hours with LPS (1  $\mu$ g/ml) applied in the latter 30 minutes. **(A)** I $\kappa$ B $\alpha$  degradation **(B)** P65 **(C)** ERK and **(D)** JNK phosphorylation was assessed by immunoblotting and data was normalised against the internal loading control, GAPDH. A representative of one of three immunoblots is shown (top). Densitometric analysis of immunoblots were performed (bottom), data shown as mean  $\pm$  SEM and are representative of three independent experiments. \*\*P  $\leq$  0.01 denotes that treatment group is significantly different from the control group, ##P  $\leq$  0.01 denotes that treatment group is significantly different from the CM group. One-way ANOVA, Tukey's post-tests.

### 2.3.3 Validation and characterisation of the polarisation of SIM-A9 microglia

Microglial activation encompasses a wide spectrum of phenotypes and the extremes of this spectrum can be induced *in vitro* by specific stimuli. LPS has been described as a trigger which polarises microglia into a pro-inflammatory state (Orihuela *et al.*, 2016). *Il1 $\beta$*  and *Nos2* (encodes iNOS) are highly associated with a pro-inflammatory state (Orihuela *et al.*, 2015). In the present work, stimulation with LPS (1  $\mu$ g/ml) caused a significant increase in the expression of *Il1 $\beta$*  by approximately 2,500-fold change at 24 hours as measured by qPCR (**figure 2.7(A)**). Expression levels of *NOS2* were also observed to be significantly upregulated by a 1,000-fold change after a 24 hour LPS stimulation but not after 4 hours (**figure 2.7(B)**). In contrast, treatment with IL-4 (20 ng/ml) is associated with inducing an anti-inflammatory phenotype (Orihuela *et al.*, 2016). IL-4 did not affect *Il1 $\beta$*  or *Nos2* expression, however, IL-4 did induce high expression levels (1,000-fold change) of the anti-inflammatory mediator *Arg1* (**figure 2.7(C)**). Thus, SIM-A9 cells are capable of being polarised into pro- and anti-inflammatory phenotypes.

To further validate these results, immunoblotting for detection of the respective proteins was performed. As indicated by the presence of the immunoreactive bands at approximately 125 kDa in the representative blots, **figure 2.8(A)** shows that iNOS was expressed after 4 and 24 hours of LPS stimulation. Densitometric quantification indicated that LPS mediated a significant upregulation of iNOS after 4 hours (2-fold change) increasing further after 24 hours (6-fold change) (**figure 2.8(B)**). Similar experiments were carried out to measure Arg1 protein expression. As shown in **figure 2.9(B)** there were no detectable differences in Arg1 protein expression with LPS or IL-4 stimulation, despite modulation of gene expression after 24 hours of IL-4 stimulation (**figure 2.7(C)**).

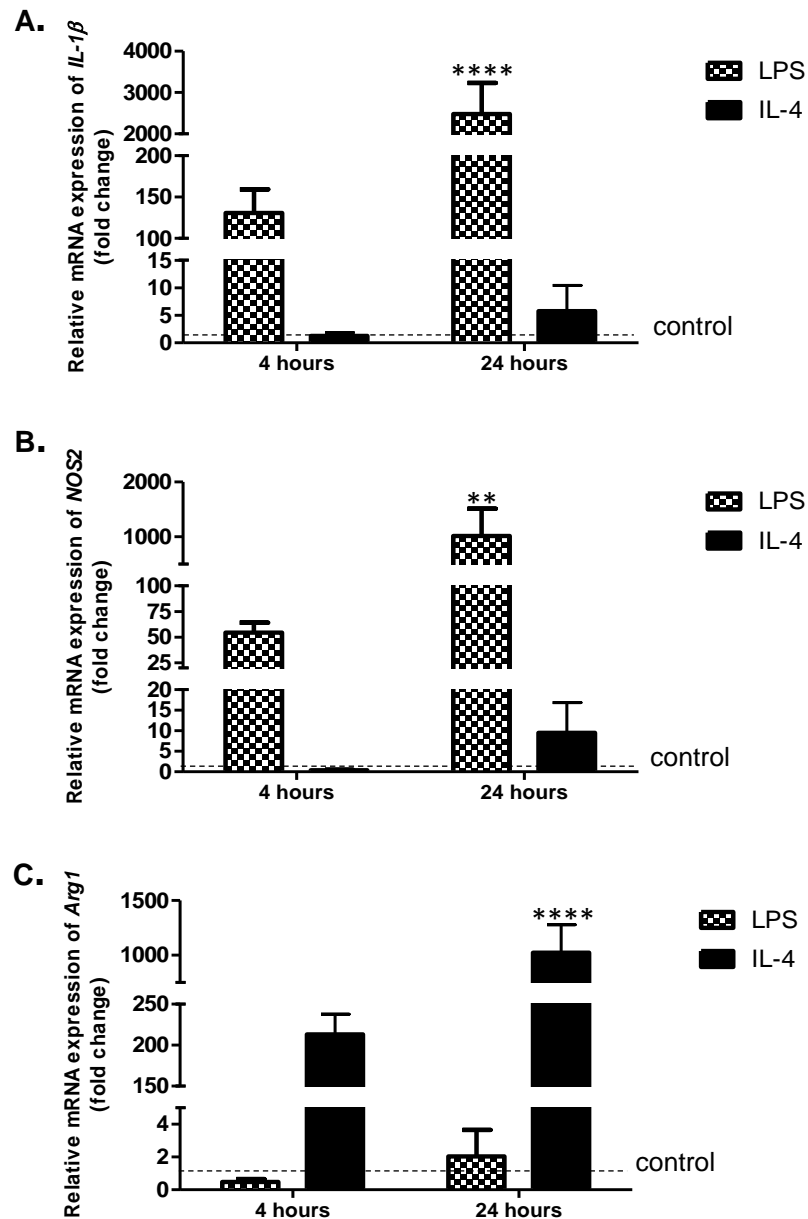
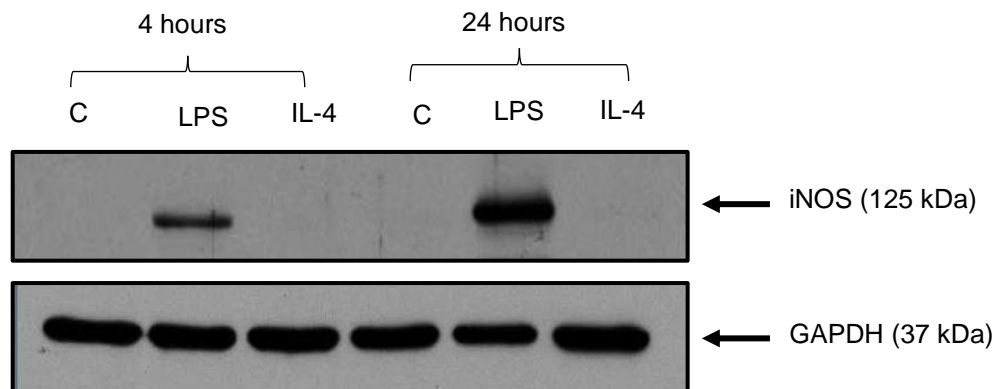


**Figure 2.7. The effect of LPS and IL-4 activation of SIM-A9 microglia cells on *Il1β*, *Nos2* and *Arg1* expression.** SIM-A9 cells were cultured and stimulated for 4 or 24 hours with LPS (1  $\mu\text{g/ml}$ ) or IL-4 (20  $\text{ng/ml}$ ) and gene expression was measured by qPCR for **(A) *Il1β*** **(B) *Nos2*** and **(C) *Arg1***. Relative expression levels of mRNA transcripts were normalised to the appropriate reference gene (*B2m* for LPS, *Sdha* for IL-4) using the  $2^{-\Delta\Delta\text{Ct}}$  method. Data shown as mean  $\pm$  SEM and are representative of four independent experiments. Data are expressed as fold-change in expression vs. relevant time point control treatment (dashed line). \* $P \leq 0.05$ , \*\* $P \leq 0.01$  \*\*\* $P \leq 0.001$ , \*\*\*\* $P \leq 0.0001$ , versus control. Two-way ANOVA, Dunnett's post-test.

A.



B.

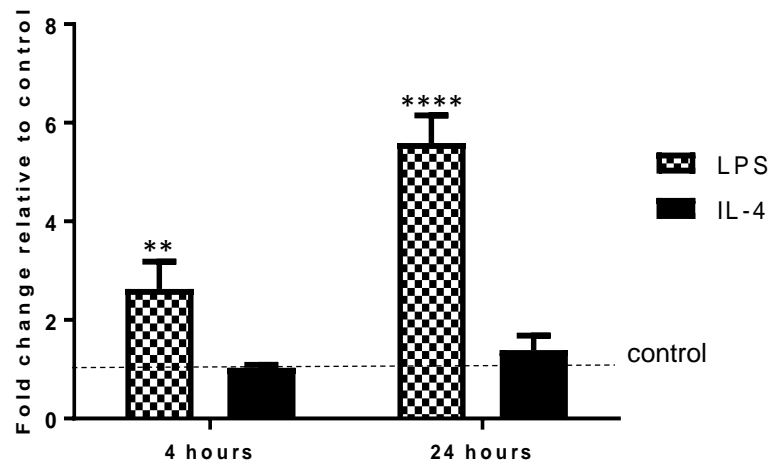


**Figure 2.8. The effect of LPS and IL-4 activation of SIM-A9 microglia cells on iNOS expression.** SIM-A9 cells were cultured and stimulated for 4 or 24 hours with LPS (1  $\mu\text{g/ml}$ ) or IL-4 (20  $\text{ng/ml}$ ). Expression of iNOS was measured by immunoblotting and data was normalised against the internal loading control, GAPDH. A representative of one of four immunoblots are shown (A). Densitometric analysis of immunoblots were performed (B), data shown as mean  $\pm$  SEM and are representative of four independent experiments. Data are expressed as fold change in expression vs. relevant time point control treatment (dashed line). \* $P \leq 0.05$ , \*\* $P \leq 0.01$  \*\*\* $P \leq 0.001$ , \*\*\*\* $P \leq 0.0001$ , versus control. Two-way ANOVA, Dunnett's post-test.

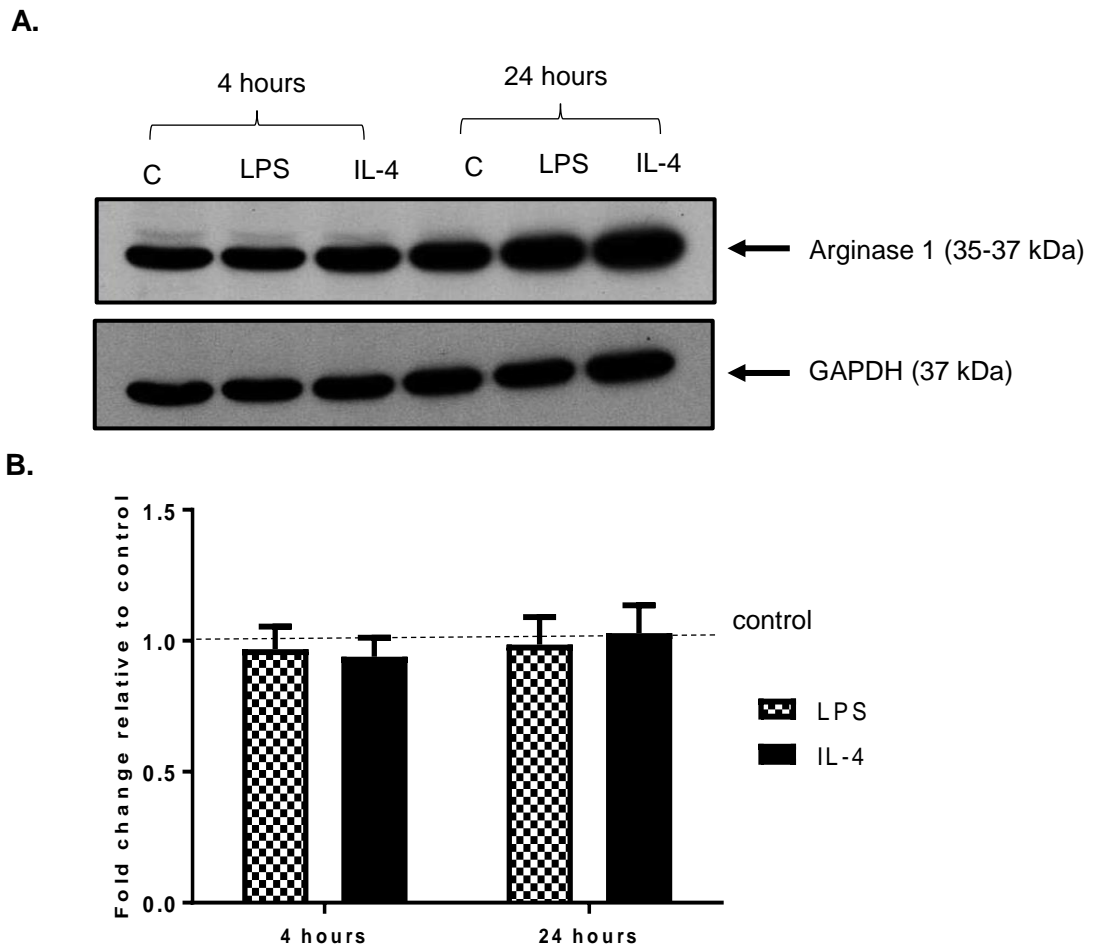


**Figure 2.9. The effect of LPS and IL-4 activation of SIM-A9 microglia cells on Arginase 1 expression.** SIM-A9 cells were cultured and stimulated for 4 or 24 hours with LPS (1  $\mu\text{g}/\text{ml}$ ) or IL-4 (20  $\text{ng}/\text{ml}$ ). Expression of Arginase 1 was measured by immunoblotting and data was normalised against the internal loading control, GAPDH. A representative of one of four immunoblots are shown **(A)**. Densitometric analysis of immunoblots were performed **(B)**, data shown as mean  $\pm$  SEM and are representative of four independent experiments. Data are expressed as fold change in expression vs. relevant time point control treatment (dashed line). Two-way ANOVA, Dunnett's post-test, data not significant.



Activated microglia produce an increased amount of NO (Shen *et al.*, 2005), thus NO secretion by SIM-A9 cells was investigated. Levels of nitrite were undetectable at 4 and 24 hours in control treated cells. Application of LPS significantly increased NO production ( $0.76 \pm 0.33$  vs  $19.62 \pm 3.71$ ) after 24 hours (**figure 2.10**) but not at 4 hours whereas IL-4 had no effect at either time point.

Taken together, these results suggest that SIM-A9 microglia can be activated and produce key inflammatory mediators.

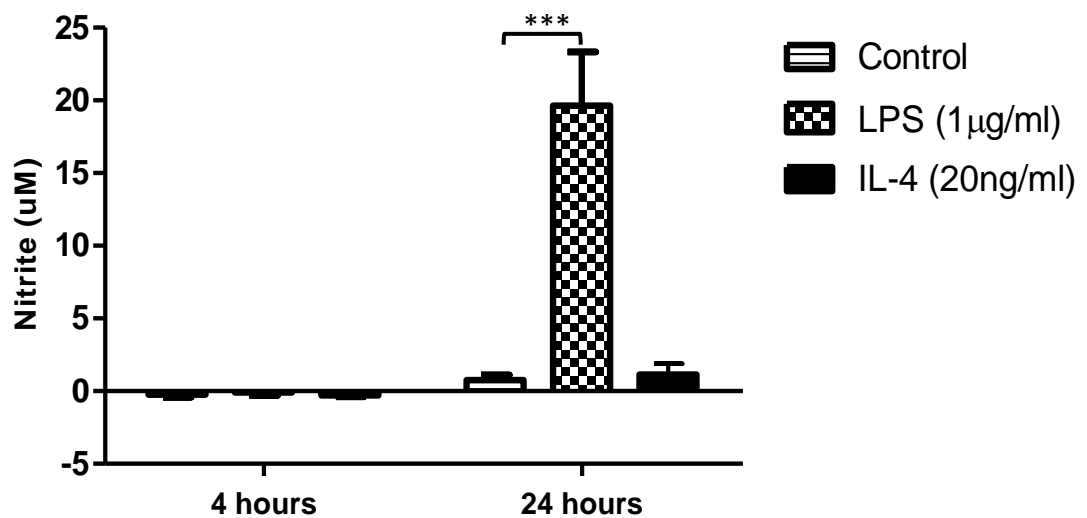


**Figure 2.10. The effect of LPS and IL-4 activation of SIM-A9 microglia cells on nitrite production.** SIM-A9 cells were cultured and stimulated for 4 or 24 hours with LPS (1 µg/ml) or IL-4 (20 ng/ml). Nitrite concentration was determined using the Griess assay. Data shown as mean  $\pm$  SEM of triplicate wells in a 96-well plate and are representative of six independent experiments. \*\*\* $P < 0.001$ , versus control. Two-way ANOVA, Dunnett's post-test.

### 2.3.4 hAMSC-CM promotes anti-inflammatory properties in microglia while dampening the pro-inflammatory properties

Given that SIM-A9 microglia activation is associated with altered expression of cytokines and mediators, the next step was to establish the effects of hAMSC-CM on microglial expression of pro- and anti-inflammatory cytokines. Upon confirming that *I11β*, *Nos2* and *Arg1* in SIM-A9 cells was significantly upregulated at the 24 hour time point, the effects of hAMSC-CM were examined.

The addition of hAMSC-CM significantly reduced mRNA expression of *I11β*, *Tnfa*, *Ccl2* in LPS induced microglia (**figure 2.11**). *I11β* mRNA levels were significantly reduced with the addition of hAMSC-CM decreasing levels from  $12.59 \pm 4.09$  in LPS alone samples down to  $2.25 \pm 0.94$  in the presence of hAMSC-CM (**figure 2.11(A)**). Similar effects were observed on *Tnfa* ( $2.106 \pm 0.46$  vs  $0.37 \pm 0.51$ ) (**figure 2.11(B)**) and *Ccl2* ( $2.29 \pm 0.17$  vs  $0.71 \pm 0.69$ ) (**figure 2.11(C)**). There was a trend to decreased levels of *Nos2* in the presence of hAMSC-CM compared to LPS alone, however results were not statistically significant (**figure 2.11(D)**). **Figure 2.11(E)** shows the effect of hAMSC-CM on the anti-inflammatory mediator *Arg1*, hAMSC-CM alone appears to induce expression which is significantly decreased upon LPS application. There was a slight increase in *Arg1* expression in the LPS + CM group, compared to LPS alone, however, a one-way ANOVA failed to find any significant differences between groups.

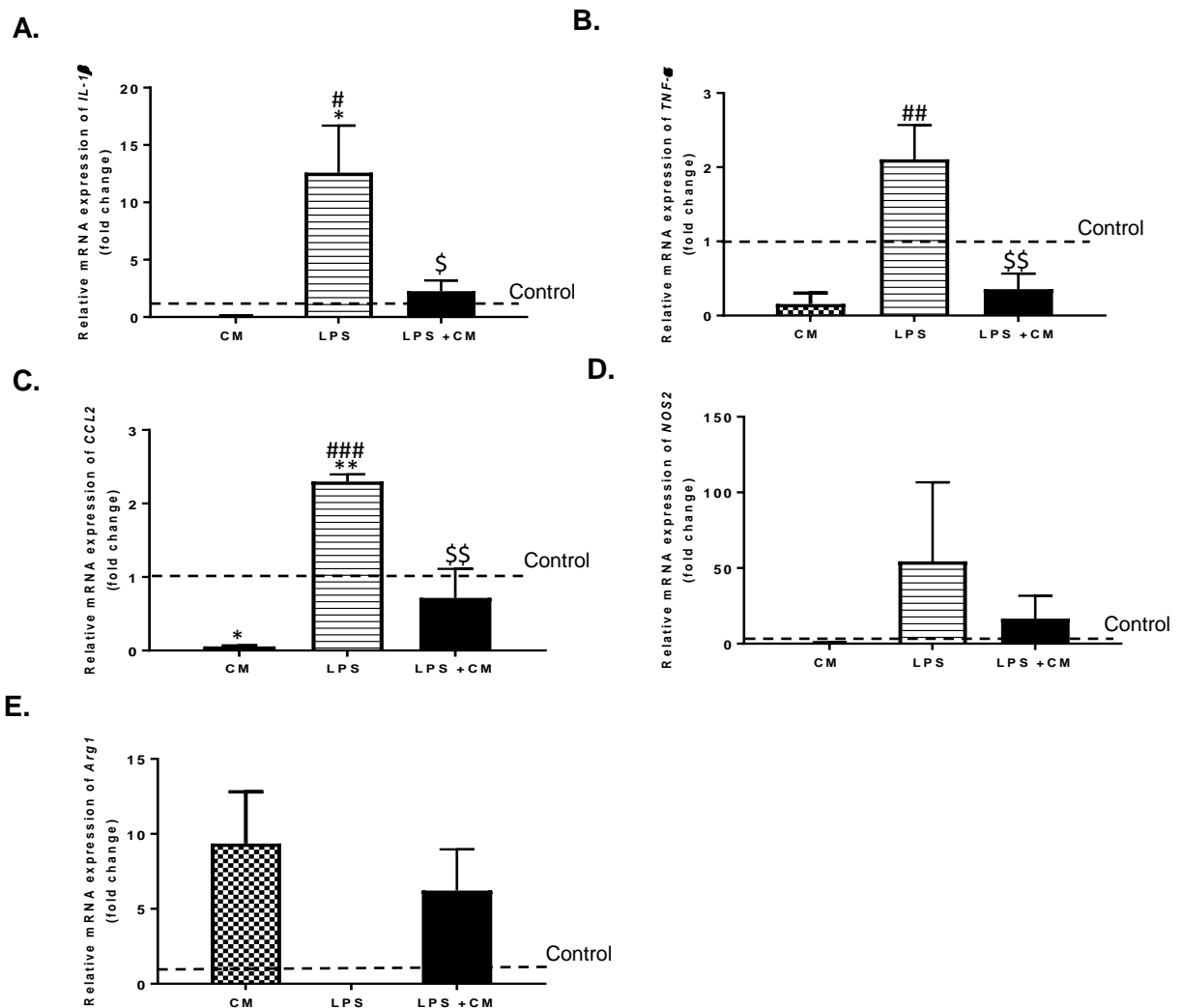


**Figure 2.11. The effect of hAMSC-CM on *Il1 $\beta$* , *Tnfa*, *Nos2*, *Ccl2* and *Arg1* expression in SIM-A9 microglia cells.** SIM-A9 cells were cultured for 24 hours with either control media (control), hAMSC-CM alone (CM), LPS (1  $\mu$ g/ml) (LPS in control media), or LPS (1  $\mu$ g/ml) + hAMSC-CM (LPS + CM) and gene expression was measured by qPCR for **(A)** *Il1 $\beta$* , **(B)** *Tnfa*, **(C)** *Ccl2* **(D)** *Nos2*, and **(E)** *Arg1*. Relative expression levels of mRNA transcripts were normalised to the appropriate reference gene (*B2M*) using the  $2^{-\Delta\Delta Ct}$  method. Data shown as mean  $\pm$  SEM and are representative of three independent experiments. Data are expressed as fold-change in expression vs. control media (dashed line). \* $P \leq 0.05$ , \*\* $P \leq 0.01$  denotes that treatment group is significantly different from the control group, # $P \leq 0.05$ , ### $P \leq 0.01$  denotes that treatment group is significantly different from the CM group, \$\$\$ $P \leq 0.001$ , \$\$\$ $P \leq 0.001$  denotes that the treatment group is significantly different from the LPS group. One-way ANOVA, Tukey's post-test.

To further characterise the phenotype of SIM-A9 cell and investigate the effect of hAMSC-CM, cells were imaged 24 hours post CM/LPS treatment. Due to the experimental limitation owing to a lower cell number being required to assess morphology, **figure 2.12** is a representative of one experiment which means limited conclusions can be drawn. From observation, it appears that, as expected from the literature (Kloss *et al.*, 2001), LPS treatment triggered microglia to change into the pro-inflammatory round amoeboid shape. Co-treatment with CM + LPS appeared to reduce the number of cells exhibiting an amoeboid shape, and appeared to increase the number of cells in the ramified shape with many cells possessing branches. Further experiments and quantitative analysis are required before any conclusions can be drawn.

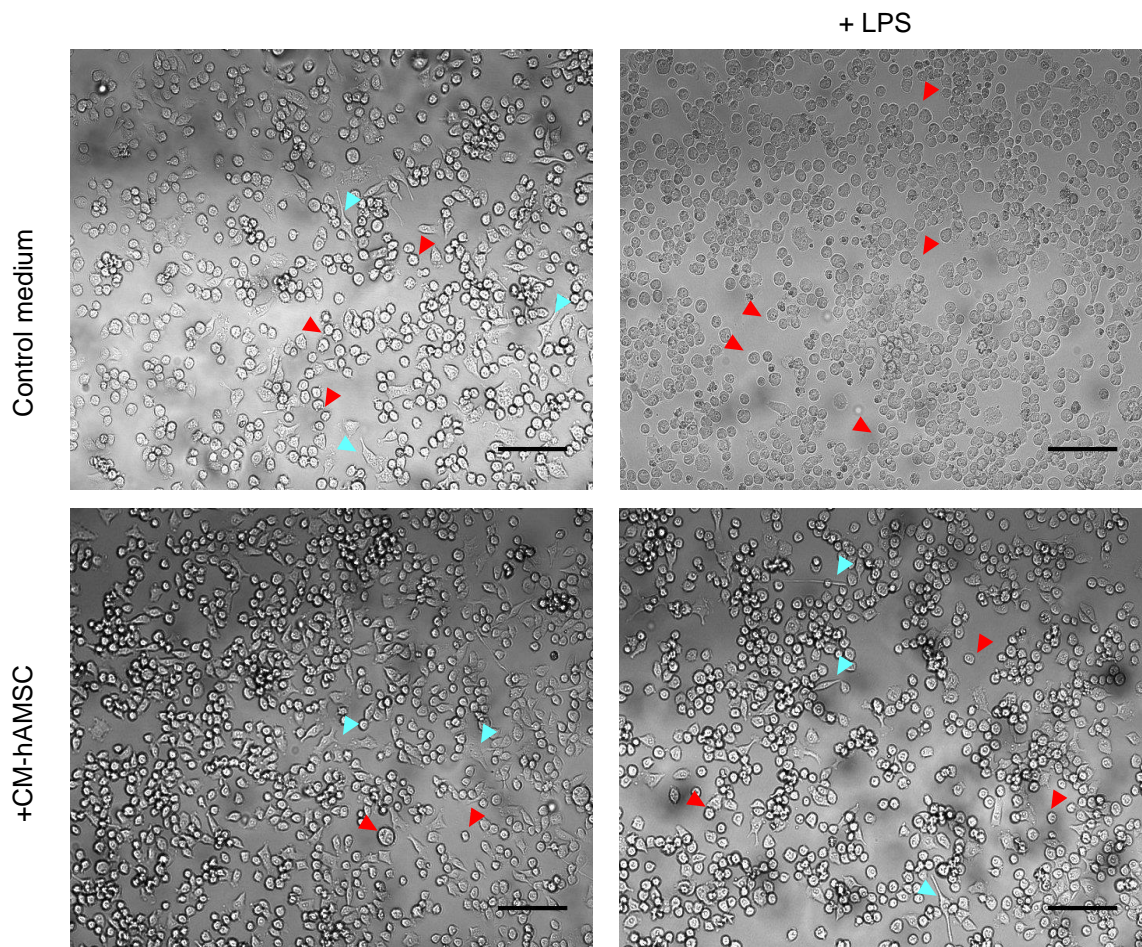


**Figure 2.12. The effect of hAMSC-CM and LPS on the morphology of SIM-A9 microglia cells.** Bright field images show the morphology of SIM-A9 cells after 24 hours exposure to either control media (neurobasal media), hAMSC-CM alone, LPS (1  $\mu\text{g/ml}$ ) (LPS in control media), or LPS (1  $\mu\text{g/ml}$ ) + hAMSC-CM. Photographs are representative of one independent experiment. Scale bars, 50  $\mu\text{m}$ . Red arrow heads indicate examples of amoeboid shaped microglia while blue arrow heads represent ramified microglia.

Nitrite secretions by SIM-A9 cells in the presence of LPS and hAMSC-CM was elucidated. LPS-induced SIM-A9 cells were incubated in hAMSC-CM + LPS for 24 hours to investigate the effects of hAMSC-CM on NO production. There was a slight decrease in NO secretions in LPS + hAMSC-CM versus LPS in control media ( $16.4 \pm 9.22$  vs  $26.11 \pm 5.65$   $\mu\text{M}$ , respectively), however, this failed to reach statistical significance (figure 2.13).

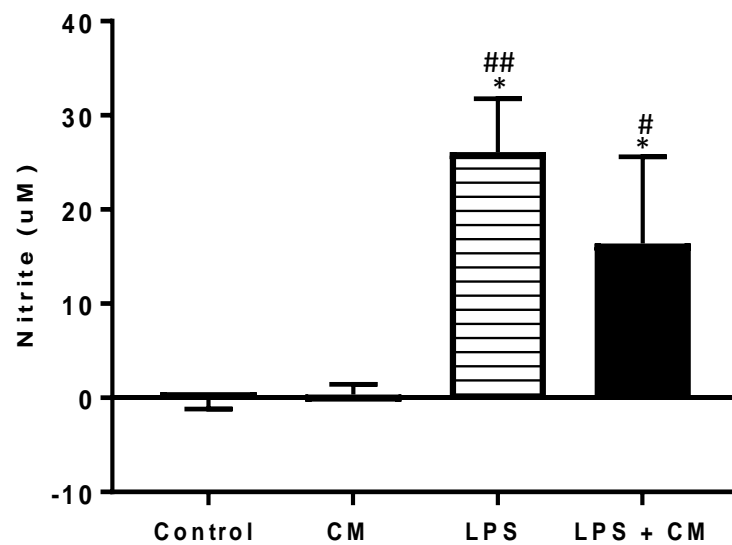


**Figure 2.13. The effect of hAMSC-CM on nitrite production in SIM-A9 microglia cells.** SIM-A9 cells were exposed to either control media (neurobasal media), hAMSC-CM alone, LPS (1  $\mu\text{g}/\text{ml}$ ) (LPS in control media), or LPS (1  $\mu\text{g}/\text{ml}$ ) + hAMSC-CM for 24 hours. Nitrite concentration was determined using the Griess assay. Data shown as mean  $\pm$  SEM of the average of triplicate wells in a 96-well plate per individual experiment and are representative of three independent experiments. \* $P \leq 0.05$ , denotes that treatment group is significantly different from the control group, # $P \leq 0.05$ , ## $P \leq 0.01$  denotes that treatment group is significantly different from the hAMSC-CM group. One-way ANOVA, Tukey's post-test.

To investigate the secretions released from SIM-A9 cells in the presence of LPS ± CM, the supernatant was collected and a cytokine proteome profiler was carried out in order to examine an array of cytokines and mediators. From the representative membranes (**figure 2.14**), hAMSC-CM appeared to decrease GM-CSF, IL-1 $\alpha$  and TNF- $\alpha$  compared to LPS stimulation alone. IL-10 expression which was non-detectable after LPS stimulation, appeared to be slightly expressed in the presence of LPS + CM. **Figure 2.15** shows the quantification of three independent experiments, in accordance with the representative immunoblot, in the presence of hAMSC-CM with LPS there was a reduction of GM-CSF ( $16.72 \pm 7.37$  to  $0.79 \pm 0.26$ ) and TNF- $\alpha$  ( $3.67 \pm 1.62$  to  $1.95 \pm 0.54$ ) (LPS vs CM +LPS, respectively), however there were no significant differences. hAMSC-CM + LPS appeared to slightly increase levels of IL-10 when compared to LPS ( $0.67 \pm 0.22$  vs  $2.39 \pm 1.29$ , LPS vs LPS + CM, respectively), however there were no significant differences between treatment groups for any of the inflammatory mediators.

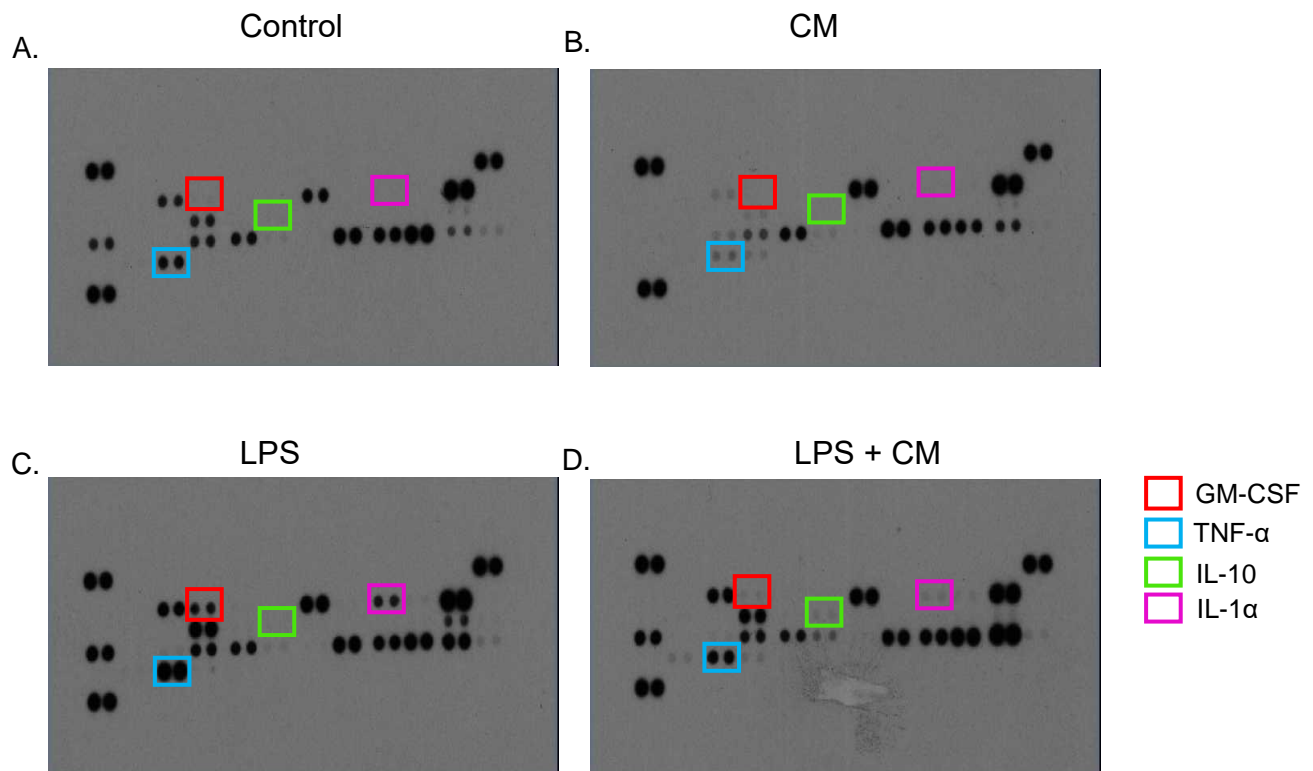


**Figure 2.14. The effect of hAMSC-CM on pro- and anti-inflammatory mediators in SIM-A9 cell lysates.** SIM-A9 cells were cultured for 24 hours with either control media (neurobasal media), hAMSC-CM alone, LPS (1  $\mu\text{g/ml}$ ) (LPS in control media), or LPS (1  $\mu\text{g/ml}$ ) + hAMSC-CM. Cell lysates were extracted and analysed using the Proteome Profiler Mouse Cytokine Array from R&D Systems®. A representative immunoblot for each treatment (A) control, (B) CM, (C) LPS, and (D) LPS + CM is shown. Blots are representative of three independent experiments. Highlighted boxes indicate mediators with the greatest change.



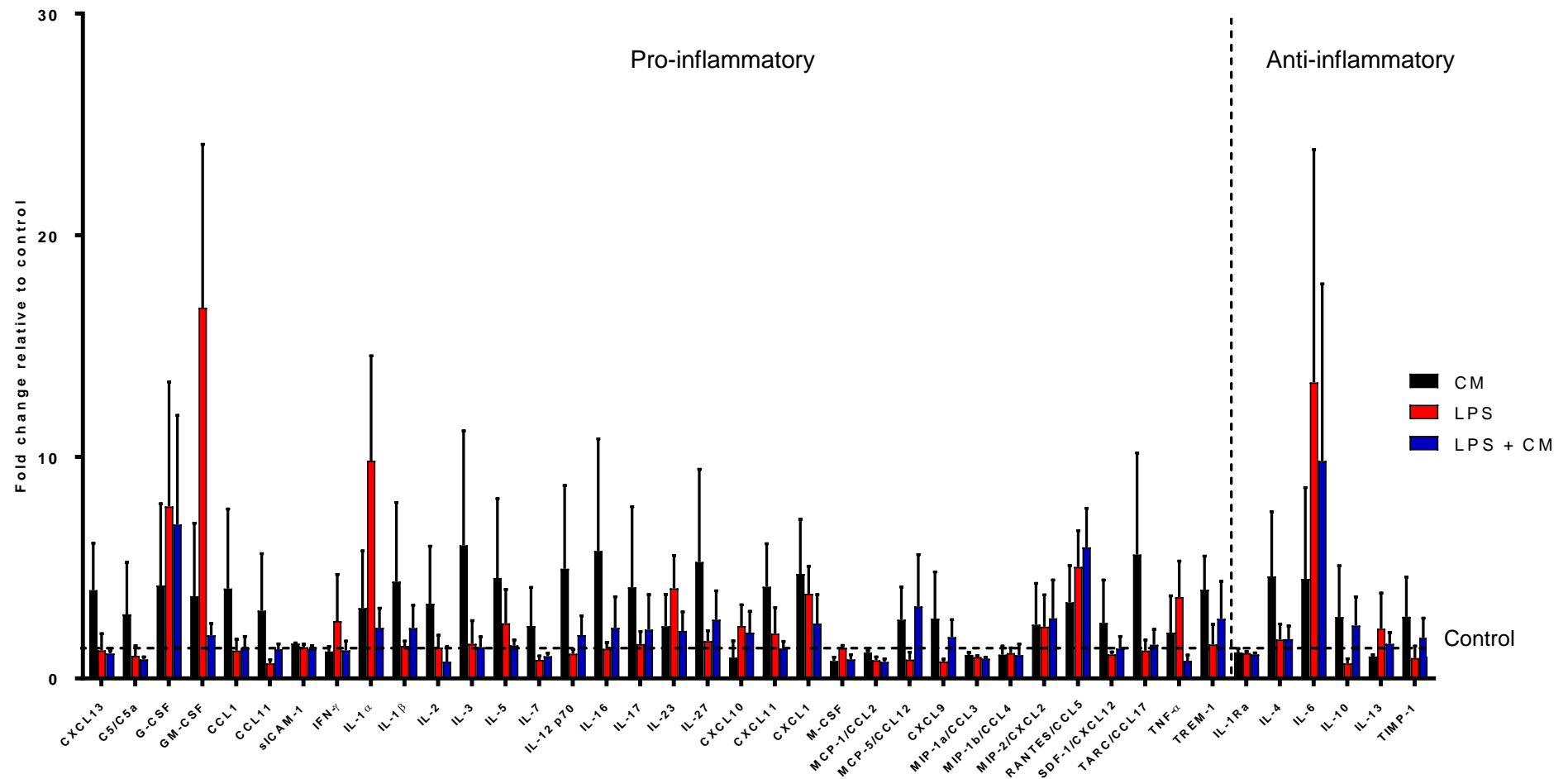


**Figure 2.15. Quantification of Proteome Profiler Mouse Cytokine Array.** SIM-A9 cells were cultured for 24 hours with either control media (neurobasal media), hAMSC-CM alone, LPS (1  $\mu\text{g/ml}$ ) (LPS in control media), or LPS (1  $\mu\text{g/ml}$ ) + hAMSC-CM. Cell supernatants were extracted and analysed using the Proteome Profiler Mouse Cytokine Array from R&D Systems®. Densitometric analysis of immunoblots were performed and spot intensities from the blots in **Figure 2.14** were quantified using image J. Data shown as mean  $\pm$  SEM and are representative of three independent experiments. Data are expressed as fold change in expression vs. control treatment (dashed line). One-way ANOVA, Tukey's post-tests, results failed to reach significance.

### 2.3.5 Establishment of primary microglia cell isolation and culture

An overview and summary of each microglia isolation protocol attempted and the results of each one is shown in **Table 2.4**.

#### 2.3.5.1 Protocol 1. The shaking method

##### Isolation and culture of murine microglia cells via enzymatic digestion

The 'shaking' method was developed in 1986 (Giulian and Baker, 1986) to harvest microglia by exploiting their differential adhesion properties with astrocytes. It involves establishing a mixed glial culture which is subsequently agitated in an orbital incubator shaker to remove the adherent microglia. The appeal of starting with this protocol was due to its simplicity, lack of specialised equipment and its common use in microglia research. **Figure 2.16** shows a representative FACS experiment where we investigated the population of CD11b<sup>+</sup> cells, on average there was a 30% CD11b<sup>+</sup> cells, indicating a poor cell purity.

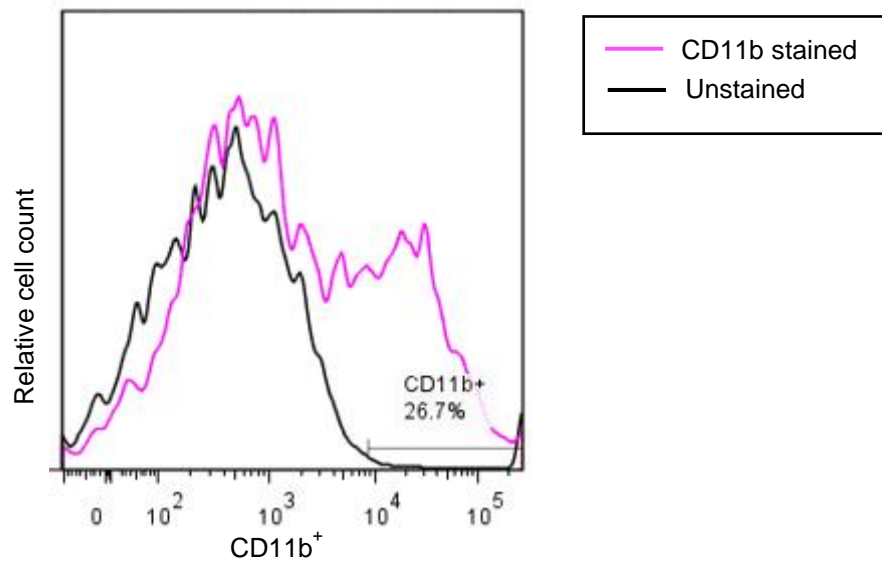


**Figure 2.16. Flow cytometry analysis of extracted microglia from a neonatal mouse brain using the shaking method (Protocol 1).** Overlay of unstained (black) and CD11b purified stained samples shows a poor enrichment of CD11b<sup>+</sup> cells using the shaking method 1 from **Table 2.4**. Representative of 3 independent microglia extractions.

Protocol number	Method of isolation	Adult/neonates	Rationale	Average purity	Problems	Troubleshooting	No. of attempts
(1)	Shaking method (Chen <i>et al.</i> , 2013)	Neonates	Most commonly used method of isolation	30%	Low microglia yield, low purity	<ul style="list-style-type: none"> <li>• PDL as an alternative to PLL</li> <li>• Longer shaking duration</li> <li>• Higher pup number</li> </ul>	3
(2)	Percoll gradient and CD11b magnetic microbeads (Grabert <i>et al.</i> , 2016)	Adults	Proven to result in high purity, adult microglia more relevant to study	80%	Poor culturing of cells, poor viability in conventional culture and microfluidic devices	<ul style="list-style-type: none"> <li>• DMEM/F12 media</li> <li>• Perfusion rate of 10ml/min instead of 5ml/min</li> <li>• P-L-L for coating</li> <li>• Use of individual columns per brain</li> <li>• Addition of + M-CSF (50ng/ml) into cultures</li> <li>• Plating cells at a higher density- <math>2.5 \times 10^5</math></li> </ul>	9
(3)	Shaking dissociation method and CD11b magnetic microbeads (Marek <i>et al.</i> , 2008)	Neonates	The shaking dissociation method produced viable culturing of cells, the CD11b magnetic microbeads produced high purity	30%	Poor purity	N/A	1
(4)	Dissociation kit, tissue homogeniser and CD11b magnetic microbeads (Harms and Tansey., 2010)	Neonates	Gentle but rapid and efficient protocol	35%	Poor viability, low purity	<ul style="list-style-type: none"> <li>• Susan Barton, Scientific support specialist from Miltenyi Biotec visited lab to oversee the technique</li> </ul>	4

**Table 2.4. Experimental protocols used for microglia isolations and the rationale, and result from each protocol.**

### 2.3.5.2 Protocol 2. Percoll gradient and CD11b Magnetic beads

We next moved on to a more recent evolved technical method, which was based on a protocol from Cardona *et al* (2006a). The protocol used in these experiments were an adapted version of the extraction by Kathleen Grabert, McColl lab (Grabert *et al.*, 2016). This technique utilises a Percoll gradient to produce a myelin-free mixed cell homogenate. Magnetic bead separation utilises anti-CD11b magnetic microbeads to bind CD11b microglia and separate microglia from the remaining brain cells using a magnetic column. To monitor the efficiency of the magnetic bead isolation, three samples were collected; 1) Pre-sort fraction (the original mixed brain cell suspension), 2) Non-selected fraction (the negative, flow-through, non-microglia) and 3) Positive selection (microglia). **Figure 2.17** displays the changes in CD11b<sup>+</sup> expression throughout the different stages of the extraction process. The pre-sort (black) contained a mix of cells within the brain and therefore showed two cell populations. Approximately an average of 80% of the brain suspension was CD11b<sup>+</sup> population. In comparison, the negative flow-through cell population retained after separation showed less than 5% CD11b<sup>+</sup> cells, indicating that the vast majority of microglia were linked with magnetic beads and were retained in the magnetic column. Positive selected samples displayed a clear CD11b<sup>+</sup> profile, showing an average microglia purity of 80%. In our hands, the issues with this technique occurred during culturing of the cells. **Figure 2.17(C)** shows the poor culturing of the CD11b<sup>+</sup> cells, the top and bottom left hand images reveals the small round cells and debris 3 days after isolation. A zoomed in image on the right-hand side of figure shows a small patch of cells which look like successfully cultured microglia cells. These patches of healthy cells were however, very sparse. Several conditions were altered in effort to try and improve the culturing of the cells, this included plating cells at a higher density, adding macrophage colony stimulating factor (M-CSF) as well as trying different coatings (**table 2.4**).

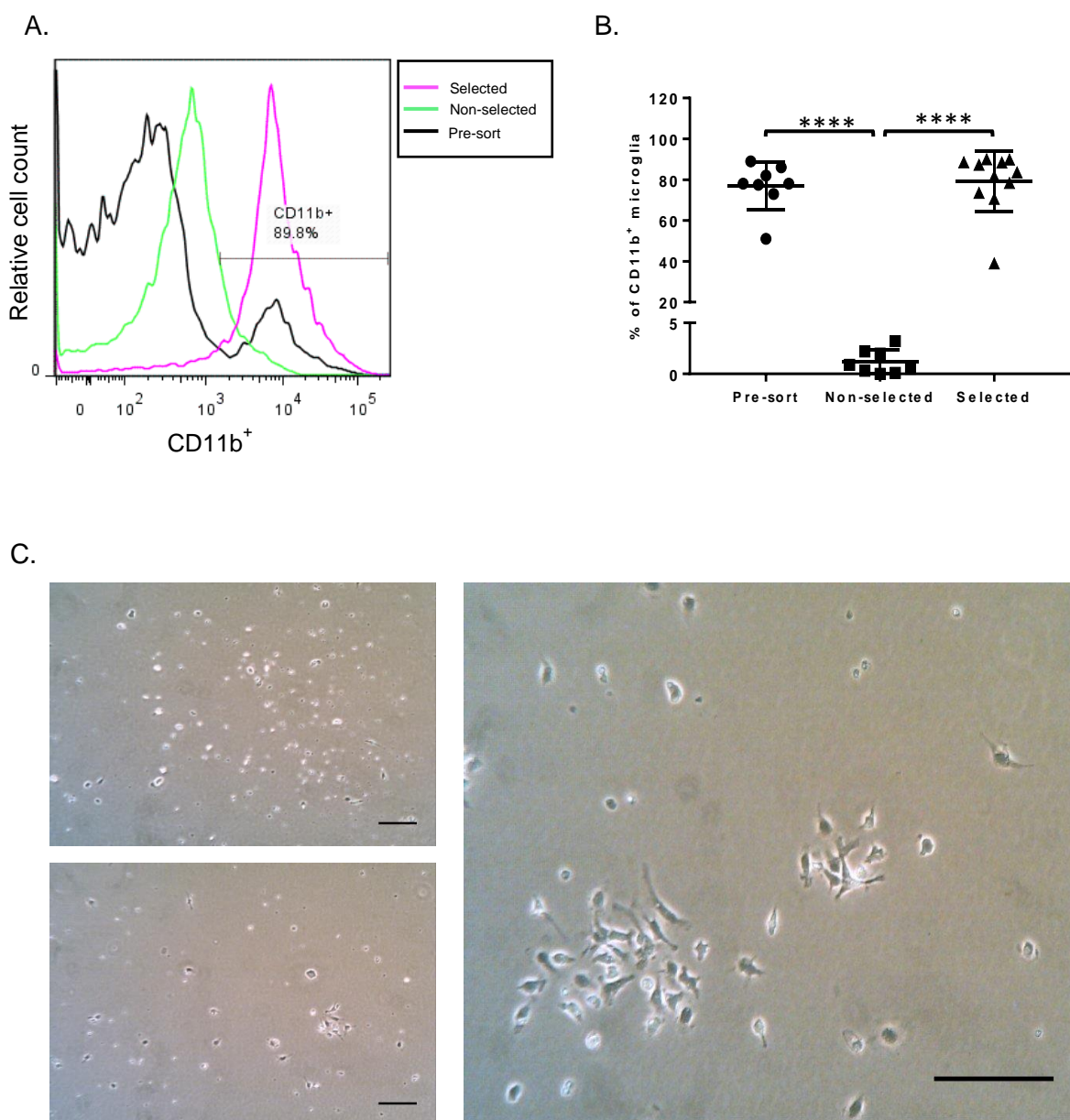


**Figure 2.17. Flow cytometry analysis and images of extracted microglia from an adult mouse brain using a Percoll gradient and CD11b magnetic beads (Protocol 2).** (A) Overlay of pre-sort (black), non-selected (green) and positive selected (pink) samples. (B) Positive selection post bead separation shows greater than 80% enrichment of CD11b<sup>+</sup> cells. Non-selected fraction displays minimal loss of <5%. (C) Shows CD11b<sup>+</sup> microglia cells at day 3 in culture, scale bars 50  $\mu$ m. Data shown as mean  $\pm$  SEM and are representative of nine independent experiments. \*\*\*\*P  $\leq$  0.0001, One-way ANOVA, Tukey's post-test.

### 2.3.5.3 Protocol 3: Shaking dissociation and CD11b magnetic microbeads

The cells from protocol 1 cultured successfully, and the extraction process of protocol 2 yielded a high microglia purity, so we next decided to combine these methods. As shown in **figure 2.18** the cells appeared to be healthy and grow in culture, however, FACS analysis revealed a poor CD11b<sup>+</sup> enrichment of 30% (data not shown).

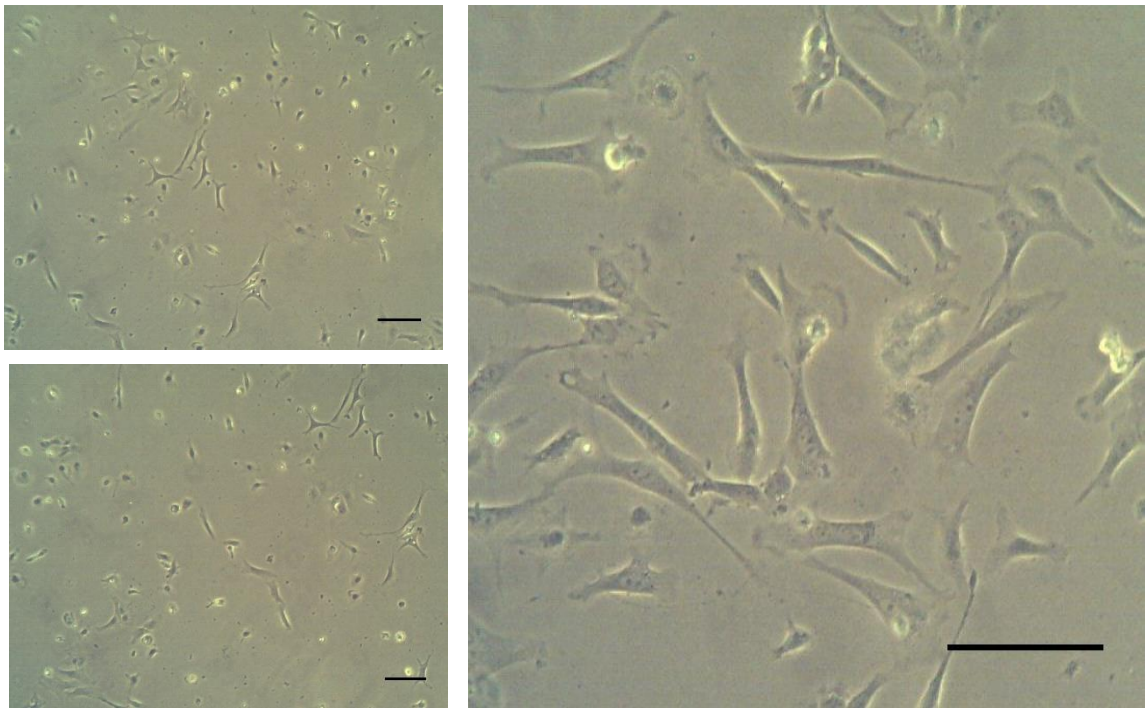


**Figure 2.18. Images of extracted microglia from a neonatal mouse at day 3 in culture using the shaking method + CD11b magnetic beads (Protocol 3). Scale bars 50  $\mu$ M.**

#### 2.3.5.4 Protocol 4: Neural Tissue Dissociation kit, GentleMACS™ and CD11b magnetic microbeads

Finally, we used a neural dissociation kit, this protocol and kit has been commercialised and therefore guaranteed to produce successful microglia cultures with a high CD11b<sup>+</sup> cell population. In our hands however, a low purity of 35% was observed (**figure 2.19**).

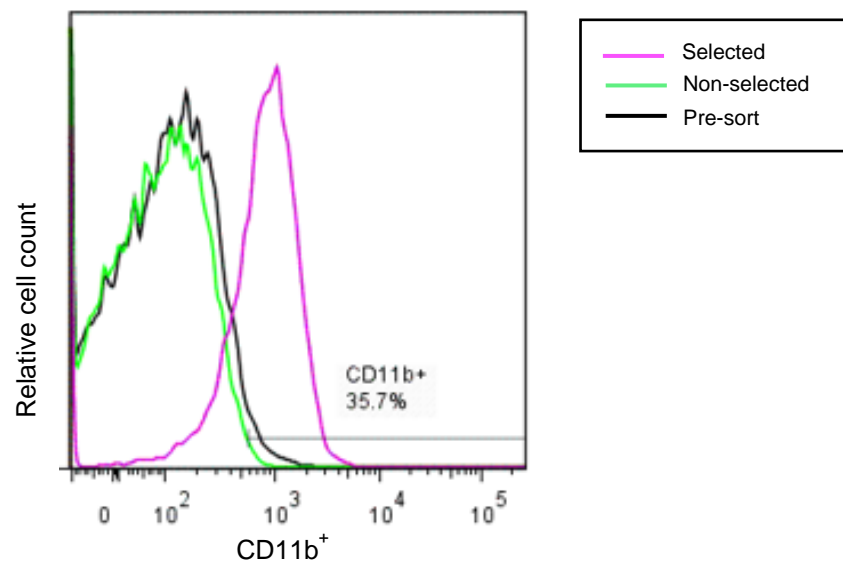


**Figure 2.19.** Flow cytometry analysis of extracted microglia from a neonatal mouse brain using the tissue dissociation kit and CD11b<sup>+</sup> magnetic beads (**Protocol 4**). Overlay of pre-sort (black), non-selected (green) and positive selected (pink) samples shows a poor enrichment of CD11b<sup>+</sup>. Representative of 4 independent microglia extractions.

## **2.4 Discussion**

The aims of this chapter were to characterise the signalling and polarisation of SIM-A9 microglia cell line and investigate the effects of hAMSC-CM and establish a protocol for primary microglia isolation.

### **2.4.1 Characterisation of the signalling of SIM-A9 microglia cell line**

Several microglia cell lines have been established via a viral vector transfection or by genetic inductions including murine BV-2, N9, MG5, EOC, HAPI and human HM06 lines (Nagai *et al.*, 2001; Stansley *et al.*, 2012). The first spontaneous immortalised microglial cell line from mouse cerebral tissue (SIM-A9) was established by Nagamoto-Combs *et al.* at the University of North Dakota, School of Medicine and Health Sciences (Nagamoto-Combs *et al.*, 2014). SIM-A9 cells are a relatively novel cell line, but emerging papers report use of the SIM-A9 cell line for various functions (Goloviznina *et al.*, 2016; McDonald *et al.*, 2016; Hung *et al.*, 2017; Krasnow *et al.*, 2017) including research involving post-ischaemic inflammation (Alhadidi and Shah, 2017). Interestingly, a recent paper reportedly used SIM-A9 cells to investigate microglia/stem cell interactions. The group used the microglia cell line to investigate the effects of activated microglia on neural stem cell (NSC) phenotype and fate in the transplanted brain (Farrell *et al.*, 2016). This reverse interaction is by note a very important and interesting point to consider; the microenvironment that microglia create and its impact on stem cell function. Although a few of these studies have touched briefly on the signalling pathways in SIM-A9 cells, there is limited characterisation of the cells in response to certain stimuli.

The present study has shown that SIM-A9 cells highly express key components of NF- $\kappa$ B signalling in response to LPS in a time and concentration dependent manner. Initial experiments using the cells examined the effect of LPS on the NF- $\kappa$ B signalling pathway by measuring degradation of I $\kappa$ B- $\alpha$  and phosphorylation of P65 as a marker for activation of the NF- $\kappa$ B pathway. I $\kappa$ B- $\alpha$  and p-P65 was assessed in the presence of LPS at various time points and concentrations. This study demonstrates that LPS is a strong agonist of NF- $\kappa$ B activation, causing I $\kappa$ B- $\alpha$  and P65 phosphorylation and subsequent NF- $\kappa$ B activation in SIM-A9 cells. The experiments carried out in the current chapter demonstrated that 30 minute LPS stimulation using 1000 ng/ml (100 ng/ml also showed activation) is the optimal conditions to induce activation of the NF- $\kappa$ B pathway. Nagamoto-Combs and colleagues used 25 ng/ml to activate SIM-A9



cells, however, after 5 minutes they failed to observe phosphorylation of I $\kappa$ B (p-I $\kappa$ B) (Nagamoto-Combs *et al.*, 2014). The low concentration of LPS and early time point compared to our experiments (25 ng/ml vs 1000 ng/ml and 5 minutes vs 30 minutes) could provide a valid explanation as to why they did not observe a significant effect of LPS on the NF- $\kappa$ B pathway. A range of LPS concentrations and times have been reported to successfully activate the NF- $\kappa$ B pathway in microglia cells, ranging from 1 ng/ml at 30 minutes (Russo *et al.*, 2004), to 100 ng/ml at 18 hours (Oh *et al.*, 2013) and 1000 ng/ml at 30 minutes (Badshah *et al.*, 2016). In agreement with our findings, LPS (100 ng/ml) was observed to cause a significant upregulation of p-P65 in BV-2 cells after a 30 minute stimulation (Lu *et al.*, 2007). In addition, it was reported that LPS-induced an increase in phosphorylation of NF- $\kappa$ B in BV-2 cells when using comparable LPS concentrations as the current work (1000 ng/ml) (Badshah *et al.*, 2016). It can therefore be concluded that the results observed in the current chapter agree with the current literature for microglia cells.

Ample evidence suggest that NF- $\kappa$ B signal cascade plays a detrimental role in cerebral ischemia owing to its function in the regulation of pro-inflammatory mediators including macrophage (M-CSF), granulocyte (G-CSF) and granulocyte macrophage (GM-CSF) colony stimulating factor, IL-1 $\beta$ , TNF- $\alpha$  and iNOS (Xia *et al.*, 2015; Baeuerle and Henkel, 1994). The importance of the signalling pathway was confirmed using mice deficient in the NF- $\kappa$ B p50 subunit, which appeared to have exhibited reduced brain injury after experimental stroke (Schneider *et al.*, 1999).

#### **2.4.2 The effects of hAMSC-CM on signalling pathways in SIM-A9 microglia cells**

In addition to the NF- $\kappa$ B pathway, we also examined components of the MAPK pathway and explored the effects of hAMSC-CM on these signalling pathways. hAMSC-CM did not affect any of the signalling pathways that we investigated. This could be due to many reasons, including the time point, hAMSC-CM availability was limited which meant that only one time-point could be examined. The data shows that after 30 minutes LPS stimulation, hAMSC-CM does not produce any effect. These signalling pathways are extremely transient, and ideally should be investigated more frequently over an extended time. Ooi *et al.*, (2014) found that MSC-CM did have an effect on signalling pathways in microglia after a 3 hour LPS stimulation. It was demonstrated that NF- $\kappa$ B and JNK expression were significantly reduced and the

MKP-1 (involved in the de-activation of MAPKs) was found to be upregulated by MSC-CM. The MAPK signalling pathway has also been shown to play an important role after stroke and in fact three interlinked signalling pathways are activated by cerebral ischemia, JNK, p38 and ERKs (Irving and Bamford, 2002). Increased ERK1/2 phosphorylation has been reported in rodents after transient, permanent MCAO and global ischemia (Irving and Bamford, 2002). Our results would suggest that previous effects of hAMSC-CM (Pischiutta *et al.*, 2016) are unlikely to be mediated by affecting JNK/p38/ERK signalling pathways in microglial cells.

#### **2.4.3 The effect of LPS and IL-4 on inflammatory mediators in SIM-A9 cells**

Microglia are activated by various inflammatory stimuli, including PAMPs (e.g. LPS) and cytokines (e.g. IL-4) (Krasnow *et al.*, 2017) which can elicit either pro-inflammatory/cytotoxic or anti-inflammatory/regenerative phenotype. For example, LPS promotes the pro-inflammatory phenotype in microglia, inducing expression of *I1 $\beta$* , *Tnfa* and *Nos2* (Stansley *et al.*, 2012). Meanwhile IL-4 promotes the anti-inflammatory phenotype inducing expression of *Arg1*, *Ym1*, and *I10* (Tang and Le, 2016). By challenging SIM-A9 cells with LPS or IL-4, it could be illustrated that SIM-A9 microglia can respond to multiple stimuli and thereby specifically up-regulate genes associated with distinct activation phenotypes. Pro-inflammatory stimuli LPS induced a similar overall gene and cytokine response in microglia in general agreement with what has previously been reported (Ransohoff and Perry 2009). We showed that LPS induced gene expression of *I1 $\beta$* , and *Nos2*, while IL-4 induced expression of *Arg1* at 24 hours in SIM-A9 microglia. IL-4 did not increase release of any cytotoxic markers and vice versa, LPS did not increase release of any regenerative markers.

These results are prototypical of microglia and there is a plethora of studies that support our findings; LPS (1  $\mu$ g/ml) induced *Nos2* expression 2,529-fold expression, and *I1 $\beta$*  by 283.6-fold expression in primary mouse microglial cells (Chhor *et al.*, 2013). The same group also revealed similar effects of IL-4 (20 ng/ml) on *Arg1* expression reporting a 2763-fold increase (Chhor *et al.*, 2013). RNA-sequencing of BV-2 cells after LPS stimulation revealed that the most markedly affected were *iNOS*, the interleukin genes, *Tnf* genes and the chemokine *Ccl2* (Das *et al.*, 2015). Furthermore, each of these pro-inflammatory markers is increased in brain injury during inflammation in particular in stroke (Chhor *et al.*, 2013). Importantly, our data

is in agreement with the original SIM-A9 paper; Nagamoto-Combs *et al.*, (2014) who also observed an increase in the expression of *Nos2* along with an upregulation of *Arg1* with upon IL-4 stimulation. Furthermore, Nagamoto-Combs reported that SIM-A9 cells demonstrated a decreased ability to express *Arg1* after a number of passages, this was evident from the lack of IL-4-stimulated *Arg1* expression at passage 40. To ensure reliable and consistent results, it should be noted that all experiments presented were carried out between cell passage 1-10. Reduced responses to external stimuli appear to be a common feature of immortalised cells, also observed in BV-2 cells (Henn *et al.*, 2009). The upregulation of *Nos2* gene expectedly caused SIM-A9 cells to subsequently produce NO, measured by the levels of nitrite present in the cell supernatant. Similar findings in SIM-A9 cells were reported when 0.1 µg/ml LPS was applied for 24 hours (Samaradivakara *et al.*, 2017). This response was also confirmed in primary microglia cells where the level of nitrite was significantly increased after LPS (1 µg/ml) by a 13-fold increase (Zhao *et al.*, 2006). In our experiments, we were unable to detect an upregulation of *Arg1* protein expression after IL-4 stimulation by western blotting. We suspect that the lack of upregulation may be due to the *Arg1* antibody used for blotting, it may be the case that optimisation of the antibody is required. The dilution of the antibody may be too high which could result in a lack of sensitivity to detect changes in levels of expression. We know from PCR results that *Arg1* gene expression is certainly upregulated so optimisation of the *Arg1* antibody is required in order to accurately detect changes in *Arg1* protein expression.

Interestingly, the induction of a pro-inflammatory phenotype also strongly decreased expression of anti-inflammatory repair/regeneration markers, in agreement with reports that acquisition of phenotype requires a complex amalgam of induction and representation of gene expression (Liao *et al.*, 2011). Here, we demonstrate the ability of SIM-A9 cells to respond to LPS and IL-4 and to produce the panel of inflammatory mediators respectively that mimics the known literature. This suggests that the SIM-A9 cell line is an efficient microglial cell line to further examine the effect of hAMSC-CM.

#### 2.4.4 The effect of hAMSC-CM on inflammatory mediators in SIM-A9 cells

Promoting a microglia neuroprotective phenotype is an emerging therapeutic goal for CNS conditions. As discussed in **section 1.6.2** the paracrine effects of MSC-released bioactive factors modify the injured microenvironment favouring reparative and restorative process (Fumagalli *et al.*, 2015). This study was targeted to elucidate the effects of hAMSC-CM in LPS-activated SIM-A9 microglia. The work described here follows on from findings of our collaborators (Pischiutta *et al.*, 2016). They showed that hAMSC-CM effect is dose-dependent in OGD injured cortical slices, and the maximal effect was obtained with 50% hAMSC-CM; this dose was therefore selected for all experiments.

Our data revealed that the addition of hAMSC-CM on LPS-activated microglia significantly reduced expression levels of pro-inflammatory cytokines *Il1 $\beta$* , *Tnfa* and *Ccl2*. The effect of MSC-CM on microglia has been reported in one previous study, Ooi *et al.*, (2014) also reported that MSC-CM suppressed the increase expression of pro-inflammatory cytokines (*Il6* and *Tnfa*) in activated primary microglia. Our data showing that hAMSC-CM decreases LPS-induced production of *Ccl2* is in disagreement with previous literature; it was reported that *Ccl2* was increased in MSC/microglia co-culture (Hegyí *et al.*, 2014; Giunti *et al.*, 2012). Rahmat *et al.*, (2013) did not observe any difference in *Ccl2* levels upon co-culture of MSC with microglia. The role of *Ccl2* appears to have conflicting reports; excessive production of *Ccl2* was associated with disease progression in stroke. The central event in post-ischaemic inflammation is recruitment of leukocytes, first neutrophils, then influx of cells of monocyte/macrophage lineage (Dirnagl *et al.*, 1999). It is thought that *Ccl2* is a crucial step of the leukocyte infiltration and its expression following ischemia to exacerbate damage (Conductier *et al.*, 2010). However, *Ccl2* has also been reported to potentially have a role in tissue repair and regulation (Fumagalli *et al.*, 2015). Data presented in this study shows that hAMSC-CM appears to increase *Arg1* expression, although it should be noted that results failed to reach statistical significance. These findings are in agreement with others that report a 3-fold enhancement of *Arg1* in LPS-stimulated microglia in the presence of MSCs (Giunti *et al.*, 2012; Hegyí *et al.*, 2014). NO production was decreased in the presence of hAMSC-CM; however, this effect was not significant. Surprisingly, literature shows that NO production was increased in the presence of MSC and MSC-CM (Rahmat *et al.*, 2013; Ooi *et al.*, 2014). The discrepancies between results may due to the fact that in the current study

conditioned media from hAMSC is used, compared with the majority of the literature that reports the use of MSC, this may cause differences in the results. Nonetheless, results show that hAMSC-CM is capable of modulating microglia cells and this is consistent with earlier reports indicating that MSCs can shift microglia from a pro-inflammatory phenotype to an anti-inflammatory phenotype (Rahmat *et al.*, 2013; Zhou *et al.*, 2009). Interestingly, in a previous study MSC were demonstrated to modulate microglia to a neuroprotective phenotype by releasing CX3CL1, also known as fractalkine (Giunti *et al.*, 2012).

Considering these interesting results, secretions from these experiments were further investigated. Results from the proteome cytokine profile revealed that hAMSC-CM failed to produce a significant effect on microglia, this lack of effect could be since secretions only were used for these experiments. It was reported that TNF- $\alpha$  was not detected in the supernatants of LPS-stimulated MSC cultures (Hegyi *et al.*, 2014). A larger sample size for this experiment is required to confirm these results. To gain insight into the effect of hAMSC-CM on microglia phenotype, initial studies involved capturing images of the cells in culture to examine morphology. Unfortunately, due to the limited volume of hAMSC-CM available, we were restrained with the experiments that could be carried out. When cells were plated at a confluency intended for morphology analysis, RNA analysis, which was our main outcome was restricted due to lack of cell confluency. Given this, experiments investigating hAMSC-CM on cell morphology is required to be repeated for further interpretation. The literature shows that, pro-inflammatory, *Il1 $\beta$* , *Nos2* high and *Arg1* low microglia-mediated phagocytosis results in neuronal loss, while an anti-inflammatory, *Il1 $\beta$* , *Nos2* low and *Arg1* high microglia may efficiently clear debris as well as promote neuron survival, decreasing ischaemic damage (Xia *et al.*, 2015).

Taken together, the data presented in this chapter so far could be interpreted as an indication that hAMSC-CM exerts a beneficial modulation of microglia, therefore, hAMSC-CM after stroke may alleviate injury by promoting anti-inflammatory properties while dampening the pro-inflammatory properties of microglia in the brain.

#### **2.4.5 Establishment of primary microglia cell isolation and culture**

Doubt has been raised regarding the value of cell lines as a model system for researching microglia function. Previous studies have revealed similarities between the BV-2 cell line with primary microglia (Henn *et al.*, 2009). However, immortalization can cause these cells to be different from primary microglia in culture or in the brain (Butovsky *et al.*, 2005; Horvath *et al.*, 2008; Stansley *et al.*, 2012). A recent study showed that cytokines associated with inflammation were significantly upregulated and these changes were found to be stronger in primary microglia than in BV-2 cells. The number of genes and the extent of fold change were significantly more modulated in primary microglia compared to BV-2 cells. Primary microglia upregulated 220 genes 2 hours post LPS, and 682 genes after 4 hours of which, are not common to the BV-2 cell line (Das *et al.*, 2016). Due to these findings, we felt it was important to investigate the effects of hAMSC-CM on primary microglia cells, and to ensure that the modulatory effects seen in SIM-A9 cells were observed consistently in primary cells. The results summarised in the end of this chapter presented the development of a consistent and efficient method to isolate single cell microglia from the whole mouse brain. Numerous protocols exist for the isolation of microglia (rodents and humans). The majority of studies use either a Percoll gradient followed by an extended centrifugation to isolate the microglia fraction (Cardona *et al.*, 2006; Lee and Tansey, 2013; Nikodemova and Watters, 2012), extensive shaking of the flask to prevent attachment of other cells (Tamashiro *et al.*, 2012), mild trypsinization (Saura *et al.*, 2003) or sorting via magnetic or fluorescence activated cell sorting (MACS/FACS) (Cardona *et al.*, 2006; Nikodemova and Watters, 2012). The shaking method first described by Giulian and Baker, 1986, utilizes dissociated brain tissue from neonatal pups to produce mixed glia cell culture. After the mixed glia cultures reach confluency, primary microglia are mechanically isolated by a brief duration of shaking. Protocol (1) was based on the published shaking method by Chen *et al.*, (2013) who reported a high purity of 90% CD11b<sup>+</sup> cells. In our hands, despite many attempts, the average purity of microglia cells in cultures was 30%. Various studies have shown that the shaking method may not be the most relevant; maintenance of primary neuron-glia cultures for extended periods of time (1-2 weeks) increases the likelihood for loss of morphological and functional microglia phenotype (Harms and Tansey 2013). In addition, the physical process of shaking the flask can cause the cells to become activated and they may take several days to return to a complete

resting phenotype (Bronstein *et al.*, 2013). Given the lack of success with the shaking method and the potential effects of the technique on the quality of microglia, we sought to try a more effective and appropriate extraction technique; Percoll gradient and CD11b magnetic bead (protocol 2). This protocol utilizes microglia from the adult mouse brain, which is a more representative model for understanding microglia function, particularly in stroke research where age is a crucial factor (Gordon *et al.*, 2011). The initial purification was based on the work of Cardona *et al.*, (2006), modified by Kathleen Grabert, McColl lab, Roslin Institute, replacing purification through FACS cell sorting with magnetic beads. Communications with the lab allowed observation of the technique as well as guidance and advice on troubleshooting. The McColl lab verified the purity and consistency of microglial extraction across brain regions (Grabert *et al.*, 2016). The results show that the extraction successfully extracted a high purity of CD11b<sup>+</sup> cells, on average yielding 80% purity. Unfortunately, we were unable to successfully culture these cells. Although patches of microglia were evident in the culture, these were sparse and mainly filled with small round cells and debris. While this protocol routinely and reliably produces healthy mouse microglia, in our hands with respect to culturing, it was unsuccessful. In attempts to try and improve culturing conditions of isolated microglia, we added M-CSF to cultures. M-CSF was found to be very useful in drastically sustaining the survival and proliferation of microglia in culture (Moussaud and Draheim 2010). M-CSF in our hands failed to improve cultures, but the use has also been shown to significantly alter microglia phenotype, particularly receptor expression and phagocytic function following exposure to M-CSF (Smith *et al.*, 2013; Rustenhoven *et al.*, 2016). It has been acknowledged that the culture of microglia prepared from adult animals is challenging and it has been reported that the culture of microglia *ex-vivo* are difficult due to extensive cell death (Moussaud and Draheim 2010). They describe a technique which involves collecting the supernatant from a mixed glia culture, excluding the shaking which they state allow for long-term culture of microglia *in vitro*. Critical parameters of this protocol which we were aware of and ensured that they were adhered to included:

- Completely removing the meningeal covering from the brain during dissection, because the presence of meninges will contribute to significant fibroblast contamination (Tamashiro *et al.*, 2012).

- The set-up of the gradient is one of the most crucial, the cell suspension in 30% Percoll must be layered over the 70% solution avoiding mix of the 30% and 70% layers to generate a defined step gradient.
- Cells were counted on a haemocytometer in trypan blue after collecting the interphase to check for sufficient cell yield and viability.
- Ensuring that cells were kept cold, on ice at all times to prevent receptor mediated endocytosis.

Next, using protocol 3, we moved onto using neonate mice, after establishment of the mixed glia culture (as described in protocol 1), the cells were separated using the CD11b magnetic beads (as described in protocol 2). It was reported that this protocol produced a yield four times that of the shaking method, and resulted in 99.5% positive CD11b staining (Marek *et al.*, 2008). This protocol resulted in the success culturing of the cells, however, FACS analysis revealed a low purity of 30%.

As a final attempt to successfully extract and isolate microglia we decided to use the MACS® Neural tissue dissociation kit with papain in conjunction with the gentle MACS dissociator (protocol 4). This allows for the gentle isolation of microglia while recovering as many cells as possible (Garcia *et al.*, 2014). Having thought that the cells may be dying in culture due to the extraction process, we utilised the MACS® Neural dissociation kit followed by CD11b magnetic beads; this technique shortens the time between brain harvesting and microglia isolation and subsequent culturing. This protocol has been reported to yield viable and highly pure (>95%) microglia population (Harms and Tansey, 2013). In our hands, this technique failed to produce a high purity of microglia (35%) due to the difficulty we were experiencing with the isolation, Miltenyi Biotec sent technical specialist, Dr Susan Barton to attend our lab and carry out the isolation alongside us. She also experienced the same problems of a low purity when examined by FACS, and concluded that our mice colony did not express the CD11b marker. Given this, we examined the CD11b expression levels in whole neonatal mice from the C57BL/6 mice strain (strain we had been using the isolations) as well as cells from BALB/C mice. The results (not shown) revealed that both strains expressed healthy levels of CD11b. Unfortunately, despite attempting many methods and modifications we were unsuccessful in culturing primary microglia and due to time restraints, we were unable to continue with our efforts. The reasons for the unsuccessful primary microglia extraction and culturing remains unknown. If time allowed, we would have continued attempting to optimise protocol 2 (Percoll



gradient and magnetic beads) as we felt this protocol produced the most successful results. The next steps to be carried out, would include a fresh preparation of the enzyme cocktail and enlisting the help of someone who regularly carries out the technique to attend our lab to do the extraction and culturing. Due to the sensitive nature of primary microglia, there could be one small error, step or fault with equipment that is responsible for the issues discussed. Upon successful culturing of primary microglia cells, future work would include repeating hAMSC-CM experiments to confirm the immunomodulatory effects observed in the SIM-A9 cell line.

In conclusion, the main findings of this chapter are that SIM-A9 cells are capable of being polarised into various phenotypes exerting many pro- and anti-inflammatory properties. This work highlights hAMSC-CM as a potential modulator of activated microglia for stroke therapy; however, work is required to further characterise the properties of hAMSC-CM. Data presented in the next chapters further characterises SIM-A9 cells examining their capacity to migrate in an environment that is relevant to stroke and examines the effect of hAMSC-CM.

#### **2.4.6 Methodological limitations**

In the current chapter, the novel SIM-A9 microglial cell line were used, this is one limitation of the study. As discussed in **section 2.4.5** the use of immortalised cell lines has many disadvantages and results obtained from cell lines should ideally be confirmed using primary microglia. It was our intention to repeat experiments on microglia extracted from adult mice, however, due to issues establishing the technique and time restrictions this was not possible. Examination of microglia in their natural environment would be ideal, it is important to consider interactions of various cell types, with the contributing signals from other cell types playing an important role in microglia function. Nonetheless, some studies require cell separation and *in vitro* analysis to gain insight and tease out possible mechanisms. Another limitation of the work in the current chapter includes the lack of analysed markers for the activation and inflammatory response of microglia. To gain further insight into the effect of hAMSC-CM on microglial cells, RNA-sequencing would provide much more information which would allow us to categorise the phenotype of microglia further.

**Chapter 3: Establishment and  
characterisation of an *in vitro* model of  
microglia migration that is relevant to  
stroke and investigation of the effects of  
hAMSC-CM**

### 3.1 Introduction and aims

In ischaemic stroke, microglia, which are activated within minutes of ischaemic onset, migrate to areas of injury through detection of chemoattractant gradients (Patel *et al.*, 2013). This subsequently results in either neurotoxic consequences by releasing inflammatory cytokines and inducing inflammation or neuroprotective effects by removing the tissue debris and pathogens and secreting anti-inflammatory cytokines and growth factors (Davalos *et al.*, 2005; Patel *et al.*, 2013). Cell migration is a complex process that involves the integration of chemotactic gradient sensing, and directed movement toward the chemotactic source (Wu *et al.*, 2014). The three most commonly studied chemoattractant agents for microglia include fractalkine, CCL21 and ADP, all of which are known to diffuse through the injured brain to engage receptors on microglia, increasing microglia motility and inducing chemotaxis (Haynes *et al.*, 2006). However, the most ubiquitous transmitter in the brain is glutamate that is present at very high concentrations in neurons and glia cells under normal homeostasis (Liu *et al.*, 2009), and in excess concentrations extracellularly after brain injury which diffuse through the brain generating a gradient towards which microglia cells could migrate (Liu *et al.*, 2009) (**figure 3.1**). However, despite the key role of glutamate in ischaemic damage, there is surprisingly little published work on glutamate-induced microglia migration. To further investigate glutamate-induced microglia migration, an *in vitro* model of microglia migration that is relevant to stroke was first established.

Understanding the migratory behaviour of microglia after brain injury and how this can be controlled therapeutically has been an area of active research. Traditional *in vitro* methods are not ideal for examining the quantitative or combinatorial nature of gradient signalling due to their inability to produce precise, long-lasting gradients. Currently, one of the most commonly used *in vitro*-based migration assays is the Boyden chamber (transwell) assay, consisting of an insert with a porous membrane lining nested in a culture plate (Boyden, 1961). In this assay, the motile cells are placed into the upper chamber, while fluid containing the chemoattractant is filled into the lower one. Migratory cells move through the porous membrane to the culture plate. The Boyden chamber is easy to perform, readily elicits chemotactic responses from cells and provides a quantitative measure of the level of migration induced by chemotaxis. However, even under ideal conditions the gradient that forms across the membrane varies over space and time and cannot be controlled to mimic the *in vivo*

situation (Keenan and Folch, 2008). In addition, cellular migration (i.e. towards a concentration gradient source) cannot be distinguished from increased non-directional motility. Another commonly used assay is the scratch assay (wound healing) in which a gap area is artificially created for cells to move across (Liang *et al.*, 2007). Although this assay can provide real-time tracking of cell movement, the process of gap creation can affect migratory behaviour and again fails to replicate the chemical gradient present after brain injury *in vivo*. The Dunn chamber, developed from the Zigmond chamber (Zicha *et al.*, 1991), consists of two concentric wells. One chamber is filled with cells re-suspended in medium, whereas the other is filled with medium containing the chemoattractant. As chemicals diffuse from the outer well to the inner one, a chemical gradient is formed. The main limitation of the Dunn chamber is that the gradient forms and dissipates within 1-2 hours, greatly limiting the cell types and questions that can be studied as some cells may take longer to respond to the gradient and limits the duration of the experiment (Chaubey *et al.*, 2011; Keenan and Folch, 2008). To overcome the drawbacks related to these assays, and to examine microglia recruitment in a more physiologically relevant model, our aim was to develop and optimise an efficient and convenient assay that mirrors the gradients observed *in vivo* after brain injury to study microglia migration by harnessing microfluidic technology. Microfluidic technology, in addition to the direct interfacing to microscopy, provides an appealing strategy to control the fluid flow necessary to create molecular concentration gradients on a scale suitable for cellular studies. Microfluidics is the science and technology of systems that process or manipulate small ( $10^{-9}$  to  $10^{-8}$  litres) amounts of fluids (Whitesides, 2006), an image of a microfluidic device is shown in **figure 3.1**.

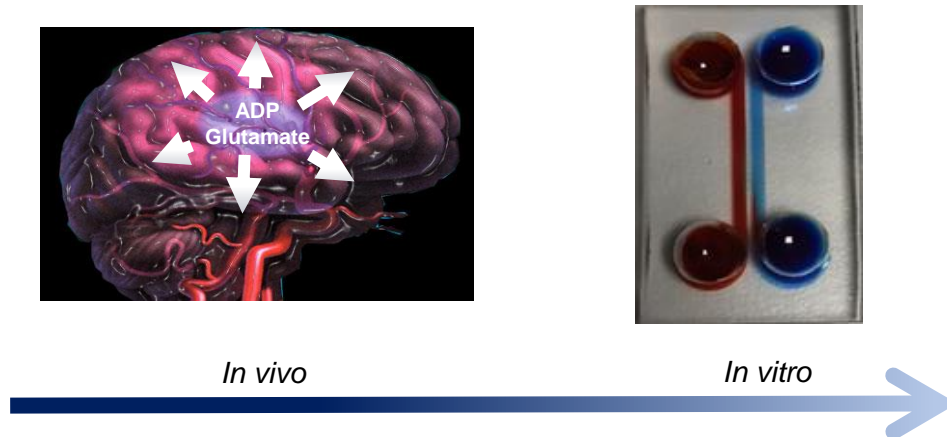


**Figure 3.1. Schema of a physiologically relevant *in vitro* model for migration studies.** ADP and glutamate as well as many other mediators are released from the ischaemic core after stroke. These chemoattractants diffuse through the brain, generating a gradient in which microglia cells migrate towards (left hand schema). Creating this gradient is an aspect that cannot be achieved using conventional culture, so, in order to achieve this, we have harnessed microfluidic technology (right hand schema), allowing a better representation of the *in vivo* situation.

Over the past years, several microfluidic-based gradient devices have been developed to investigate different biological questions. Microfluidic platforms for gradient generation can be classified into 5 categories: laminar flow gradients, static gradients, 3 dimensional (3D) gradients, 1D gradients and immobilized gradients (Zhang *et al.*, 2015). For studies of cell migration on 2D substrates, as in the present study, under the effects of soluble chemoattractant gradients, laminar flow-based and static gradient devices are the most commonly used (Zhang *et al.*, 2015). A laminar flow-based microfluidic device, offers precisely controlled stable gradients over time, however, the shear stress induced by the constant flow can affect cellular migration as well as inducing undesired signalling events (Berthier and Beebe, 2014). Therefore, we decided that using a microfluidic device with a static gradient generator would be the most appropriate to answer our questions.

A static microfluidic gradient generation method uses free-diffusion of water-soluble molecules. A basic example of a microfluidic device that can be used for migration is

a two-reservoir chamber device connected by one or an array of microchannels (a channel with at least one dimension below 1 mm). One of the reservoir chambers is loaded with cells re-suspended in medium (known as the 'sink'), whereas the other is filled with medium containing a chemoattractant (known as the 'source'). A stable concentration gradient develops between the two reservoir chambers in the connecting microchannels as the molecules diffuse from source to sink (**figure 3.2**) (Kramer *et al.*, 2013). The chemical species enter the channel by diffusion through the source region and creates a concentration gradient along the length of a channel. A source/sink concept is used to create a pseudo steady state in the system where the concentration at a point does not vary dramatically with time (Abhyankar *et al.*, 2006). Abhyankar *et al.*, (2006) developed an elegant and simple flow-free gradient generator composed of reservoirs connected by a straight channel. This pseudo steady state gradient was maintained for more than 24 hours (**figure 3.2(B)**).

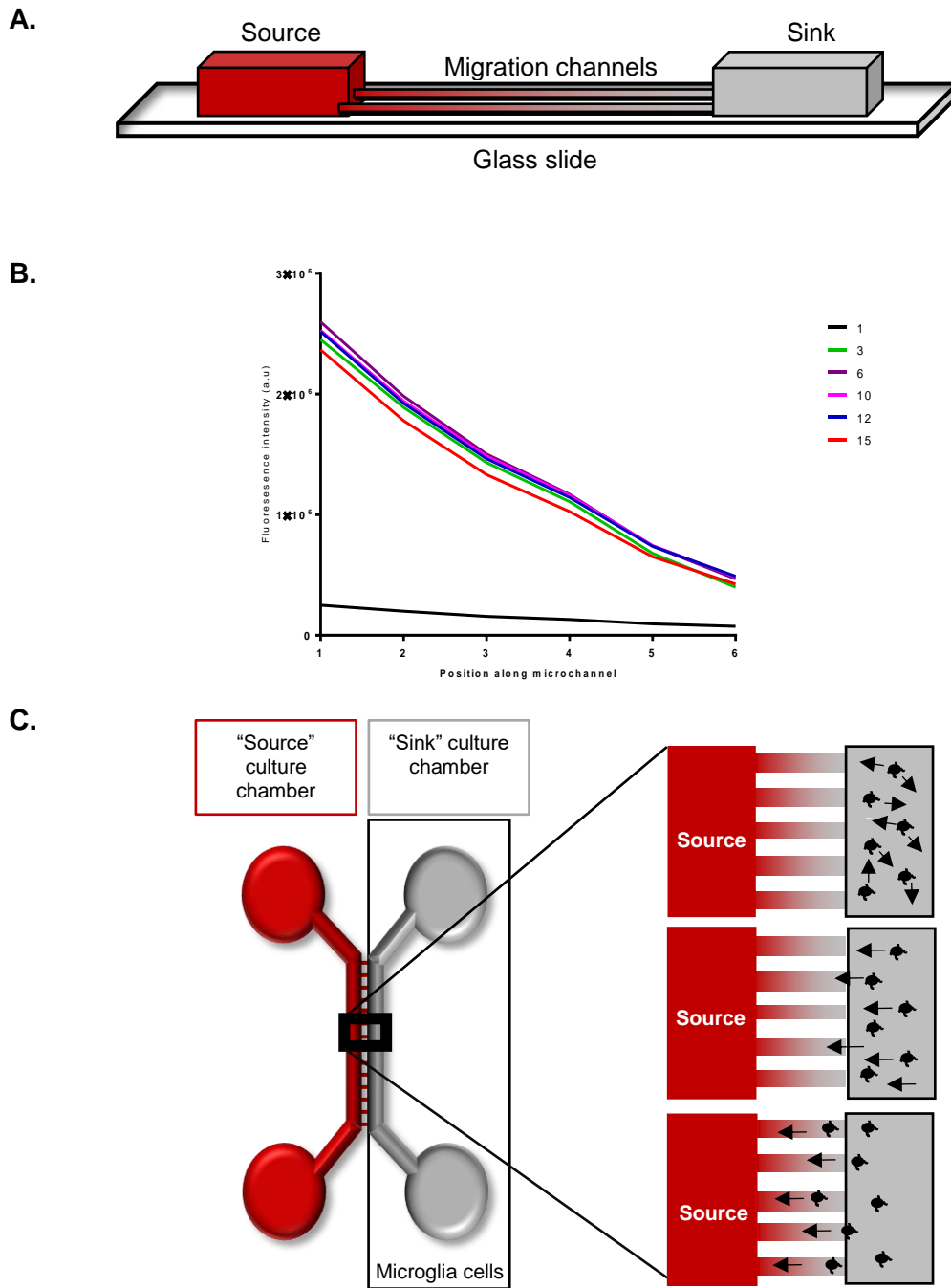


**Figure 3.2. Static gradient generator. (A)** A cross-section schematic of a microfluidic device shows the source/sink reservoirs connected by a microchannel where the gradient will be generated. **(B)** Shows the time dependent establishment of a concentration gradient across the width (length) of the microchannel. **(C)** Schematic representation of a microfluidic device showing the direction of cell migration from the sink reservoir towards the chemoattractant source.

The main difference of a microfluidic approach compared to conventional macroscale methods is the use of microchannels with high fluidic resistance (Kim *et al.*, 2010). These obstacles provide physical barrier against convective flow and fluidically isolate the gradient forming region (microchannel) from the source and the sink regions. Because transport of molecules occurs by diffusion, the concentration gradient evolves over time until a steady state is achieved when influx and outflux transport are balanced (Abhyankar *et al.*, 2006).

Diffusion is the process by which a concentrated group of particles in a volume will, by Brownian motion (the erratic random movement of microscope particles in a fluid, as a result of continuous bombardment from molecules of the surrounding medium), spread out over time so that the average concentration of particles throughout the volume is constant. Diffusion can be modelled in one dimension by the equation  $d^2=2Dt$ , where  $d$  is the distance a particle moves in the time,  $t$  and  $D$  is the diffusion coefficient of the particle. Because distance varies to the square power, diffusion becomes very important on the microscale e.g. haemoglobin ( $D= 7 \times 10^{-7} \text{ cm}^2\text{s}^{-1}$ ) in water takes  $10^6$  seconds to diffuse 1 cm but only 1 second to diffuse 10  $\mu\text{m}$ . Therefore, in a 1 cm wide tube, diffusion of haemoglobin is not usually an important consideration but in a microchannel 10  $\mu\text{m}$  wide, the distance travelled due to diffusion becomes important. Since diffusion times can be short at the microscale, microchannels can be used to create concentration gradients (Beebe *et al.*, 2002).

The choice of technology allows us to examine microglia recruitment in a model that mimics the *in vivo* conditions of the brain's environment after stroke and subsequently examine the effect of hAMSC-CM.

The aims of the work described in this chapter were to:

1. Establish a microfluidic device which allows for microglia culture and seeding.
2. Optimise conditions to provide a suitable long-lasting chemoattractant gradient.
3. Characterise microglia migration using an established chemoattractant.
4. Examine the effects of microglia phenotype on microglia migration.
5. Investigate the effects of hAMSC-CM on microglia migration.



## **3.2 Materials and Methods**

### **3.2.1 BV-2 cells**

Initial optimisation studies involved usage of BV2 cells that were a generous gift from Dr McColl of the Roslin Institute, Edinburgh. BV2 is a murine microglia cell line immortalised with v-raf/v-myc gene-carrying retrovirus J2 (JOSE). The cells were preserved in a solution containing neat FBS and 10% dimethyl sulfoxide (DMSO) at a cell concentration of  $5 \times 10^6$  cells/ml and in liquid nitrogen.

In culture, BV2 cells were grown in Dulbecco's modified Eagle's medium (DMEM) containing 5% FCS, 1% L-glutamine, 1% penicillin and 1% streptomycin at 37°C, 5% CO<sub>2</sub>. Cells were either sub cultured or inserted into a microfluidic device before reaching 90% confluency by harvesting with 0.25% trypsin containing 1mM EDTA for 5 minutes at 37°C, 5% CO<sub>2</sub>.

### **3.2.2 Microfluidic device preparation**

Microfluidic devices were fabricated in polydimethylsiloxane (PDMS) using standard soft lithography techniques. Silicon masters were designed and produced by Dr Michele Zagnoni, Electronic and electrical engineering (EEE), University of Strathclyde.

To create the microfluidic channels, PDMS was poured onto the silicon master at a 10:1 ratio of base to curing agent (PDMS and curing agent both, DowCorning, Michigan), and degassed in a vacuum desiccator chamber for 30 minutes to remove bubbles. The degassed PDMS was placed in to an oven at 80°C to cure for at least 2 hours. The PDMS was allowed to cool for approximately 30 minutes before preparation. The cured PDMS was then cut out of the master using a scalpel. The block of PDMS, containing several devices, was then sliced into individual devices. Holes were punched (8 mm diameter) using a biopsy punch (Stiefel, SmithKline Beecham, UK) to obtain the inlet and outlet wells for each device. The PDMS devices and microscope glass slides (Fisher Scientific, UK) were then cleaned using scotch tape. Tape was applied firmly to the surface of the PDMS or glass slide and then removed to ensure any dust or particles were removed from the surface.

Bonding of microfluidic devices was carried out by treatment of PDMS and glass slides within an oxygen plasma chamber (Pico A, Diener Electronic, Germany). By

briefly exposing the surface of PDMS and silicon glass to low pressure oxygen plasma, silanol groups (-Si-OH) are formed on the treated surfaces. When both surfaces are brought into contact they quickly form covalent bonds (-Si-O-Si) making the devices irreversibly bonded to the glass slide. Once exposed to oxygen plasma (0.26 mBar, 90 W, 6 s), the devices were placed feature side down on to the surface of the glass. Manual compression between the PDMS and the glass was used to ensure conformal contact. Three devices were bonded onto one slide, as shown in **figure 3.3**.

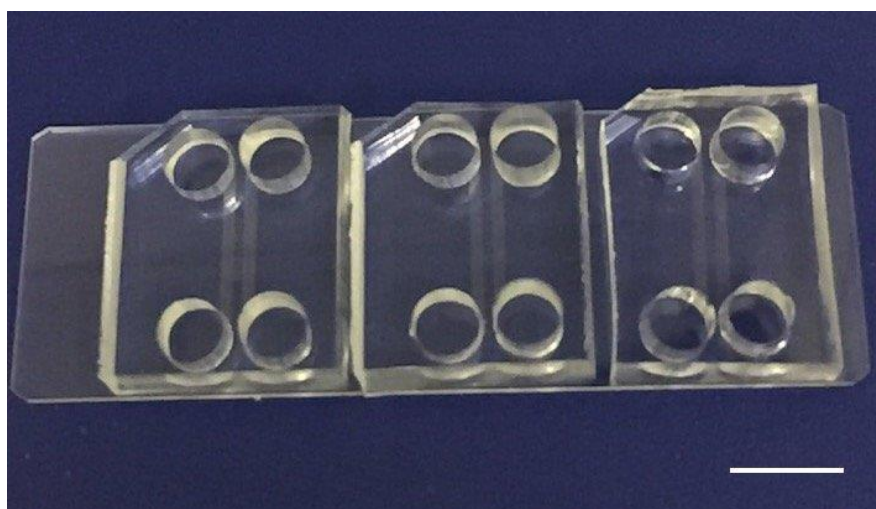


**Figure 3.3. Example of microfluidic devices.** A photograph of three microfluidic devices bonded to a single microscope glass slide. Scale bar, 10 mm.

Once cured, the PDMS quickly becomes hydrophobic, however, upon oxygen plasma exposure, the surfaces of PDMS are temporarily rendered hydrophilic. Once the devices were bonded on the glass slide, the entire system was exposed once again to oxygen plasma (0.26 mBar, 200 W, 1 minute) before the wells were filled with deionised water. As soon as devices were flooded with water they were placed into a large petri dish and left with the lid open inside a UV sterilisation cabinet for 5 minutes. The lid was then closed and the dish left under UV light for a further 5 minutes. The closed dish, now containing sterile devices, was removed, wrapped in parafilm and transported to a sterile cell culture hood.

Prior to cell seeding, the devices were flooded with poly-L-lysine (PLL, 10 µg/ml) (Sigma, UK) for 1 hour to coat the chambers and microchannels for adequate cell adhesion. Finally, devices were washed three times with 5% DMEM prior to cell injection.

### **3.2.3 Insertion of cells into the microfluidic devices**

As shown in **figure 3.2(C)**, devices consisted of two chambers (12 mm long, 1 mm wide, 100 µm deep) connected by 10 microchannels (1 mm long, 100 µm wide, 5 µm deep). Each chamber has an inlet and an outlet well. 5 µl of media was first placed into the inlet well of the non-cell containing chamber to ensure cells from the cell-containing chamber would not cross into the microchannels. Immediately after, 5 µl of microglia cell suspension (as described in **section 2.2.1**) were loaded into the inlet well of the other chamber at a density of  $2.5 \times 10^6$  cells per ml and incubated for 15 minutes before each well was filled with 80 µl of DMEM, containing 5% FCS, 1% L-glutamine, 1% penicillin and 1% streptomycin. Devices were placed in a round culture dish alongside a petri dish containing DMEM and kept in a humidified incubator at 37°C, 5% CO<sub>2</sub>. The extra Petri dish next to the devices served to increase the humidity within the closed Petri dish and prevented significant evaporation from the device wells.

### **3.2.4 Gradient characterisation**

In cell migration studies, fluorescent molecules are commonly used to visualize a gradient for its characterization. In our experiments, we used calcein (Sigma, UK). A challenge for static gradient generation resides in maintaining a diffusion-dominant environment in the presence of pressure differences that can occur in experimental situations. Unwanted pressure differences generate convection and can prevent the setup of a stable gradient (Berthier *et al.*, 2010). To prevent pressure differences, the device was first loaded with 80 µl media in each inlet, this was then removed and 80 µl media was placed in the sink (cell-side inlet well) reservoir, while simultaneously, 75 µl of calcein was placed in the source (non-cell inlet well) reservoir. The 5 µl volume difference was introduced to create a slow flow of medium in the direction of the source that was extinguished after 10 minutes. This strategy ensured that potential small differences in the well volumes (due to fabrication inaccuracies) did not create unwanted cross-contamination of the chemoattractant agent into the cell

chamber. Eventually, the flow will equilibrate and the chemoattractant gradient will form through diffusion, also allowing enough time for setting up of the device on the microscope for live-cell time-lapse experiments. The device was then gently covered with a glass slide to prevent liquid evaporation prior to imaging inside a small microscope stage incubator (Tokai Hit, Japan).

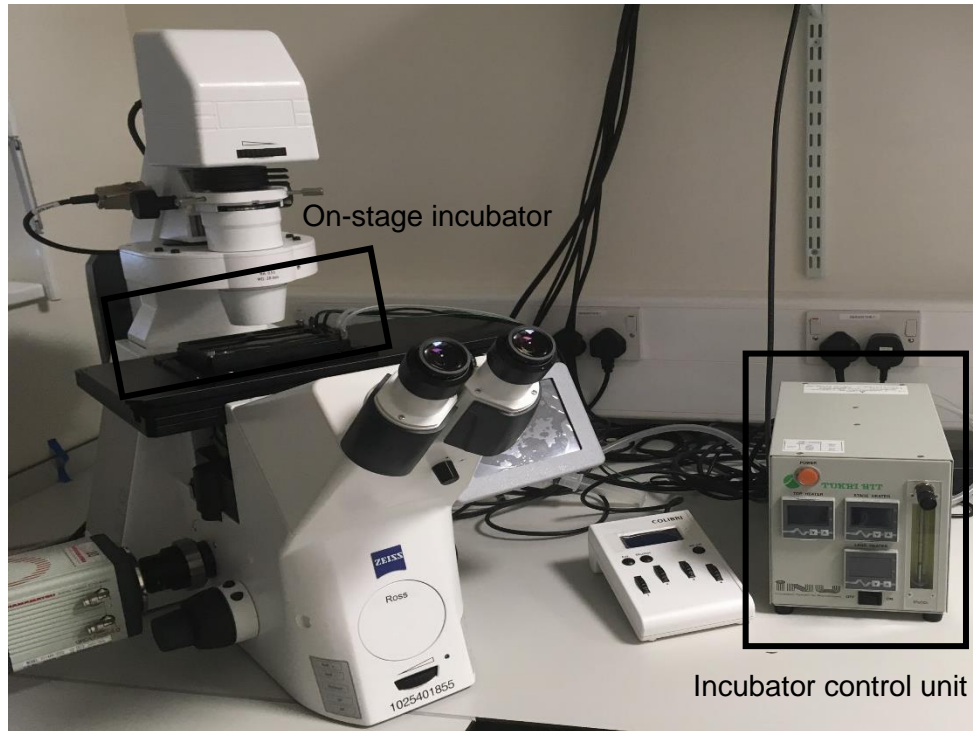
### **3.2.5 Set up of migration experiments**

BV-2 or SIM-A9 cells were seeded into microfluidic devices, and let to rest for at least 2 hours in the incubator before, the devices were carefully transported to the engineering department for time-lapse experiments. Migration experiments were set up 24 hours after cell seeding. Once conditions that produced a long-lasting gradient were established, the same protocol (as above) was used for migration experiments, replacing calcein with media containing the desired chemoattractant agent: ADP (Adenosine 5'-diphosphate sodium salt, Sigma, UK) or glutamate (L-Glutamic acid, Tocris Bioscience, UK). For hAMSC-CM experiments, hAMSC-CM with/without LPS or control media (neurobasal basal) with/without LPS was replaced in the cell-containing well at the same time as glutamate (in control media) was added into the non-cell containing well (same procedure as described in **section 3.2.4**).

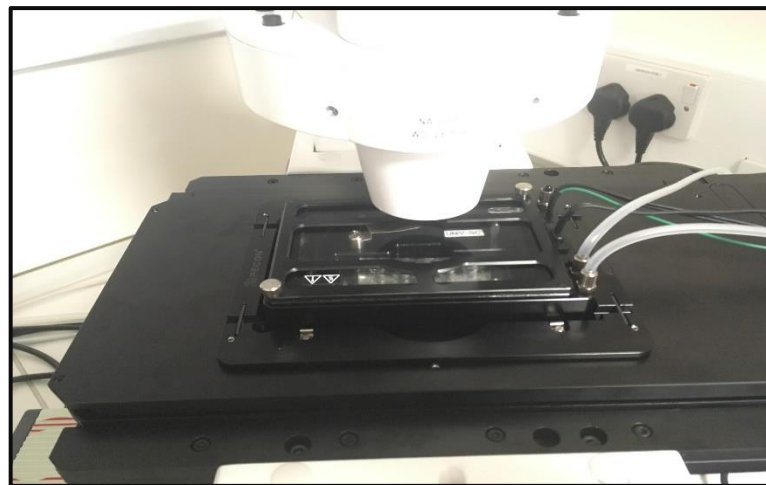
### **3.2.6 Real-time imaging**

A Zeiss Observer A1 inverted epifluorescence microscope (Nikon, Japan) equipped with Zen controlled Zeiss AxioCam Mrm camera and a cage on-stage incubator system (Tokai Hit, Japan) (pre-warmed before loading the devices) was used for the time lapse imaging (**figure 3.4**). The microscope was fully automated for imaging multiple positions in sequence, and equipped with long working distance objectives to rapidly acquire high-resolution phase contrast images. The on-stage incubator system included an enclosure, a temperature-control and CO<sub>2</sub> module. For our experiments, two positions, one capturing the top half of the device focusing on the migration channels and the second capturing the bottom half of the device, were imaged. A total of 6 positions were recorded per experiment (3 devices x 2 positions). At each position, phase contrast images were taken every 3 minutes over a period of 15 hours.

A.



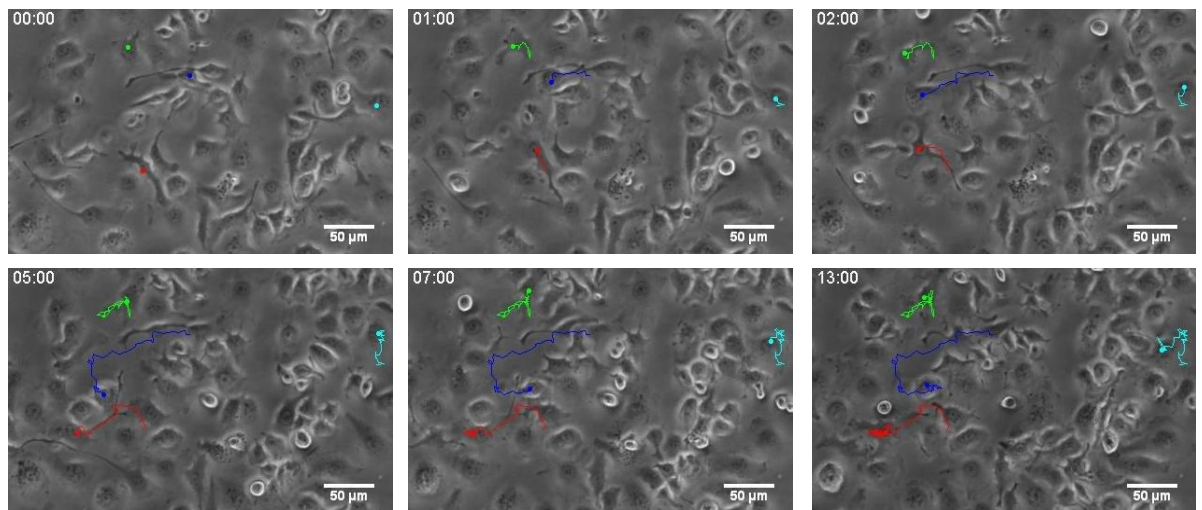
B.



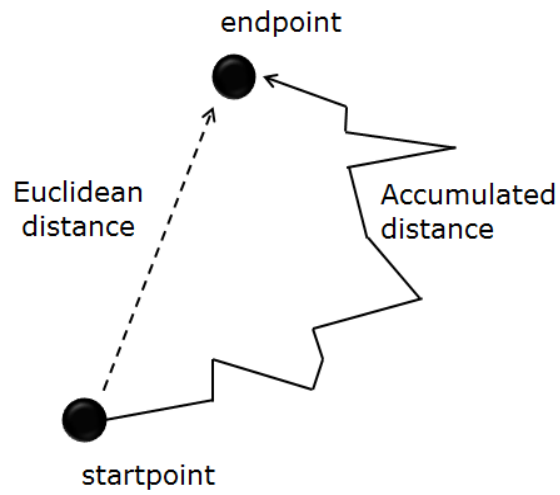
**Figure 3.4.** Example of an experimental set-up using an on-stage incubator. Photographs of **(A)** the on-stage incubator set up on the microscope connected to the control unit for the on-stage incubator used to maintain the temperature and CO<sub>2</sub>. **(B)** A close image of the on-stage incubator with an example of a device inside. Source of images 'with modifications' from Kay McMillian, personal communication.

### 3.2.7 Analysis of cell migration

Carl Zeiss Image Data Files (CZI) were imported into Image J and converted into Audio Video Interleave (AVI) files. Tracking analysis of time-lapse microphotographs was performed by Image J manual tracking plugin (**figure 3.5**). The generated tracking data was transferred into the Chemotaxis and Migration Tool program 2.0 (Ibidi) to calculate several quantitative data as well as the migration cell track paths. Cell migration was characterised in terms of three parameters: Speed of migration (velocity), Accumulated distance (the sum of all incremental movements), and Euclidean distance (the length of the straight line between the cell start and end-point) (**figure 3.6**).



**Figure 3.5. Snapshot images demonstrating manual cell tracking of BV-2 microglia cells within microfluidic devices.** Images show tracked cells (green, blue, red and turquoise) over 13 hours using Image J manual tracking plugin. Scale bar, 50  $\mu\text{m}$ .

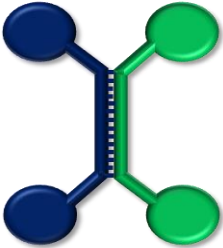
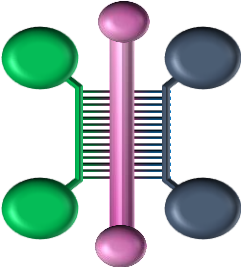
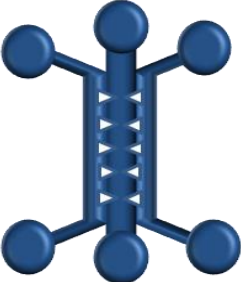
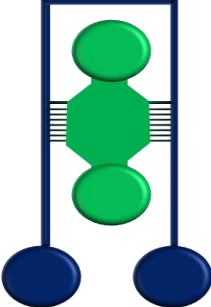
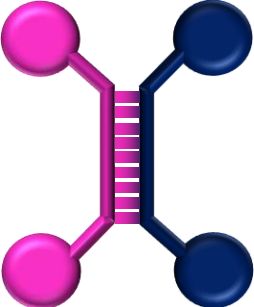


**Figure 3.6. Schematic illustrating the definitions in the 2D cell trajectory plots.** Euclidean distance is the measure of overall distance the cell has travelled from start point to end-point. Accumulated distance is the total of the distance the cell has moved, despite direction.

### 3.3 Results

The aim of this chapter was to create microfluidic devices and optimise associated protocols to examine microglia migration in response to chemoattractant agents found *in vivo* post stroke environment. The initial aim was to ensure that microglia cells were viable and capable of surviving for long-term culturing within devices. Initial studies in these experiments utilised BV-2 microglia cells (described in **section 3.2.1**). Due to complications arising with the survival of BV-2 cells in the microfluidics devices, SIM-A9 cells were used thereafter (for all experiments described in **figures 3.14-3.17**). For initial studies to optimise conditions for culture of microglia cells, several devices that were readily available were utilised (**table 3.1**).



Device number	Schema of device	Dimensions of microchannels	Problems
1.		10 $\mu\text{m}$ wide 250 $\mu\text{m}$ long	The microchannels were too small for microglia migration. Cells got stuck and died.
2.		15 $\mu\text{m}$ wide 1.2 cm long	Channels were not wide enough for cells to migrate through.
3.		N/A	Space between pillars was too large to allow for uniform cell seeding.
4.		100 $\mu\text{m}$ wide 500-1000 $\mu\text{m}$ long	Results were not reproducible as difficulty seeding cells close enough to the microchannels for cells to respond to chemoattractant.
5.		100 $\mu\text{m}$ wide 1000 $\mu\text{m}$ long	No problems identified - device optimised for microglia migration.

**Table 3.1. A summary of the five microfluidic devices used in this chapter.**

### 3.3.1 Microglia cells survive and proliferate within microfluidic devices

Device 1, as illustrated in **figure 3.2**, consists of two culturing chambers connected by an array of microchannels. 4',6-Diamidino-2-Phenylindole, Dihydrochloride (DAPI), a fluorescent stain that binds strongly to A-T rich regions in DNA, can pass through an intact cell membrane and can be used to stain live and dead cells. DAPI used in combination with Propidium Iodide (PI), which is fluorescent intercalating agent, can be used to evaluate cell viability and is useful to differentiate dead, and healthy cells. To ensure that microglia cells can survive and proliferate in the microfluidic device, an initial experiment using DAPI and PI staining was carried out after 6 days of culture within the device. **Figure 3.7** shows that BV-2 cells can successfully be cultured in microfluidic devices. DAPI/PI staining shows that most cells stain DAPI positive with only a few PI positive cells at day 6 in culture. However, **Figure 3.7(D)** demonstrates that the cells within the microchannels appear to be dead, staining positive for PI. This suggests that the microchannels in device 1 are too small for microglia cells and results in their cell death. However, before optimising the microchannels for migration, it was important to ensure that the cells motility within the device was also optimised, which leads nicely into our next aim; to optimise device coating.

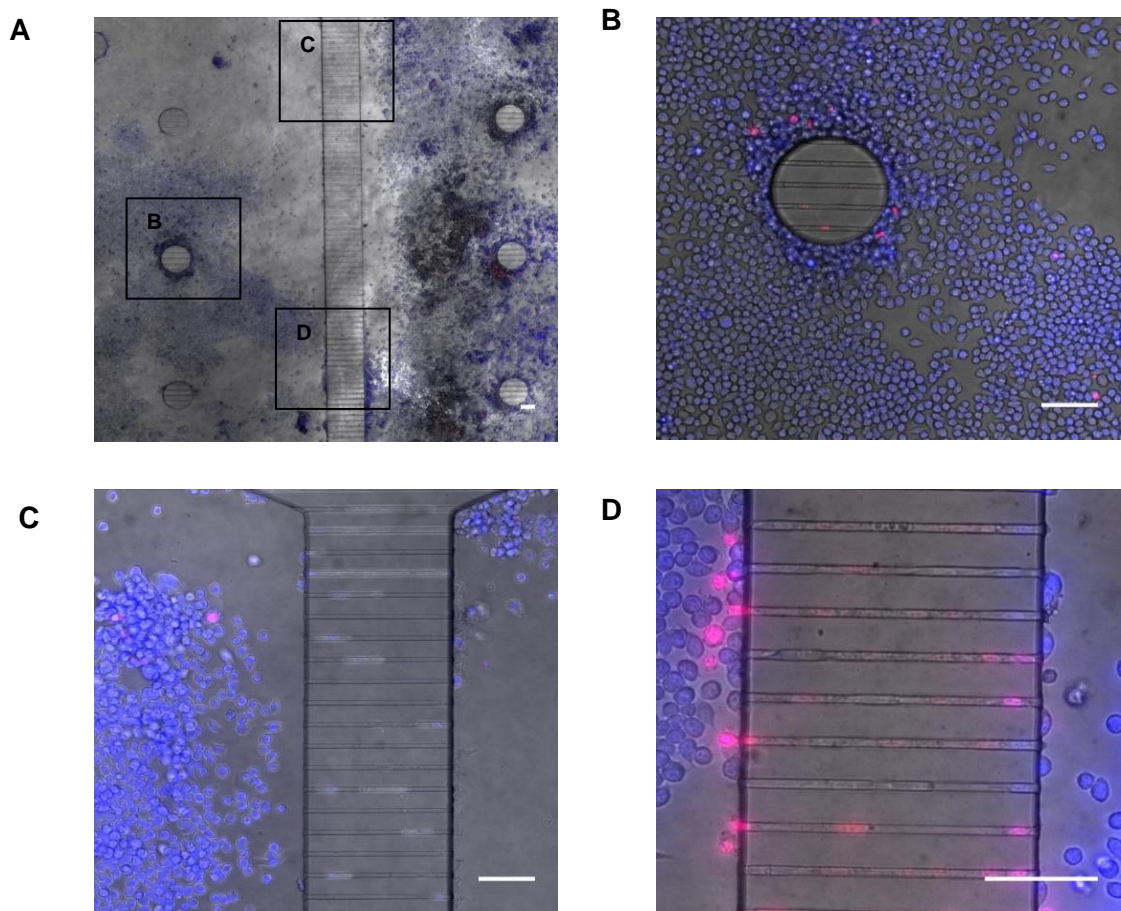


**Fig 3.7. DAPI and Propidium iodide stained BV-2 microglia cells 6 days after insertion into microfluidic devices. (A)** Overview of the device (device 1, **table 3.1**) at 2.5x magnification **(B)** and **(C)** x10 magnification **(D)** x20 magnification show that BV-2 cells can successfully be cultured in the device with **(D)** suggesting that cells within the microchannels die. Blue: Hoechst stain, red: Propidium iodide (PI). Scale bars, 100  $\mu\text{m}$ .

### 3.3.2 Optimisation of coatings of microfluidic devices

Microglia cells were cultured directly onto a glass slide; therefore, an essential step in device preparation is to coat the device to promote cell adhesion. Poly-D-Lysine (PDL), is in current use in our lab for neuronal cultures, however, it was noted that a previous study investigating primary microglia in microfluidic devices used fibronectin (Amadio *et al.*, 2013). To examine, whether PDL and fibronectin were both suitable or if one of the two provided more efficient adhesion while allowing for optimal cell motility, a short pilot study was conducted. Cells were seeded into device 1; cell motility solely within the culturing chambers was measured. Under basal 'resting' conditions, cells were recorded over a period of 15 hours, with 12 cell paths from each condition (PDL and fibronectin) tracked and three parameters quantified. Results revealed that there were no differences in distance travelled or the speed at which the cells move at, concluding that both PDL and fibronectin are both viable adhesion coatings for microglia in microfluidic devices (**figure 3.8**). It should be noted that experiments from this point forward were all conducted on PDL coated devices. The next aim was to validate a device with associated protocols for efficient cell seeding in the chambers (allow for cells to be placed next to the microchannels to sense the gradient), and that microchannels were optimised to allow microglia cells to migrate through these efficiently.

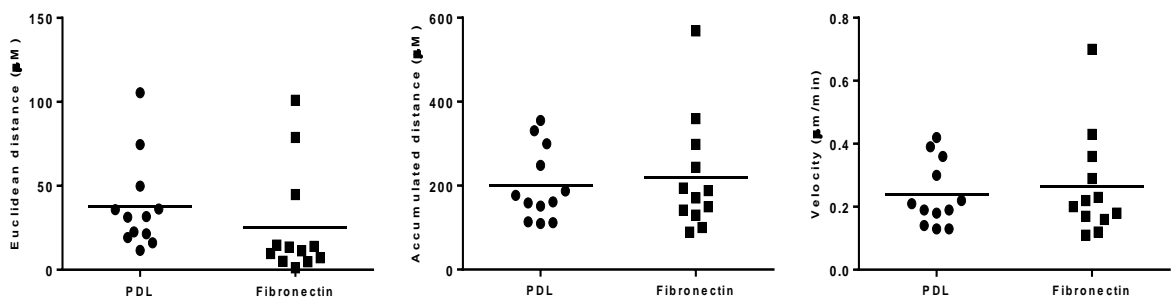


**Figure 3.8. The effect of PDL and fibronectin coating on BV-2 microglia cell motility.** 12 cells were tracked and quantification of their paths were quantified in Image J. The Euclidean distance ( $\mu\text{m}$ ), accumulated distance ( $\mu\text{m}$ ) and velocity ( $\mu\text{m}/\text{min}$ ) show there is no difference in microglia motility between either coating. Data representative of one individual experiment.

### 3.3.3 Results from readily available devices

**Table 3.1** provides a summary of each device used within this chapter, devices 1-4 were readily available so we examined these first. Device 1, consisted of microchannels that are 10  $\mu\text{m}$  wide, and as shown above, these channels were proven to be too small for microglia to migrate through (**figure 3.7**).

To overcome this problem, device 2 was adopted which is a three-chamber device, connected by an array of microchannels that are 15  $\mu\text{m}$  wide. This device is advantageous due to its three distinct chambers that allow for cells to be seeded in the middle chamber, while two different chemoattractant agents can be inserted into the top and bottom chamber setting up two different gradient conditions, allowing cells to migrate both sides. With the microchannels being 15  $\mu\text{m}$  wide instead of 10  $\mu\text{m}$  it was hypothesised that this would provide microglia with a larger space to survive and migrate through. **Figure 3.9** demonstrates that from the cells being seeded within the device at 0 hours (**figure 3.9(A)**), to 10.7 hours after seeding (**figure 3.9(B)**), there was no noticeable migration through the channels and cells also appeared to be stuck in the microchannels. It was concluded that device 2 would not be appropriate to study migration, with the small microchannel width restricting microglia movement.

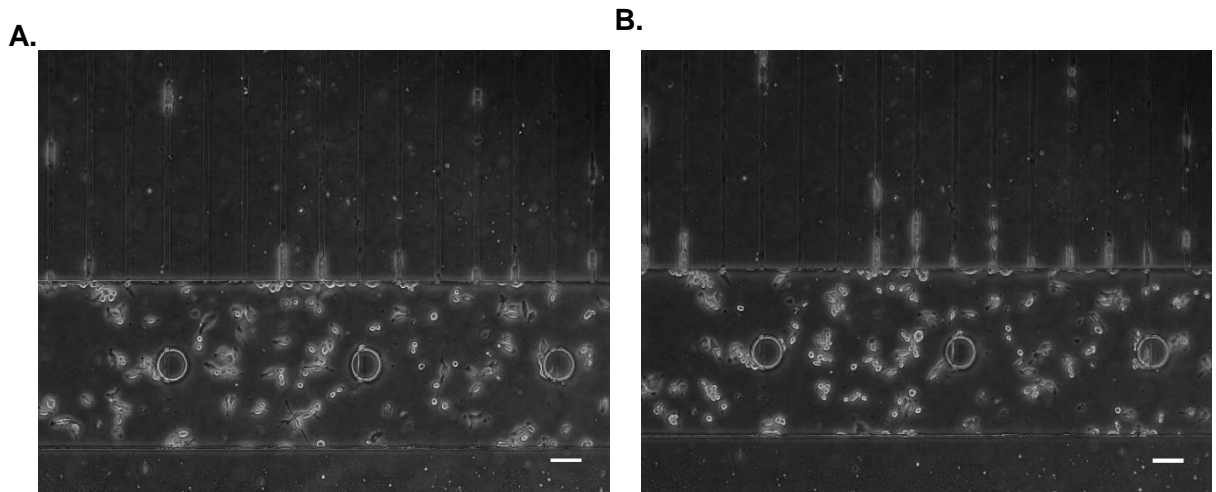


**Figure 3.9. BV-2 microglia cells within device 2.** Snapshot image from time lapse recording at **(A)** 0 hours and **(B)** 10.7 hours. Scale bar, 100  $\mu\text{m}$ .

To overcome the problem with the microchannels, we next moved onto device 3 in which microchannels were replaced with small pillars which possess a larger space between them than microchannels. Ideally cells would be seeded within the two sides of the device, and we would be able to visualise migration through the pillars into the main channel. Unfortunately, we obtained uneven cell distribution throughout this device. During seeding, cells flowed through the pillars and into the remaining chambers, which did not allow for uniform seeding; resulting in cell seeding that was unreproducible (**figure 3.10**).

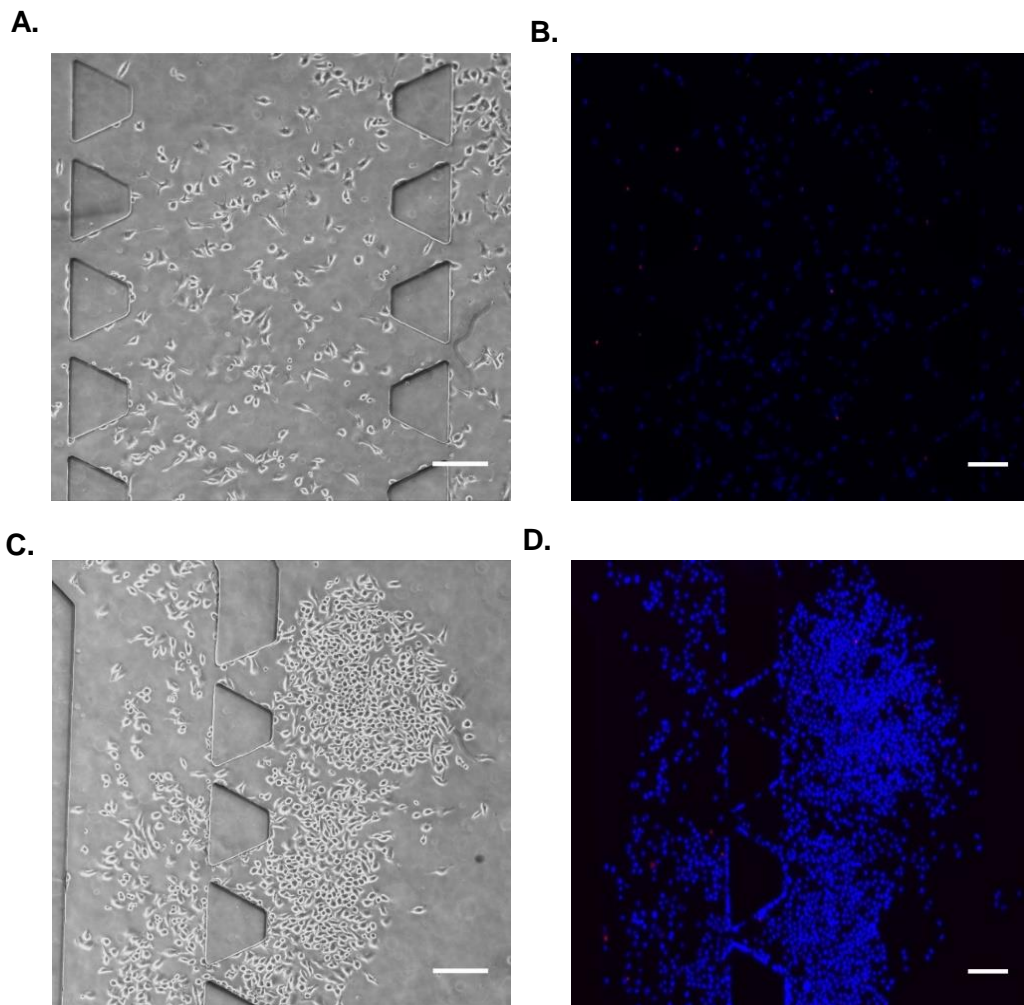


**Figure 3.10. Images of BV-2 cells in device 3, illustrating uneven cell distribution 24 hours after seeding.** Device (A) and (C) and their corresponding Hoechst and PI stained images (B) and (D) respectively. Images demonstrate uneven and unreproducible cell distribution within microfluidic devices. Blue: Hoechst stain, red: Propidium iodine (PI). Scale bar, 100  $\mu\text{m}$ .

Therefore, the use of pillars was evidently not beneficial and device 4 which is another 3-chamber version of device, consisting of one inner chamber that is surrounded by a second outer chamber with two sets of microchannels, again, allowing for two gradients to be established (**Figure 3.11**). The channel width in this device is 100  $\mu\text{m}$  which was a sufficient diameter for microglia cells to happily migrate through. The next step was to ensure that a successful and long-lasting gradient could be established within the device. **Figure 3.11** demonstrates that a gradient was established within the microchannels as visualised using Fluorescein. The outer chamber becomes fully filled with fluorescein moving from a high concentration at the start of the microchannel down to a low concentration within each microchannel.

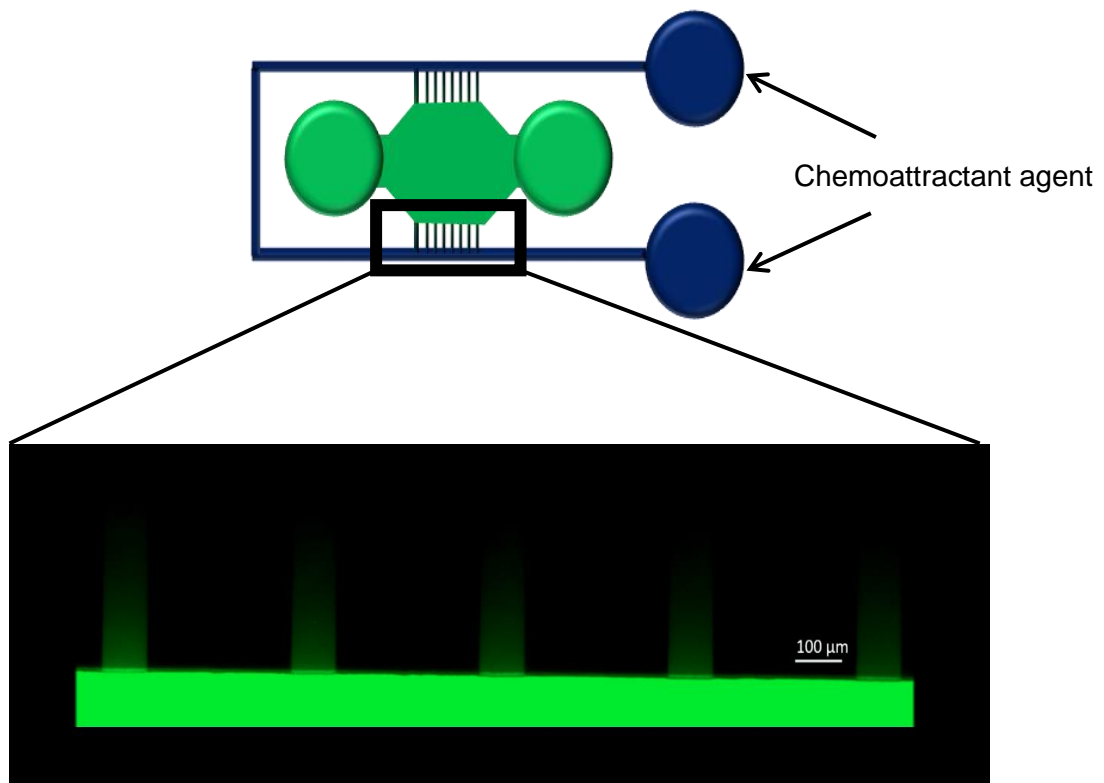


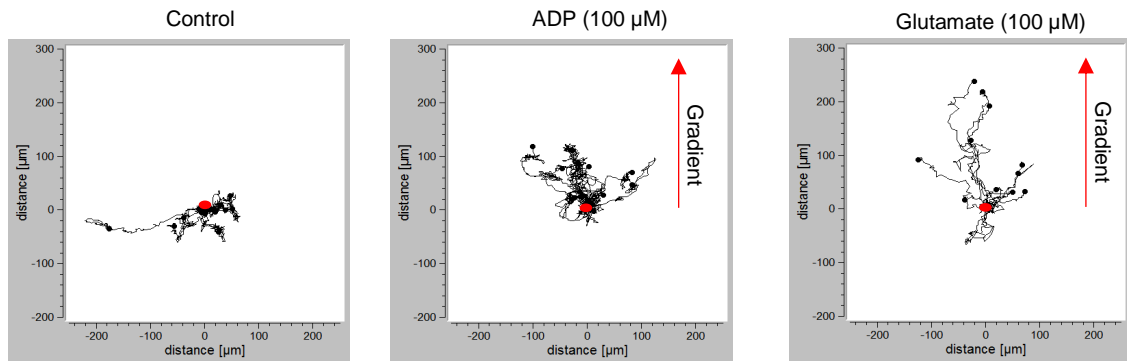
**Figure 3.11. A gradient can successfully be established within microchannels in device 4.** Fluorescent image showing fluorescein filling the source chamber, while a gradient is established within the microchannels. Scale bar, 100  $\mu\text{m}$ .



With successful gradient established in device 4, this device was used for initial migration experiments. Microglia cells were seeded into the device to investigate migration towards glutamate and ADP concentration gradients. **Figure 3.12(A)** illustrates the paths for 12 individual cells from the one experiment, each cell track is coincided into a common starting point (red dot). The cell path is demonstrated by the black lines, with the black dot representing the cells endpoint and each axis representing the distance travelled in both directions ( $\mu\text{m}$ ). In control experiment, with media (DMEM) only in the source chamber, we observed high spontaneous movement of microglia cells with their processes extending and retracting but importantly no preferred migration direction. In contrast, with ADP ( $100 \mu\text{M}$ ) or glutamate ( $100 \mu\text{M}$ ) in the source chamber, there was directional migration of microglia towards the source of ADP and glutamate. From initial observations from one experiment, glutamate and ADP increased the Euclidean distance of microglia whereas, ADP increased microglia's accumulated distance (**figure 3.12(B)**). Although further experiments would be required before conclusions can be drawn, this experiment does show feasibility of quantification of glutamate and ADP-induced migration, the former of which will be the main focus of this chapter given the paucity of literature in this area as detailed above.

However, although the number of cells at initial loading were controlled and the insertion technique was kept constant, we observed uneven distribution of cells in the chambers. Due to the design of the device where the cell seeding chamber has the flow of two microchannels coming in from the top and bottom set of microchannels, when cells were being inserted, the flow from each direction pushed the cells to settle in the middle of the chamber. This resulted in difficulties in trying to get the cells close enough to the microchannels so they could sense the gradient. This led to unreproducible results and so we decided to fabricate a new device geometry, specifically designed to overcome the above-mentioned problems.

**A.**



**B.**

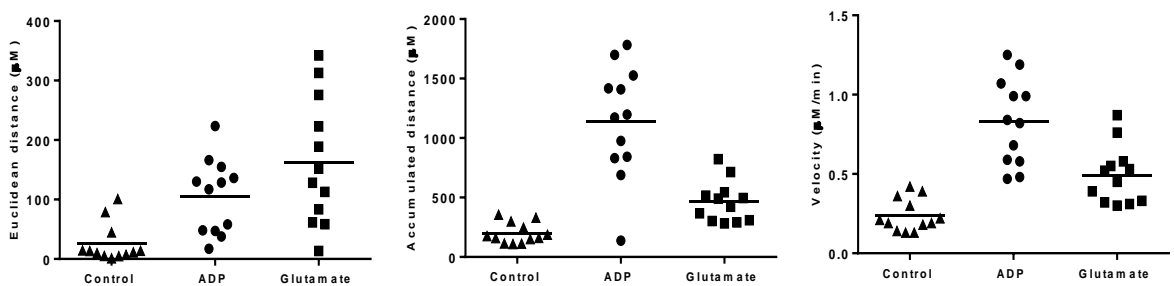


**Figure 3.12. The effect of a glutamate and ADP gradient on BV-2 microglia cells.**

**(A)** Scatter plots of the movement of 12 microglia cells in microfluidic devices when exposed to a gradient of Dulbecco's modified Eagles Medium (DMEM) (left), ADP (100  $\mu\text{M}$ ) (middle) and glutamate (100  $\mu\text{M}$ ) (right). Red dot represents the cells start point, black dot represents the cells end-point. **(B)** Euclidean distance, accumulated distance and velocity of BV-2 microglia in response to DMEM) (left), ADP (100  $\mu\text{M}$ ) (middle) and glutamate (100  $\mu\text{M}$ ) (right). Data are from one independent experiment.

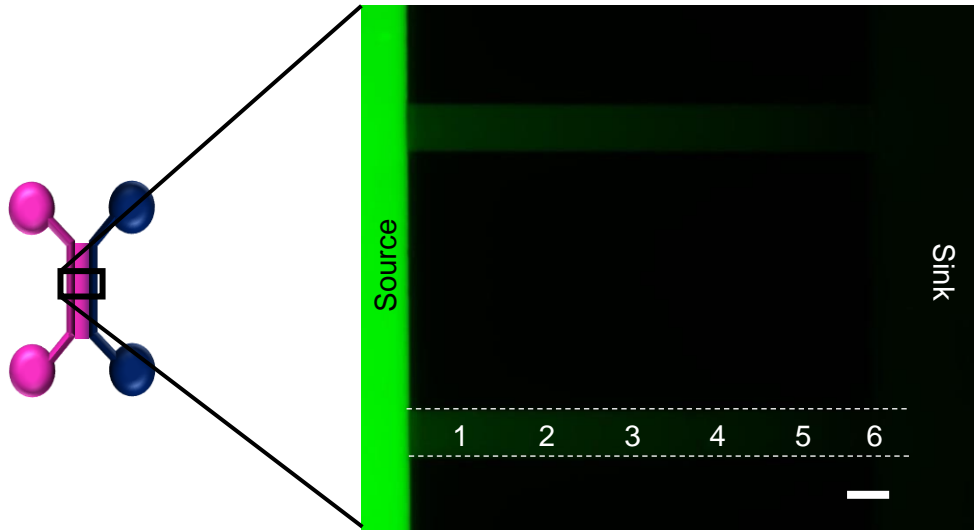
### 3.3.4 New generation of devices

Device 5 was designed based on the structure of device 1; it was the simplest and best geometry but it was optimised to contain wider channels to prevent cells getting stuck. The design consists of two parallel cell seeding chambers that are separated with a series of microchannels that are suitable for a gradient to be established within but also large enough for cells to migrate through. A group of eight devices, all similar structures possessing slightly different dimensions (different lengths, widths and number of microchannels) were designed and fabricated (by Dr Zagnoni). The device that was chosen to proceed with comprised of 10 microchannels, each 1 mm long and 100  $\mu\text{m}$  wide.

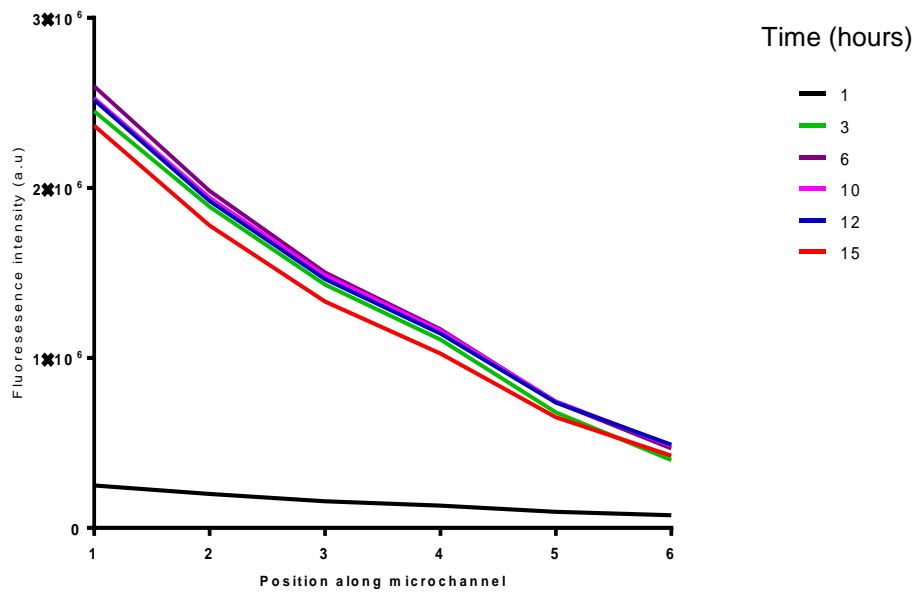
The initial aim was to create a concentration gradient that was established as quickly as possible and maintained constantly for as long as possible. The gradient was characterised using calcein (100  $\mu\text{M}$ ), a fluorescent dye commonly used to visualise and quantify gradient formation. Fluorescent images were taken every 3 minutes for 15 hours using an inverted fluorescence microscope. The fluorescence intensities in the region of the migration were recorded as shown in **figure 3.13(A)** and analysed in Image J. During the gradient characterisation, upon introduction of the fluorophore into the reservoir, the dye fills the 'source' chamber, before slowly diffusing into the microchannels. **Figure 3.13(B)** shows the gradient slopes along the migration channels at 1, 3, 6, 10 and 15 hours, respectively. The selected hours indicate that at 1 hour the gradient is still being established (due to an initial flow, discussed below), after 3 hours the gradient has fully formed, and this is steadily maintained until the end of the experiment (15 hours). **Figure 3.13(C)** illustrates the gradient profile of each position along the microchannel over time during the gradient development.

The rate of diffusion of a molecule depends on its molecular mass and environmental temperature, these two factors affecting the kinetic energy of a particle. Therefore, at a constant temperature, the rate at which a molecule diffuses is inversely proportional to its molecular mass. Gradient characterisation experiments were carried out using calcein. The molecular weight of calcein is 622 g/mol, compared to glutamate which has a molecular weight of 147 g/mol, resulting in a higher diffusion rate with glutamate compared to calcein. To allow for this difference, a slight volume difference of 5  $\mu\text{l}$  was created, allowing an initial flow that will eventually even out, hence explaining why the gradient takes slightly longer to be established (3 hours).

A.



B.



C.

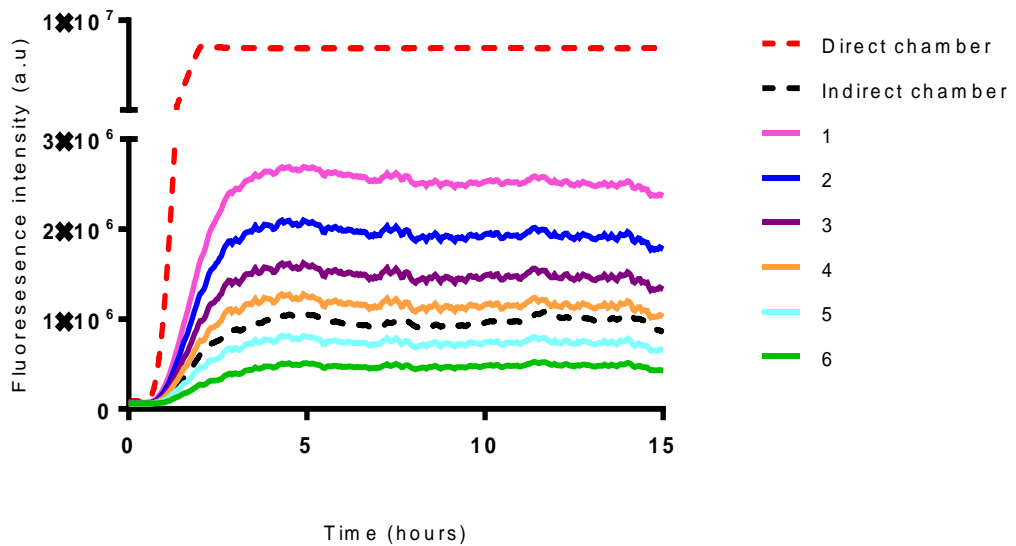


**Figure 3.13. Characterisation of the gradient development.** (A) Fluorescent image shows the calcein gradient along a microchannel connecting the source and sink chamber. Dashed white lines indicate the boundary of the microchannel, 1-6 represents the positions along the channel measured in (B) and (C). Scale bar, 100  $\mu\text{M}$ . (B) Gradient profile along the migration channel at different time (1, 3, 6, 10, 12, and 15 hours). (C) Illustrates the gradient profile of each position within the microchannel over time as the gradient develops.

### 3.3.5 The effect of LPS and IL-4 treatment on glutamate-induced migration in SIM-A9 microglia cells

Microglia migration in response to a gradient of glutamate was investigated using device 5. The microglia (as described in **section 3.2.3**) are added to the device by adding a small volume concentrated cells into the sink chamber. As previously observed, under control conditions (DMEM in the source chamber), in absence of any chemotactic agent; microglia cells are randomly motile, but in no directed migration. Visualisation of the cells movement and path can be seen in **figure 3.14(A)**, which displays representative cell paths from 24 individual cells. In the presence of a gradient of glutamate (100uM glutamate in the source chamber), the microglia migrate out of the 'sink' region and begin to migrate along the glutamate gradient that was established in the microchannels. The cell paths demonstrate that SIM-A9 cells migrate up the concentration gradient towards the source of glutamate (**figure 3.16**).

The Euclidean distance of microglia was significantly increased in the presence of a glutamate gradient compared to control ( $139.2 \pm 23.13 \mu\text{m}$  vs  $44.34 \pm 7.86 \mu\text{m}$ , respectively). The pro-inflammatory inducer, LPS added directly to the cells in the sink chamber, significantly inhibited microglia's ability to migrate in response to a glutamate gradient. The Euclidean distance of microglia was significantly decreased from  $139.2 \pm 23.13 \mu\text{m}$  in the presence of a glutamate gradient, to  $52.45 \pm 12.19 \mu\text{m}$  in the presence of direct LPS on the cells (**figure 3.14(B)**). The effect of LPS on glutamate-induced migration is also reflected in the cell path diagrams, producing paths similar to control, where they remain motile, yet, their directional migration is limited.

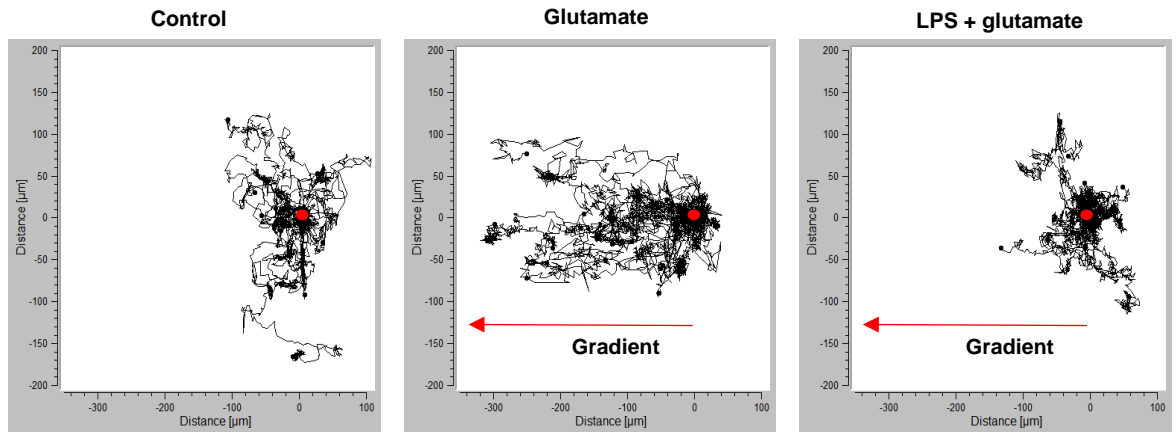
Given that inducing a pro-inflammatory phenotype had such pronounced effect on microglia migration, we next investigated the effect of inducing an anti-inflammatory phenotype on glutamate-induced microglia migration. As expected glutamate increased the Euclidean distance of cells compared to control cells ( $63.88 \pm 18.07 \mu\text{M}$  vs.  $22.61 \pm 5.66 \mu\text{M}$ , respectively), despite a one-way ANOVA failing to reach statistical significance, a trend to an increase was observed (**figure 3.15(B)**). Interestingly, inducing an anti-inflammatory phenotype, using IL-4 significantly increased the Euclidean distance of SIM-A9 cells from  $63.88 \pm 18.07 \mu\text{M}$  with glutamate alone, to  $111.4 \pm 35.76 \mu\text{M}$  in the presence of direct IL-4 and a glutamate gradient (**figure 3.15(B)**). The effect of IL-4 on glutamate-induced migration is further

reflected in their cell paths, **figure 3.15(A)** illustrating cells migrating towards the source of glutamate; which is further enhanced in the presence of IL-4.

As revealed in **figure 3.14(B)** and **3.15(B)** the average migratory speed (velocity) and the accumulated distance of microglia cells exposed to glutamate, LPS and IL-4 were compared. There was no significant effect of any of the treatments on the velocity or the accumulated distance of microglia.

The logical conclusions are that when microglia are induced into a pro-inflammatory phenotype (direct LPS treatment), their migratory capabilities are significantly reduced. This is compared with microglia cells that are induced into an anti-inflammatory phenotype (direct IL-4 treatment) where, their migratory capabilities are significantly increased. This is discussed in **section 3.4**, but if this is the case, this opens doors for immunomodulatory agents, such as MSCs, to control microglia migration, which is explored in the next section of this chapter.

**A.**



**B.**

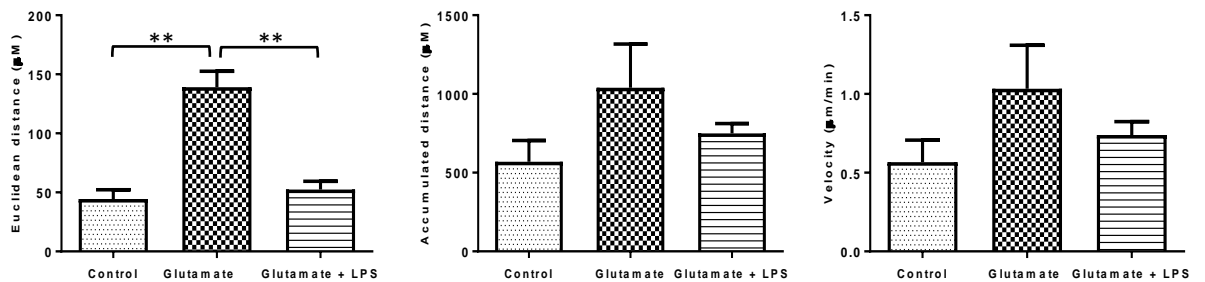
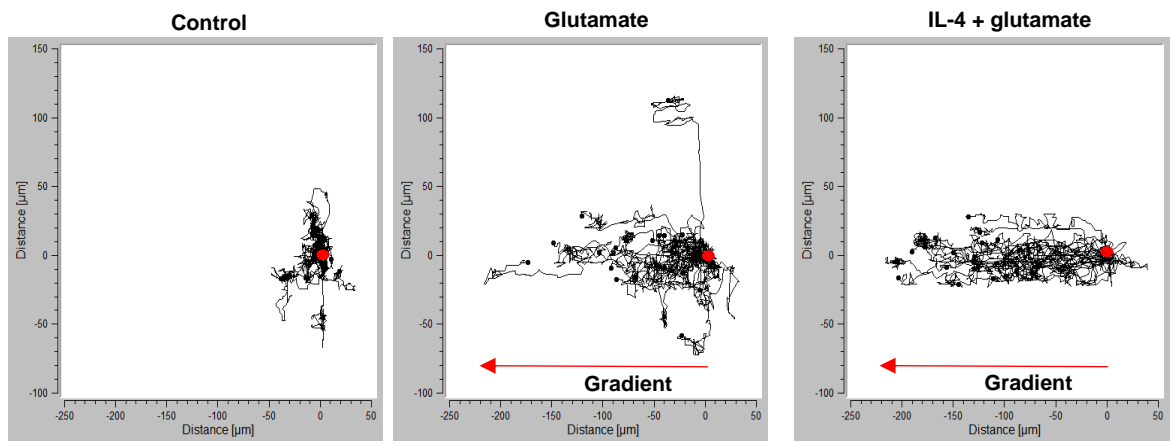


**Figure 3.14. LPS inhibited glutamate-induced SIM-A9 microglia cell migration in microfluidic devices. (A)** Scatter plots taken from one representative experiment showing the movement of 24 microglia cells in microfluidic devices when exposed to a gradient of Dulbecco's Modified Eagles Medium (DMEM) (left), glutamate (100 µM) gradient (middle) and direct LPS (1 µg/ml) and a glutamate (100 µM) gradient (right). The red dot represents the cells start point, while the black dots represents the cells end-point. **(B)** Euclidean distance (left), accumulated distance (middle) and velocity (right) of SIM-A9 microglia in response to DMEM, glutamate (100 µM) gradient, and direct LPS (1 µg/ml) with a glutamate (100 µM) gradient. Data shown as mean ± SEM and a combination of three independent experiments. \*\*P ≤ 0.01, One-way ANOVA, Tukey's post-test.



**A.**



**B.**

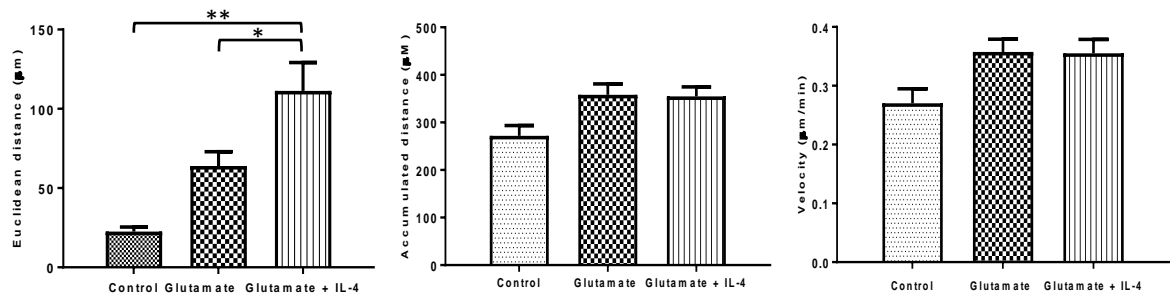


**Figure 3.15. IL-4 enhanced glutamate-induced SIM-A9 microglia cell migration in microfluidic devices.** Time lapse imaging was performed and images were captured every 3 minutes over a period of 15 hours. **(A)** Scatter plots taken from one representative experiment showing the movement of 24 microglia cells in microfluidic devices when exposed to a gradient of Dulbecco's Modified Eagles Medium (DMEM) (left), glutamate (100 µM) gradient (middle) and direct IL-4 (20 ng/ml) and a glutamate (100 µM) gradient (right). The red dot represents the cells start point, while the black dots represents the cells end-point. **(B)** Euclidean distance (left), accumulated distance (middle) and velocity (right) of SIM-A9 microglia in response to DMEM, glutamate (100 µM) gradient and direct IL-4 (20 ng/ml) with a glutamate (100 µM) gradient. Data shown as mean ± SEM and a combination of four independent experiments. \*P ≤ 0.05, \*\*P ≤ 0.01, One-way ANOVA, Tukey's post-test.

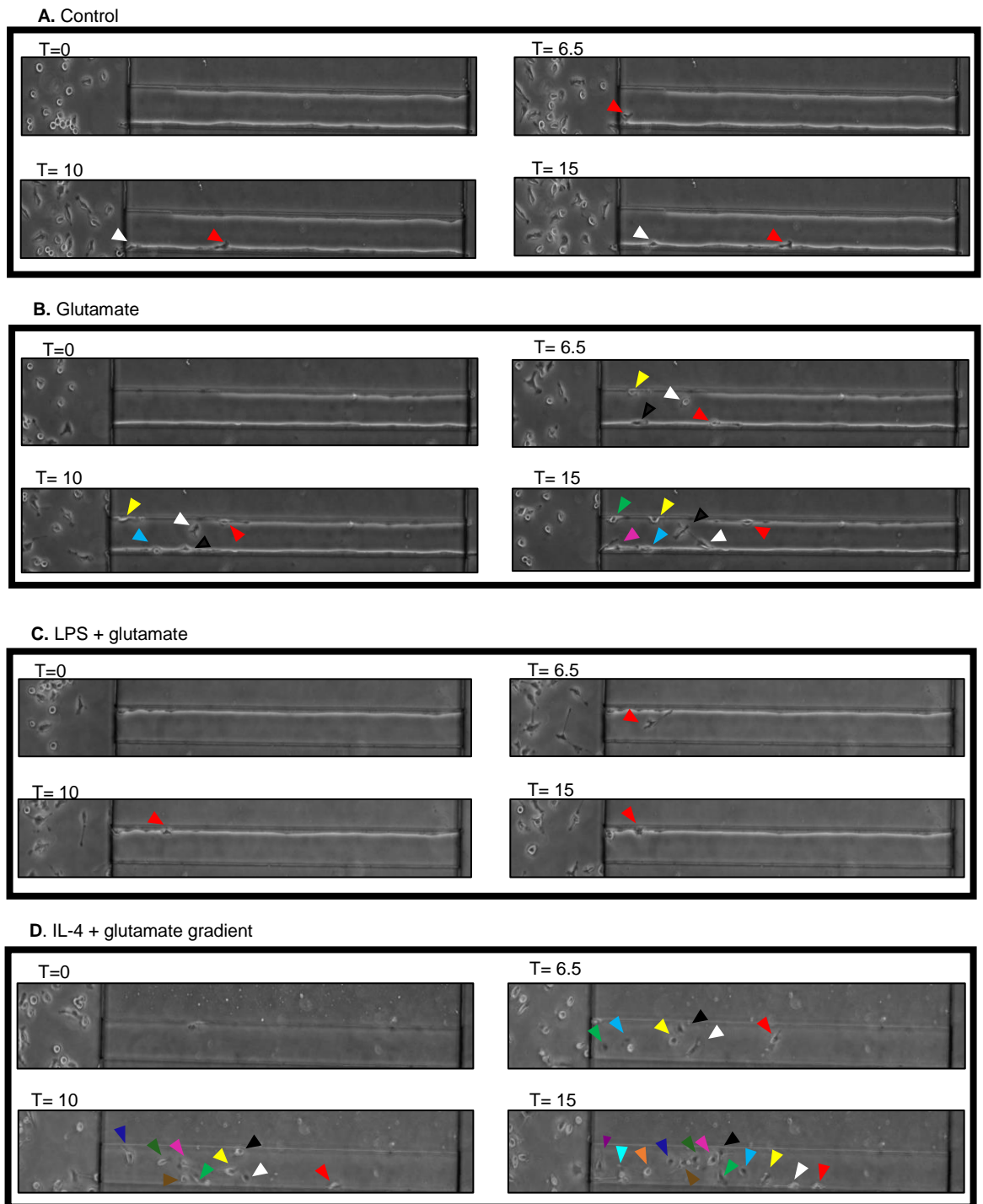


**Figure 3.16. Modulation of glutamate-induced migration by LPS and IL-4.** Snapshot images from one representative experiment of SIM-A9 microglia. In response to **(A)** control, DMEM gradient, **(B)** a glutamate (100  $\mu$ M) gradient, **(C)** direct LPS (1  $\mu$ g/ml) and a glutamate (100  $\mu$ M) gradient **(D)** direct IL-4 (20 ng/ml) and a glutamate (100  $\mu$ M) gradient. Different coloured arrow heads represent individual microglial cells within the microchannels.

### 3.3.6 The effect of hAMSC-CM treatment on glutamate-induced migration in SIM-A9 microglia cells

The final aim of this chapter was to investigate the effects of hAMSC-CM on microglia migration using the current established migration model. In hAMSC-CM experiments, the control cells are exposed to a different medium, (neurobasal medium instead of DMEM). Neurobasal medium is the base of the conditioned media, so it was important to ensure that any effects observed was due to hAMSC-CM and not the different base medium. To ensure that the change of media did not affect the cell behaviour, glutamate alone, and LPS treatments were repeated to ensure the same effects were observed in the presence of neurobasal media. **Figure 3.17(A)** shows the paths of SIM-A9 microglia and, upon introduction of a glutamate-gradient, cells migrated towards the source of glutamate. In the presence of direct LPS, glutamate-induced migration was inhibited. Cells moved randomly without any direction, as previously seen with LPS treatment. Interestingly, when cells were directly applied with LPS and hAMSC-CM under presence of a glutamate gradient, migration was restored, with cells once again migrating towards increasing concentrations of glutamate. These results are reflected in the quantified data; direct LPS significantly inhibited the Euclidean distance of microglia cells when compared to glutamate alone ( $18.44 \pm 3.99 \mu\text{M}$  vs.  $50.07 \pm 5.27 \mu\text{M}$ , respectively). The addition of hAMSC-CM significantly reversed the inhibitory effect of LPS on glutamate-induced migration, almost fully restoring the Euclidean distance from  $18.44 \pm 3.99 \mu\text{M}$  to  $39.98 \pm 13.23 \mu\text{M}$ , respectively. Representative snapshot images of cells migrating into the microchannels at different time points are shown in **figure 3.18**.

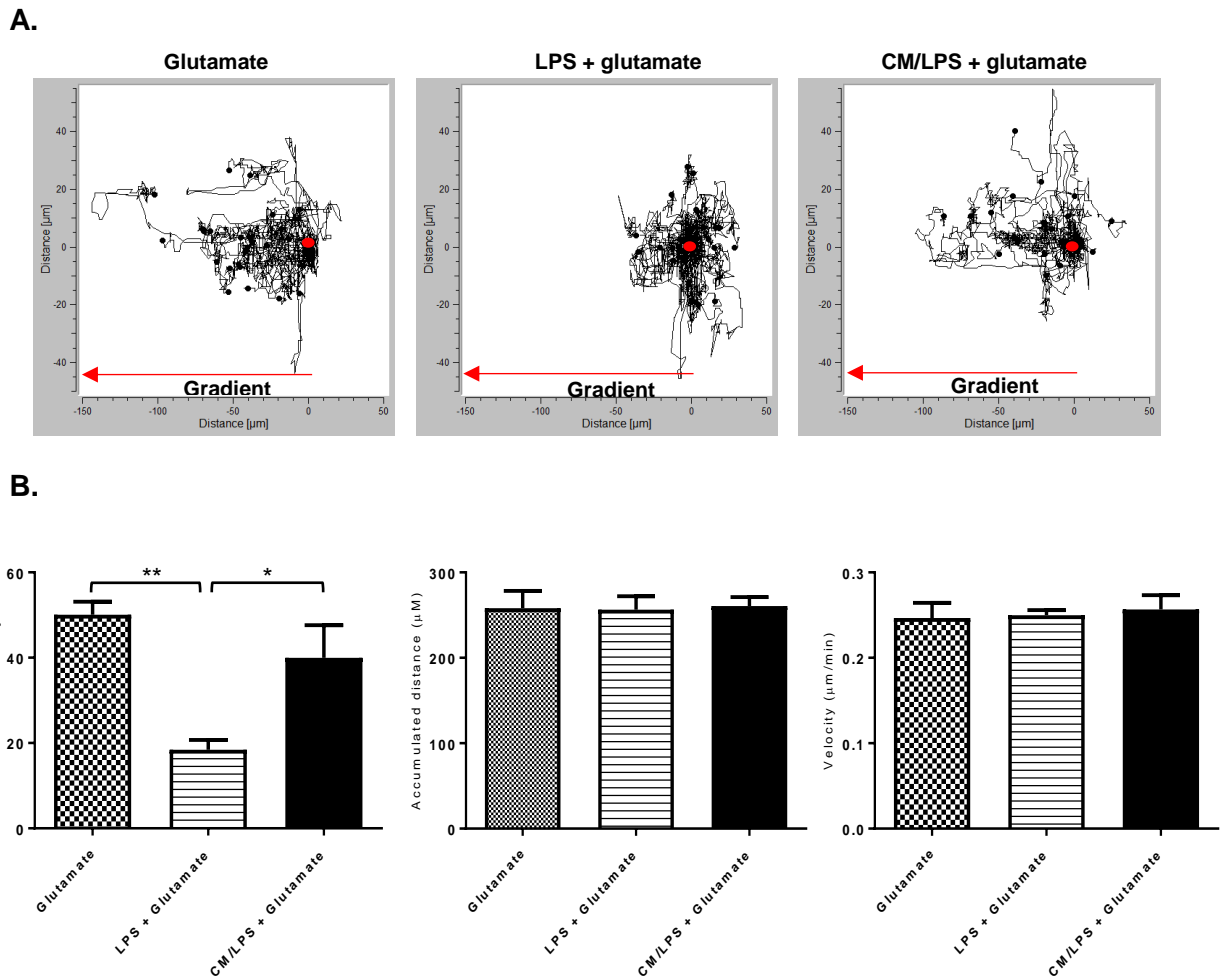


**Figure 3.17. hAMSC-CM reverses the inhibitory effect of LPS on glutamate-induced SIM-A9 microglia cell migration in microfluidic devices.** Time lapse imaging was performed, and images were captured every 3 minutes over a period of 15 hours. **(A)** Scatter plots taken from one representative experiment showing the movement of 24 microglia cells in microfluidic devices when exposed to a glutamate (100  $\mu\text{M}$ ) gradient in neurobasal medium (left), direct LPS (1  $\mu\text{g}/\text{ml}$ ) and a glutamate (100  $\mu\text{M}$ ) gradient in neurobasal medium (middle), and direct CM-and LPS (1  $\mu\text{g}/\text{ml}$ ) and a glutamate (100  $\mu\text{M}$ ) gradient (right). The red dot represents the cells start point, while the black dots represents the cells end-points. **B)** Euclidean distance (left), accumulated distance (middle) and velocity (right) of SIM-A9 microglia in response to glutamate (100  $\mu\text{M}$ ) gradient in neurobasal medium, direct LPS (1  $\mu\text{g}/\text{ml}$ ) and a glutamate (100  $\mu\text{M}$ ) gradient in neurobasal medium and direct hAMSC-CM and LPS (1  $\mu\text{g}/\text{ml}$ ) and a glutamate (100  $\mu\text{M}$ ) gradient. Data shown as mean  $\pm$  SEM and a combination of four independent experiments. \* $P \leq 0.05$ , \*\* $P \leq 0.01$ , One-way ANOVA, Tukey's post-test.

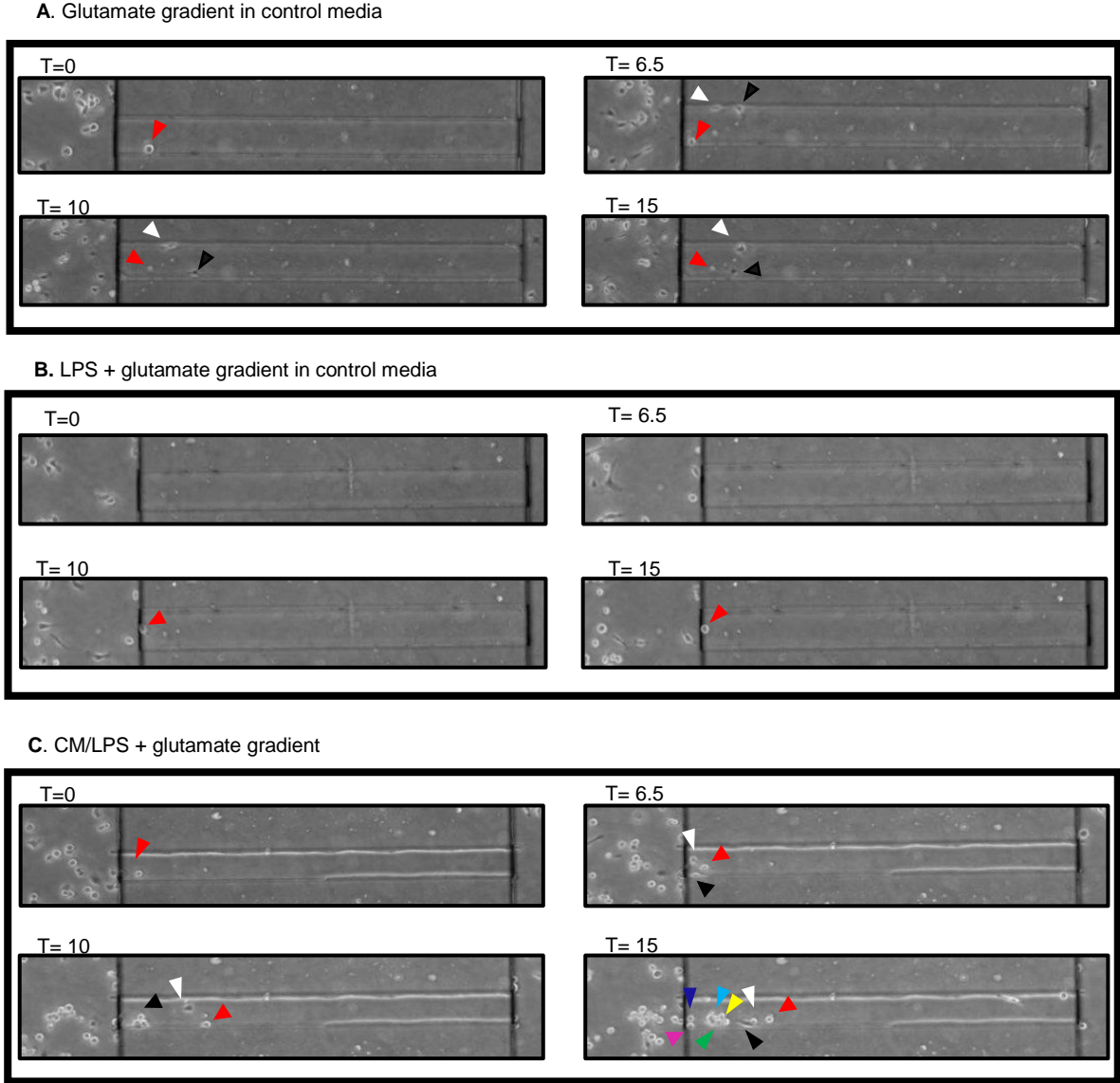


**Figure 3.18. hAMSC-CM reversed the inhibitory effect of LPS on glutamate-induced microglia migration.** SIM-A9 microglia response to **(A)** a glutamate (100  $\mu$ M) gradient in neurobasal medium, **(B)** direct LPS (1  $\mu$ g/ml) and a glutamate (100  $\mu$ M) gradient in neurobasal medium **(C)** direct CM and LPS (1  $\mu$ g/ml) and a glutamate (100  $\mu$ M) gradient. Arrow heads indicate microglia cells.

### 3.4 Discussion

#### 3.4.1 The use of microfluidic technology to study microglia migration

The main aim of this chapter was to develop a microfluidic assay to examine microglia migration in response to the chemoattractant properties of several molecules. The ability to treat cells with chemical gradients *in vitro* is a valuable tool for mimicking the *in vivo* environment. In this chapter, we showed that using microfluidic technology: 1) a chemical gradient could be established within the microchannels of the microfluidic device and was stable over a period of 15 hours and 2) microglia survival and migration towards an increasing glutamate concentration gradient was achieved. The large volume sink reservoir at the end of the chambers helped to maintain the chemical gradient without allowing the chemical species to accumulate in the chambers. In order to limit fluid flow resulting from small pressure differences, the optimised fabricated migration channels were shallow in height (5  $\mu\text{M}$ ) and narrow in width (100  $\mu\text{M}$ ), and the cell chambers were 20 times deeper in height (100  $\mu\text{M}$ ) and 12 mm in length. This design helped to create a high fluidic resistance within the migration channels to minimize the convective flow from the glutamate loading site due to any unwanted pressure differences. Using this method, we demonstrated that SIM-A9 microglia cells exhibit spontaneous motility in control conditions; SIM-A9 microglia cells respond to a glutamate gradient migrating towards the source; a pro-inflammatory inhibited glutamate-induced microglia migration, whereas, an anti-inflammatory stimulus enhanced glutamate-induced migration; and exposure to hAMSC-CM reversed the inhibitory effects of LPS, restoring glutamate-induced migration. The results of these findings are discussed below.

An important observation during migration experiments was the motility of microglia under basal conditions, with no chemoattractant. Experiments showed that microglia in the control group possessed a degree of random motility as shown in the cell path graphs and accumulated distance data. The time-lapse images showed that the SIM-A9 microglia cells extend and retract their processes continuously with many of the cell bodies randomly migrating through the device. In preliminary studies BV-2 cells were utilised, however, due to experimental complications, the SIM-A9 cell line were used. It should be noted that previous reports have noted that BV-2 failed to give reliable results in chemotaxis experiments (Graeber and Streit, 2010).

A study investigating the motility of primary microglia in microfluidic devices utilised similar devices to device 5 used for migration experiments in the current chapter. Amadio *et al.*, (2013) used fibronectin-coated microchannels with a width of 12-18  $\mu\text{M}$  and a length of 500  $\mu\text{M}$ . Interestingly, in that study, the authors recorded the spontaneous migration of microglia, in the absence of a chemoattractant. Detection of microglia migrating through the microchannels was observed with one cell completing the full length of 500  $\mu\text{M}$  in 11.5 hours. The average accumulated distance of microglia over the 20 hour recording was reported  $409.2 \pm 199.6 \mu\text{M}$  with the mean velocity noted to be  $0.35 \pm 0.145 \mu\text{M}/\text{min}$ . Although this experiment was conducted with primary microglia cells, interestingly, our results of control cells (no chemoattractant, spontaneous movement) produce very similar findings to Amadio and colleagues [average accumulated distance for control cells;  $569.9 \pm 134.7 \mu\text{M}$ , mean velocity of control cells;  $0.56 \pm 0.13 \mu\text{M}/\text{min}$ ] validating our results of the basal motility of microglia. It should be noted that when we used a device with a similar microchannel width as Amadio and colleagues (device 2, 15  $\mu\text{M}$ ), it was too small for microglia cells and did not allow efficient migration through the microchannels. We observed a degree of spontaneous movement of 'resting' microglia, in absence of a chemoattractant gradient, cells including their cell body randomly moved through the device, nonetheless, there was no directed migration.

These findings are also observed *in vivo* and it has been shown that in acutely isolated living slices from adult brain-injured mice when microglia cells are reactive they can migrate rapidly at peak velocity  $\geq 10 \mu\text{m}/\text{min}$  (Carbonell *et al.*, 2005). By using *in vivo* two-photon imaging in the neocortex, it was found that microglia cells are highly active in their presumed 'resting state'; continually surveying their microenvironment with extremely motile processes and protrusions (Nimmerjahn *et al.*, 2005). Davalos and authors reported that only microglia processes are highly dynamic in the intact brain, reaching up to several  $\mu\text{M}$ 's in length or retracting until they completely disappear (Davalos *et al.*, 2005).

### 3.4.2 A glutamate gradient induces migration of SIM-A9 microglial cells

Using microfluidic technology to introduce a chemical gradient of glutamate, we observed chemotaxis of SIM-A9 cells in response to glutamate (100  $\mu\text{M}$ ). Glutamate is the major excitatory neurotransmitter of the CNS with ambient levels of glutamate measuring between 0.5  $\mu\text{M}$  and 2  $\mu\text{M}$  in the extracellular space of unstimulated parenchyma (Meldrum, 2000). Perturbations in the homeostasis, such as under ischaemic conditions, can lead to large amounts of glutamate being released from neurons, astrocytes and microglia. The present work shows that gradients of glutamate can strongly attract microglia, suggesting that the ischaemic-released glutamate can strongly attract microglia migrating to the area of pathology, similarly to ATP and chemokines. ATP/ADP is a well-known chemoattractant for microglia and a plethora of evidence suggests that migration is mediated by the stimulation of P2Y<sub>12</sub> with ATP from damaged cells (Honda *et al.*, 2001; Davalos *et al.*, 2005; Haynes *et al.*, 2006; Ohsawa *et al.*, 2012).

In agreement with our findings, Liu *et al.*, (2009) also reported that glutamate acted as a chemoattractant agent for microglia in spinal cord slices. Using the Dunn chamber, they report a distance migrated of approximately 10  $\mu\text{M}$  in control cells compared to 20  $\mu\text{M}$  in cells treated with Glutamate (100  $\mu\text{M}$ ). These reported distances are a lot smaller than we report, lack of migration parameter for example accumulated and Euclidean distance could be a possible limitation of this study.

Liu *et al.* (2009) also examined the mechanisms in which glutamate can induce chemotaxis of microglia cells. They examined the possibility that, as glutamate triggers ATP release from microglia cells (Liu *et al.*, 2006), the increase in motility induced by glutamate may be due to the evoked release of ATP acting on P2Y<sub>12</sub> receptors. However, their results showed that blocking purinergic receptors with suramin and PPADS had no antagonistic effects on glutamate-driven chemotaxis of microglia neither did the ATP degrading enzyme apyrase. Given that reactive microglia possess group I (mGlutR1,5), group II (mGlutR2,3) and group III (mGlutR4,6,8) metabotropic glutamate receptors as well as AMPA ionotropic receptors but not NMDA receptors (Liu *et al.*, 2009, Pocock and Kettenmann, 2007), taken together these results suggest that microglia chemotaxis is due to a direct effect of glutamate on AMPA and metabotropic glutamate receptors rather than indirectly through ATP released from microglia by glutamate (Liu *et al.*, 2009).



In disagreement with this, Fontainhas *et al.*, (2011) reported that retinal microglia cells respond directly to ATP but not to glutamatergic or GABAergic agonists. They indicate that glutamate-induced migration may be indirectly mediated, with ATP acting as an intermediate signal. They conclude that glutamate and GABA receptors are likely to be absent on the surface of resting microglia in intact tissue and that the regulatory effects are mediated indirectly through a secondary signal, likely to be ATP.

### **3.4.3 The effect of LPS and IL-4 treatment on glutamate-induced migration in SIM-A9 microglia cells**

In this set of experiments, we assessed the effects of pro- and anti-inflammatory agents (LPS and IL-4, respectively) on glutamate-induced microglia migration. The results from this chapter suggest that the microglia resting or surveillant phenotype is associated with the ability of these cells to migrate in response to danger signals, such as glutamate. This ability is enhanced when microglial cells are exposed to anti-inflammatory molecules such as IL-4 but is lost when cells are exposed to LPS. As far as we are aware, there are no studies that investigate the effect of microglia phenotype on glutamate-induced migration. However, similar findings have been observed with ADP-induced migration. It has been reported that microglia chemotactic response to ADP is reversed upon microglia activation. De Simone and authors used Boyden chambers to show that in the presence of 10  $\mu$ M ADP, the anti-inflammatory mediator, TGF- $\beta$  significantly increased the migratory activity of freshly isolated microglia cells, while LPS inhibited it. They elucidate the mechanism to show that TGF- $\beta$  increased both migration and P2Y<sub>1</sub> and P2Y<sub>12</sub> receptor expression, while LPS strongly inhibited both. These interpretations are further supported by the observation that microglia migratory response to ATP was reversed following LPS activation, during which a loss of P2Y<sub>12</sub> expression was reported (Haynes *et al.*, 2006). It has been proposed that there is connection between P2Y<sub>12</sub> and A<sub>2A</sub> receptor expression in microglia: downregulation of P2Y<sub>12</sub> expression is accompanied by a strong upregulation of the adenosine A<sub>2A</sub> receptors. Studies have demonstrated that activated microglia assume their characteristic amoeboid morphology because of A<sub>2A</sub>-driven process retraction (Orr *et al.*, 2009). It has been hypothesised that the type of predominant receptor (P2Y<sub>12</sub> vs A<sub>2A</sub>) determines microglia motility (Orr *et al.*, 2009). The expression of adenosine receptors could not be detected on quiescent, ramified microglia *in vitro* unless microglia were activated by LPS, which lead to the upregulation of A<sub>2A</sub> and down-regulation of the P2Y<sub>12</sub> receptor (Madry and Attwell,

2015). Interestingly, P2Y<sub>12</sub> receptors have been reportedly downregulated in microglia after stroke (Domercq *et al.*, 2013). Considering the contrasting effects of ATP on resting vs activated microglia (Orr *et al.*, 2009), Gyoneva and colleagues tested the ability of activated microglia in LPS-injected mice to respond to laser-induced tissue damage. Results showed that microglia in LPS-treated animals approached the ablation at a slower rate than microglia in control animals (Gyoneva *et al.*, 2014), in agreement with the present results

#### **3.4.4 The effect of hAMSC-CM treatment on glutamate-induced migration in SIM-A9 microglia cells**

In the current study, we demonstrate the ability of hAMSC-CM to reverse the inhibitory effects of LPS on glutamate-induced microglia migration. The effect of conditioned media from MSCs on microglia migration have not been investigated (as far as we are aware) until now. The results demonstrate that hAMSC-CM reverses the inhibitory effect of LPS on glutamate-induced migration. Taken together with the results in the previous chapter, where the addition of hAMSC-CM significantly reduced LPS-induced inflammatory response, these results suggest that hAMSC-CM modulates microglia cells into an anti-inflammatory phenotype and thus increasing their migratory capacity. It should be noted that the overall distances travelled in the set of hAMSC-CM experiments are lower when compared to the previous LPS and IL-4 experiments. We hypothesise that this is due to the difference in control media, it would suggest that SIM-A9 microglia cells may not be as functional in the neurobasal medium compared to DMEM.

A previous study investigated the effect of MSC/microglia co-culture on microglia migration using mouse MSCs and BV-2 microglia cells. Interestingly, BV-2 cells migrated towards MSCs but their migration was not significantly affected by soluble factors secreted by unprimed or LPS-primed MSCs (Rahmat *et al.*, 2013). The authors concluded that microglia are compelled to be in close proximity to MSCs. Differences in our results could be due to cells/secretions used, and the MSC source; they use MSC from the bone marrow, in comparison, we use MSCs extracted from the umbilical cord. The migration assay used was the Boyden chamber, which cannot distinguish between directed migration and increased non-directional cell motility and could explain the contrasting conclusions. Contrary to the results we observed with secretions from hAMSCs, Yuan *et al.*, (2015) showed that Scutellarin, a Chinese

herbal compound with anti-oxidants effects halted microglia migration. It was reported that the FCS-induced migration of BV-2 cells towards the lower compartment treated with Scutellarin, was significantly decreased compared with the control (Yuan *et al.*, 2015). Differences between our results and those of Yuan *et al.*, (2015) could be due to the lack of gradient in Yuan *et al.*, (2015). Without a gradient, it is likely the chemoattractant (20% FCS) producing an increase in overall motility rather than directed migration as measured in the present study.

Although in the current study the microfluidic device was designed to study microglia migration, depending on the size of the cell of interest, further cell types could be examined. In addition to microglia migration, microfluidic devices have been shown to be utilised for migration of many cell type across various field of research. Recently, use of microfluidic devices filled with hydrogels have been created to study the migration of lung cancer cells under different cancer invasion microenvironments (Anguiano *et al.*, 2017). Another group, used microfluidic devices to track the migration of dendritic cells towards immobilized gradients of the chemokine CCL21 (Schwarz *et al.*, 2016).

Further studies are required to elucidate the mechanisms involved in glutamate-induced migration, the effect of phenotype on receptor expression and the mechanisms involved in hAMSC-CM enhanced microglia migration. Using an interdisciplinary approach, the study of microglia migration was investigated. By mimicking a simplified *in vivo* post stroke situation, microfluidic technologies can help to understand the role of microglia and the effect of possible therapies for example, hAMSC-CM.

In conclusion, the main findings of this chapter are that; SIM-A9 microglia cells can migrate towards a glutamate gradient, this migration is dependent on the phenotype of microglia cells, with a pro-inflammatory stimulus inhibiting migration, and an anti-inflammatory stimulus enhancing migration. The results also show that hAMSC-CM is capable of reversing LPS inhibitory effect of glutamate-induced migration, agreeing with our findings in the previous chapter and further confirming the potential of hAMSC-CM to modulate microglia. The next chapter investigates the effect of hAMSC-CM on the acute inflammatory response post MCAO.

### **3.4.5 Methodological limitations**

Possible limitations of the current work include the use of the SIM-A9 cell line as opposed to primary cells as discussed in **section 2.4.6**. It should be noted that a glutamate gradient was established to induce migration of microglial cells, the *in vivo* environment would consist of many chemoattract molecules combined, for example, ADP, ATP, CCL21, and CX3CL1. Chemoattractant molecules are released from many other cell types as well as cell to cell interactions with microglia which could inhibit or increase migratory signals. The current model of microglia migration does not take the contributing effects of other cell types or the addition of several chemoattractant molecules into consideration and this is a limitation of the study.

**Chapter 4: Establishment of the middle cerebral artery occlusion model in mice and investigation of the effect of hAMSC-CM on the acute inflammatory response post-MCAO**

#### 4.1 Introduction and aims

In previous chapters, it was demonstrated that conditioned media from human amniotic mesenchymal stromal stem cells (hAMSC-CM) is capable of modulating microglia's inflammatory response *in vitro*. hAMSC-CM has previously been shown by our collaborators to have a beneficial effect *in vivo*. Intravenous or intracerebral injection of hAMSC-CM after traumatic brain injury led to early and persistent brain protection (up to 5 weeks) (Pischiutta *et al.*, 2016). In addition, Pischiutta and colleagues have produced pilot data showing that hAMSC-CM improves functional recovery after stroke (Pischiutta *et al.*, personal communication). Cortical slices injured by oxygen-glucose deprivation and treated with hAMSC and hAMSC-CM showed comparable protective effects including neuronal rescue, promotion of M2 microglia polarisation and induction of tropic factors (Pischiutta *et al.*, 2016). As such, it is important to investigate the potential of hAMSC-CM to modulate inflammation *in vivo* following ischaemic damage. Therefore, the aim of this chapter is to establish if the potent immunomodulatory effects on microglia shown *in vitro* in the previous chapters are evident *in vivo* after experimental stroke which may, at least in part, mediate the beneficial effects of hAMSC-CM after stroke. Specifically, we examined the acute (24 hours) effects of hAMSC-CM on inflammatory and microglia specific markers after experimental stroke. To allow for the assessment of hAMSC-CM to modulate the expression of inflammatory markers following ischaemic damage, a key objective of this project was to establish and gain reproducible infarcts in a mouse model of ischaemic stroke using the intraluminal thread model (ILT).

In order to identify the mechanisms that underlie cerebral ischemia and to develop new agents for stroke therapy, a variety of animal stroke models have been developed. The MCA is the most commonly affected blood vessel in human ischaemic stroke, thus, techniques that occlude this artery are the closest to human ischaemic stroke. Models of middle cerebral artery occlusion (MCAO) have been established in many species including rodents, rabbits, pigs, dogs, cats and primates (Krafft *et al.*, 2012). Larger species have obvious advantages of large gyrencephalic brains with grey/white matter proportions closer to humans (Howells *et al.*, 2010), however rodents are the most common species used. Rodents are favoured mainly because, they are more ethically approved, their cost including maintenance is lower and their vascular anatomy is similar to man (Macrae, 2011). A major advantage of establishing the MCAO model in mice is the prospect of using genetically engineered mice to help

elucidate potential mechanisms of actions in future work. In addition, mice were the chosen species in the present work as the microglial cell line used in previous chapters was derived from mice, specifically the C57BL/6 strain. Only male mice were used in the current study, due to sex differences that arise in stroke; related to sex steroid hormones, particularly oestrogen that could cause complications in the results observed (Reeves *et al.*, 2008).

There are many different animal models, each with advantages and disadvantages, and can be divided into two main categories, depending on the requirement of a craniectomy (opening of the skull to allow direct access to cerebral arteries). Following a craniectomy, the MCA can be occluded by various methods. A popular method is by electrocoagulation of the blood at a particular point on the vessel and further dissection of the vessel (Tamura *et al.*, 1981). Other methods include mechanical occlusion by clip or ligatures or pharmacologically using a vasoconstrictor, for example endothelin-1 (Macrae *et al.*, 1993). Other models include stereotaxic injection of endothelin-1 which involves the need for a burr hole rather than a craniectomy (Sharkey *et al.*, 1993). Models of MCAO that do not require craniectomy and that allow the skull to remain intact include an intravascular approach by advancing a filament or embolus to the origin of the MCA. The current most widely used method is the intraluminal filament (or suture) model (ILT) (insertion of a filament through the internal carotid artery) first introduced by Kozuimi *et al.*, (1986) with the first modification made to the model by Longa *et al.*, (1989) to reduce subarachnoid haemorrhage by coating the suture. The filament traverses the artery until it reaches the origin of the MCA, where it can be left in position for varying lengths of time and subsequently removed or alternatively it can be left in place permanently. Removal of the filament allows reperfusion, attempting to replicate vascular recanalization, permitting the study of ischemia/reperfusion injury. An advantage associated with this technique is the ability to directly control the extent of damage, depending on the type of filament, whether the filament is removed, the length of occlusion period, and the period of reperfusion. Since the filament is advanced along the internal carotid artery to reach the origin of the MCA, other arteries that branch off the internal carotid can also be occluded and can cause collateral damage that is not directly related to MCA occlusion (McColl *et al.*, 2004). The ILT model is more severe, and results in a higher mortality rate when compared to other methods such as the electrocoagulation model, which although is permanent model, is less severe.

Emerging data indicate that the transient MCAO model may better mimic the pathophysiology of human stroke compared to permanent occlusion (Jin *et al.*, 2010). In human stroke, cerebral vessel occlusion is seldom permanent and inflammation plays a critical role in the pathophysiology of ischemia/reperfusion (Zuidema and Zhang, 2010). For these reasons, the intraluminal thread model was the method chosen to induce ischaemic damage.

The aims of the work described in this chapter were to:

1. Establish reproducibility of the intraluminal thread model of transient middle cerebral occlusion in mice.
2. Investigate the effect of hAMSC-CM on the acute inflammatory response post MCAO.



## **4.2 Materials and methods**

### **4.2.1 Surgical Techniques**

#### **4.2.1.1 Preparation of animals for surgery**

All animal experiments were carried out on C57BL/6 male mice, aged 10-12 weeks old, weighing 25-30g (bred in-house) in accordance with UK Home Office Guidelines on the Operation of the Animals (Scientific Procedures) Act 1986 (Project Licence No. PPL60/3775; Personal Licence No. PIL 60/4469). All procedures were carried out in accordance with ARRIVE guidelines wherever possible (Kilkenny *et al.*, 2010, **table 4.1**).

*Anaesthesia:* Animals were placed in a Perspex box and anaesthesia was induced by inhalation of 3% isoflurane/1000ml/min oxygen (O<sub>2</sub>) for approximately 3-4 minutes. The mice were then transferred to a face mask and anaesthesia was reduced to 2% isoflurane/1000ml/min O<sub>2</sub> which was maintained for 20 minutes and then subsequently reduced and maintained 1.5 ± 0.5% isoflurane/1000ml/min O<sub>2</sub> depending on the animals breathing rate. Excessive isoflurane and O<sub>2</sub> were actively scavenged using an aldorsorber unit (Shirley Alder & Co, Cardiff, UK).

*Temperature:* Throughout all procedures the animal's body temperature was monitored using a rectal probe (Harvard Apparatus, UK) and maintained at 37 ± 0.5°C using an automatic heat mat (Harvard Apparatus, UK).

#### **4.2.1.2 ILT model of transient MCAO**

The area around the neck was wiped in a circular motion three times with iodine. Either lignocaine (3% w/v) a topical local anaesthetic was applied or Ropivacaine (Naropin®) (4 mg/kg) was injected subcutaneously prior to making a midline neck incision. The neck incision was opened further using rounded blunt scissors to fully expose the submandibular gland. The submandibular gland was then dissected and retracted onto paper which was kept moist throughout surgery with sterile saline. The left common carotid artery (LCCA) and its bifurcation to the left external carotid artery (LECA) and the left internal carotid artery (LICA) were exposed by blunt dissection of the overlying connective tissue using tweezers and tri-swabs (Royem, Scientific, UK). Next, the left superior thyroid artery (STA), a branch of the LECA, was electrocoagulated using a diathermy probe (Eschmann equipment, Lancing, UK) and dissected. The following ligatures (6-0 silk thread) (Henry Schein, UK) were made in

order. 1) Thread was placed under the LICA by first passing it under the left common carotid artery (LCCA) and then passing the trailing end under the LECA, this was left untied and taped down to the operating surface for manipulation throughout the procedure. 2) A permanent ligature was placed under the ECA which was double knotted distally from the bifurcation of the LCCA. 3) A thread was loosely tied between the LCCA and LECA bifurcation point. 4) A final thread around the LCCA was placed to lift the LCCA to allow placement of a 13 mm microaneurysm clip. The segment of vessel distal to the first ligature on the LECA was electro-coagulated. Tension was applied to the thread around the LICA to cease blood flow along the LICA. Next, a small incision was made on the abluminal surface of the LECA, and a silicon-rubber coated monofilament (20mm length of which 9mm is coated with silicone giving an overall diameter of  $0.23\pm 0.01$ mm) (Docol Corporation, Sharon, USA) was inserted approximately 9mm until its tip sat at the bifurcation with the LCCA and LICA. The filament was held in place by tightening the loosely tied thread on the LECA. The coagulated area distal to the ligature on the LECA was cut and pulled to give an angle to the LICA. Tension on the thread around the LICA was released and the filament was advanced until resistance was met indicating the filament had reached the origin of the middle cerebral artery (**figure 4.2**). At this point the filament was tied in place and remained for 45 minutes. The filament was then carefully removed and the insertion incision was electro-coagulated and the microaneurysm clip removed. The submandibular gland was replaced to its original position and the surgical wound sealed with 5-0 suture. Finally, the isoflurane was turned off and the mouse was placed on its side to receive 100% O<sub>2</sub> for 1 minute and given 500µl sterile saline (Henry Schein, UK) intraperitoneally.

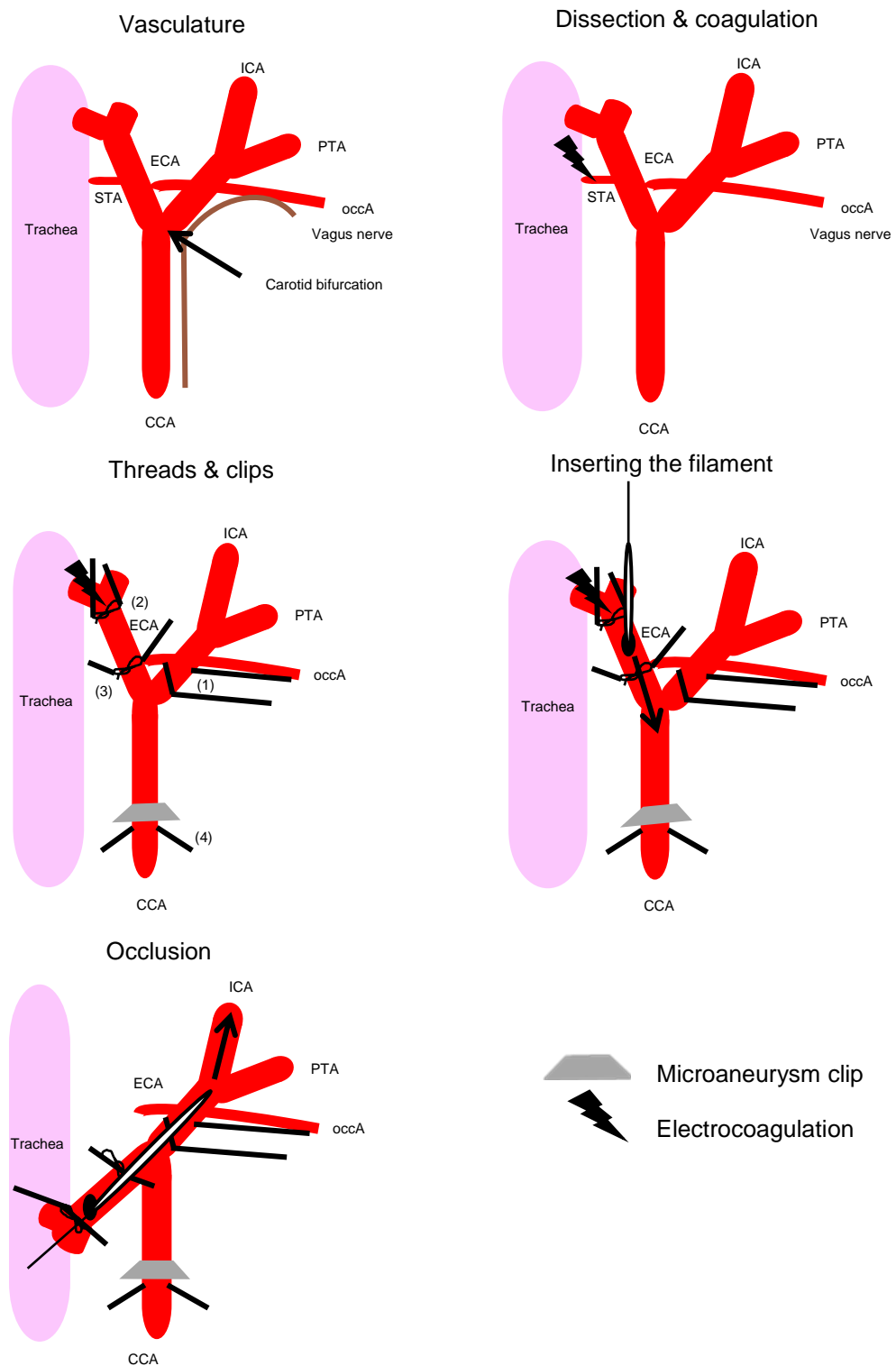


**Figure 4.2. A schematic representation of the intraluminal filament middle cerebral artery occlusion surgery.** Described in section 4.2.2. Abbreviations, ECA, external carotid artery; ICA, internal carotid artery; CCA, common carotid artery; STA, superior thyroid artery; occA, occipital artery; PTA, pterygopalatine.

## 4.2.2 Experimental protocol

### **Study 1: Establishment of reproducibility of the intraluminal thread model of transient middle cerebral occlusion in mice**

C57BL/6 male mice, aged 10-12 weeks old, weighing 25-30g (bred in-house) (n=3) underwent a 45 minute transient MCAO followed by a 72 hour recovery period. After the 72 hour recovery period mice were terminated by carbon dioxide (CO<sub>2</sub>) and dislocation of the neck, the brains were immediately removed and flash frozen (**section 4.2.5**). Animals were only included in the data analysis if they fulfilled the criteria of no sign of haemorrhage on the brain.

### **Study 2: Investigation of the effect of hAMSC-CM on the acute inflammatory response post MCAO.**

All work in this thesis involving the use of hAMSC-CM was carried out with several collaborators (Dr Elisa R Zanier, Dr Francesca Pischiutta, Prof Ornella Parolini, and Dr Antonietta Silini).

The experiment was designed using the Experimental Design Assistant (EDA) produced by 3R's (<https://eda.nc3rs.org.uk/eda/modelEditor/index/25240>). Mice underwent a 45 minute transient MCAO, followed by an intravenous (IV) tail vein injection of either control or conditioned media 3 hours post MCAO (**figure 4.1**). Following a 24 hour recovery period, mice underwent Bederson scoring assessment and mice were terminated by decapitation (without anaesthetic). The brain was immediately dissected and trunk blood was collected and processed. Animals were only included in the data analysis if they fulfilled the following criteria:

1. Scored 1 or more on the Bederson score
2. No sign of haemorrhage on the brain on visual inspection during dissection

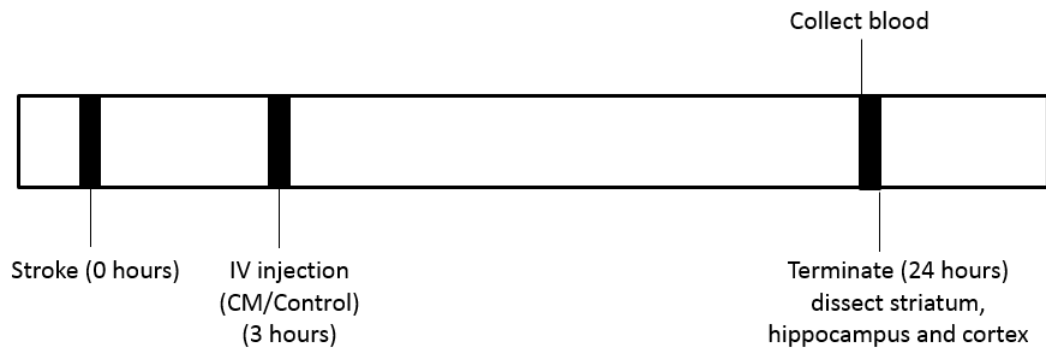


**Figure 4.1. Experimental and treatment protocol for study 2.** Following stroke surgery (45 minute MCAO), conditioned media or control media (Neurobasal) was injected intravenously into the tail vein 3 hours post MCAO.

Methods	Details								
Study design	<p>Groups:</p> <ol style="list-style-type: none"> <li>1. MCAO + control media</li> <li>2. MCAO + conditioned media</li> </ol> <p>-Randomisation/blinded to treatment as described below</p> <p>-Previous house partners were grouped with mice that received surgery on same day</p>								
Experimental procedures	<p>-45 minute MCAO using filament model</p> <p>-Administration of 100% CM or control medium (200 µl) intravenously through tail vein 3 hours post-MCAO</p>								
Experimental animals	C57BL/6 male mice, aged 10-12 weeks old, weighing 25-30g (bred in-house)								
Housing and husbandry	Animals were housed in groups with conditions of a temperature controlled environment with a 12-hour light dark cycle and were given access to food and water <i>ad libitum</i> .								
Sample size	<p>8 mice per group (as calculated by power calculation, shown below) + 15% drop out rate, 2 groups = 18 mice in total for experiment</p> <p>2-Sample t Test</p> <p>Testing mean 1 = mean 2 (versus ≠)</p> <p>Calculating power for mean 1 = mean 2 + difference</p> <p>α = 0.05 Assumed standard deviation = 15</p> <table border="1" style="margin-left: auto; margin-right: auto;"> <thead> <tr> <th>Difference</th> <th>Sample Size</th> <th>Target Power</th> <th>Actual Power</th> </tr> </thead> <tbody> <tr> <td>30</td> <td>8</td> <td>0.95</td> <td>0.960221</td> </tr> </tbody> </table> <p>The sample size is for each group.</p>	Difference	Sample Size	Target Power	Actual Power	30	8	0.95	0.960221
Difference	Sample Size	Target Power	Actual Power						
30	8	0.95	0.960221						
Allocating animals to experimental groups	<p>Random and blinded by using an independent investigator:</p> <p>-Randomisation of mice selection using coin toss, allocation concealment by an independent investigator and randomisation of control/CM using coin toss.</p>								
Experimental outcomes	<p>-Primary endpoints: gene expression for microglia phenotype (e.g. Arg-1/Ym-1, iNOS) per region (striatum, hippocampus and cortex)</p> <p>-Secondary endpoints: analysis of plasma</p>								
Statistical methods	Statistical analysis was performed using the graph and statistics software of GraphPad Prism (GraphPad Software Inc., USA). An unpaired t-test was performed between the control and CM animal group								

**Table 4.1. Details of the experimental methods for study 2 as advised by the ARRIVE guidelines (Kilkenny *et al.*, 2010).**

#### **4.2.3 Intravenous injection of hAMSC-CM**

hAMSC-CM (1x) or control media (neurobasal medium) were thawed and placed into a syringe and needle by an independent investigator. Intravenous administration of material can be technically difficult, therefore, use of a restraining device was required. Extra care and attention was paid when using the restraining device being careful not to do any damage to the wound and sutures considering the sensitive timing so soon after the MCAO surgery. It is common practise to stimulate dilation of the tail veins in mice, this was achieved by placing them into a warmer environment (37 °C) for 30 minutes before the injection was due. Three hours after MCAO surgery, hAMSC-CM or control media (200 µl) was intravenously injected into the mouse tail vein and mice were placed back into their recovery cage.

#### **4.2.4 Bederson scoring**

In study 2, all animals were evaluated at 24 hours post MCAO using a scoring system developed to detect neurological impairments following stroke established by Bederson (Bederson *et al.*, 1986) to establish if occlusion had been successful. Tests include forelimb flexion, resistance to lateral push and circling behaviour. Using the Bederson scoring, a grading scale of 0-3 (**table 4.4**) is used to assess behavioural deficits after stroke. This scoring scale is a quick and simple way to reveal basic neurological deficits and was used for confirmation of a successful MCAO. Ischaemic animals will have significantly more neurological deficits than non-ischaemic animals, resulting in a higher score (Schaar *et al.*, 2010).

Severity	Grade	Observation
Normal	Grade 0:	No observable deficit
Moderate	Grade 1:	Forelimb flexion
Severe	Grade 2:	Decreased resistance to lateral push (and forelimb flexion) without circling
	Grade 3:	Same behaviour as grade 2, with circling

**Table 4.2. Bederson neurological examination grading system (Bederson *et al.*, 1986).**

#### **4.2.5 Termination of Experiment and Processing Tissue**

In study 1 (reproducibility study), 72 hours post MCAO, each animal was terminated by cervical dislocation and the animal was decapitated and the brain was removed immediately, fresh frozen and histology was performed (detailed below).

In study 2 (hAMSC-CM study), at 24 hours post MCAO, mice were terminated by decapitation (without anaesthesia, to ensure no effect on the immune system). Trunk blood was collected into an EDTA-coated tube, and the brain removed and placed on a cold petri dish on ice. The ipsilateral (hemisphere of damage (LHS)) and contralateral (opposing hemisphere to damage (RHS)) hippocampus, striatum and cortex was dissected separately and placed into a 1.5ml centrifugation tube containing 5:1 volume ratio of RNAlater™ solution for RNA analysis (detailed below).

##### **4.2.5.1 Fresh Freezing**

By placing on dry ice isopentane was cooled to -42°C, the fresh brains were then immediately removed and placed into the isopentane solution for 2-3 minutes. The brain was then removed, placed in tin foil and subsequently stored at -18°C.



#### 4.2.5.2 Sectioning of Tissue

Brains were coated with embedding matrix prior to slicing. Coronal sections (20  $\mu\text{M}$ ) were taken on to glass slides at 8 pre-determined levels based on Osborne *et al.*, (1987). The 8 coronal sections were taken at the level of the olfactory tract, nucleus accumbens, septal nuclei, globus pallidus, anterior hypothalamus, lateral habenula, medial geniculate and the aqueduct. The coronal sections were taken based on known physiological landmarks (**figure 4.3**); including the presence of olfactory tract and forceps of the corpus callosum, anterior commissure, ventral hippocampal commissure, progressive hippocampal development (over 3 sections) and the aqueduct. Two sections were collected onto each slide and one slide from each coronal level was stained with Haematoxylin and Eosin to measure volume of tissue damage.

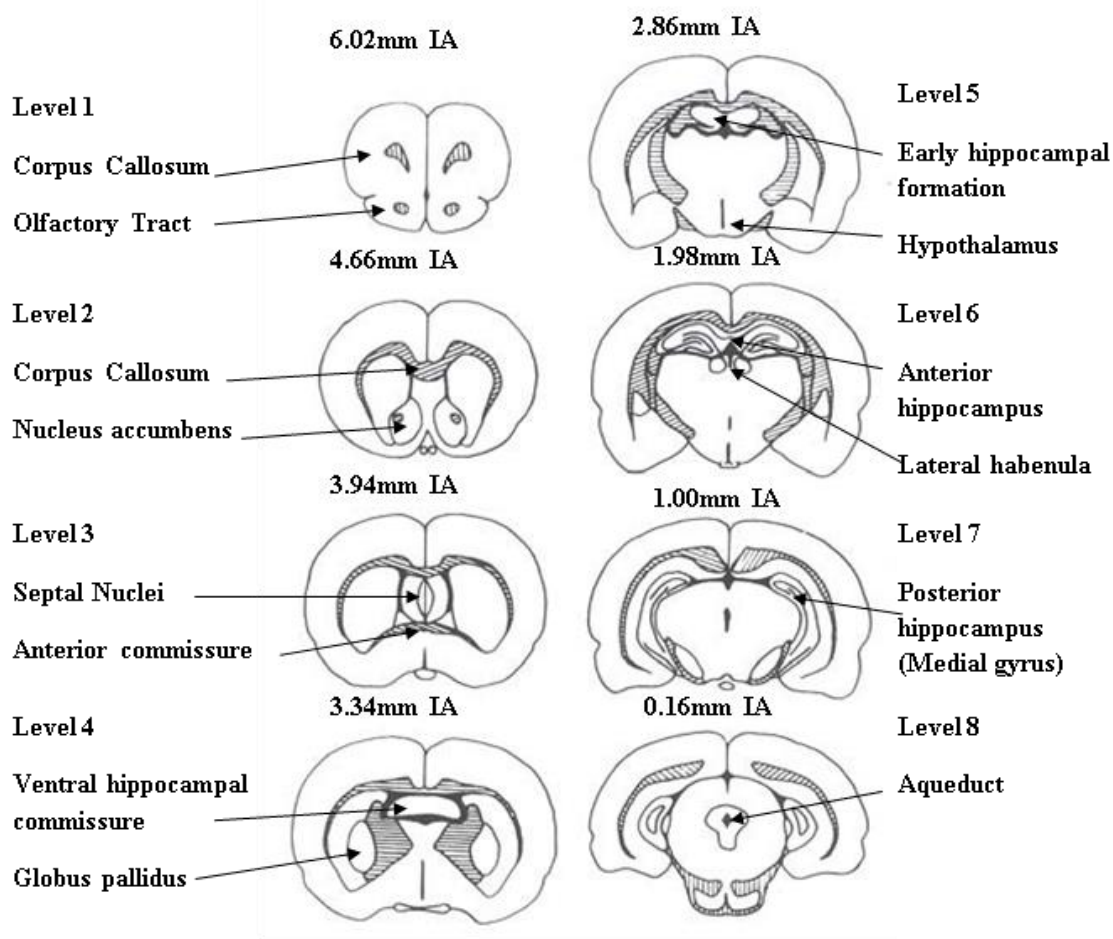


**Figure 4.3. The eight distinct anatomical landmarks collected for quantification of lesion and oedema volume. A visual representation and the distance from the interaural line are provided for each level. Adapted from Osborne *et al.*, (1987).**

#### **4.2.5.3 Haematoxylin and Eosin Staining**

H &E staining is used routinely to identify regions of ischaemic damage. Eosin stains connective tissue and cytoplasm pink, while haematoxylin stains nuclei dark blue. Coronal tissue sections on glass microscope slides were initially post fixed in 4% paraformaldehyde (PFA) (Sigma, Poole, UK) for 10 minutes, then washed in tap water for 3 minutes. The tissue was then dehydrated and rehydrated through graded alcohol concentrations, the slides were placed in 70%, 90%, 100% then back into the 90% and 70%, each for 2 minutes. Slides were washed in tap water before stained in Haematoxylin (1% w/v in absolute ethanol) (Sigma, Poole, UK) for 4 minutes followed by a wash in running water. Sections were differentiated in acid alcohol (500ml of 100% ethanol, 5ml of concentrated HCl) for 2 minutes and washed again. The sections were then placed in Scots tap water substitute for 1 minute, washed again before being immersed in Eosin Y (1% w/v aqueous) (Sigma, Poole, UK) and then rinsed in running tap water until the water ran clear. The tissue was then dehydrated through 70%, 90% and 100% ethanol for 4 minutes each before clearing in two changes of histoclear for 2 minutes each. Slides were then mounted with a coverslip using DPX mounting medium (Sigma, Poole, UK).

#### **4.2.6 Measurement of ischaemic damage and oedema**

The H&E stained sections, representative of the forebrain, were placed under a densitometer (MCID, InterFocus Imaging Ltd, Cambridge, UK) and analysed for measurement of infarct volume and oedema. For each level, the ipsilateral and contralateral hemispheric areas were measured, as well as the area of ischaemic damage represented by regions of pallor. The volumes of each hemisphere and the lesion were calculated by graphing the area of each of the eight levels against their Interaural (IA) distance. In order to produce the hemispheric and lesion volumes the area under the curve was then calculated; where Y Intersected X at 7.9mm IA and 0.1 mm IA.

Lesion volume was expressed as:

$$(\text{Volume of Lesion}/\text{Volume of ipsilateral hemisphere}) \times 100$$

Oedema volume was expressed as a percentage increase in the ipsilateral hemisphere over the contralateral volume as:

$$((\text{Volume of Ipsilateral hemisphere}-\text{Volume of Contralateral hemisphere})/\text{Volume of Contralateral hemisphere}) \times 100$$

#### **4.2.7 Collection of plasma from blood samples**

Serum is the liquid fraction of whole blood that is collected after the blood can clot. Whole blood was collected in anticoagulant-treated tube (Plastic whole blood tube with spray-coated K<sub>2</sub>EDTA, BD Bioscience, UK). Cells were removed from plasma by centrifugation for 15 minutes at 2,000 x g, 4°C. The resulting supernatant was designated plasma, the liquid was immediately transferred to a clean 1.5 ml centrifugation tube using a Pasteur pipette. The samples were maintained on ice at 2-8°C while being handled and subsequently stored at -80°C immediately.

#### **4.2.8 RNA extraction from regional brain homogenates using RNeasy Plus Universal Mini kit**

##### **RNA extraction**

RNA from regional brain homogenates (striatum, hippocampus and cortex) was isolated using the procedure of the RNeasy Plus Universal Mini Kit (Qiagen). Brain regions were stored in RNAlater™ solution for 24 hours at 4°C before being placed into a fresh Eppendorf tube and stored at -80°C for long term storage. For disruption and homogenisation, one stainless steel cone ball (6.0 mm diameter) (Retsch, UK) along with 900 µl QIAzol lysis reagent was placed into the 2 ml tube containing the individual tissue. The tube was placed into the Tissue Lyser mixer (TissueLyser, MM301, Retsch, UK) for 1 minute at 30 1/s, repeated twice. Lysates were placed into a new tube and procedures were performed according to manufacturer's instructions at room temperature. RNA quality assessment, cDNA synthesis, selection of the most appropriate house-keeping gene and qRT-PCR was carried out as described in **section 2.2.4**, using the set of primers listed in **table 4.5**.

<b>Gene name</b>	<b>Forward primer</b>	<b>Reverse primer</b>
<i>Qars</i>	GGTGACCTGGCTGGGTATAC	TGGCCTTTGAGCTCTTCCAC
<i>B2m</i>	TCCTTCAGCAAGGACTGGTCT	CATGTCTCGATCCCAGTAGACG
<i>Sdha</i>	CGCCTAAACATGCAGAAGTCG	TCCAAACCATTCCCCTGTCTG
<i>Tnfa</i>	CCCACGTCGTAGCAAACCA	AGAACCTGGGAGTAGACAAGGT
<i>Cd86</i>	ACAGGAACAACCTGGACTCTACG	TCACTGAAGTTGGCGATCACT
<i>Cd68</i>	GGAAGAAAGGCTTGGGGCAT	ACTCGGGCTCTGATGTAGGT
<i>Chil3</i>	AGAGTGCTGATCTCAATGTGGATTC	GTAGGGGCACCAATTCCAGTC
<i>Arg1</i>	TACAAGACAGGGCTCCTTTCAG	TGGTTACCCTCCCGTTGAGT
<i>Mrc1</i>	ACCTGGGGACCTGGTTGTAT	CCTCGCGTCCAATAGCTGAA
<i>Socs3</i>	GGGGAGCCCCCTTTGTAGACT	CGGGGAGCTAGTCCCGAA
<i>Ccl2</i>	AGCTGTAGTTTTTGTCAACCAAGC	GACCTTAGGGCAGATGCAGT
<i>Il1<math>\beta</math></i>	AGCTTCCTTGTGCAAGTGTCT	TTGGAAGCAGCCCTTCATCTT
<i>Il10</i>	TGAATTCCCTGGGTGAGAAGC	GACACCTTGGTCTTGGAGCTTA
<i>Igf1</i>	TACTTCAACAAGCCCACAGGC	ATAGAGCGGGCTGCTTTTGT
<i>Vegfa</i>	TCCGAAACCATGAACTTTCTGC	GAACTTGATCACTTCATGGGACTTC
<i>Gfap</i>	GGCAGAAGCTCCAAGATGAAAC	GATCTCCTCCTCCAGCGATTC

**Table 4.5. Sequence of oligonucleotides of housekeeping genes and genes of interest. Primers used in qRT-PCR with an annealing temperature of 60°C.**

### 4.3. Results

#### 4.3.1 Result from study 1: Reproducibility of the ILT model in mice

The initial aim of the chapter was to ensure that a reproducible model of transient MCAO could be established. Before further investigation into the effect of hAMSC-CM post MCAO, it was important to ensure that the technique produced reproducible lesions in our hands. The infarct and oedema volumes only were quantified in this initial study as the aim of the work was to establish and validate the surgical procedure. The lesion and oedema volume for three representative mice are discussed in this chapter. In this study, mice were recovered for 72 hours to allow the infarct to fully develop. **Figure 4.4(A)** shows infarct development in all three animals after a 45 minute occlusion, which suggest successful insertion of the filament. The percentage infarct volume varied between animals; 35.6, 39.5 and 43.1%, producing a mean infarct of 39.4%. The co-efficient of variation shows the extent of variability in relation to the mean of the population, therefore measuring how variable results are. The co-efficient of variation was calculated as:

Standard deviation / mean x 100:

$$3.75144 / 39.41 \times 100$$

$$= 9.5\%$$

The results produced a variance of 9.5%, suggesting a reasonable low variation in lesion size between animals. There was visible oedema of the ipsilateral hemisphere at 72 hours after MCAO quantified in **figure 4.5(B)**. Oedema was not consistent as percentages ranged from 25.2%, 27.1% down to 13.9%.

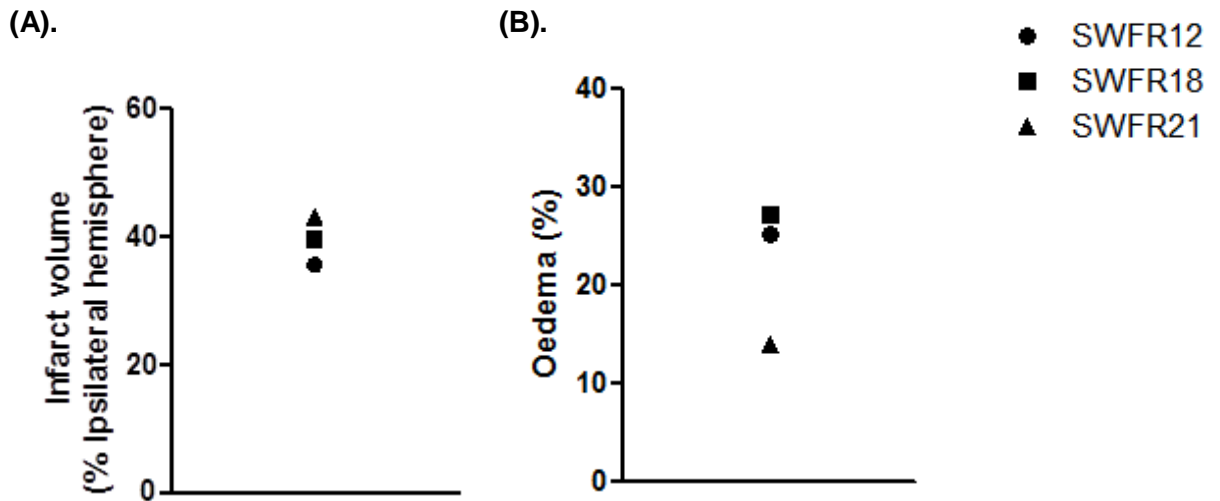


**Figure 4.4. (A) Infarct volume and (B) Oedema percentage in animals 72 hours post MCAO.** Lesion volume is expressed as percentage of the ipsilateral hemisphere and oedema as a percentage of hemisphere as described in **section 4.2.7**. SWFR12, SWFR18 and SWFR21 represent individual identity codes of the mice used in the study.

#### 4.3.2 Results from study 2: hAMSC-CM study

To examine the effect of hAMSC-CM on the acute inflammatory response it was decided to recover animals for 24 hours (Perego *et al.*, 2011). In this study, RNA was extracted from the ipsilateral striatum (hemisphere of infarction), and inflammatory markers were examined.

Surgery was performed on twenty-five mice (n=25). One mouse (n=1) died while under anaesthesia and one (n=1) had to be put down due to a technical issue. Overall, there were three mortalities in the study, one death during the IV injection; one death after barrel rolling inside the restrainer (n=1) (before treatment was given) and two deaths occurred during the night (n=2) (**figure 4.5**). Twenty experimental animals remained (n=20), two mice were excluded from the results as they failed to meet the inclusion criteria, scoring 0 on the Bederson scoring examination (**table 4.6**). It is important to note that the allocated treatment group of the mice excluded remained blinded to the investigator to ensure there was no bias in exclusion. This resulted in eighteen animals in total for RNA analysis (n=18), all of which displayed circling

behaviour after MCAO and scored three on the Bederson examination. During the RNA extraction process, one brain failed to produce high quality RNA required for analysis. After decoding of the treatment groups at the end of data analysis, it was revealed that there were nine animals, (n=9) that received hAMSC-CM and eight animals (n=8) that received the control media (**figure 4.5**).

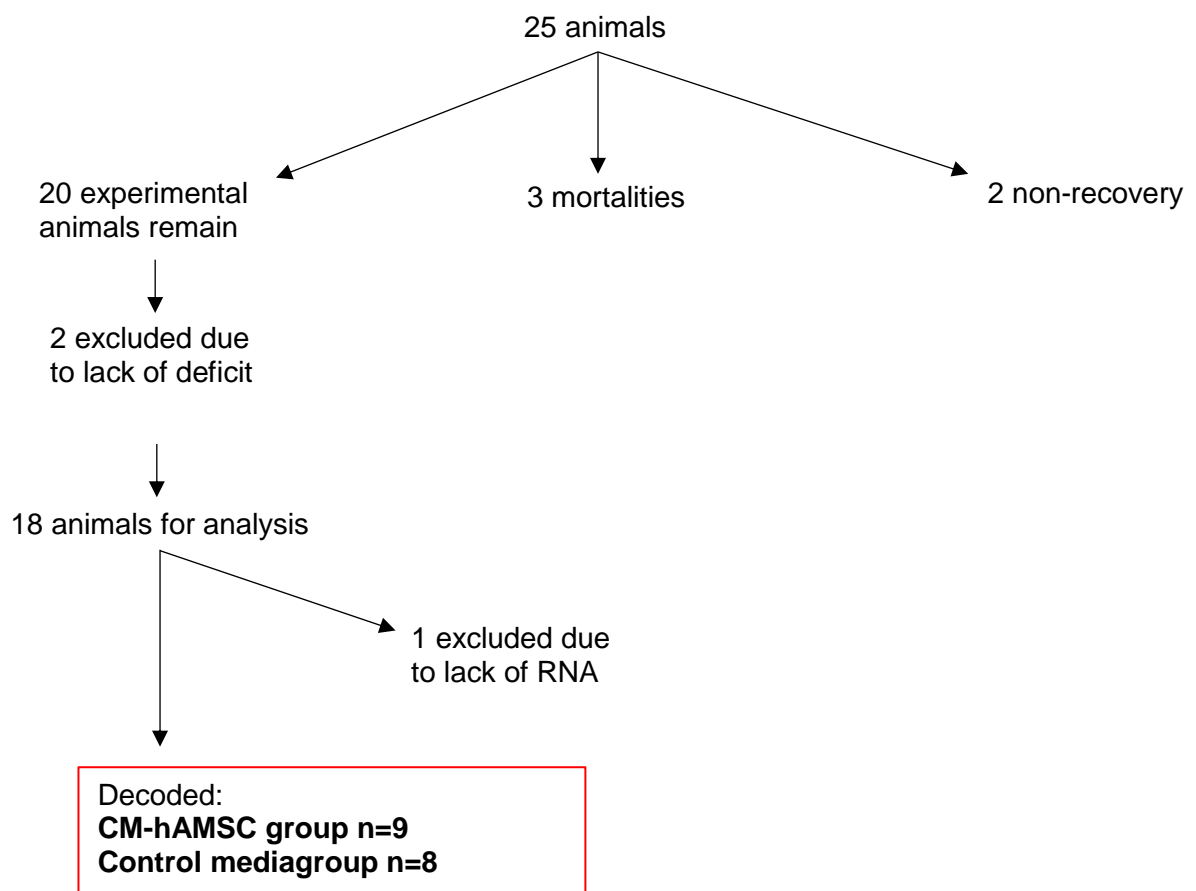


**Figure 4.5. Flow-chart showing total experimental animals used in study 2.**



<b>Animal ID</b>	<b>Grade</b>
CM01	3
CM02	3
CM03	0
CM04	3
CM05	3
CM06	3
CM07	3
CM08	3
CM11	3
CM15	3
CM16	3
CM17	3
CM18	3
CM19	3
CM20	3
CM21	3
CM22	3
CM23	0
CM24	3
CM25	3

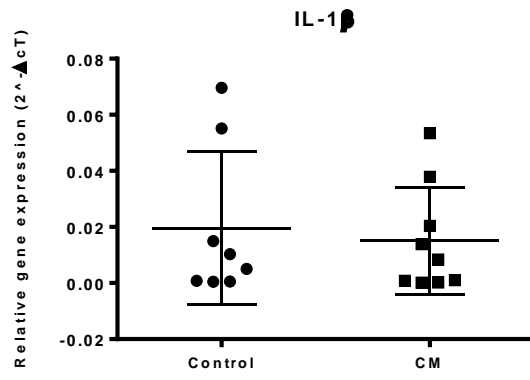
**Table 4.6. Results of the Bederson neurological scoring examine in experimental animals 24 hours post MCAO in study 2.**

To investigate the potential of hAMSC-CM to modulate the inflammatory response *in vivo*, the effect of hAMSC-CM on expression of pro- and anti-inflammatory associated genes was compared with that of control media. Unfortunately, due to time restrictions, we were limited to only analysing the striatum.

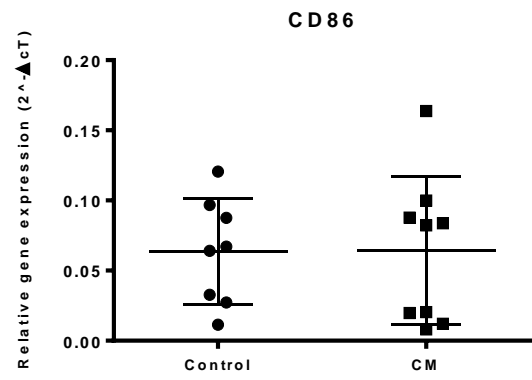
There was no statistical difference in the expression of pro-inflammatory genes, *Il1 $\beta$*  or *Tnfa* in hAMSC-CM vs control groups (**Figure 4.7**). In addition, hAMSC-CM had no effect on the relative expression of cell surface markers *Cd86* and *Cd68* compared to control media. *Ccl2* (monocyte chemoattractant protein-1), which is involved in recruiting immune cells, alongside the leukocyte marker *Cd11b* and *Gfap* (Glial fibrillary acidic protein) also remained unchanged with hAMSC-CM treatment compared to control media treatment (**figure 4.7**).

There was no change in the expression of anti-inflammatory genes, *Arg1* and *Ym1* in hAMSC-CM vs control group (Figure 4.8). In addition, hAMSC-CM had no effect on the relative expression of the pattern recognition receptor, *Mrc1* (mannose receptor C type-1) (*Cd206*) or anti-inflammatory cytokine *Il10* compared to control media. Growth factor *Igf1* (insulin-like growth factor-1) and *Socs3* (suppressor of cytokine signalling 3) also failed to be different between the hAMSC-CM and control group (**figure 4.8**).

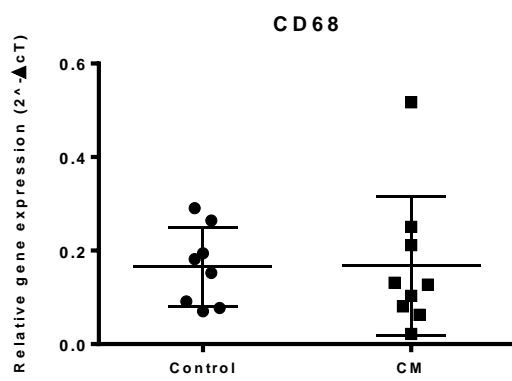
(A)



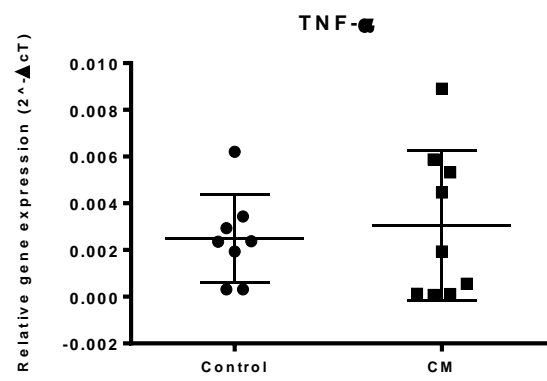
(B)



(C)



(D)



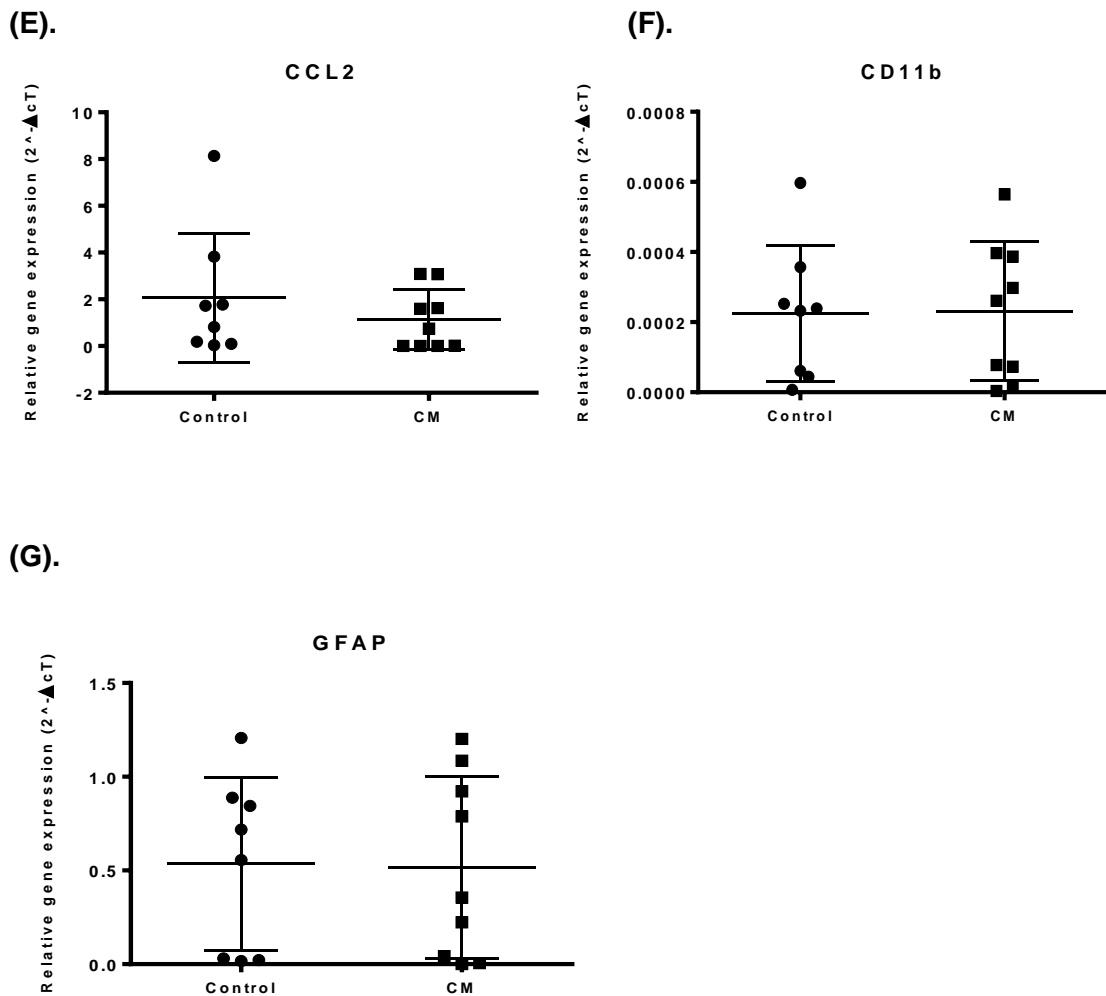
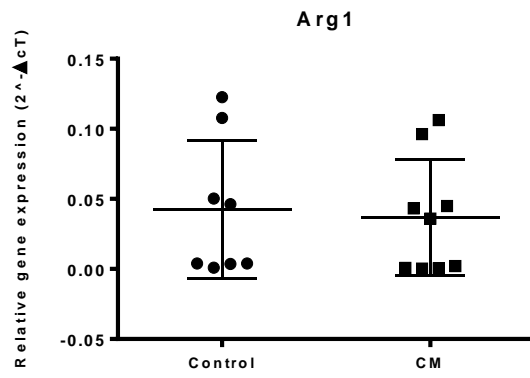
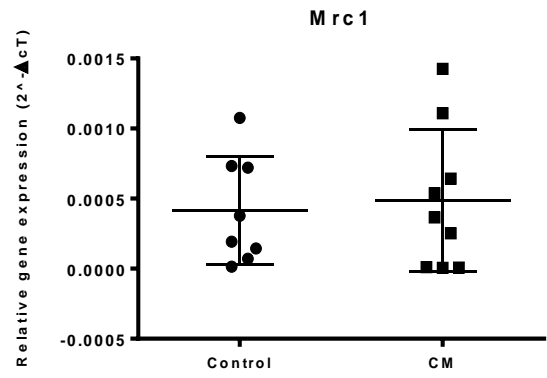


**Figure 4.6. The effect of hAMSC-CM on ipsilateral striatal pro-inflammatory gene expression 24 hours after MCAO.** hAMSC-CM (labelled CM on graph) or control media (neurobasal, labelled control on graph) was intravenously injected into mice 3 hours post MCAO. Graphs show the effect of hAMSC-CM or control media on **(A)** Interleukin-1 $\beta$  (*Il1 $\beta$* ), **(B)** cell surface markers *Cd86* and **(C)** *Cd68* **(D)** Tumour necrosis factor  $\alpha$  (*Tnfa*) **(E)** chemokine ligand-2 (*Ccl2*) **(F)** the microglia marker cluster of differentiation molecule 11b (*Cd11b*) and **(G)** the astrocytic marker astrocytic glial fibrillary (*Gfap*). Data expressed as relative expression ( $2^{-\Delta\Delta Ct}$ ), control group n=8, CM group n=9. Lines represent mean  $\pm$  SEM, unpaired t-test.

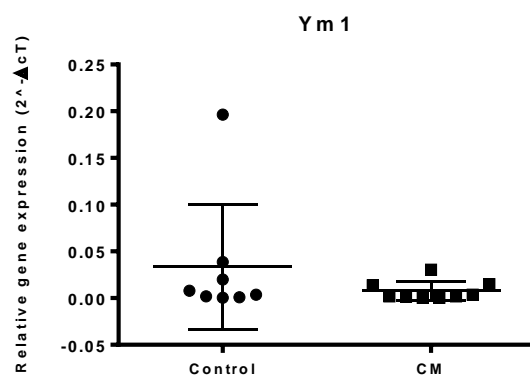
(A)



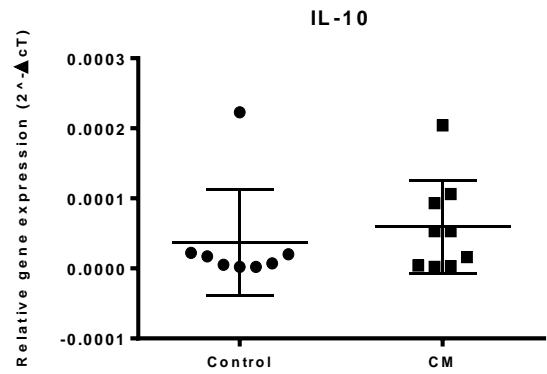
(B)



(C)



(D)



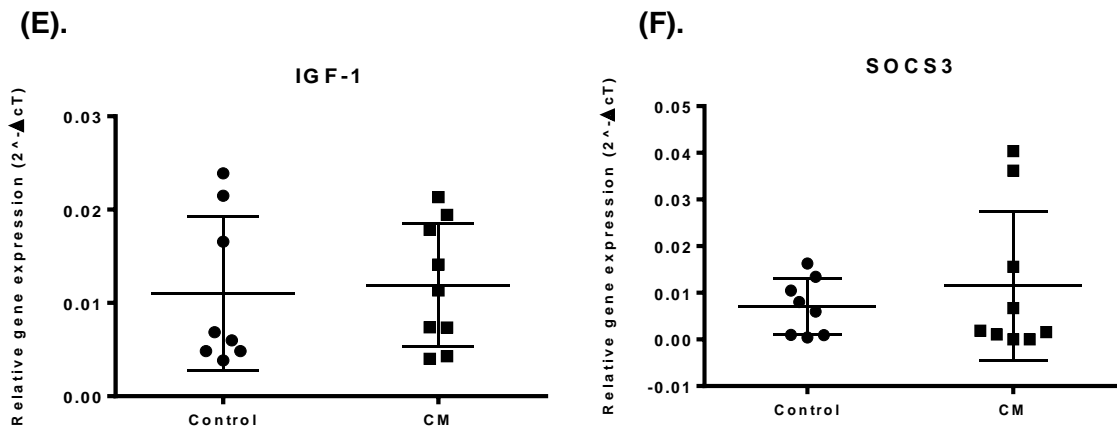


**Figure 4.7. The effect of hAMSC-CM on ipsilateral striatal anti-inflammatory gene expression 24 hours after MCAO.** Human amniotic mesenchymal stromal cell conditioned media (hAMSC-CM) or control media (neurobasal) was intravenously injected into mice 3 hours post MCAO. Graphs show the effect of hAMSC-CM or control media on **(A)** Arginase-1 (*Arg1*) **(B)** Mannose receptor C type-1 (*Mrc1*) **(C)** Chitinase-like protein-3 (*Chil3*) **(D)** Interleukin-10 (*Il10*) **(E)** Insulin-like growth factor-1 (*Igf1*) **(F)** Suppressor of cytokine signalling 3 (*Socs3*). Data expressed as relative expression (2<sup>-ΔΔCT</sup>), control group n=8, CM group n=9. Lines represent mean +/- SEM, unpaired t-test.

## 4.4 Discussion

### 4.4.1 Reproducibility of the ILT model in mice

While the overall aim of this chapter was to investigate the effect of hAMSC-CM on inflammatory mediators after MCAO, the initial aim was to ensure the model of MCAO was established and consistent in our hands. Therefore, the first experiment in the chapter included a short reproducibility study. The aim of the study was to establish an intraluminal thread model of transient middle cerebral occlusion in mice producing reproducible infarction volumes with low rates of mortality and morbidity in animals.

All animals in the study successfully resulted in an infarct, Infarct volume and oedema are related to the severity of ischaemic injury as with a large infarct there are a greater number of injured cells causing an increase in cytotoxic oedema and severe injury associated with breakdown of the blood brain barrier and vasogenic oedema. In this study the recovery period was 72 hours, to allow evolution of infarct after reperfusion commences (Liu and McCullough, 2011). In our hands, a 45 minute MCAO produced a mean infarct volume of 39.4% this is comparable to several studies reporting the mean infarct percentage to be  $40 \pm 5\%$  after a 24 hour recovery (Chiang *et al.*, 2011) and 48% infarct volume after a permanent MCAO in C57 mice (Carmichael, 2005). The current study resulted in a standard deviation of infarct of 3.75%, this is in agreement with a report that states that 15% standard deviation produces strong lesion reproducibility (Rousselet *et al.*, 2012).

The present study showed a low variability of infarct volume producing a coefficient of variation of 9.5%. Filament diameter is carefully matched to a defined body weight in rodents in order to help ensure adequate and consistent occlusion of the MCA origin. In both of the present studies, mice with a body weight of 25-30g and a filament size of  $0.23 \pm 0.01\text{mm}$  were used which is evidently a good match to produce reproducible lesions. McColl *et al.*, (2004) used a narrow weight range of  $29 \pm 0.9\text{g}$ , proving to increase reproducibility of infarct volume by reducing the chance of residual flow around the filament. Variation in this model using mice may also be due to differences in the posterior communicating arteries (PcomAs) amongst the commonly used C57BL/6 mouse strain. The PcomAs connect the anterior and posterior portions of the circle of Willis, and it was shown that 10% of mice possess a complete circle of Willis compared to 90% who had either one or both PcomAs absent (McColl *et al.*,

2004). This is important to consider as it is a possible reason why some mice do not show any deficit after MCAO, this was observed in study 2 where two mice were excluded from the study due to lack of deficit.

In conclusion, this study produced a low co-efficient of variance for infarct volume indicating that this model produced reproducible infarcts. This suggests that this is a suitable model of MCAO to examine the effects of hAMSC-CM.

#### **4.4.2 The effect of hAMSC-CM on inflammatory marker expression after a 45 minute MCAO in mice**

The ultimate aim of the work described in the current chapter was to examine the effects of hAMSC-CM injected into mice 3 hours post MCAO on various inflammatory marker expression.

The results of the present study indicate no effect of hAMSC-CM on inflammatory responses in the striatum after stroke. This disagrees with several published and unpublished pilot studies undertaken with hAMSCs or hAMSC-CM, the same source as used in this thesis, by our collaborators. These are summarised in **table 4.7**. The first work by Zanier *et al.*, (2011) transplanted hAMSCs intracerebrally 24 hours after of traumatic brain injury (TBI). Results showed an upregulation of CD11b and a decrease in the phagocytic marker, CD68 after 7 days of injury and improved sensorimotor function 5 weeks after injury. The latest publication, also in the TBI model, showed that both intracerebral (IC) and intravenous (IV) injection of hAMSC significantly improved sensorimotor function after 5 weeks (Pischiutta *et al.*, 2016). This study also revealed the potent effects of hAMSC-CM in comparison to hAMSC in organic brain slices post oxygen-glucose deprivation (OGD). The study that most closely resembles the experimental design of the current work is unpublished work described in study 4 in **table 4.7**. This was a pilot study where the authors injected hAMSC-CM, lyophilized to a 4 x concentration, intravenously 24 hours after a 60 minute MCAO in mice, hAMSC-CM was found to significantly improve sensorimotor function after 4 weeks of injury (Pischiutta *et al.*, 2016, personal communication).



Study	Model	Cells/ CM	Admin	Timing	Dose	Outcomes
Current chapter	45 minute MCAO	CM	IV	3 hours	1 x CM	No effect on inflammatory markers (24 hours)
<b>(1).</b> (Zanier <i>et al.</i> , 2011)	TBI	Cells	IC	24 hours	150,000 cells / 5 µl	Microglia/macrophage markers (7 days) Improved behaviour (30 days)
<b>(2).</b> (Pischiutta <i>et al.</i> , 2016)	TBI	Cells	IC + IV	24 hours	IC: 150,000 in 5 µl IV: 10 <sup>6</sup> cells in 200 µl	Improved sensorimotor function (5 weeks)
<b>(3).</b> Unpublished pilot data (Zanier <i>et al.</i> )	TBI	CM	IC	1 and 3 hours	1 x CM	Improved sensorimotor function (5 weeks)
<b>(4).</b> Unpublished pilot data (Zanier <i>et al.</i> )	60 minute MCAO	CM	IV	24 hours	4 x CM (lyophilized CM)	Improved sensorimotor function (4 weeks)
<b>(5).</b> (Pischiutta <i>et al.</i> , 2016)	OGD on cortical slices	Cells and CM	N/A	1 hour post OGD	600,000 hAMSC/well or 50% CM	Both treatments significantly reduced PI incorporation and upregulated CD11b expression compared to ODG

**Table 4.7. Key features of the published and unpublished work carried out on the effects of hAMSC or hAMSC-CM after TBI, MCAo or OGD.**

There are various methodological considerations that may account for the disagreement of our results with those of our collaborators. These will be discussed in the following text and then put into context with the rest of the literature and include; concentration of hAMSC-CM, route of administration, timing of treatment, timing of analysis, brain region analysed, and technological weaknesses.

The only study performed on stroke by our collaborators (study 4, **table 4.7**) used 4 x hAMSC-CM (lyophilized hAMSC-CM). However, in our collaborators experience, there was a lack of reproducibility in the concentration of the lyophilized hAMSC-CM and it was discovered that there were problems with the company producing the lyophilized hAMSC-CM. It was next investigated if 'plain' one times hAMSC-CM was capable of exerting a beneficial effect. A pilot study showed that 1 x hAMSC-CM injected IC 1 and 3 hours after TBI showed significant recovery 5 weeks post injury (study 3, table 4.7, personal communication). It was therefore decided in the present study to inject 1 x hAMSC-CM 3 hours after MCAO. However, it is important to note that in that TBI study IC administration was used whereas in the present study, IV administration was used (as described below) to copy that of the stroke study (study 4). Therefore, the combined less potent and less direct route of administration could explain the lack of effect in the present study. The other difference between our results and our collaborators' results is the timing of outcome measure. Our collaborators are primarily interested in behavioural outcomes; hence they perform long-term recovery studies, and we were primarily interested in the acute inflammatory response, which led to a 24 hour recovery period, a time point when inflammation is at its peak as described below.

Many studies indicate that hAMSCs treatment can promote functional recovery and reduce infarction in animal models of MCAO (Ding *et al.*, 2007; Hsieh *et al.*, 2013; Liao *et al.*, 2009). There is limited information regarding the impact of hAMSC-CM in stroke *in vivo*, however, it has been shown that administration of hAMSC-CM prevents the progression of bleomycin-induced lung fibrosis (Cargnoni *et al.*, 2014; Cargnoni *et al.*, 2012). For this reason, when discussing methodological considerations, comparisons will be made with MSCs in general, due to the lack of studies involving the use of conditioned media.

In our study, hAMSC-CM was injected 3 hours post stroke, the timing of injection was decided as recovery was 24 hours which ruled out any later timings and our

collaborators had previously shown its effectiveness. In rat models of ischaemia, MSCs were injected into the tail vein 1 hour, 12 hours, 1, 3, 5 and 7 days after injury. The authors concluded that MSC transplant 12 hours after ischemia was the optimal time, showing the highest neurological functional recovery and the lowest degree of cerebral damage (Hosseini *et al.*, 2015). This might suggest that 12 hours post stroke would be a more successful time for injection, however, it should be noted that this study was for MSCs and not conditioned media.

In this work, a time-point of 24 hours was chosen for analysis of inflammatory markers. The expression of cytokines and chemokines after reperfusion has been shown to be extremely transient: *Il1 $\beta$*  mRNA expression was shown to peak early after reperfusion (1 hour), but also at later times (6-24 hours) showing biphasic expression. Similar results were observed with *Tnfa*, showing to peak for a second time at 24-36 hours (Brea *et al.*, 2009). A study investigating the dynamics of microglia/macrophage polarisation after ischemia revealed that the levels of 'M1' pro-inflammatory genes (*Nos2*, *Cd11b* and *Cd86*) were gradually increased from day 3 onwards. In contrast, mRNA expression of 'M2' anti-inflammatory markers (*Cd206*, *Arg1*, *Ccl2*, *Ym1* and *Il10*) were induced between 1-3 days after MCAO. It is worth noting that when the authors measured CD206 and Iba1 double staining, there was no difference in expression levels between the cortex and the striatum (Hu *et al.*, 2012). Of note, there are many inconsistencies in the literature about the time course of recruitment of various inflammatory cells in the brain following ischemia, even in the same experimental models (Jin *et al.*, 2010). It was reported that microglia and macrophages started to appear 12 hours after ischemia and were significantly upregulated after 24 hours (Gelderblom *et al.*, 2009). In agreement, activated microglia (CX3CR1<sup>+</sup> cells) was significantly upregulated in the brain parenchyma 24 hours following MCAO (Zanier *et al.*, 2015). In comparison, it was found that there was a significant increase of CD11b<sup>+</sup> cells in the ischaemic region by 18 and 24 hours, further increasing at 48 and 72 hours (Stevens *et al.*, 2002). A previous study reported that post-ischaemic microglia proliferation peaks at 48-72 hours after focal cerebral ischemia (Denes *et al.*, 2007).

Had microglia been examined at a later point (72 hours), it is possible that a more marked effect in the striatum might have been observed with hAMSC-CM treatment. If a later time point was assumed it would also be valuable to examine lesion volume. Unfortunately, it was not possible to measure lesion volume in this work, in this case

it would be necessary to have availability to MRI, or have multiple cohorts of animals, with some inflammatory markers and others sacrificed for histological assessment. Administration and time of analysis in mouse models of MCAO needs to be further optimised in future work to fully elucidate any effect of hAMSC-CM.

Recent studies have shown that the degree of protection by MSCs in *in vivo* brain injury models, is dependent on the route of administration (Pischiutta *et al.*, 2016). Regarding the delivery route, we choose to deliver hAMSC-CM intravenously through the tail vein. Although injecting IC offers the direct localised administration, it is very invasive leading to poor clinical translation. The literature shows that MSCs are capable of modulating the systemic immune response and it has been revealed that IV is adequate for immunomodulatory effects (Honma *et al.*, 2006). A plethora of administration routes have been shown to be optimal for stem cell treatment including; intracerebral (IC), intra-arterial (IA), intraperitoneal (IP), intranasal (IN) and intravenous (IV) while the most appropriate route remains unknown (Rodríguez-Frutos *et al.*, 2016). Intravenously administered exogenous BMSCs are capable of entering the brain, migrating, surviving and improving recovery (Chen *et al.*, 2001). It was demonstrated that IV administration is capable of dampening inflammation, and thus preventing secondary cell death: IV human BMSC administration 60 days after stroke migrated to the spleen, attenuated stroke-induced inflammation and decreased infarct area in the striatum (Acosta *et al.*, 2015). Similar findings are observed in the clinical context, it was observed that IV infusion of autologous MSCs improved neurological deficits with patients with several stroke (Bang *et al.*, 2005).

The ipsilateral and contralateral striatum, cortex and hippocampi were collected from each experimental brain. It was anticipated that all tissue could be analysed, however, unfortunately due to time restrictions, it was only possible to analyse one area; the ipsilateral striatum. The ipsilateral striatum has been shown to be the most damaged area after MCAO and it was therefore believed that it would be the most appropriate tissue to start with. In MCAO reperfusion, the striatum remains densely ischaemic, with the cortex returning to control blood flow values. Thus, in MCAO striatal infarction is an ischaemic core and cortical infarction is a region of delayed, progressive neuronal death (the ischaemic penumbra) (Carmichael, 2005). This is supported by previous studies demonstrating that at 24 hours, the ischaemic damage was confined to the ipsilateral striatum (Denes *et al.*, 2007). In contrast, reports have suggested that a clear infarction is observed in the striatal and cortical tissue at 24 hours after

MCAO (McColl *et al.*, 2007). Differences in infarction areas is likely due to technique and lab variability, none the less, damage within the striatum is expected. Having said that, the cortex would have more viable tissue which may be better suited for immune cell recruitment. A previous study from our collaborators also failed to observe an effect of hAMSC-CM in the striatum after TBI but did see a change in the cortex (Personal communication, Zanier). Future work should therefore include further analysis of the cortex.

Blood from all experimental animals was collected and plasma was subsequently processed and stored. It would have been useful to measure cytokine/chemokine levels in the blood plasma, unfortunately due to time restrictions this was not in the scope of the current work. It could be the case that although a local immune modulation was not observed, hAMSC-CM could have immunomodulatory effects on the systemic immune response. A peripheral effect of human AMSC have been shown to reduce stroke-induced brain injury. Attenuation of pro-inflammatory factors including IL-1, TNF- $\alpha$ , IL-23, IL-17 and IL-10 in the peripheral blood serum was observed at 12, 24 and 72 hours after MCAO (Cheng *et al.*, 2015). Given this, a cytokine array examining cytokines and chemokines present in the blood plasma would be valuable. On the occasion that the study is repeated, examination of peripheral immune organs such as the thymus, spleen and lymph nodes would be an interesting future avenue to explore.

Technological weaknesses in the study which should be considered include optimisation of PCR. It should be noted that expression levels of all primers are relatively low, this could suggest poor expression levels of the genes of interest or possibly reduced primer efficiency. In these experiments, we assume 100% primer efficiency, this means that during the logarithmic phase of the reaction, the PCR product of interest is doubling with each cycle. However, the efficiency of PCR can be affected by multiple factors (e.g. primer, temperature). A primer efficiency test can be performed and allows for the actual amplification rate to be integrated into the calculation. The concentration of primers had been optimised in previous cell studies, however, ideally the concentration would be further optimised for the current study using tissue. The most appropriate reference gene was optimised using the program RefFinder, however, primer efficiency was not carried out. If time had permitted, it would have been useful to include a MCAO only and sham group into the study, this

would have allowed us to ensure that an appropriate up or down regulation of genes was observed post MCAO.

This chapter of work has investigated the therapeutic potential of hAMSC-CM in experimental stroke. As discussed above, there are a plethora of factors that may be responsible for this lack of effect.

Further work would benefit from further optimisation of timing of hAMSC-CM injection as well as the timing of termination and analysis. The concentration of hAMSC-CM would ideally be lyophilised to 4x in order to be comparable with findings of our collaborators (**table 4.7**). Given the potent effects of hAMSC-CM on microglia migration *in vitro* (**section 3.3.6**), further work should include an *in vivo* study using 2-photon or histological analysis of microglia location and polarisation/morphology. Previous findings with hAMSC-CM *in vivo* and our findings *in vitro* suggests that hAMSC-CM might still be an attractive therapeutic option for the treatment of ischaemic stroke.

#### **4.4.3 Methodological limitations**

Several methodological limitations have been discussed within the previous section (**section 4.4.2**) and includes the timing of injection, the timing of termination, the concentration of hASMC-CM used, as well as the route of administration of hAMSC-CM. Another limitation of the methodological approach used is the variability of the extent of damage produced by the 45 minute MCAO. If the extent of damage produced is considerably variable across the animals, it is difficult to fairly compare treatment groups. One possible solution for this would be to measure the extent of damage using MRI to ensure all animals have a similar lesion size, however, access to MRI can be difficult. Ensuring reproducibility in the model prior to the study, as well as excluding animals with no deficit should have helped to alleviate animal variability.

## **Chapter 5: General Discussion**

## 5.1 Summary of aims and results

This thesis was set out to investigate the ability of hAMSC-CM to modulate the inflammatory response of microglia cells. Given that the aim was to develop a better understanding of hAMSC-CM and its effect on microglia, several *in vitro* and *in vivo* approaches were used. This work has included the development of a new experimental set up for examining microglia migration using a novel microglial cell line.

### 5.1.1 Summary of main findings

#### Chapter 2

- The microglia cell line SIM-A9 cells were responsive to pro- and anti-inflammatory stimuli triggering signalling and polarisation rendering them suitable for investigating the immunomodulatory effects of hAMSC-CM.
- hAMSC-CM had no effect on the signalling pathways of microglia after 30 minutes stimulation with LPS.
- hAMSC-CM significantly reduced *IL1 $\beta$* , *Tnfa* and *Ccl2* gene expression compared to LPS alone group.
- Protocols used to extract primary microglia from the neonatal and adult mouse did not produce purity, reproducibility or good survival in culture.

#### Chapter 3

- SIM-A9 microglial cells survive and proliferate within optimised microfluidic devices
- The optimal conditions for a chemical gradient that was quick to be established and that can be maintained was established in the microfluidic devices
- A glutamate (100  $\mu$ m) gradient induced a significant increase in the Euclidean distance of SIM-A9 cells
- Direct application of LPS significantly inhibited glutamate-induced microglia migration
- IL-4 application significantly increased glutamate-induced migration
- Direct application of hAMSC-CM restored the inhibitory effect of LPS on glutamate-induced migration restoring microglia migration



## Chapter 4

- Reproducible results were obtained for a 45 minute MCAO model in mice producing a low co-efficient of variance (9.5%) for lesion size
- Intravenous injection of hAMSC-CM 3 hours post MCAO did not elicit any effect on pro- or anti-inflammatory gene expression

### 5.2 Future directions

There are many areas relating to this work that need to be investigated in the future including the developing and evaluation of new *in vitro* models relevant to stroke which combines neurons, astrocytes and microglia to investigate the cumulative effect of the cell interactions.

Firstly, further optimisations regarding extracting and culturing primary microglia cells should be a priority. It is important to confirm that hAMSC-CM produces similar results in freshly isolated microglia as already observed in the SIM-A9 cell line.

Optimisation of the microfluidic devices was a significant part of the current project and although time consuming, the use of microfluidic devices have provided us with more detailed information. While the migration device is an improvement on the currently used migration assays, further optimisation could be carried out for a more detailed analysis including exact timing of gradient vs migration of the cells. Incorporating immunofluorescent staining into the time lapse in order to monitor the expression levels of specific proteins and receptors that are potentially involved in the migration process would also be beneficial and would allow us to gain insight into the mechanism of hAMSC-CM and how it is exerted its effects.

To harness the benefits of microfluidic devices, alternative device set ups should be explored. It is essential to examine and understand what effect hAMSC-CM has on neurons and astrocyte functional networks in the presence and absences of insult and microglia. This could help to investigate whether the modulatory effect that we observe on microglia is pertinent to the protective effects of hAMSC-CM after insult. Using a device already available in the department (**figure 5.1**) primary mixed hippocampal and microglia cultures can be cultured in the five chambers for 10 days to develop functional synapses. Each condition, with microglia and microglia/CM can be applied in only one chamber without the others being cross contaminated. Live-

dead cell stains and calcium imaging will be carried out to investigate mortality and effects of treatment on functional communications between cells from different chamber (+/- direct application of LPS and CM and with/without insults and with/without microglia). These experiments could determine whether microglia are needed for this protection and if microglia are needed, whether the phenotype of microglia is anti-inflammatory could be assessed by comparing expression markers.

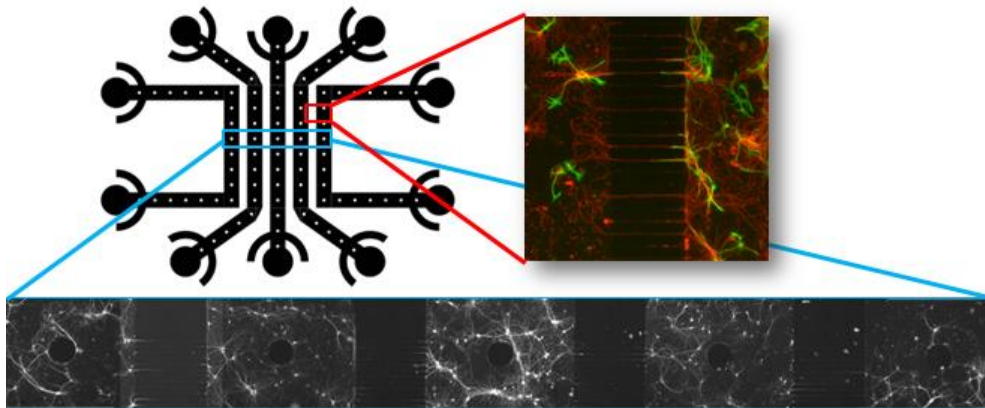


**Figure 5.1. Five chamber microfluidic device.** Chambers are connected through microchannels into which only processes can grow and form functional synapses between the chambers. Fluorescence image showing GFAP (green) and MAP2 (red) staining.

The *in vivo* data failed to reveal an effect of hAMSC-CM on various inflammatory markers, as already discussed, there are several variables that could influence this. Further work should be carried out to establish the optimal timing of hAMSC-CM injection as well as the optimal route of administration.

### 5.3 Further implications

#### 5.3.1 What are the mechanisms involved in hAMSC-CM modulation of microglia?

In the present study, combining several techniques including multidisciplinary collaboration, we show that hAMSC release protective mediators which are capable of modulating microglial cells. Our collaborators used sequential size-exclusion and gel-filtration chromatography to identify a hAMSC-CM sub-fraction which specifically displayed highly protective properties in their *in vitro* OGD injury model. They demonstrated that this fraction, identified as FrA2, is enriched for bioactive properties with a molecular weight smaller than 700 Da, not including proteins or ribonucleic acids (Pischiutta *et al.*, 2016). A series of molecules that were identified by metabolomic profiling are of interest, whose abundance is increased in the active hAMSC-CM fraction, thus suggesting metabolites as possible drivers of the observed protection. Interestingly, the fraction was found to be rich in lysine, taurine, alpha-aminoadipic-acid and spermidine, for which neuroprotective effects have been reported. After ischemia, polyamine catabolism is disrupted (Adibhatla *et al.*, 2002), including depletion of spermine and spermidine, whose antioxidant and free radical scavenger properties are well known (Lovaas, 1997). Therefore, hAMSC-CM may serve as an extracellular source of spermidine, to restore the polyamine pathway in damaged tissue.

Similar neuroprotective effects are potentiated by taurine supplementation which acts through multiple neuroprotective mechanisms in the CNS (Menzie *et al.*, 2013). Taurine is a sulphur containing amino acid found abundantly in mammals. It has been shown to have neuroprotective mechanisms in the CNS such as: regulating cellular osmolarity, an anti-oxidant, neuromodulator of GABAergic transmission, maintaining calcium homeostasis, inhibiting glutamate excitotoxicity, attenuating endoplasmic reticulum stress, modulating the mitochondrial pore permeability and downregulating inflammatory mediators (Menzie *et al.*, 2013).

hAMSC-CM FrA2 was found to be rich in kynurenine, kynurenine is a metabolite of the amino acid L-tryptophan used for the production of niacin. The pathway generates quinolinic acid, an agonist at NMDA-sensitive glutamate receptors but also a glutamate antagonist, resulting in a double-edged sword paradigm (Amori *et al.*, 2009). Availability of kynurenine as precursor of NMDA antagonist molecules might

have beneficial effects, however, it has previously been reported that inhibiting the kynurenine pathway reduces brain damage in animal models of stroke (Darlington *et al.*, 2007).

Intravenous administration of arginine has been shown to be protective against cerebral ischemia insults decreasing infarction size (Kondoh *et al.*, 2010). Voluntary ingestion of lysine in drinking water tends to reduce the incidence of stroke in stroke-prone spontaneous hypertensive rats (Kondoh *et al.*, 2010).

It could be hypothesised that protective mediators released from hAMSC are small molecules/metabolites that are able to stimulate the survival pathways and endogenous trophic/repairative support.

### **5.3.2 Clinical relevance**

The ultimate aim of researching stroke in animal models is to identify potential therapies which can be translated to the treatment of human disease. In pre-clinical studies, over 1000 potential therapies have been trialled, yet after nearly 200 clinical trials, all attempts of neuroprotection have failed (Minnerup *et al.*, 2012). The only real effective treatment available in acute stroke which can reduce injury severity is tissue plasminogen activator (tPA), which was initially developed for myocardial ischaemia, and it not ideal due to its limitations and possible devastating consequences. For this reason, along with increasing prevalence of stroke due to an ageing population, it is essential that new stroke therapies are developed (Albers and Olivot, 2007).

Stem cell conditioned media treatment has several advantages over the current treatment, tPA; in order to receive rtPA treatment, stroke patients must undergo MRI to confirm an ischaemic stroke has indeed occurred, which could possibly delay treatment and result in patients missing the optimal time window. Conditioned media injection IV or IA could prove to be an extremely valuable tool allowing ambulance treatment to modulate the acute immune response post stroke before admittance to hospital. This evidence shows that conditioned media could be a potential straight forward therapy for stroke and could be simply injected, acting on the systemic immune response.

Current hurdles that the use of adult stem cells face include; a limited source of engraftable cells, and the possible transplanted cell-mediated adverse effects including tumour formation, cells trapped within lung or brain vessels, coagulation

activation and immune rejection (Bang *et al.*, 2016). It is tempting to speculate that a cell-free treatment, based on the use of hAMSC-CM, could potentially replace cell transplantation, particularly when tissue repair via paracrine bioactive molecules rather than tissue regeneration via cell replacement/ differentiation is required, with this strategy also offering a series of added advantages. Of note, all placental tissues/fluids are easily available after birth without invasive procedures which means that hAMSC-CM can be produced easily and in large quantities. hAMSC-CM can be stored efficiently because it maintains its anti-fibrotic efficacy after the lyophilization process. As a cell-free treatment, it reduces the risk of adverse immunologic reactions, infectious risks and other potential long-term negative effects caused by the presence of exogenous cells. Finally, it is also conceivable that hAMSC-CM could be administered safely via intravenous injection, avoiding clot formation and lung capillary entrapment (Cargnoni *et al.*, 2012).

## Chapter 6: References

- Abhyankar, V., Lokuta, M., Huttenlocher, A., and Beebe, D. (2006) Characterization of a Membrane-Based Gradient Generator for Use in Cell-Signaling Studies. *Lab on a Chip*, **6**, 389–393.
- Acosta, S., Tajiri, N., Hoover, J., Kaneko, Y., and Borlongan, C. (2015) Intravenous Bone Marrow Stem Cell Grafts Preferentially Migrate to Spleen and Abrogate Chronic Inflammation in Stroke. *Stroke*, **46**, 2616–2627.
- Adibhatla, M., Hatcher, J., Sailor, K., and Dempsey, R.. (2002) Polyamines and Central Nervous System Injury: Spermine and Spermidine Decrease Following Transient Focal Cerebral Ischemia in Spontaneously Hypertensive Rats. *Brain Res*, **938**, 81–86.
- Akira, S., and Takeda, K. (2004) Functions of Toll-like Receptors: Lessons from KO Mice. *Comptes Rendus - Biologies*, **327**, 581–589.
- Albers, G., and Olivot, J. M. (2007) Intravenous Alteplase for Acute Ischaemic Stroke. *The Lancet*, **369**, 249–250.
- Alhadidi, Q., and Shah, Z. (2017) Cofilin Mediates LPS-Induced Microglial Cell Activation and Associated Neurotoxicity Through Activation of NF- $\kappa$ B and JAK/STAT Pathway. *Molecular Neurobiology*, 1–16.
- Amadio, S., De Ninno, A., Montilli, C., Businaro, L., Gerardino, A., and Volonté, C. (2013) Plasticity of Primary Microglia on Micropatterned Geometries and Spontaneous Long-Distance Migration in Microfluidic Channels. *BMC Neuroscience* **14**, 1-12.
- Amori, L., Guidetti, P., Pellicciari, R, Kajii, Y., and Schwarcz, R. (2009) On the Relationship between the Two Branches of the Kynurenine Pathway in the Rat Brain *in vivo*. *Journal of Neurochemistry*, **109**, 316–325.
- Anderson, D J. (2001) Stem Cells and Pattern Formation in the Nervous System: The Possible versus the Actual. *Neuron*, **30**, 19–35.
- Anguiano, M., Carlos, C., Martin, M., Ederra, C., Rafael, P., Xabier, M., and Gorka, M. (2017) Characterization of Three-Dimensional Cancer Cell Migration in Mixed Collagen-Matrigel Scaffolds Using Microfluidics and Image Analysis. *PLoS ONE*, **12**, 1-24.

- Badoer, E. (2010) Microglia: Activation in Acute and Chronic Inflammatory States and in Response to Cardiovascular Dysfunction. *The International Journal of Biochemistry & Cell Biology*, **42**,1580–1585.
- Badshah, H., Ali, T., and Kim, M. (2016) Osmotin Attenuates LPS-Induced Neuroinflammation and Memory Impairments via the TLR4/NFκB Signaling Pathway. *Scientific Reports*, **6**, 1-3.
- Baeuerle, P, A., and Henkel, T. (1994) Function And Activation Of Nf-Kappa-B In the Immune-System. *Annual Review of Immunology*, **12**, 141–179.
- Bang, O. Y., Kim, E., Cha, J., and Moon, G. (2016) Adult Stem Cell Therapy for Stroke: Challenges and Progress. *Journal of Stroke*, **18**, 256–266.
- Bang, O, Y., Lee, J, S., Lee, P., and Lee, G. (2005) Autologous Mesenchymal Stem Cell Transplantation in Stroke Patients. *Annals of Neurology*, **57**, 874–882.
- Bederson. J, B., Pitts, L. H., Tsuji, M., Nishimura, M, C., Davis, R, L., and Bartkowski, H. (1986) Rat Middle Cerebral Artery Occlusion: Evaluation of the Model and Development of a Neurologic Examination. *Stroke, a Journal of Cerebral Circulation*, **17**, 472–476.
- Beebe, D., Mensing, G., and Walker, G. M. (2002) Physics and Applications of Microfluidics in Biology. *Annual Review of Biomedical Engineering*, **4**, 261–86.
- Benjamin, E. J., Blaha, M., Chiuve, S., Cushman, M., Das, S., Deo, R., and De Ferranti, S (2017) *Heart Disease and Stroke Statistics—2017 Update: A Report From the American Heart Association. Circulation.*
- Berthier, E., and Beebe, D. (2014) *Lab chip*, **14**, 3241–3247.
- Bhasin, A., Srivastava, M., Mohanty, S., Bhatia, R., Kumaran, S. S., and Bose, S. (2013) Stem Cell Therapy: A Clinical Trial of Stroke. *Clin Neurol Neurosurg*, **115**, 1003–1008.
- Biber, K., Neumann, H., Kazuhide, I., and Boddeke, H. (2007) Neuronal ‘On’ and ‘Off’ Signals Control Microglia. *Trends in Neurosciences*, **30**, 596–602.
- Boltze, J., Ina, K., Geiger, K., Reich, D., Gunther, A., Buhrlé, C., Egger, D., Kamprad, M., and Emmrich, F. (2005) Experimental Treatment of Stroke in Spontaneously Hypertensive Rats by CD34+ and CD34- Cord Blood Cells. *German Medical Science*, **3**, 1-13.

- Borlongan, Cesar V., Martin Hadman, Cyndy Davis Sanberg, and Paul R. Sanberg. (2004) Central Nervous System Entry of Peripherally Injected Umbilical Cord Blood Cells Is Not Required for Neuroprotection in Stroke. *Stroke*, **35**, 2385–2389.
- Boyden, S. (1961) The chemotactic effect of mixtures of antibody and antigen on polymorphonuclear leukocytes. *Journal of Experimental Medicine*, 453–466.
- Brea, David, Tomás Sobrino, Pedro Ramos-Cabrera, and José Castillo. (2009) Inflammatory and Neuroimmunomodulatory Changes in Acute Cerebral Ischemia. *Cerebrovascular Diseases*, **27**, 48–64.
- Bronstein, Robert, Luisa Torres, Jillian C Nissen, and Stella E Tsirka. (2013) Culturing Microglia from the Neonatal and Adult Central Nervous System.” *Journal of Visualized Experiments : JoVE*, **78**.
- Burr, S., Francesco, D., and Oliver, G. (2013) Mesenchymal Stromal Cells and Regulatory T Cells: The Yin and Yang of Peripheral Tolerance. *Immunology and Cell Biology*, **91**, 12–18.
- Bustin, S., Vladimir, B., Jeremy, G., Huggett, K., and Reinhold, M. (2009) The MIQE Guidelines. *Clinical Chemistry*, **55**, 611–622.
- Butovsky, O., Talpalar, A., Ben-Yaakov, K., and Schwartz, M. (2005) Activation of Microglia by Aggregated  $\beta$ -Amyloid or Lipopolysaccharide Impairs MHC-II Expression and Renders Them Cytotoxic Whereas IFN- $\gamma$  and IL-4 Render Them Protective. *Molecular and Cellular Neuroscience*, **29**, 381–393.
- Caplan, A. (1991) Mesenchymal Stem Cells. *Journal of orthopaedic research*, **9**, 641-650.
- Carbonell, S., Shin-Ichi, M., Alan, H., and Mandell, J. (2005) Migration of Perilesional Microglia after Focal Brain Injury and Modulation by CC Chemokine Receptor 5. *The Journal of Neuroscience*, **25**, 7040-7047.
- Cardona, A., DeRen, H., Sasse, M and Ransohoff, R. (2006) Isolation of Murine Microglial Cells for RNA Analysis or Flow Cytometry. *Nature Protocols*, **1**, 947–951.
- Cargnoni, A., Piccinelli, E. C., Ressel, L., Rossi, D., Magatti, M., Toschi, I., Cesari, V., Albertini, M., Mazzola, S., and Parolini, O. (2014) Conditioned Medium from



Amniotic Membrane-Derived Cells Prevents Lung Fibrosis and Preserves Blood Gas Exchanges in Bleomycin-Injured Mice-Specificity of the Effects and Insights into Possible Mechanisms. *Cytotherapy*, **16**, 17–32.

Cargnoni, A., Ressel, L., Rossi, D., Poli, A., Arienti, D., Lombardi, G., and Parolini, O. (2012) Conditioned Medium from Amniotic Mesenchymal Tissue Cells Reduces Progression of Bleomycin-Induced Lung Fibrosis. *Cytotherapy*, **14**, 153–161.

Carmichael, S. (2005) Rodent Models of Focal Stroke: Size, Mechanism, and Purpose. *The Journal of the American Society for Experimental NeuroTherapeutics*, **2**, 396–409.

Ceulemans, A. G., Zgavc, T., Kooijman, R., Hachimi-Idrissi, S., Sarre, S., and Michotte, Y. (2010) The Dual Role of the Neuroinflammatory Response after Ischemic Stroke: Modulatory Effects of Hypothermia. *J Neuroinflammation*, **7**, 1-18.

Chamorro, Á., Meisel, A., Planas, A., Urra, X., Beek, D., and Roland, V. (2012) The Immunology of Acute Stroke. *Nature Reviews Neurology*, **8**, 401–410.

Chapman, G., Moores, K., Harrison, D., Campbell, C., Stewart, B., and Strijbos, P. (2000) Fractalkine Cleavage from Neuronal Membranes Represents an Acute Event in the Inflammatory Response to Excitotoxic Brain Damage. *The Journal of Neuroscience*, **20**, 1-5.

Chaubey, S., Ridley, A., and Wells, C. (2011) Using the Dunn Chemotaxis Chamber to Analyse Primary Cell Migration in Real Time. *Methods in Molecular Biology*, **769**, 41-51.

Chen, J., Li, Y., Wang, L., Zhang, Z., Lu, D., Lu, M., and Chopp, M. (2001) Therapeutic Benefit of Intravenous Administration of Bone Marrow Stromal Cells After Cerebral Ischemia in Rats. *Stroke*, **32**, 1005–1011.

Chen, X., Zhang, Y., Sadadcharam, G., Cui, W., and Wang, J. (2013) Isolation, Purification and Culture of Primary Murine Microglial Cells. *Bio-protocol*, **3**, 1–6.

Cheng, Q., Zhang, Z., Zhang, S., Yang, H., Zhang, X., Pan, J., and Weng, L. (2015) Human Umbilical Cord Mesenchymal Stem Cells Protect against Ischemic Brain Injury in Mouse by Regulating Peripheral Immunoinflammation. *Brain Research*, **1594**, 293–304.

- Chhor, V., Charpentier, T., Lebon, S., Oré, M., Celador, I., Josserand, J., and Degos, V (2013) Characterization of Phenotype Markers and Neuronotoxic Potential of Polarised Primary Microglia *in vitro*. *Brain, Behavior, and Immunity*, **32**, 70–85.
- Chiang, T., Messing, R., and Chou, W. H. (2011) Mouse Model of Middle Cerebral Artery Occlusion. *Journal of Visualized Experiments*, **48**, 10-12.
- Chiu, I., Morimoto, E., Goodarzi, H., Liao, J., O’Keeffe, S., Phatnani, H., and Muratet, M (2013) A Neurodegeneration-Specific Gene-Expression Signature of Acutely Isolated Microglia from an Amyotrophic Lateral Sclerosis Mouse Model. *Cell Reports*, **4**, 385–401.
- Conductier, G., Blondeau, N., Guyon, A., Nahon, J., and Rovère, C. (2010) The Role of Monocyte Chemoattractant Protein MCP1/CCL2 in Neuroinflammatory Diseases. *Journal of Neuroimmunology* **224**, 93–100.
- Daadi, M. M., Maag, A-L., and Steinberg, G. (2008) Adherent Self-Renewable Human Embryonic Stem Cell-Derived Neural Stem Cell Line: Functional Engraftment in Experimental Stroke Model. *PloS One*, **3**, 1-6.
- Darlington, L. G., Mackay, G.M., Forrest, C. M., Stoy, N., George, C., and Stone, T. (2007) Altered Kynurenine Metabolism Correlates with Infarct Volume in Stroke. *European Journal of Neuroscience*, **26**, 2211–2221.
- Das, A., Chai, J., Kim, S., Park, K. S., Lee, Y. S., Jung, K., and Chai, Y. G. (2015) Dual RNA Sequencing Reveals the Expression of Unique Transcriptomic Signatures in Lipopolysaccharide-Induced BV-2 Microglial Cells. *Plos One*, **10**, 1-26.
- Das, A., Kim, S., Arifuzzaman, S., Yoon, T., Chai, J., Lee, Y. S., Park, K. S., Jung, K., and Chai, Y. G. (2016) Transcriptome Sequencing Reveals That LPS-Triggered Transcriptional Responses in Established Microglia BV2 Cell Lines Are Poorly Representative of Primary Microglia. *Journal of Neuroinflammation*, **13**, 1-18.
- Davalos, D., Grutzendler, J., Yang, G., Kim, J., Zuo, Y., Jung, S., Littman, D., Dustin, M and Gan, W-B. (2005) ATP Mediates Rapid Microglial Response to Local Brain Injury *in vivo*. *Nature Neuroscience*, **8**, 752–758.
- De Simone, R., Elena, C., De Nuccio, C., Ajmone-Cat, M., Visentin, S., and

- Minghetti, L. (2010) TGF- $\beta$  and LPS modulate ADP-induced migration of microglial cells through P2Y1 and P2Y12 receptor expression. *Journal of Neurochemistry*, **115**, 450-459.
- Dénes, A., Ferenczi, S., Halász, J., Környei, Z., and Kovács, K. (2008) Role of CX3CR1 (Fractalkine Receptor) in Brain Damage and Inflammation Induced by Focal Cerebral Ischemia in Mouse. *Journal of Cerebral Blood Flow and Metabolism*, **28**, 1707–1721.
- Denes, A., Vidyasagar, R., Feng, J., Narvainen, J., McColl, B., Kauppinen, R., and Allan, S. (2007) Proliferating Resident Microglia after Focal Cerebral Ischaemia in Mice. *Journal of Cerebral Blood Flow and Metabolism*, **27**, 1941–1953.
- Ding, D-C., Chang, Y-S., Shyu, W-C., and Lin, S-Z. (2015) Human Umbilical Cord Mesenchymal Stem Cells: A New Era for Stem Cell Therapy. *Cell Transplantation*, **24**, 339–347.
- Ding, D-C, Lin, C-H., Shyu, W-C., and Lin, S-Z. (2013) *Review Neural Stem Cells and Stroke*, **22**, 619–630.
- Ding, D-C., Shyu, W-C., Chiang, M-F., Lin, S., Chang, Y., Wang, H., Su, C and Li, H. (2007) Enhancement of Neuroplasticity through Upregulation of  $\beta$ 1-Integrin in Human Umbilical Cord-Derived Stromal Cell Implanted Stroke Model. *Neurobiology of Disease*, **27**, 339–353.
- Dirnagl, U., Iadecola, C and Moskowitz, M. (1999) Pathobiology of Ischaemic Stroke: An Integrated View. *Trends in Neurosciences*, **22**, 391–397.
- Dissing-Olesen, L., LeDue, J., Rungta, R., Hefendehl, J., Choi, H.B., and MacVicar, B. A. (2014) Activation of Neuronal NMDA Receptors Triggers Transient ATP-Mediated Microglial Process Outgrowth. *Journal of Neuroscience*, **34**, 10511–10527.
- Domercq, M., Vázquez-Villoldo, N., and Matute, C.(2013) Neurotransmitter Signaling in the Pathophysiology of Microglia. *Frontiers in Cellular Neuroscience*, **7**, 1-17.
- Doyle, K. P., Simon, P. R., and Stenzel-Poore, M. (2008) Mechanisms of Ischemic Brain Damage. *Neuropharmacology*, **55**, 310–318.
- Duncombe, T., Tentori, A., and Herr, A. (2015) Microfluidics: Reframing Biological

- Enquiry. *Nature Reviews Molecular Cell Biology*, **16**, 554–567.
- Eckert, M. A., Vu, Q., Xie, K., Yu, J., Liao, W., Cramer, S and Zhao, W. (2013) Evidence for High Translational Potential of Mesenchymal Stromal Cell Therapy to Improve Recovery from Ischemic Stroke. *Journal of Cerebral Blood Flow & Metabolism*, **33**, 1322–1334.
- EIAlI, A., and Rivest, S. (2016) Microglia Ontology and Signaling. *Frontiers in Cell and Developmental Biology*, **4**, 1-14.
- Emsley, H. C. A., Smith, C. J., Georgiou, R.F., Vail, A., Hopkins, S. J., Rothwell, N. J., and Tyrrell, P. J. (2005) A Randomised Phase II Study of Interleukin-1 Receptor Antagonist in Acute Stroke Patients. *Journal of Neurology, Neurosurgery, and Psychiatry*, **76**, 1366–1372.
- Farrell, K., Borazjani, A., Damaser, M and Kothapalli, C. (2016) Differential Regulation of NSC Phenotype and Genotype by Chronically Activated Microglia within Cocultures. *Integr. Biol.*, **8**, 1145–1157.
- Feigin, V. L., Forouzanfar, F. M., Krishnamurthi, R., Mensah, A. G., Connor, M., Bennett, D., and Moran, A . (2014) Global and Regional Burden of Stroke during 1990-2010: Findings from the Global Burden of Disease Study. *The Lancet*, **383**, 245–255.
- Fisher, M. (2004) Current Concepts of the Ischemic Penumbra: Introduction. *Stroke* **35**, 2657–2658.
- Fontainhas, A. M., Wang, M., Liang, J. K., Chen, S., Mettu, P., Damani, M., Fariss, R., Li, W., and Wong, W. (2011) Microglial Morphology and Dynamic Behavior Is Regulated by Ionotropic Glutamatergic and GABAergic Neurotransmission. *PLoS ONE*, **6**, 1-14.
- Fraga, J. S., Silva, N. A., Lourenço, A. S., Gonçalves, V., Neves, N. M., Reis, R. L., Rodrigues, A. J., Manadas, B., Sousa, N., and Salgado, A. J. (2013) Unveiling the Effects of the Secretome of Mesenchymal Progenitors from the Umbilical Cord in Different Neuronal Cell Populations. *Biochimie*, **95**, 2297–2303.
- Fu, Y., Liu, Q., Anrather, J., and Shi, F-D. (2015) Immune Interventions in Stroke. *Nature Reviews. Neurology*, **11**, 524–535.
- Fumagalli, S., Perego, C., Ortolano, F and De Simoni, M. G. (2013) CX3CR1

- Deficiency Induces an Early Protective Inflammatory Environment in Ischemic Mice. *Glia*, **61**, 827–842.
- Fumagalli, S., Perego, C., Pischiutta, F., Zanier, E., and De Simoni, M. G. (2015) The Ischemic Environment Drives Microglia and Macrophage Function. *Frontiers in Neurology*, **6**, 1–19.
- Garcia, J. A., Cardona, S. M., and Cardona, A. (2014) Isolation and Analysis of Mouse Microglial Cells. *Current Protocols in Immunology*, **104**, 1-18
- Gelderblom, M., Leypoldt, F., Steinbach, F., Behrens, D., Choe, C-U., Siler, D., and Arumugam, T. (2009) Temporal and Spatial Dynamics of Cerebral Immune Cell Accumulation in Stroke. *Stroke; a Journal of Cerebral Circulation*, **40**, 1849–1857.
- Gennai, S., Monsel, A., Hao, Q., Liu, J., Gudapati, V., Barbier, E. L., and Lee, J. W. (2015) Cell-Based Therapy for Traumatic Brain Injury. *British Journal of Anaesthesia*, **115**, 203–212.
- Ginhoux, F., Greter, M., Leboeuf, M., Nandi, S., See, P., Gokhan, S., and Mehler, M. F. (2010) Fate Mapping Analysis Reveals That Adult Microglia Derive from Primitive Macrophages. *Science*, **330**, 841–845.
- Giulian, D, and Baker, T. J. (1986) Characterization of Ameboid Microglia Isolated from Developing Mammalian Brain. *The Journal of Neuroscience*, **6**, 2163–2178.
- Giunti, D., Parodi, B., Usai, C., Vergani, L., Casazza, S., Bruzzone, S., Mancardi, G., and Uccelli, A. (2012) Mesenchymal Stem Cells Shape Microglia Effector Functions through the Release of CX3CL1. *Stem Cells*, **30**, 2044–2053.
- Goloviznina, N. A., Verghese, S., Yoon, Y. M., Taratula, O., Marks, D., and Kurre, P. (2016) Mesenchymal Stromal Cell-Derived Extracellular Vesicles Promote Myeloid-Biased Multipotent Hematopoietic Progenitor Expansion via Toll-like Receptor Engagement. *Journal of Biological Chemistry*, **291**, 24607–24617.
- Gordon, R., Hogan, C., Neal, L. M., Anantharam, V., Kanthasamy, A., and Kanthasamy, A. (2011) A Simple Magnetic Separation Method for High-Yield Isolation of Pure Primary Microglia. *Journal of Neuroscience Methods*, **194**, 287–296.

- Grabert, K., Michoel, T., Karavolos, M., Clohisey, S., Baillie, K., Stevens, M., Freeman, T., Summers, K., and McColl, B. (2016) Microglial Brain Region-Dependent Diversity and Selective Regional Sensitivities to Aging. *Nature Neuroscience*, **19**, 504–516.
- Graeber, M. B., and Streit, J. W. (2010) Microglia: Biology and Pathology. *Acta Neuropathologica*, **119**, 89–105.
- Gregersen, R., Lambertsen, K., and Finsen, B. (2000) Microglia and Macrophages Are the Major Source of Tumor Necrosis Factor in Permanent Middle Cerebral Artery Occlusion in Mice. *Journal of Cerebral Blood Flow and Metabolism*, **20**, 53–65.
- Gyoneva, S., Davalos, D., Biswas, D., Swanger, S., Garnier-Amblard, E., Loth, F., Akassoglou, K., and Traynelis, S. (2014) Systemic Inflammation Regulates Microglial Response to Tissue Damage *in vivo*. *Glia*, **62**, 1345–1360.
- Harms, A.S., and Tansey, M. G. (2013) Isolation of Murine Postnatal Brain Microglia for Phenotypic Characterization Using Magnetic Cell Separation Technology. *Methods in Molecular Biology*, **1041**, 33–39.
- Haynes, S. E., Hollopeter, G., Yang, G., Kurpius, D., Dailey, M. E., Gan, W-B., and Julius, D. (2006) The P<sub>2</sub>Y<sub>12</sub> Receptor Regulates Microglial Activation by Extracellular Nucleotides. *Nature Neuroscience*, **9**, 1512–1519.
- Hegyí, B., Kornyei, Z., Ferenczi, S., Fekete, R., Kudlik, G., Kovacs, K., Madarasz, E., and Uher, F. (2014) Regulation of Mouse Microglia Activation and Effector Functions by Bone Marrow-Derived Mesenchymal Stem Cells. *Experimental Biology*, **49**, 1–56.
- Henn, A., Lund, S., Hedtj, M., Schrattenholz, A., Porzgen, P., and Leist, M. (2009) The Suitability of BV2 Cells as Alternative Model System for Primary Microglia Cultures or for Animal Experiments Examining Brain Inflammation. *Alternatives to Animal Experimentation*, **26**, 83–94.
- Herx, L. M., Rivest, S., and Yong, V. W. (2000) Central Nervous System-Initiated Inflammation and Neurotrophism in Trauma: IL-1 Is Required for the Production of Ciliary Neurotrophic Factor. *The Journal of Immunology*, **165**, 2232–2239.
- Hicks, A. U., Lappalainen, R., Narkilahti, S., Suuronen, R., Corbett, D., Sivenius, J.,

- Hovatta, O., and Jolkkonen, J. (2009) Transplantation of Human Embryonic Stem Cell-Derived Neural Precursor Cells and Enriched Environment after Cortical Stroke in Rats: Cell Survival and Functional Recovery. *The European Journal of Neuroscience*, **29**, 562–574.
- Honda, S., Sasaki, Y., Ohsawa, K., Imai, Y., Nakamura, Y., Inoue, K., and Kohsaka, S. (2001) Extracellular ATP or ADP Induce Chemotaxis of Cultured Microglia through Gi/o-Coupled P2Y Receptors. *The Journal of Neuroscience*, **21**, 1975–1982.
- Honma, T., Honmou, O., Iihoshi, S., Harada, K., Houkin, K., Hamada, H., and Kocsis, J. D. (2006) Intravenous Infusion of Immortalized Human Mesenchymal Stem Cells Protects against Injury in a Cerebral Ischemia Model in Adult Rat. *Experimental Neurology*, **199**, 56–66.
- Horvath, R. J., Nutile-McMenemy, N., Alkaitis, M. S., and Deleo, J. (2008) Differential Migration, LPS-Induced Cytokine, Chemokine, and NO Expression in Immortalized BV-2 and HAPI Cell Lines and Primary Microglial Cultures. *Journal of Neurochemistry*, **107**, 557–569.
- Hosseini, S.M., Farahmandnia, M., Razi, Z., Delavarifar, S., and Shakibajahromi, B. (2015) 12 Hours After Cerebral Ischemia Is the Optimal Time for Bone Marrow Mesenchymal Stem Cell Transplantation. *Neural Regeneration Research*, **10**, 904-908.
- Howells, D. W., Porritt, M.J., Rewell, S. S. J., O'Collins, V., Sena, E. S., Bart van der Worp, H., Traystman, R. J., and Macleod, M. R. (2010) Different Strokes for Different Folks: The Rich Diversity of Animal Models of Focal Cerebral Ischemia. *Journal of Cerebral Blood Flow and Metabolism*, **30**, 1412–1431.
- Hsieh, J. Y., Wang, H. W., Chang, S. J., Liao, K. H., Lee, I. H., Lin, S., Wu, C. H., Lin, W. Y., and Cheng, S. M. (2013) Mesenchymal Stem Cells from Human Umbilical Cord Express Preferentially Secreted Factors Related to Neuroprotection, Neurogenesis, and Angiogenesis. *PLoS ONE*, **8**, 1–11.
- Hsuan, Y. C. Y., Lin, C. H., Chang, C. P., and Lin, M. T. (2016) Mesenchymal Stem Cell-Based Treatments for Stroke, Neural Trauma, and Heat Stroke. *Brain and Behavior*, **6**, 1–11.
- Hu, H., Li, Z., Zhu, X., Lin, R., and Chen, L. (2014) Salidroside Reduces Cell

- Mobility via NF-  $\kappa$  B and MAPK Signaling in LPS-Induced BV2 Microglial Cells. *Evidence-Based Complementary and Alternative Medicine*, **2014**, 1-9.
- Hu, X., Li, P., Guo, Y., Wang, H., Leak, R. K., Chen, S., Gao, Y., and Chen, J. (2012) Microglia/macrophage Polarization Dynamics Reveal Novel Mechanism of Injury Expansion after Focal Cerebral Ischemia. *Stroke*, **43**, 3063–3070.
- Huang, P., Gebhart, N., Richelson, E., Brott, T. G., Meschia, J. F., and Zubair, A. C. (2014) Mechanism of Mesenchymal Stem Cell-Induced Neuron Recovery and Anti-Inflammation. *Cytotherapy*, **0**, 1-9.
- Hung, Y.Y., Lin, C-C., Kang, H-T., and Huang, T-L. (2017) TFAIP3, a Negative Regulator of the TLR Signaling Pathway, Is a Potential Predictive Biomarker of Response to Antidepressant Treatment in Major Depressive Disorder. *Brain, Behavior, and Immunity*, **59**, 265–272.
- Hutchison, E. R., Kawamoto, E. M., Taub, D. D., Lal, A., Abdelmohsen, K., Zhang, Y., and Wood, W. H. (2013) Evidence for miR-181 Involvement in Neuroinflammatory Responses of Astrocytes. *Glia*, **61**, 1018–1028.
- Iadecola, C., and Anrather, J. (2011) The Immunology of Stroke: From Mechanisms to Translation. *Nature Medicine*, **17**, 796–808.
- Imitola, J., Raddassi, K., Park, K., Mueller, F-J., Nieto, M., Teng, Y. D., and Frenkel, D. (2004) Directed Migration of Neural Stem Cells to Sites of CNS Injury by the Stromal Cell-Derived Factor 1 CXC Chemokine Receptor 4 Pathway. **101**, 18117–18122.
- Irino, Y., Nakamura, Y., Inoue, K., Kohsaka, S and Ohsawa, K. (2008) Akt Activation Is Involved in P2Y<sub>12</sub> Receptor-Mediated Chemotaxis of Microglia. *Journal of Neuroscience Research*, **86**, 511–519.
- Irving, E. A., and Bamford, M. (2002) Role of Mitogen- and Stress-Activated Kinases in Ischemic Injury. *Journal of Cerebral Blood Flow and Metabolism*, **22**, 631–647.
- Jiang, Y., Zhu, W., Zhu, J., Wu, L., Xu, G., and Liu, X.. (2013) Feasibility of Delivering Mesenchymal Stem Cells via Catheter to the Proximal End of the Lesion Artery in Patients with Stroke in the Territory of the Middle Cerebral Artery. *Cell Transplantation*, **22**, 2291–2298.



- Jin, R., Yang, G., and Li, G. (2010) Inflammatory Mechanisms in Ischemic Stroke: Role of Inflammatory Cells. *Journal of Leukocyte Biology*, **87**, 779–789.
- Jose, S., Tan, S. W., Ooi, Y. Y., Ramasamy, R., and Vidyadaran, S. (2014) Mesenchymal Stem Cells Exert Anti-Proliferative Effect on Lipopolysaccharide-Stimulated BV2 Microglia by Reducing Tumour Necrosis Factor- $\alpha$  Levels. *Journal of Neuroinflammation*, **11**.
- Kahle, M. P., and Bix, G. J. (2013) Neuronal Restoration Following Ischemic Stroke. *Neurorehabilitation and Neural Repair*, **27**, 469–478.
- Kalladka, D., and Muir, K. (2014) Brain Repair: Cell Therapy in Stroke. *Stem Cells and Cloning : Advances and Applications*, **7**, 31–44.
- Kawai, H., Yamashita, T., Ohta, Y., Deguchi, K., Nagotani, S., Zhang, X., Ikeda, Y., Matsuura, T and Abe, K. (2010) Tridermal Tumorigenesis of Induced Pluripotent Stem Cells Transplanted in Ischemic Brain. *Journal of Cerebral Blood Flow and Metabolism*, **30**, 1487–1493.
- Keenan, M. T., and Folch, A. (2008) Biomolecular Gradients in Cell Culture Systems. **8**, 1–44.
- Khalil, M, Ronda, J., Weintraub, M., Jain, K., Silver, R and Silverman, A. J. (2007) Brain Mast Cell Relationship to Neurovasculature during Development. *Brain Research*, **1171**, 18–29.
- Kilkenny, C., Browne, W. J., Cuthill, I. C., Emerson, M and Altman, D. G. (2010) Improving Bioscience Research Reporting: The ARRIVE Guidelines for Reporting Animal Research. *PLoS Biology*, **8**.
- Kim, E.S., Ahn, S. Y., Im, G. H., Sung, D. K., Park, Y. R., Choi, H., and Choi, S. (2012) Human Umbilical Cord Blood-derived Mesenchymal Stem Cell Transplantation Attenuates Severe Brain Injury by Permanent Middle Cerebral Artery Occlusion in Newborn Rats. *Pediatric Research*, **72**, 277–284.
- Kim, J., Choi, J. S., Yu, M., Nam, K., Piao, C., Kim, S., Lee, M., Han, P., Park, and Lee, J. (2006) HMGB1, a Novel Cytokine-Like Mediator Linking Acute Neuronal Death and Delayed Neuroinflammation in the Postischemic Brain. *Journal of Neuroscience*, **26**, 6413–6421.
- Kim, S., Kim, H. J., and Jeon, N. L. (2010) Biological Applications of Microfluidic

Gradient Devices. *Integrative Biology : Quantitative Biosciences from Nano to Macro*, **2**, 584–603.

- Kim, Y.-J., Park, H.-J., Lee, G., Bang, O. Y., Ahn, Y. H., Joe, E. Kim, H. O., and Lee, P. H. (2009) Neuroprotective Effects of Human Mesenchymal Stem Cells on Dopaminergic Neurons through Anti-Inflammatory Action. *Glia*, **57**, 13–23.
- Kondoh, T., Kameishi, M., Mallick, H. N., Ono, T., and Torii, K. (2010) Lysine and Arginine Reduce the Effects of Cerebral Ischemic Insults and Inhibit Glutamate-Induced Neuronal Activity in Rats. *Frontiers in Integrative Neuroscience*, **4**, 1-10.
- Kostulas, N. (2002) Dendritic Cells Are Present in Ischemic Brain After Permanent Middle Cerebral Artery Occlusion in the Rat. *Stroke*, **33**, 1129–1134.
- Krafft, P. R., Bailey, E. L., Lekic, T., Rolland, W. B., Altay, O., Tang, J., Wardlaw, J. M., Zhang, J. H., and Sudlow, C. A. M. (2012) Etiology of Stroke and Choice of Models. *International Journal of Stroke*, **7**, 398–406.
- Kramer, N., Walzl, A., Unger, C., Rosner, M., Krupitza, G., Hengstchlager, M., and Dolznig, H. (2013) *In Vitro* Cell Migration and Invasion Assays. *Reviews in Mutation Research*, **752**, 10–24.
- Kranz, A., Wagner, D.-C., Kamprad, M., Scholz, M., Schmidt, U. R., Nitzsche, F., Aberman, Z., Emmrich, F., Riegelsberger, U. M., and Boltze, J. (2010) Transplantation of Placenta-Derived Mesenchymal Stromal Cells upon Experimental Stroke in Rats. *Brain Research*, **1315**, 128–136.
- Krasnow, S. M., Knoll, J. B., Verghese, S. C., Levasseur, P. R., and Marks, D. R. (2017) Amplification and Propagation of Interleukin-1 $\beta$  Signaling by Murine Brain Endothelial and Glial Cells. *Journal of Neuroinflammation*, **14**, 1-18.
- Ladecola, C., and Anrather, J. (2012) The Immunology of Stroke: From Mechanisms to Translation. *Nat Med*, **17**, 796–808.
- Lakhan, S. E., Kirchgessner, A., and Hofer, M. (2009) Inflammatory Mechanisms in Ischemic Stroke: Therapeutic Approaches. *Journal of Translational Medicine*, **7**, 1-11.
- Lalancette-Hébert, M., Gowing, G., Simard, A., Weng, Y. C., and Kriz, J. (2007) Selective Ablation of Proliferating Microglial Cells Exacerbates Ischemic Injury

- in the Brain. *The Journal of Neuroscience*, **27**, 2596–2605.
- Lee, J-K., and Tansey, M. G. (2013) Microglia. *Methods Mol Biol*, **1041**, 17–23.
- Leonardo, C. C., Hall, A. A., Collier, L. A., Ajmo, C. T., Willing, A. E., and Pennypacker, K. R. (2010) Human Umbilical Cord Blood Cell Therapy Blocks the Morphological Change and Recruitment of CD11b-Expressing, Isolectin-Binding Proinflammatory Cells after Middle Cerebral Artery Occlusion. *Journal of Neuroscience Research*, **88**, 1213–1222.
- Li, F., Miao, Z-N., Xu, Y-Y., Zheng, S-Y., Qin, M-D., Gu, Y-Z., and Zhang, X-G. (2012) Transplantation of Human Amniotic Mesenchymal Stem Cells in the Treatment of Focal Cerebral Ischemia. *Molecular Medicine Reports*, **6**, 625–630.
- Liang, C-C., Park, A, Y., and Guan, J-L. (2007) *In Vitro* Scratch Assay: A Convenient and Inexpensive Method for Analysis of Cell Migration in Vitro. *Nat. Protoc.*, **2**, 329–333.
- Liao, W., Xie, J., Zhong, J., Liu, Y., Du, L., Zhou, B., and Xu, J. (2009) Therapeutic Effect of Human Umbilical Cord Multipotent Mesenchymal Stromal Cells in a Rat Model of Stroke. *Transplantation*, **87**, 350–359.
- Liao, X., Sharma, N and Kapadia, F. (2011) Krüppel-like Factor 4 Regulates Macrophage Polarization. *The Journal of Clinical Investigation*, **121**, 2736–2749.
- Liu, F., and McCullough, L. D. (2011) Middle Cerebral Artery Occlusion Model in Rodents: Methods and Potential Pitfalls. *Journal of Biomedicine & Biotechnology*.
- Liu, G.J., Kalous, A., Werry, E. L., and Bennett, M. R. (2006) Purine Release from Spinal Cord Microglia after Elevation of Calcium by Glutamate. *Molecular Pharmacology*, **70**, 851–859.
- Liu, G. J., Nagarajah, R., Banati, R. B., and Bennett, M. R. (2009) Glutamate Induces Directed Chemotaxis of Microglia. *European Journal of Neuroscience*, **29**, 1108–1118.
- Liu, X-L., Zhang, W and Tang, S-J. (2014) Intracranial Transplantation of Human Adipose-Derived Stem Cells Promotes the Expression of Neurotrophic Factors

and Nerve Repair in Rats of Cerebral Ischemia-Reperfusion Injury. *International Journal of Clinical and Experimental Pathology*, **7**, 174–183.

Locatelli, F., Bersano, A., Ballabio, E., Lanfranconi, S., Papadimitriou, D., Strazzer, S., Bresolin, N., Comi, G. P and Corti, S. (2009) Stem Cell Therapy in Stroke. *Cellular and Molecular Life Sciences*, **66**, 757–772.

Lovaas, E. (1997) Antioxidative and Metal-Chelating Effects of Polyamines. *Advances in Pharmacology*, **38**, 119-149.

Lu, D-Y., Tang, C-H., Liou, H-C., Teng, C-M., Jeng, K-C. G., Kuo, S-C., Lee, F-Y., and Fu, W-M. (2007) YC-1 Attenuates LPS-Induced Proinflammatory Responses and Activation of Nuclear Factor-kappaB in Microglia. *British Journal of Pharmacology*, **151**, 396–405.

Lu, D., Sanberg, P. R., Mahmood, A., Li, Y., Wang, L., Sanchez-Ramos, J., and Chopp, M. (2002) Intravenous Administration of Human Umbilical Cord Blood Reduces Neurological Deficit in the Rat after Traumatic Brain Injury. *Cell Transplantation*, **11**, 275-281.

Ma, S., Zhong, D., Chen, H., Zheng, Y., Sun, Y., Luo, J., Li, H., Li, G., and Yin, Y. (2013) The Immunomodulatory Effect of Bone Marrow Stromal Cells (BMSCs) on Interleukin (IL)-23/IL-17-Mediated Ischemic Stroke in Mice. *Journal of Neuroimmunology*, **257**, 28–35.

Ma, Y., Wang, J., Wang, Y., and Yang, G-Y. (2016) The Biphasic Function of Microglia in Ischemic Stroke. *Progress in Neurobiology*, **157**, 1-25.

Macrae, I. M. (2011) Preclinical Stroke Research-Advantages and Disadvantages of the Most Common Rodent Models of Focal Ischaemia. *British Journal of Pharmacology*, **164**, 1062–1078.

Macrae, M., Robinson, M. J., Graham, D., Reid, J. L., and McCulloch, J. (1993) Endothelin-L-Induced Reductions in Cerebral Blood Flow: Dose Dependency, Time Course, and Neuropathological Consequences. *Journal of Cerebral Blood Flow and Metabolism*, **13**, 276–84.

Macrez, R., Ali, C., Toutirais, O., Le Mauff, B., Defier, G., Dirnagl, U., and Denis, V. D. (2011) Stroke and the Immune System: From Pathophysiology to New Therapeutic Strategies. *The Lancet Neurology*, **10**, 471–480.

- Madinier, A., Bertrand, N., Mossiat, C., Prigent-Tessier, A., Beley, A., Marie, C., and Garnier, P. (2009) Microglial Involvement in Neuroplastic Changes Following Focal Brain Ischemia in Rats. *PLoS ONE*, **4**, 1-12.
- Madry, C., and Attwell, D. (2015) Receptors, Ion Channels, and Signaling Mechanisms Underlying Microglial Dynamics. *Journal of Biological Chemistry*, **290**, 12443–12450.
- Marek, R., Caruso, M., Rostami, A., Grinspan, J. B., and Das Sarma, J. (2008) Magnetic Cell Sorting: A Fast and Effective Method of Concurrent Isolation of High Purity Viable Astrocytes and Microglia from Neonatal Mouse Brain Tissue. *Journal of Neuroscience Methods*, **175**, 108–118.
- Martinez, F. O., and Gordon, S. (2014) The M1 and M2 Paradigm of Macrophage Activation: Time for Reassessment. *Prime Reports*, **6**, 1–13.
- McColl, B. W., Rothwell, N. J., and Allan, S. M. (2007) Systemic Inflammatory Stimulus Potentiates the Acute Phase and CXC Chemokine Responses to Experimental Stroke and Exacerbates Brain Damage via Interleukin-1- and Neutrophil-Dependent Mechanisms. *Journal of Neuroscience*, **27**, 4403–4412.
- McColl, B. W., Carswell, H. V., McCulloch, J., and Horsburgh, K. (2004) Extension of Cerebral Hypoperfusion and Ischaemic Pathology beyond MCA Territory after Intraluminal Filament Occlusion in C57Bl/6J Mice. *Brain Research*, **997**, 15–23.
- McColl, B. W., Allan, S. M., and Rothwell, N. J. (2009) Systemic Infection, Inflammation and Acute Ischemic Stroke. *Neuroscience*, **158**, 1049–1061.
- McCoy, M. K., and Tansey, M. G. (2008) TNF Signaling Inhibition in the CNS: Implications for Normal Brain Function and Neurodegenerative Disease. *Journal of Neuroinflammation*, **5**, 1-13.
- McCulloch, L., Smith, C. J., and McColl, B. W. (2017) Adrenergic-Mediated Loss of Splenic Marginal Zone B Cells Contributes to Infection Susceptibility after Stroke. *Nature Communications*, **8**, 1-15.
- McDonald, L., Liu, B., Taraboletti, A., Whiddon, K., Shriver, L. P., Konopka, M., Liu, Q., and Pang, Y. (2016) Fluorescent Flavonoids for Endoplasmic Reticulum Cell Imaging. *Journal of Materials Chemistry*, **4**, 7902–7908.

- Meldrum, B. S. (2000) Glutamate as a Neurotransmitter in the Brain: Review of Physiology and Pathology. *The Journal of Nutrition*, 130,
- Menzie, J., Prentice, H., and Wu, J-Y. (2013) Neuroprotective Mechanisms of Taurine against Ischemic Stroke. *Brain Sci.*, **3**, 877–907.
- Minnerup, J., Sutherland, B, A., Buchan, A. M., and Kleinschnitz, C. (2012) Neuroprotection for Stroke: Current Status and Future Perspectives. *International Journal of Molecular Sciences*, **13**, 11753–1172.
- Mittelbronn, M. (2014) The M1/M2 Immune Polarization Concept in Microglia: A Fair Transfer? *Neuroimmunology and Neuroinflammation*, **1**, 6-7.
- Morrison, H. W., and Filosa, J. A. (2013) A Quantitative Spatiotemporal Analysis of Microglia Morphology during Ischemic Stroke and Reperfusion. *Journal of Neuroinflammation*, **10**, 1-20.
- Moskowitz, M. A., Lo, E. H., and Iadecola, C. (2010) The Science of Stroke: Mechanisms in Search of Treatments. *Neuron*, **67**, 181–198.
- Moussaud, S., and Draheim, H. J. (2010) A New Method to Isolate Microglia from Adult Mice and Culture Them for an Extended Period of Time. *Journal of Neuroscience Methods*, **187**, 243–253.
- Murugan, M., Ling, E-A., and Kaur, C. (2013) Glutamate Receptors in Microglia. *CNS & Neurological Disorders Drug Targets*, **12**, 773–784.
- Nagai, A., Nakagawa, E., Hatori, K., Choi, H. B., McLarnon, J. G., Lee, M. A., and Kim, S. U. (2001) Generation and Characterization of Immortalized Human Microglial Cell Lines: Expression of Cytokines and Chemokines. *Neurobiology of Disease*, **8**, 1057–1068.
- Nagamoto-Combs, K., Kulas, J and Combs, C. K. (2014) A Novel Cell Line from Spontaneously Immortalized Murine Microglia. *Journal of Neuroscience Methods*, **233**, 187–198.
- Napetschnig, J., and Wu, H. (2013) Molecular Basis of NF- $\kappa$ B Signaling. *Annual Review of Biophysics*, **42**, 443–468.
- Napoli, I., and Neumann, H. (2009) Microglial Clearance Function in Health and Disease. *Neuroscience*, **158**, 1030–1038.
- Nayak, D., Roth, T. L., and McGavern, D. B. (2014) Microglia Development and

- Function. *Annu Rev Immunol.*, **32**, 367–402.
- Neumann, J., Gunzer, M., Gutzeit, H. O., Ullrich, O., Reymann, C. G., and Dinkel, K. (2006) Microglia Provide Neuroprotection after Ischemia. *The FASEB Journal : Official Publication of the Federation of American Societies for Experimental Biology*, **20**, 714–716.
- Newcomb, J. D., Ajmo, C. T., Sanberg, C. D., Sanberg, P. R., Pennypacker, K. R., and Willing, A. E. (2006) Timing of Cord Blood Treatment after Experimental Stroke Determines Therapeutic Efficacy. *Cell Transplantation*, **15**, 213–223.
- Nikodemova, M., and Watters, J. J. (2012) Efficient Isolation of Live Microglia with Preserved Phenotypes from Adult Mouse Brain. *Journal of Neuroinflammation*, **9**, 1-10.
- Nimmerjahn, A., Kirchhoff, F., and Helmchen, F. (2005) Resting Microglial Cells Are Highly Dynamic Surveillants of Brain Parenchyma *in vivo*. *Neuroforum*, **11**, 95–96.
- Nishizawa, Y. (2001) Glutamate Release and Neuronal Damage in Ischemia. *Life Sciences*, **69**, 369–381.
- Noda, M., Nakanishi, H., Nabekura, J., and Akaike, N. (2000) AMPA – Kainate Subtypes of Glutamate Receptor in Rat Cerebral Microglia. *The Journal of Neuroscience*, **20**, 251–258.
- Oh, W. J., Jung, U., Eom, H. S., Shin, H. J., and Park, H. R. (2013) Inhibition of Lipopolysaccharide-Induced Proinflammatory Responses by Buddleja Officinalis Extract in BV-2 Microglial Cells via Negative Regulation of NF- $\kappa$ B and ERK1/2 Signaling. *Molecules*, **18**, 9195–9206.
- Ohmi, K., Greenberg, D. S., Rajavel, K. S., Ryazantsev, S., Li, H. H., and Neufeld, E. F. (2003) Activated Microglia in Cortex of Mouse Models of Mucopolysaccharidoses I and IIIB. *Proceedings of the National Academy of Sciences of the United States of America*, **100**, 1902–1907.
- Ohsawa, K., Sanagi, T., Nakamura, Y., Suzuki, E., Inoue, K., and Kohsaka, S. (2012) Adenosine A3 Receptor Is Involved in ADP-Induced Microglial Process Extension and Migration. *Journal of Neurochemistry*, **121**, 217–227.
- Ohtaki, H., Ylostalo, J. H., Foraker, J. E., Robinson, A. P., Reger, R. L., Shioda, S.,

- and Prockop, D. J. (2008) Stem/progenitor Cells from Bone Marrow Decrease Neuronal Death in Global Ischemia by Modulation of Inflammatory/immune Responses. *Proceedings of the National Academy of Sciences of the United States of America*, **105**, 14638–14643.
- Ooi, Yin. Y., Dheen, S. T., and Tay, S. S. W. (2014) Paracrine Effects of Mesenchymal Stem Cells-Conditioned Medium on Microglial Cytokines Expression and Nitric Oxide Production. *Neuroimmunomodulation*, **22**, 233–242.
- Ooi, Y. Y., Ramasamy, R., Rahmat, Z., Subramaiam, H., Tan, S. W., Abdullah, M., Israf, D.A., and Vidyadaran, S. (2010) Bone Marrow-Derived Mesenchymal Stem Cells Modulate BV2 Microglia Responses to Lipopolysaccharide. *International Immunopharmacology*, **10**, 1532–1540.
- Orihuela, R., McPherson, C. A., and Harry, G. J. (2016) Microglial M1/M2 Polarization and Metabolic States. *British Journal of Pharmacology*, **173**, 649–65.
- Orr, A. G., Orr, A. L., Li, X-J., Gross, R. E., and Traynelis, S. F. (2009) Adenosine A2A Receptor Mediates Microglia Process Retraction. *Nature Neuroscience*, **12**, 872–878.
- Osborne, K. A., Shigeno, T., Balarsky, A. M., Ford, I., McCulloch, J., Teasdale, G. M., and Graham, D. I. (1987) Quantitative Assessment of Early Brain Damage in a Rat Model of Focal Cerebral Ischaemia. *Journal of Neurology, Neurosurgery, and Psychiatry*, **50**, 402–410.
- Paolicelli, R., Bolasco, G., Pagani, F., Maggi, L., Scianni, M., Panzanelli, P., and Giustetto, M. (2011) Synaptic Pruning by Microglia Is Necessary for Normal Brain Development. *Acta Neurobiologiae Experimentalis*, **72**, 1–17.
- Patel, A. R., Ritzel, R., McCullough, L. D., and Liu, F. (2013) Microglia and Ischemic Stroke: A Double-Edged Sword. *International Journal of Physiology, Pathophysiology and Pharmacology*, **5**, 73–90.
- Patkar, S., Tate, R., Modo, M., Plevin, R., and Carswell, H. V. O. (2012) Conditionally Immortalised Neural Stem Cells Promote Functional Recovery and Brain Plasticity after Transient Focal Cerebral Ischaemia in Mice. *Stem Cell Research*, **8**, 14–25.



- Peña, I. D., Borlongan, C., Shen, G., and Davis, W. (2017) Strategies to Extend Thrombolytic Time Window for Ischemic Stroke Treatment: An Unmet Clinical Need. *Journal of Stroke*, **19**, 50–60.
- Perego, C., Fumagalli, S., and De Simoni, M-G. (2011) Temporal Pattern of Expression and Colocalization of Microglia/macrophage Phenotype Markers Following Brain Ischemic Injury in Mice. *Journal of Neuroinflammation*, **8**, 1-19.
- Pischiutta, F., Brunelli, L., Romele, P., Silini, A., Sammali, E., Paracchini, L., Marchini, S., and Talamini, S. (2016) Protection of Brain Injury by Amniotic Mesenchymal Stromal Cell-Secreted Metabolites. *Critical Care Medicine*, **44**, 118–1131.
- Pocock, J. M., and Kettenmann, H. (2007) Neurotransmitter Receptors on Microglia. *Trends in Neurosciences*, **30**, 527–535.
- Pradillo, J. M., Murray, K. N., Coutts, G. A., Moraga, A., Oroz-Gonjar, F., Boutin, H., Moro, M.A., Lizasoain, I., Rothwell, N. J., and Allan, S. M. (2017) Reparative Effects of Interleukin-1 Receptor Antagonist in Young and Aged/co-Morbid Rodents after Cerebral Ischemia. *Brain, Behavior, and Immunity*, **61**, 117–126.
- Price, J, and Williams, P. B. (2001) Neural Stem Cells. *Current Opinion in Neurobiology*, **11**, 564–567.
- Prinz, M., and Priller, J. (2014) Microglia and Brain Macrophages in the Molecular Age: From Origin to Neuropsychiatric Disease. *Nature Reviews Neuroscience*, **15**, 300–312.
- Rahmat, Z., Jose, S., Ramasamy, R., and Vidyadaran, S. (2013) Reciprocal Interactions of Mouse Bone Marrow-Derived Mesenchymal Stem Cells and BV2 Microglia after Lipopolysaccharide Stimulation. *Stem Cell Research & Therapy*, **4**, 1-11.
- Raichle, M. E. (2014) Bold insights. *Cognitive Neuroscience*, **11**, 112–113.
- Ransohoff, R. M. (2016) A Polarizing Question: Do M1 and M2 Microglia Exist? *Nature Neuroscience*, **19**, 987–991.
- Ransohoff, R. M., and Perry, H. V. (2009) Microglial Physiology: Unique Stimuli, Specialized Responses. *Annual Review of Immunology*, **27**, 119–145.
- Rodríguez-Frutos, B., Otero-Ortega, L., Gutiérrez-Fernández, M., Fuentes, B.,

- Ramos-Cejudo, J., and Díez-Tejedor, E. (2016) Stem Cell Therapy and Administration Routes After Stroke. *Translational Stroke Research*, **7**, 378–387.
- Rousselet, E., Kriz, J., and Seidah, N. G. (2012) Mouse Model of Intraluminal MCAO: Cerebral Infarct Evaluation by Cresyl Violet Staining. *Journal of Visualized Experiments*, **69**, 1–5.
- Russo, C. D., Boullerne, A. I., Gavrilyuk, V., and Feinstein, D. L. (2004) Inhibition of Microglial Inflammatory Responses by Norepinephrine: Effects on Nitric Oxide and Interleukin-1beta Production. *Journal of Neuroinflammation*, **1**, 1-15.
- Rustenhoven, J., Park, T. I-H., Schweder, P., Scotter, J., Correia, J., Smith, A. M., and Gibbons, H. M. (2016) Isolation of Highly Enriched Primary Human Microglia for Functional Studies. *Scientific Reports*, **6**, 1-11.
- Samaradivakara, S. P., Samarasekera, R., Viranga, L. M., Shiroma, T. M., Handunnetti, O. V.D.S., Weerasena, J., Taylor, W. R., Alhadidi, Q., and Shah, Z. A. (2017) Bioactivities of N-Hexane Fraction of *Vateria Copallifera* and GC-MS Analysis of Its Phytoconstituents. *Industrial Crops and Products*, **97**, 87–92.
- Saura, J., Tusell, J. M. and Serratosa, J. (2003) High-Yield Isolation of Murine Microglia by Mild Trypsinization. *Glia*, **44**, 183–89.
- Schaar, K. L, Brenneman, M. M., and Savitz, S. I. (2010) Functional Assessments in the Rodent Stroke Model. *Experimental & Translational Stroke Medicine*, **2**, 1-11.
- Schielke, G. P., Yang, G. Y., Shivers, B. D., and Betz, A. L. (1998) Reduced Ischemic Brain Injury in Interleukin-1 Beta Converting Enzyme Deficientmice. *J.Cereb.Blood Flow Metab*, **18**, 180–185.
- Schmitz, M. L., and Baeuerle, P. A. (1991) The p65 Subunit Is Responsible for the Strong Transcription Activating Potential of NF-Kappa B. *The EMBO Journal*, **10**, 3805–3817.
- Schneider, A., Martin-Villalba, A., Weih, F., Vogel, J., Wirth, T., and Schwaninger, M. (1999) NF-kappaB Is Activated and Promotes Cell Death in Focal Cerebral Ischemia. *Nature Medicine*, **5**, 554–559.

- Schwarting, S., Litwak, S., Hao, W., Bähr, M., Weise, J., and Neumann, H. (2008) Hematopoietic Stem Cells Reduce Postischemic Inflammation and Ameliorate Ischemic Brain Injury. *Stroke; a Journal of Cerebral Circulation*, **39**, 2867–2875.
- Schwarz, J., Bierbaum, V., Merrin, J., Frank, T., Hauschild, R., Bollenbach, T., Tay, S., Sixt, M and Mehling, M. (2016) A Microfluidic Device for Measuring Cell Migration towards Substrate-Bound and Soluble Chemokine Gradients. *Scientific Reports*, **6**, 1-12.
- Sharkey, J., Ritchie, I. M., and Kelly, P. A. T. (1993) Perivascular Microapplication of Endothelin-1: A New Model of Focal Cerebral Ischaemia in the Rat. *Journal of Cerebral Blood Flow & Metabolism*, **13**, 865–871.
- Shichita, T., Sugiyama, Y., Ooboshi, H., Sugimori, H., Nakagawa, R., Takada, I., Iwaki, T. (2009) Pivotal Role of Cerebral Interleukin-17–producing  $\gamma\delta$ T Cells in the Delayed Phase of Ischemic Brain Injury. *Nature Medicine*, **15**, 946–950.
- Shih, R-H., Wang, C-Y., and Yang, C-M. (2015) NF-kappaB Signaling Pathways in Neurological Inflammation: A Mini Review. *Frontiers in Molecular Neuroscience*, **8**, 1–8.
- Sierra, C., Coca, A., and Schiffrin, E. L. (2011) Vascular Mechanisms in the Pathogenesis of Stroke. *Current Hypertension Reports*, **13**, 200–207.
- Smith, A. M., Gibbons, H. M., Oldfield, R. L., Bergin, P.M., Mee, E. W., Curtis, M. A., Faull, R. L. M., and Dragunow, M. (2013) M-CSF Increases Proliferation and Phagocytosis While Modulating Receptor and Transcription Factor Expression in Adult Human Microglia. *Journal of Neuroinflammation*, **10**, 1-15.
- Sousa, C., Biber, K., and Michelucci, A. (2017) Cellular and Molecular Characterization of Microglia: A Unique Immune Cell Population. *Frontiers in Immunology*, **8**, 1-17.
- Stansley, B., Post, J., and Hensley, K. (2012) A Comparative Review of Cell Culture Systems for the Study of Microglial Biology in Alzheimer’s Disease. *Journal of Neuroinflammation*, **9**, 1-8.
- Stevens, S. L., Bao, J., Hollis, J., Lessov, N. S., Clark, W. M., and Stenzel-Poore, M. P. (2002) The Use of Flow Cytometry to Evaluate Temporal Changes in Inflammatory Cells Following Focal Cerebral Ischemia in Mice. *Brain Res.*,

**932**, 110–119.

Sun, S-C. (2011) Non-Canonical NF- $\kappa$ B Signaling Pathway. *Cell Research*, **21**, 71–85.

Svensson, C., Part, K., K nnis-Beres, K., Kaldm e, M., Fernaeus, S. Z. and Land, T. (2011) Pro-Survival Effects of JNK and p38 MAPK Pathways in LPS-Induced Activation of BV-2 Cells. *Biochemical and Biophysical Research Communications*, **406**, 488–92.

Tamashiro, T. T., Dalgard, C. L., and Byrnes, K. R.. (2012) Primary Microglia Isolation from Mixed Glial Cell Cultures of Neonatal Rat Brain Tissue. *Journal of Visualized Experiments : JoVE*, **66**, 1-5.

Tamura, A., Graham, D. I., McCulloch, J., and Teasdale, G. M. (1981) Focal Cerebral Ischaemia in the Rat: Description of Technique and Early Neuropathological Consequences Following Middle Cerebral Artery Occlusion. *Journal of Cerebral Blood Flow and Metabolism*, **1**, 53–60.

Tang, G., Liu, Y., Zhang, Z., Lu, Y., Wang, Y., Huang, J., Li, Y., Chen, X., Gu, X., and Yang, G. Y. (2014) Mesenchymal Stem Cells Maintain Blood-Brain Barrier Integrity by Inhibiting Aquaporin-4 Upregulation after Cerebral Ischemia.” *Stem Cells*, **32**, 3150–3162.

Tang, Y., and Le, W. (2016) Differential Roles of M1 and M2 Microglia in Neurodegenerative Diseases. *Molecular Neurobiology*, **53**, 1181–1194.

Tarozzo, G., Campanella, M., Ghiani, M., Bulfone, A., and Beltramo, M. (2002) Expression of Fractalkine and Its Receptor, CX3CR1, in Response to Ischaemia-Reperfusion Brain Injury in the Rat. *European Journal of Neuroscience*, **15**, 1663–1668.

Taylor, R. A., and Sansing, L. H. (2013) Microglial Responses after Ischemic Stroke and Intracerebral Hemorrhage. *Clinical & Developmental Immunology*, **2013**, 1-10.

Teixeira, F. G., Carvalho, M. M., Neves-Carvalho, A., Panchalingam, K. A., Behie, L. A., Pinto, L., Sousa, N., and Salgado, A. J. (2015) Secretome of Mesenchymal Progenitors from the Umbilical Cord Acts as Modulator of Neural/Glial Proliferation and Differentiation. *Stem Cell Reviews and Reports*, **11**, 288–297.

- Terskikh, A. V., Bryant, P. J., and Schwartz, P. H. (2006) Mammalian Stem Cells. *Pediatric Research*, **59**, 13-20.
- Thanos, D., and Maniatis, T. (1995) NF-Kappa B: A Lesson in Family Values. *Cell*, **80**, 529–532.
- Thored, P., Heldmann, U., Gomes-Leal, W., Gisler, R., Darsalia, V., Taneera, J., Nygren, J. M. (2009) Long-Term Accumulation of Microglia with Proneurogenic Phenotype Concomitant with Persistent Neurogenesis in Adult Subventricular Zone after Stroke. *Glia*, **57**, 835–849.
- Tobin, M. K., Bonds, J. A., Minshall, D. M., Pelligrino, D. A., Testai, F. D., and Lazarov, O. (2014) Neurogenesis and Inflammation after Ischemic Stroke: What Is Known and Where We Go from Here. *Journal of Cerebral Blood Flow and Metabolism*, **34**, 1573–1584.
- Tremblay, M. E., Lowery, R. L., and Majewska, A. R. (2010) Microglial Interactions with Synapses Are Modulated by Visual Experience. *PLoS Biology*, **8**, 1-16.
- Vendrame, M., Gemma, C., Pennypacker, K. R., Bickford, P. C., Sanberg, C. D., Sanberg, P. R., and Willing, A. E. (2006) Cord Blood Rescues Stroke-Induced Changes in Splenocyte Phenotype and Function. *Experimental Neurology*, **199**, 191–200.
- Wake, H., Moorhouse, A. J., Jinno, S., Kohsaka, S., and Nabekura, J. (2009) Resting Microglia Directly Monitor the Functional State of Synapses *in vivo* and Determine the Fate of Ischemic Terminals. *Journal of Neuroscience*, **29**, 3974–3980.
- Wang, L-Q, Lin, Z-Z., Zhang, H-X., Shao, B., Xiao, L., Jiang, H-G., and Zhuge, Q-C. (2014) Timing and Dose Regimens of Marrow Mesenchymal Stem Cell Transplantation Affect the Outcomes and Neuroinflammatory Response After Ischemic Stroke. *CNS Neuroscience & Therapeutics*, **1**, 1–10.
- Wang, Q., Tang, X. N., and Yenari, M. A. (2007) The Inflammatory Response in Stroke. *Journal of Neuroimmunology*, **184**, 53–68.
- Warlow, C., Sudlow, C., Dennis, M., Wardlaw, J., and Sandercock, P. (2003) Stroke. *The Lancet*, **362**, 1211–1224.
- Weise, G., Lorenz, M., Pösel, C., Riegelsberger, U. M., Störbeck, V., Kamprad, M.,

- Kranz, A., Wagner, D-C., and Boltze, J. (2014) Transplantation of Cryopreserved Human Umbilical Cord Blood Mononuclear Cells Does Not Induce Sustained Recovery after Experimental Stroke in Spontaneously Hypertensive Rats. *Journal of Cerebral Blood Flow & Metabolism*, **34**, 1–9.
- Whiteside, S. T., Epinat, J-C., Rice, N. R., and Israël, A. (1997) I Kappa B Epsilon, a Novel Member of the I Kappa B Family, Controls RelA and cRel NF-Kappa B Activity. *The EMBO Journal*, **16**, 1413–1426.
- Whitesides, G. M. (2006) The Origins and the Future of Microfluidics. *Nature*, **442**, 368–373.
- Wink, D. A., Hanbauer, I., Laval, F., Cook, J. A., Krishna, M. C., and Mitchell, J. B. (1994) Nitric Oxide Protects against the Cytotoxic Effects of Reactive Oxygen Species. *Ann N Y Acad Sci.*, **738**, 265–78.
- Wu, H-J., Liu, Y-J., Li, H-Q., Chen, C., Dou, Y., Lou, H-F., Ho, M. S., Li, X-M., Gao, Z., and Duan, S. (2014) Analysis of Microglial Migration by a Micropipette Assay. *Nature Protocols*, **9**, 491–500.
- Xia, C.Y., Zhang, S., Gao, Y., Wang, Z. Z., and Chen, N. H. (2015) Selective Modulation of Microglia Polarization to M2 Phenotype for Stroke Treatment. *International Immunopharmacology*, **25**, 377–382.
- Yan, K., Zhang, R., Sun, C., Chen, L., Li, P., Liu, Y., and Peng, L. (2013) Bone Marrow-Derived Mesenchymal Stem Cells Maintain the Resting Phenotype of Microglia and Inhibit Microglial Activation. *PloS One*, **8**, 1-8.
- Ye, J., Coulouris, G., Zaretskaya, I., Cutcutache, I., Rozen, S., and Madden, T. L. (2012) Primer-BLAST: A Tool to Design Target-Specific Primers for Polymerase Chain Reaction. *BMC Bioinformatics*, **13**, 1-11.
- Yuan, Y., Rangarajan, P., Kan, E. M., Wu, Y., Wu, C., and Ling, E-A. (2015) Scutellarin Regulates the Notch Pathway and Affects the Migration and Morphological Transformation of Activated Microglia in Experimentally Induced Cerebral Ischemia in Rats and in Activated BV-2 Microglia. *Journal of Neuroinflammation*, **12**,1-21.
- Zanier, E. R., Marchesi, F., Ortolano, F., Perego, C., Arabian, M., Zoerle, T., Sammali, E., Pischiutta, F and De Simoni, M-G. (2015) Fractalkine Receptor Deficiency Is Associated with Early Protection, but Late Worsening of Outcome

- Following Brain Trauma in Mice. *Journal of Neurotrauma*, **33**, 1060-1072.
- Zanier, E. R., Montinaro, M., Viganò, M., Villa, P., Fumagalli, S., Pischiutta, F., Longhi, L., Leoni, M. L., Rebullà, P., Stocchetti, N., Lazzari, L., and De Simoni, M-G. (2011) Human Umbilical Cord Blood Mesenchymal Stem Cells Protect Mice Brain after Trauma. *Critical Care Medicine*, **39**, 2501–2510.
- Zhang, H., Lohcharoenkal, W., Sun, J., Li, X., Wang, L., Wu, N., Rojanasakul, Y., and Liu, Y. (2015) Microfluidic Gradient Device for Studying Mesothelial Cell Migration and the Effect of Chronic Carbon Nanotube Exposure. *J Micromech Microeng.*, **25**, 1-11.
- Zhang, L., Dong, L-Y., Li, Y-J., Hong, Z., and Wei, W-S. (2012) The microRNA miR-181c Controls Microglia-Mediated Neuronal Apoptosis by Suppressing Tumor Necrosis Factor, **9**, 1–12.
- Zhang, R., Liu, Y., Yan, K., Chen, L., Chen, X-R., Li, P., Chen, F-F., and Jiang, X-D. (2013) Anti-Inflammatory and Immunomodulatory Mechanisms of Mesenchymal Stem Cell Transplantation in Experimental Traumatic Brain Injury. *Journal of Neuroinflammation*, **10**, 1-12.
- Zhao, W., Xie, W., Xiao, Q., Beers, D. R., and Appel, S. H. (2006) Protective Effects of an Anti-Inflammatory Cytokine, Interleukin-4, on Motoneuron Toxicity Induced by Activated Microglia. *Journal of Neurochemistry*, **99**, 1176–1187.
- Zhao, X., Zhang, Y., Strong, R., Zhang, J., Grotta, J. C., and Aronowski, J. (2007) Distinct Patterns of Intracerebral Hemorrhage-Induced Alterations in NF- $\kappa$ B Subunit, iNOS, and COX-2 Expression. *Journal of Neurochemistry*, **101**, 652–663.
- Zhou, C., Zhang, C., Chi, S., Xu, Y., Teng, J., Wang, H., Song, Y and Zhao, R. (2009) Effects of Human Marrow Stromal Cells on Activation of Microglial Cells and Production of Inflammatory Factors Induced by Lipopolysaccharide. *Brain Research*, **1269**, 23–30.
- Zhu, Y., Guan, Y-M., Huang, H-I and Wang, Q-S. (2014) Human Umbilical Cord Blood Mesenchymal Stem Cell Transplantation Suppresses Inflammatory Responses and Neuronal Apoptosis during Early Stage of Focal Cerebral Ischemia in Rabbits. *Acta Pharmacologica Sinica*, **35**, 585–591.
- Zicha, D., Dunn, G. A., and Brown, A. F. (1991) A New Direct-Viewing Chemotaxis

Chamber. *Journal of Cell Science*, **99**, 769–775.

Zuidema, M. Y., and Zhang, C. (2010) Ischemia/reperfusion Injury: The Role of Immune Cells. *World J Cardiol*, **2**, 325–332.